Isolated Induction Generator , Induction Motor Scheme For Borehole Pump And Other Application

by

MAGED AHMED ABU - ADMA

B.Sc., M.Sc, M.B.W.E.A.

Thesis submitted to the University of London

for the degree of Doctor of Philosophy

and Diploma of Imperial College

Department of Electrical Engineering

Imperial college of science and Technology

April 1989

"In The Name of Allah, The Merciful,
The beneficient."

TO MY FATHER

ABSTRACT

This thesis presents a study of a scheme in which an induction motor is supplied from a capacitor–excited induction generator. The scheme is one of a number in which the output of a prime mover is converted into electrical form for convenient transmission to one, or a small number of electric motor–driven mechanical loads.

Prospective advantages of this scheme include the complete absence of brushes on the electrical machines, the use of standard low–cost induction machines, freedom from synchronizing difficulties, an absence of electronic power converters and field exciters. The absence of self–excitation at low speeds can be an advantage when the scheme is driven by a prime mover such as a wind turbine having only modest starting torques.

A prediction technique for the system, based on non–linear models of the generator and motor, has been evolved. The prediction method enables the effects of changes in machine parameters and operating conditions to be assessed. The analysis is based on the steady–state equivalent circuit model for induction machines, saturation being allowed for by making each machine's magnetizing inductance dependent on the calculated air gap flux level.

Four simulation codes have been developed for predicting the steady–state performance. The first two deal with operation of the generator and capacitor bank alone. The generator speed at which voltage build up occurs and the value of the final voltage at the end of build–up period are predicted. The other two deal with the operation of the generator and capacitor bank when connected to an induction motor–driven pump. The prediction technique has

been used to demonstrate the way in which the scheme operates:

a) when the capacitor is varied to maintain constant voltage;

b) when the capacitance is varied to maintain constant voltage/frequency;

c) with constant capacitance.

In each of the first two cases, a capacitance regulator in the form of a stepped switching scheme or regulator using a parallel inductor would be needed. The influence of the pump size in relation to the power ratings of the two induction machines has been investigated. Comparisons between predictions and experimental results from a laboratory rig show good agreement.

Further simulation codes have been formulated enabling the scheme's response to a time–varying prime mover torque to be estimated. Valid for conditions where changes are relatively small within one cycle of a.c. operation, these codes have been used to investigate the start–up behaviour of the scheme under:

a) constant generator speed;

b) variable generator speed in combination with wind turbine.

Predictions have been made for the system operated in two ways:

i) with a switched, capacitor bank;

ii) with a fully controlled capacitor bank operated so as to give a constant rate of voltage increase during the motor starting period.

It is found that a motor isolating switch, closed only after self–excitation has occurred, is necessary to avoid the need for very large capacitor bank values. Even with the motor isolating switch, the 'fixed' capacitor scheme's operation is much improved if the capacitor bank is sectionalised into 2 or 3 parts.

ACKNOWLEDGEMENTS

I would like to express my extreme gratitude to my supervisor Dr. H.R. Bolton of the Department of Electrical Engineering, Imperial College, for his continuous support, guidance, advice and invaluable encouragement during the course of the work.

I would also like to thank Dr. L.L. Freris for many useful suggestions and helpful discussions.

Thanks are also due to the Egyptian government and Overseas Research Scholarship Committee for their financial support during the project. I also wish to acknowledge the help of my colleague E. El-Halafawy for collecting the data concerning the viability of wind pump schemes for Egypt.

I would like to thank Mr. F. Briggs – technician in the laboratory for his advice throughout the experimental parts of the project.

Last but not least, I must thank my wife, Mona, for her care, encouragement and her sharing of my joys and sorrows all these years.

CONTENTS

List of Principal Symbols

C	Capacitor per phase
D	Rotor blade diameter
C_p	Power coefficient
f	System frequency
H	Total pumping head
I_c	Capacitive exciting current
I_{mog}	Generator magnetizing current
I_{mom}	Motor magnetizing current
I_{1g}	Generator stator current
$I_{1g\ react}$	Reactive component of generator stator current
I_{1m}	Motor stator current
$I_{1m\ react}$	Reactive component of motor stator current
I_{2g}	Generator rotor current
I_{2m}	Motor rotor current
J_g	Generator moment of inertia
J_m	Motor moment of inertia
J_p	Pump moment of inertia
J_{tur}	Turbine moment of inertia
J_w	Water moment of inertia
k_g	Gear box ratio
k_p	Pump constant
n_g	Generator speed
n_m	Motor speed
$P_{g.elec}$	Generator electric power
$P_{g.loss}$	Generator losses
$P_{g.mech}$	Generator mechanical power
$P_{m.elec}$	Motor electric power
$P_{m.mech}$	Motor mechanical power

P_{tur}	Turbine power
$P_{w.F}$	Windage and friction power loss
$(P.F)_g$	Generator power factor
$(P.F)_m$	Motor power factor
P_{2g}	Rotor output power
Q_{day}	Average daily wind pump output
Q_g	Generator reactive power
Q_m	Motor reactive power
R_{mg}	Generator magnetizing resistance
R_{mm}	Motor magnetizing resistance
R_{1g}	Generator stator resistance
R_{1m}	Motor stator resistance
R_{2g}	Generator rotor resistance
R_{2m}	Motor rotor resistance
R	Wind turbine radius
R_L	Load resistance
S_g	Generator slip
S_m	Motor slip
$T_{acc.g}$	Generator accelerating toque
$T_{acc.m}$	Motor accelerating torque
$T_{elec.g}$	Generator electric torque
$T_{elec.m}$	Motor electric torque
T_p	Pump torque
T_{tur}	Wind turbine torque
V_t	Generator terminal voltage
V_g	Generator air gap voltage
V_m	Motor air gap voltage
V_w	Wind speed
$V_{w(op)}$	Optimum wind speed

w	System angular frequency
w_g	Generator angular frequency
$w_{g(op)}$	Optimum generator angular frequency
w_m	Motor angular frequency
w_{tur}	Turbine speed
X_c	Capacitor reactance
X_{mg}	Generator magnetizing reactance
X_{nm}	Motor magnetizing reactance
X_{1g}	Motor stator leakage reactance
X_{2g}	Generator rotor leakage reactance
X_{2m}	Motor stator leakage reactance
Z_{ing}	Generator input impedance
Z_{inm}	Motor input impedance
ρ_{air}	Air density
λ	Tip−speed ratio
δ_{wg}	Generator speed increment
δ_{wm}	Motor speed increment
δ_t	Time increment
η_g	Generator efficiency
η_m	Motor efficiency
$\eta_{overall}$	Overall efficiency

CHAPTER 1

INTRODUCTION

1.1 The Nature of Wind Energy

The thesis primarily concerns wind–powered borehole pumps and some introductory remarks about wind energy are appropriate. References from [1-1] to [1-14] contain concise accounts of the basic nature of wind energy. As reference [1-14] states: 'Wind energy is a highly variable energy source, and geographical factors are very important'. The main influences on wind conditions are described in reference [1-15]. Chief amongst these are terrain, climatic regime, height, season and time of day. The variable nature of wind speeds from instant to instant is a challenge to the wind energy system designer and the strong influence of location on mean wind speeds makes the siting of wind energy convertion equipment a critical matter. Water pumping is an example of an application where the short term variation in wind speed is of relatively small importance, and the scheme investigated in the project and reported in this thesis enables the siting of the wind turbine to be less determined by the borehole or surface pump location than in cases where the pump turbine is directly mechanically connected to the turbine.

The basic relations for wind turbine and pump behaviour are set out in appendices 1 and 2 respectively.

1.2 Wind Energy in Agriculture

The application of wind energy to agriculture is not a new idea, and in many parts of the world wind power is successfully used for water pumping. There is evidence that the ancient Egyptians used windmills as early as 3600 B.C. to pump water to irrigate their arid fields. Europe subsequently imported the technology from the East. A big step forward was made by the Dutch, probably the first to introduce the horizontal–axis windmill around the 12th century. At the begining of the 20th century some hundreds of thousands of machines were in operation throughout the world [1-1]. In the last several decades wind pump numbers have decreased considerably as diesel and electrically powered pumps have come into use. Wind pumps are however still used extensively in remote parts of Australia, North America and South America [1-2]. This is probably due to the high cost of fuel in remote areas, and the frequent lack of mains electricity there, together with the ability of many pumping schemes to accept an intermittent mode of operation. In recent years a number of organisations have sought to improve the traditional wind pumps, most notably the Intermediate Technology Development Europe and the Dutch T.N.O. National Organization. Over the last 10 years, many installations of new wind pumps have made in numerous Third World Countries for small scale irrigation and rural water supplies [1-3] and [1-4]. The new machines are capable of powering pumps from 0.1 to 200 Kw.

The obvious advantages of using wind energy are

1] It is a nondepletable and non–polluting resource.

2] Fuel costs are zero.

3] Its use affords a considerable degree of independence from outside energy resources and from the distribution of these resources.

And the major disadvantages are:

1] Low energy density which means a relatively large capture area.

2] Intermittent and variable behaviour of the wind.

3] High initial capital cost [1-5] per mean Kw.

1.3 Centrifugal Pumps

The ideal load for a wind rotor operating in a variable wind is one whose torque–speed characteristic matches the optimum torque–wind speed characteristic of the wind rotor. Ideally the torque should be proportional to the square of the operating speed [1-6]. Centrifugal pumps have in fact a load torque proportional to the square of the rotor speed. However, they generally run at speeds at least ten times the operating speed of typical wind rotors, making the use of some form of a step–up essential.

Fig. (1.1) shows a schematic drawing of a centrifugal pump connected to a wind rotor [1–6]. There are 3 basic types of centrifugal pumps: the impeller–radial type, the mixed flow type and the axial type. For use in wind pump systems, the radial type are of greatest interest, due to their higher pressure coefficient and resulting ability to deal with larger static heads [1-7].

The main advantages of the centrifugal pumps are:

1] It is relatively unaffected by water impurities.

2] It is less affected by dry-running than the piston pump.

3] It operates smoothly, without oscillating parts.

Even for typical low head agricultural applications such as drainage and irrigation, a combination of wind turbine and centrifugal pump may hence be superior to classical systems [1-7]. The disadvantages of the centrifugal pumps are the need to incorporate a step−up gear box with its attendant problems of failure risk, extra friction and increased referred inertia.

1.4 Directly−Coupled versus Indirectly −Coupled Wind−Pumping Systems

Directly-coupled wind turbines need to be located directly over the pump. Unfortunately, the borehole or other water source is frequently sheltered from the wind by trees or buildings or is located in a sheltered valley or depression. Experience with commercialization has confirmed that many opportunities for applying wind pumps are compromised or even lost due to difficulties in siting the wind turbine [1.8]. Where used, the directly coupled, traditional farm−type water−pumping windmill has proved reliable, but its high solidity makes the blading and supporting structure relatively heavy and expensive, and its matching with the usual simple positive displacement pump is poor [1−9].

With an indirect coupling, the wind turbine can be located some distance (horizontally) from the pump. The wind velocity can be considerably higher on local raised or high ground, or even in nearby land which is less sheltered than that at the pump location. Fig. (1.2) shows the way in which the generator and pump can each be located for best operating conditions [1−10]. Since the power in the wind varies as the cube the wind speed, the benefits from separating a wind turbine from its pump can be significant. A further advantage is that the percentage of the time the wind will exceed the cut−in velocity will be greater, reducing storage requirements (and costs). Finally the

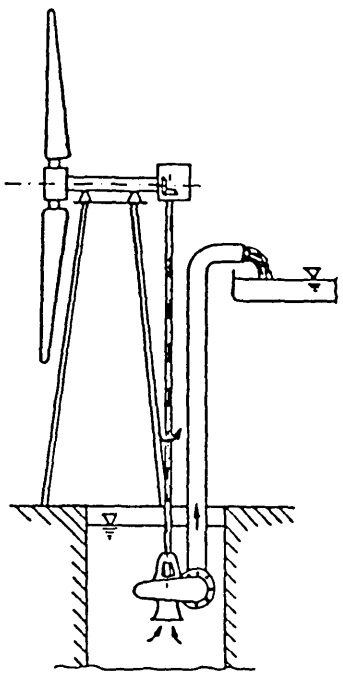

Fig. (1. 1) Schematic drawing of a centrifugal pump connected to a wind rotor.

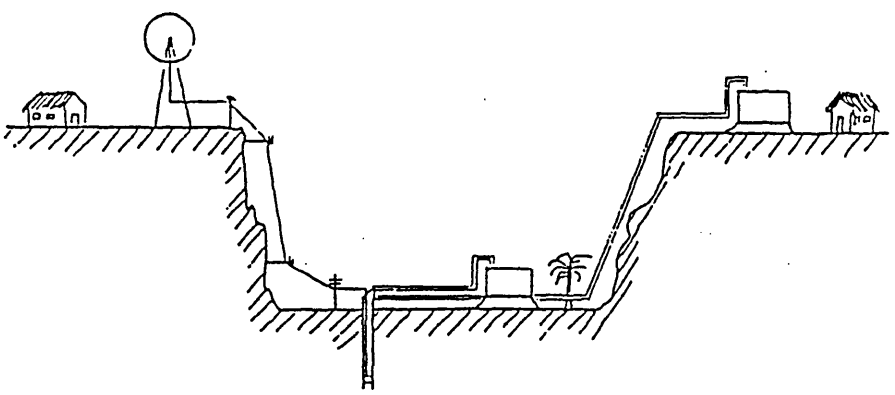

Fig. (1.2) Optimum placement for the turbine and the pump .

air-flow at an exposed location is generally less turbulent and therefore the fatigue life of key components is likely to be improved. It is hence useful to consider methods of indirect coupling.

The most feasible transmission systems can be identified as mechanical, electrical, hydraulic and pneumatic. The rate of increase of cost with seperation distance is a direct function of transmission line cost per unit length. Low pressure pneumatic hose is significantly cheaper than other options; electric cable is ranked next, followed by hydraulic pipe. Mechanical shafts etc. are the most expensive . The mechanical system however involves the least cost of energy conversion equipment. Hydraulic and pneumatic pumps and motors are probably less costly than electrical ones, but life times are generally less, particularly in comparison with commutator less equipment. A significant advantage enjoyed by hydraulic pumps is their high torque per size, enabling a direct connection between wind rotor and pump to be used, eliminating the need for a gearbox. Direct drive electrical generators are apt to be costly and heavy but are not unknown in windpower applications.

1.5 Wind Electric Pump Systems

Over the past decade a large number of types of wind–driven electric generator units have been developed. A particular feature is the increase in power rating of commercially available units. Whereas direct – coupled wind pumps have rotor diameters limited to approx. 5m, those in commercially available wind–electric units range up to and beyond 20m. Few of these so far have been applied to water pumping or irrigation, though a few projects have been reported in the literature [1-11], [1-23] and [1-24]. When an electrically coupled

wind turbine pump system using available components is developed, it is obviously the job of the designer to select those components that will be well matched and will give a system which satisfies the output requirements at minimum cost and with adequate reliability, subject to the types of local maintenance skills and spares likely to be available. Reference [1-11] reports

an economic comparison between the wind electric pump system and a diesel pump.

The author concluded that the systems were economically comparable, the electrical transmission system having the disadvantage of high initial cost and the diesel engine the disadvantage of dependency on unpredictable oil prices. Electric pumping for deep well pumping, irrigation and agriculture [1-23] would therefore appear to be a promising application of wind energy in certain circumstances likely to be competitive with to conventional systems particularly in remote sites. References [1-23] and [1-24] are discussed later in this chapter.

1.6 Water Storage in Irrigation System

Wind pump output is not constant with time and one of the methods used to facilitate the water management of a wind pump irrigation system is the inclusion of a storage tank in the system [1-3] , [1-4].
For small scale systems, water storage is cheap in comparison with electric storage using batteries [1-9].

In many systems, there is no water demand during the night and the pump output during this period is either stored in a tank or lost if the tank is already

full. Similarly, if the daily water requirements are met during the day, any pump output in excess of these requirements is again either stored in a tank or lost if the tank happens to be full. If the farmer does not have enough water from either wind pump or tank, however, a water deficit occurs. It has been found in practice that, for a site with a typical diurnal wind pattern, a tank capacity in the range of 1 to 2 times the average daily wind pumps output (Reference [1-3]) gives a good compromise between cost and water availability. Of the average daily wind pump output given by:

$$Q_{day} = 0.69 \frac{V_w^3 D^2}{H} \qquad (1-1)$$

where:

V_w: average wind speed m/sec

D : rotor diameter m

H : Total pumping head m,

70% to 80% of the potential wind pump output is available for use by the farmer [1−3].

1.7 Wind Energy Utilisation in Egypt

Oil is responsible for 75% of the total energy consumption in Egypt, the writer's home country. At present Egypt is an oil exporter, but in the future this situation is expected to reverse. Because of this and the likely upward long term oil price trend as world reserves diminish, the assessment of renewable energy resources such as wind is obviously important. Egypt is a large country and a nationally interconnected grid system is non-viable. The isolation of many of the smaller towns, villages and settlements necessitates the adoption of isolated local electricity networks of relatively small rating. Fuel costs are high

due to the transportation distances involved and the case for some form of renewable energy conversion is correspondingly stronger.

1.7.1 Wind Program For Egypt

An evaluation of the size of the wind energy resource available in Egypt has been under way since 1972 as a program conducted by the Egyptian Ministry of Electricity and Energy [1-25]. The first part of this program was to gather existing wind data and to determine the most promising area for wind energy exploration. The second part was to survey existing Egyptian industrial capabilities to determine the feasibility of local wind energy conversion equipment manufacture.

It was generally concluded from this program that the most promising areas were the Mediterranean coast to the north and the Red Sea Coast (especially between Hurghada and Ras Gharib) to the east. On the north coast, wind is thought to be certainly suitable with small machines for irrigation and/or providing comparatively small amounts of electricity. Concerning the Red Sea coast, it is felt that the prospects for obtaining a significant amount of commercial power from wind energy for the electric grid are bright.

The disadvantage of the Red Sea coast is that this area is the best oil gas–producing region in Egypt. Concerning the capability of Egyptian industry, it was found that considerable diversity does exist to manufacture wind energy systems locally, including those of smaller size to be used for auxiliary electricity and water pumping, together with somewhat larger systems [1-1].

1.7.2 Viability of Wind Pumping Scheme for Egypt

A visit to Egypt to collect data concerning the viability of wind pumping schemes incorporating electrically–powered borehole pumps was made by the writer. The specific data required were graphs or tables of month–by–month mean wind speeds for a number of appropriate locations. The locations where wind–power electric pumps could be viable would be where local electricity supplies are absent, where under–ground water conditions are satisfactory and where the average wind speed (e.g. over a 3–hour period at the windiest part of each day) would exceed 3 meters per second or so. From the EMA data, it was found that these conditions were all satisfied at a promising site called 'East of Oweinat' – near the Egyptian frontiers with Libya and Sudan, west of Aswan. The costs of fuel transportation to a diesel station there or of erecting power lines from Aswan would be high.

1.7.3 Wind Recorders at the 'East of Oweinat' Area

Fig. (1–3) shows a map of Egypt on which the annual mean wind speeds (m/sec) in the most promising areas for wind energy exploitation [1-26] are shown. Wind velocity frequency data for the East of Oweinat area for the period 1980 to 1984 is illustrated in table (1.1). It also shows the mean wind speed (knots) for each month. The mean monthly minimum wind speed is 31.3 Km/hr in December and January, and its mean maximum is 32.4 Km/hr in September. Fig. (1–4) shows the mean wind speed (knots) versus months for the period from 1980 until 1984. It is clear that the monthly average wind speeds change considerably, but in general the highest value occurred in spring and summer and the lowest in autumn. The prevailing wind direction is

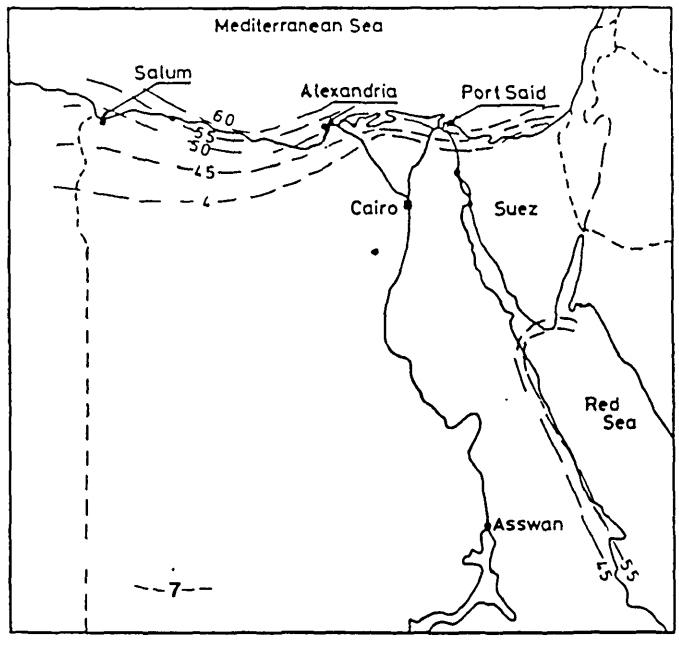

Fig. (1.3) Map of Egypt on which annual mean wind speed (m/sec.) .

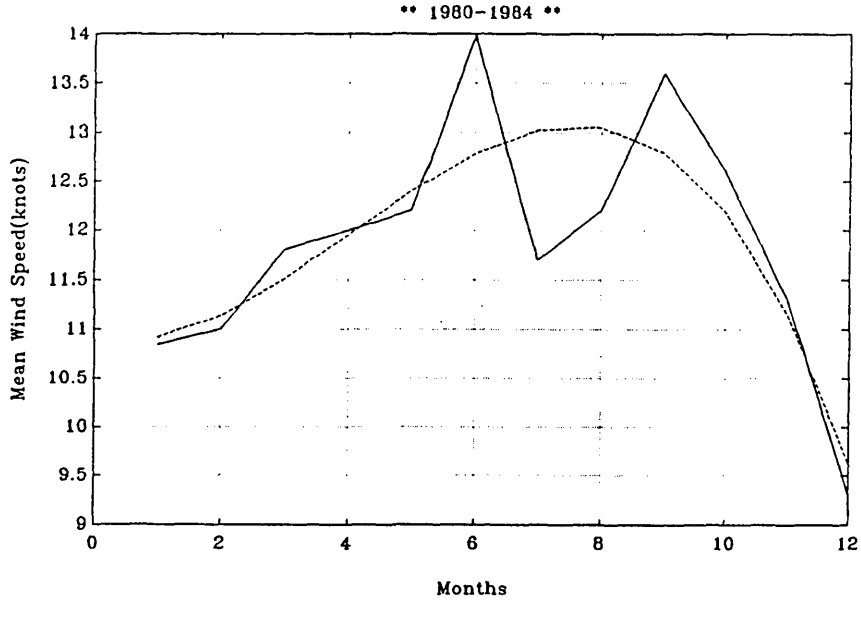

Fig. (1.4) Mean wind speed (Knots) versus months .

-1980 – 1984

Months	Mean wind speed (knots)	Surface wind speed (knots) Percentage frequency of wind blowing within the following speed ranges							
		1-3	4-6	7-10	11-16	17-21	22-27	28-33	>34
Jan.	10.84	4.90	15.1	30.4	33.9	11.4	2.80	0.00	0.00
Feb.	11.00	4.50	16.5	27.8	32.8	11.7	4.80	0.00	0.00
Mar.	11.8	3.50	14.1	25.8	32.8	12.8	6.10	1.90	0.00
Apr.	12.00	3.90	13,7	21.4	31.4	16.7	7.70	0.50	0.00
May	12.20	2.10	12.1	23.6	35.4	15.1	6.90	0.70	0.00
June	13.98	2.00	5.90	16.4	42.5	20.0	8.90	1.80	0.00
July	11.70	1.50	9.60	29.1	42.4	12.6	2.40	0.00	0.00
Aug.	12.20	1.20	6.40	27.9	50.0	11.0	2.50	0.00	0.00
Sep.	13.60	0.00	5.70	20.9	45.6	18.5	7.40	0.00	0.00
Oct.	12.60	1.70	6.20	24.2	46.2	16.9	2.97	0.00	0.00
Nov.	11.30	1.00	15.9	30.7	39.4	10.4	2.30	0.00	0.00
Dec.	9.30	7.40	20.0	34.9	31.6	5.20	0.00	0.00	0.00
Annual mean	11.8	2.8	11.8	26.1	38.6	13.5	4.6	0.00	0.00

Table (1.1)

generally in the northwest to northeast. Strong wind blows frequently during April, developing occasionally into sand storms, while throughout the period July–October moderate to calm wind prevails. The number of hours of surface wind within specified speed ranges at the area for the period from 1980 to 1984 is illustrated in table (1–2). It is clear that the number of hours within the 7 to 10 knot and 11 to 16 knot speed ranges are sufficient for viable wind exploitation.

1.7.4 Climatic Conditions

The climatological observations recorded at the GPC Camp, meteorological station indicate that the study area lies within the arid zone, being warm in winter and rather hot in summer, with wide diurnal variations and almost no precipitation.

The average monthly temperature ranges between 12.2° in December and 31.5°C in July. The relative humidity ranges from 11% in May to 41.3% in December. The rather hot periods, prevailing from the end of May to the end of July, are always associated with extreme dryness, with humidity reducing to 11%. Natural evaporation rates range between 9.7 mm/day during January to 31.1 mm/day during July.

1.7.5 Under–ground Water Conditions

A ground water resources evaluation study was carried out in the East of Oweinat area, as a part of the comprehensive hydro–agricultural investigation program, initiated in 1978 by the General Petroleum Company (GPC) [1–27].

1980 - 1884

Months	Number of hours of occurrence of surface wind within specified ranges							
	1 - 3	4 - 6	7 - 10	11-16	17-21	22-27	28-33	> 34
Jan.	20	61	122	137	46	11	0	0
Feb.	17	61	103	121	43	18	0	0
Mar.	14	57	104	132	52	24	8	1
Apr.	15	53	83	122	65	30	2	0
May	8	49	95	142	61	28	3	0
June	8	23	64	166	78	35	7	0
July	6	39	117	171	51	10	2	1
Aug.	5	26	112	202	45	10	1	0
Sep.	3	22	82	178	72	29	3	0
Oct.	7	25	97	186	68	12	0	0
Nov.	4	62	120	154	41	9	0	0
Dec.	30	81	141	127	21	1	0	0

Table (1.2)

The object of the study was to quantify the exploitable ground water resources of the Nubia aquifer system, which can be feasibly utilized for irrigating areas of proven good soil, with long–term reliability and good economy. The intensive hydrogeological study covered an area of 4250 Km^2 in the mid–west part of the East Oweinat regional study area. The ground water in the East Oweinat area is reasonably pure and is reckoned to be suitable for irrigation purposes. Preliminary evaluation of the ground water resource is estimate for the intensive study area to be about 285×10^6 m^3/annum for an exploitation period of 100 years and a maximum allowed pumping lift of 100 m. 245×10^6 m^3/annum of this will be extracted from the recoverable static reserves. With the present production – well design – practice in the East Oweinat area, an optimum pumping rate of 200–400 m^3/hr can be achieved, with anticipated drawdowns ranging from 6 to 27m.

1.8 Wind–Electric Pumping Scheme

This thesis presents an analysis of a specific type of wind pumping scheme based on a capacitor–excited three phase induction generator driven by a wind turbine supplying a three phase induction motor driving a centrifugal pump.

Although there is some literature (refs from [1-28] to [1-39]) dealing with mains–connected induction generators, and some literature (refs from [1-40] to [1-62]) dealing with capacitor–excited induction generators feeding isolated resistance or simple R–L loads, it is believed to be the first time that an investigation in quantitative terms has been made of a capacitor–excited induction generator scheme with an induction motor as its sole load.

The electrical system configuration belongs to that family of isolated energy conversion and transmission systems in which the output of a prime mover is converted into electrical form for consumption in one or a small number of motor loads.

The most well known examples of such systems are perhaps the diesel/ alternator/rectifier/dc motor schemes found on railway locomotives, drilling rigs and some mountain cable car installations, the petrol engine/alternator/motor units investigated for hybrid battery vehicles, and the turbine/alternator/synchronous motor drives used on turbo–electric ships. Flexibility of operation and simplification of speed control are in most cases the key benefits bestowed by the adoption of an 'electrical stage' between the prime mover and the ultimate mechanical load, and the steady state and dynamic behaviour patterns of the most popular type of scheme have been analysed and formulated for some years.

A number of preliminary remarks can be made about the present scheme's likely operating features:

1] The absence of any sort of frequency converter means that when the scheme is operating normally, the motor speed will tend to track the generator speed fairly closely (the two being roughly related by the machine's pole number ratio). The variable and somewhat unpredictable nature of the motor/pump speed is of course much more acceptable in water pumping schemes than in many other drive applications.

2] The absence of voltage build–up at low speeds in the induction generator will leave the turbine virtually unloaded there, helping the turbine–start–up process.

3] Because both the wind turbine and the centifugal pump have cubic power–speed curves, a good power match can be expected over a considerable range of wind speeds. Note that this power matching feature would be shared by schemes having other electrical system configurations.

4] The use of an electric rather than a mechanical connection between turbine and pump can bring a reduced risk of mechanical shock and enables a standard submersible commercial electric pump to be considered. Such pumps are available for a wide range of heads and flow.

1.9 Electrical System Options

In addition to the scheme considered, other system configuration options exist.

1] A wound–field synchronous a.c. generator (or alternator) on the turbine, and an induction motor driving the pump. This could perhaps be thought of as the most conventional of the options.

2] D.C. generator feeding a d.c. to a.c. inverter, in turn feeding an induction motor pump.

3] Permanent magnet synchronous a.c. generator feeding an induction motor pump.

4] Generator of any type feeding a converter–fed brushless d.c. pump. (Note that such pumps have been developed for solar–voltaic–powered schemes due to their enhanced efficiency).

As indicated above, the three types of electrical machines normally used as generators are the d.c. machine, the induction machine and the synchronous machine. Each of these has its own constructional and performance characteristics.

Though the d.c. machine has many characteristics which fit well with a wind–generation system, it is costly and does not have the features of ruggedness and serviceability which are also desirable in a generator called on to operate reliably for perhaps 4000 hours per year for 20 years.

Synchronous generators have been widely used in wind–energy schemes, particularly in mains–connected ones of relatively high rated power (primarily because of their good efficiency at full load and the controllable nature of their VAr demand). The synchronous generator's ability to supply the induction pump's VArs make it a strong contender for the present scheme and reference [1–11] does in fact report an investigation into a pumping scheme based as a synchronous generator. However, the generator possesses a wound rotor or a permanent magnet rotor construction, and is hence somewhat more costly and less robust than an induction generator, and this will affect overall system costs and reliability levels.

Cage induction machines have been used for almost 100 years, are universally established in the motoring roles, and are increasingly used in the generator mode for small/medium hydro and mains–connected wind energy conversion applications [1–63].

Squirrel cage induction machines of course have no brushes. The rotor conductors are copper bars or are of aluminium cast directly in the slots in the lamination stack, making the rotor simple, inexpensive, and mechanically rugged. An induction generator's efficiency can be near to that of a synchronous generator's at similar rating and operating conditions, while because of its simple construction and installation requirements (no field supply system etc.), the induction machine is generally considerably cheaper in cost per rated Kw [1-64]. The absence of a field supply system perhaps incorporating auxiliary batteries and automatic voltage regulating (AVR) devices further boosts their reliability advantages. Although the low output voltage of d.c. and synchronous generators at low speeds will also lead to low turbine loading, the complete absence (apart from residual) of voltage build up with a capacitor–excited induction generator until a critical speed is reached means that turbine start–up will be easier and faster in the latter case unless special excitation control features are incorporated in the d.c. and synchronous generator cases.

Finally, the induction generator exhibits a high level of internal (rotor current) damping to sudden speed disturbances and hence may often provide sufficient compliance virtually to eliminate the torque pulsations due to gusting. Hence the higher frequency components of frequency fluctuations seen by the motor are likely to be largely damped out. This will reduce motor slip losses, raise

efficiency and will minimise the risks of motor pull–out during extreme conditions [1-65].

1.10 Some Drawbacks of Induction Generator Schemes

1] Induction generators demand significant amounts of reactive power. The weight, cost, volume and finite life time of the capacitor bank needed for the scheme envisaged obviously affect the corresponding quality factors of the overall system. Some sort of regulating and/or switching scheme is likely to be needed for the capacitor bank, possibly similar in cost etc. to the field regulator needed for a d.c. or synchronous generator. (Note: as is shown later, two simple 3 phase contacters are thought to suffice in many cases for the Ind. Gen. scheme).

2] The Induction Generator is likely to possess a smaller overload capability and cannot sustain a short circuit unless special measures (or de–rating) are employed.

3] Even under fixed shaft speed conditions, the induction generator's output frequency varies with load (slip must vary as power varies). Although this matters little in the present case because the frequency variation is small, predictions about pump behaviour and motor operating points are obviously made more difficult.

4] The sensitivity of the output voltage to the generator shaft and to load is generally high. With a motor load, the impedance presented to the generator varies considerably, particularly during motor starting, aggravating

the problem. Hence system design is made difficult. With incorrect system design, voltage collapse and/or motor stall are more likely than with a d.c. or a synchronous generator. Over–excitation and over–voltage may also be a risk.

5] General efficiency is likely to fall off significantly if the operating slip is not maintained within a well defined range.

6] Although the cage rotor is normally thought of as being very rugged, in application where vibration levels and/or thermal cycling are high, cage fractures are a common failure mode [1-62]. Both may occur in wind turbine applications.

7] In contrast with schemes employing inverters (which offer independence between the generator and motor speeds – helpful for power matching etc), the direct connected induction generator/induction motor scheme proposed possesses 'limited–slip' or fluid–clutch type properties at least under normal working conditions. This means that (unless pole–changing techniques, etc. are adopted) design and operational flexibility is rather limited.

8] Finally, any control that one wishes to exert must generally be carried out through changes to a capacitor bank, requiring the use of some form of power switch. This introduces adverse development, maintenance and operational implications.

1.11 Previous work on Wind Pumping Schemes with Electrical Transmission

Two papers were found in the literature. Reference [1−11] reports the results of work on a wind−electric−water pumping scheme designed by 'consultancy services for wind Energy in Developing countries' (CWD), a Dutch National organization. In this scheme, a synchronous generator (described by the authors as a synchronous compound generator), driven by the turbine supplies a three phase induction motor driving a centrifugal pump. Very few details of the scheme were given (2 block diagrams only) and the paper did not present any electrical analysis of the scheme's operation. However, an interesting outline account is given as follows of the steps necessary for systematic design of their type of system.

The starting points relate to the wind and water data prevalent at the location under consideration; with the desired flow output and static head, the required hydraulic power can be found. From commercially available ranges of pumps and generators a suitable pump and generator can be chosen. The capacity of the generator must be large enough to supply the large starting current required by the induction pump motor. The gear box ratio mainly depends on the optimum speed of the turbine and generator, the former speed being the more important. The gear box efficiency is estimated in order to obtain the required turbine shaft power. A complete matching procedure is then carried out for the turbine and its load, with the help of the power−speed curves of both turbine and load, as supplied by manufacturers or obtained through calculations or experiments. The gradient of the load curve depends on the gear box ratio. Before a final decision on the gear box ratio is made, the

starting behaviour, working point stability and degree of over loading of the system is assessed. After establishing the transmission ratio a gear box can be chosen, and the previously estimated gear efficiency checked. Design iterations are carried out if necessary. The authors considered two ways of limiting the voltage, the first being an 'electric buffer' or control system between the generator and the pump. The second option is a mechanical control device that limits the turbine and/or the generator speed.

The system was found to perform smoothly, and no starting or stability problems occurred. No breakdowns occurred during the eight months' test period. The overall efficiency (including pump and wind rotor) of the system was 7% at the design speed, this being below the expected efficiency of 11% due mainly to a speed limiting device on the turbine. In spite of the low overall efficiency, the authors found that the system could be competitive with diesel pumps.

Reference [1-23] reports the test results of work on a Riva Calzoni single blade 3.5 Kw rated wind generator, feeding a 1.5 Kw caprari submersible induction motor–driven pump. This scheme was designed by ENEA (Italian Board for R & D on Nuclear and Alternative Energies). A test well has been built, 100 meters deep using 0.5 meters diameter steel tube. The tube is closed at its lower end, so that it acts as a type of well, and the water level can be varied in order to change the static head over the pump. In this scheme, the generator used is a synchronous rather than an induction generator. Designed for generation at remote sites with a generator pole number of 16, the generator was direct coupled to the wind turbine, thus avoiding the gear box weight, losses and failure risks. The alternator was rated at 4 KVA and was

self–excited using a rectifier bridge between the a.c. output and the field winding.

The criteria adopted by the authors for the design of the plant were categorized under three headings:

a) criteria for generator–motor matching;

b) criteria for the determination of size and type of pump;

c) pump starting criteria.

In respect of (a), the basic criterion is to feed the pump motor at a constant v/f basis, at least for frequency values greater than a so called 'saturation frequency'. For the self–excited alternator used (rectifier and field in shunt), the only way to get a linear v/f relationship (normally resulting from an approximately constant field–current) at frequencies lower than the saturation frequency (where the output voltage climbs with speed so tending to produce steadily increasing field current) is to limit the field current at a maximum value less than the saturation field current.

So far as item (b) is concerned, the authors mention the importance of choosing approximately

i) The maximum generator speed;

ii) The wind speed at which pump output flow should commence and of dealing with the question of power matching optimization.

In respect of point (c), (pump starting criteria) the authors draw attention to the need for the alternator to be able to start the electric pump without excessive current overloads, since there is a risk of voltage collapse due to the cumulative effect of voltage regulation due to the high starting currents on the

field voltage.

The authors suggest two starting techniques:

i) "Switching" mode, in which a motor isolating switch is closed only when the generator output voltage and frequency are sufficient to produce water flow.

ii) "Soft starting" mode, in which the generator and motor are permanently connected.

Tests on two pumps, of 1.5 and 2.2 Kw, showed that the scheme's main problem was the loss of excitation of the alternator. This was apt to occur with the 2.2 Kw pump with the type (i) scheme or with either pump in the "soft starting mode" type (ii) scheme. To avoid this, the authors suggested the use of a modified alternator field current incorporating series compounding with the alternator output current as well as its voltage affecting the field voltage. The authors investigated the wind speeds needed for pumping action to commence with a relatively high head (60m) imposed on the pump. The wind speeds found were 6.5 m/sec and 2.4 m/sec for the 1.5 and 2.2 Kw pump respectively.

1.12 The Object of the Induction Scheme

The heart of the scheme, the capacitor excited induction generator–induction motor combination, has, it is believed, been very little investigated or analysed previously (A third year undergraduate project done in the department of Electrical Engineering at Imperial College, which made a preliminary investigation only of certain practical aspects of the scheme, is the sole relevant

material found). The absence of any analytic treatment in literature (or even of any test data) of the induction generator/induction motor scheme, the possible edge in terms of equipment simplicity and cost that this scheme may well possess over the competing electrical alternatives, and the existence of a suitable application, viz wind turbine–powered borehole pumping, were the principal spurs to the current investigation.

It is worth recording finally that the estimation techniques developed during the project reported in this thesis, together with the know–how gained, are being used in a current industry – collaborative SERC project (GR/E 83740 Development of a sail–wing wind turbine with electrical transmission for water–pumping applications (Oct '87 to '90) being led by a departmental colleague: Dr. L.L. Freris. Present plans are for such a scheme to form the heart of new wind pumps on the Plain of Lasithi on Crete.

1.13 Thesis Structure

Chapter 1 of the thesis has made reference to the basic principles of wind turbine behaviour, has described the case for remote–site borehole pumping with reference to Egyptian conditions and has summarised the principal system options for wind–powered borehole–pumping schemes. The remainder of the thesis presents in detail the results of the investigation into the particular type of scheme described in section 1.8.

Chapter 2 describes the analytical techniques used to predict the steady–state behaviour of the electrical parts of the scheme.

Chapter 3 presents results for operation under no–load and on–load conditions, both constant voltage and constant v/f conditions with fully controlled

capacitor banks being examined. Electrical factors affecting the selection of pumps and generators are outlined in this chapter.

Chapter 4 presents the results of work into the behaviour of the system when fixed and sectionalized capacitor banks are employed.

Chapter 5 examines the starting behaviour of the system under constant generator speed conditions and considers the case for motor isolation during the initial self–excitation phase.

The analysis is extended in chapter 6 to include the wind turbine itself. Results of work into the starting behaviour of the complete system under constant–speed conditions are presented.

Conclusions are drawn in chapter 7 and suggestions made for further work.

CHAPTER 2

STEADY STATE ANALYSIS TECHNIQUES

2.1 Introduction

The steady state analysis described in this chapter is based on the steady state equivalent circuit model for induction machines and the saturation in each machine is taken into account by making each magnetizing inductance dependent on the calculated air gap flux level. Four prediction programs were evolved:

a) The first one deals with operation of the generator connected to a capacitor Bank only, the bank being envisaged as regulated so as to maintain specified voltage conditions. This enables complete terminal voltage versus capacitance (or capacitor current) characteristics at different generator speeds to be obtained.

b) The second deals with variable speed operation of the generator when connected only to a capacitor bank of specified value. The analysis predicts the generator speed at which voltage build up occurs and the value of the final voltage at the end of build up period.

c) The third deals with the operation of the generator and regulated capacitor bank when connected to an induction motor pump.

In the third program, the simulation code has been developed to predict the electrical scheme's performance versus generator shaft speeds under fixed V

and fixed voltage per frequency conditions.

d) The fourth deals with the operation of the generator with a sectionalized capacitor scheme when connected to an induction motor pump. The sectionalized capacitor scheme incorporates two groups of capacitors – one left permanently connected, the other switched into and out of circuit either en–block or in two stages (Further details in chapter 4).

The fourth program accordingly includes a simulation code evolved to investigate the operation of the scheme with constant capacitance at different generator shaft speeds.

Further codes, described in chapters 5 and 6, were written to predict the start–up behaviour of the system under constant generator speed and the start–up behaviour of the complete system in combination with the wind turbine, at constant wind speed.

2.2 Basis for Analysis

Although the electrical parts of the scheme shown in Fig. (2.1) are simple constructionally, the analysis is complicated by the strong coupling between the phenomena in the two machines and by the key role saturation in fixing operating voltages with capacitor excited induction generator schemes. The analysis is based throughout on the steady state single phase equivalent circuit of the induction machine. Such an approach is of course valid when rms conditions are changing relatively slowly. If conditions are changing at a fast rate (say by more than 10% per cycle), the behaviour of the generator,

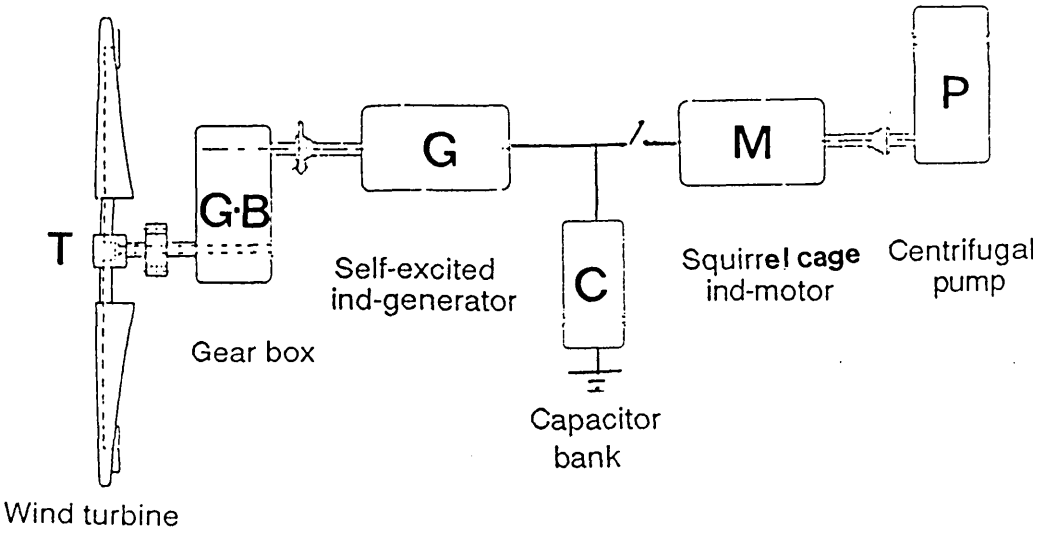

Fig. (2.1) Wind electric pumping scheme.

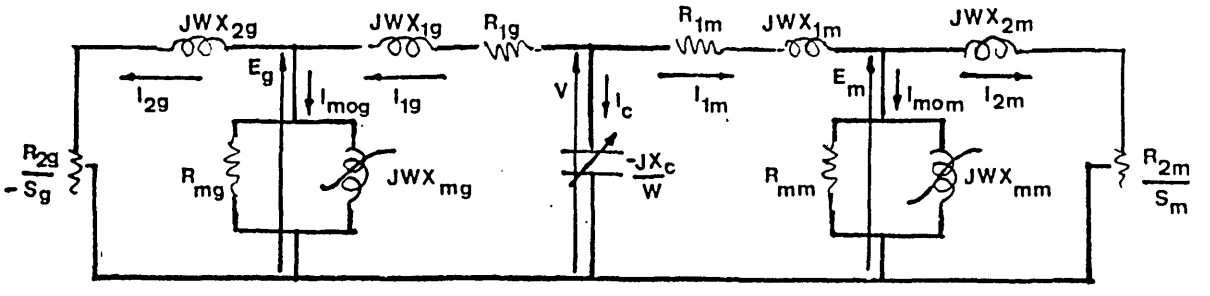

Fig. (2.2) Equivalent circuit of induction gen.-motor system

capacitor bank and motor will be affected to a greater or lesser extent by transient phenomena. In the present case the justification for using a steady state basis is two–fold.

(a) The rates of change of shaft speeds are relatively low due to the significant inertias of turbine, generator, motor and pump.

(b) The project involved a system study incorporating consideration not only of motor, capacitor bank and generator but also pump and turbine, and of system characteristics over a wide range of operating conditions. The use of instantaneous models of the electrical components of the system (such as phase or d–q models) would have led to a large and probably unacceptable increase in computation times.

It has to be admitted that under certain conditions, the rates of change of rms electrical quantities will exceed occasionally the 10% per cycle suggested above as the limit figure for 'steady state' operation. The conditions involved are considered to be (a) generated voltage build–up (b) motor run–up in the vicinity of peak torque. The voltage build–up process in a capacitor–excited induction generator was analysed using an instantaneous model in a recent paper [2–1]. The analysis presented in this thesis is unlikely, it is thought, to predict the exact voltage versus time trajectory correctly. However, the analysis is felt to be capable of predicting the generator speed at which voltage build–up occurs, and the value of the final voltage at the end of the build–up period. So far as the operation of the entire system is concerned, trajectory errors may not be of great importance. Similar remarks may be made about motor behaviour during motor run–up. The final motor speed is likely to be predicted well in spite of probable errors in respect of the duration of the starting process.

The full steady−state single−phase equivalent circuit for the electrical components of the scheme is shown in Fig. (2.2).

Throughout the thesis, all quantities (voltages, currents, torques, slips, speeds, powers, KVArs etc.) are expressed in per unit form. Speeds are referred to a base synchronous speed n_S at the base frequency f_S of 50 Hz. In Fig (2.2), all the reactances are expressed at the base frequency. The base angular frequency is denoted by $w_S = 2\pi f_S$, and w denotes the actual angular electrical frequency as a per−unit of the base angular frequency w_S. Per unit definitions are included in the Appendix 3.

2.3 Simulation Techniques

Simulation codes have been developed for predictions, iterative procedures being used to deal with the non−linearities and the interactions between the phenomena in the various components. As stated above four principal prediction programs were evolved: The first two deal with operation of the generator and capacitor bank alone (the 'no−load' programs). The third and fourth deal with the operation of the generator and capacitor bank when connected to the induction motor pump (the 'on−load' programs). In all cases, the generator shaft speed w_g was treated as known input quantity. The equivalent circuits used are shown in Figs (2.2) and (2.3).

2.3.1 Simulation of No−load Operation with Regulated Capacitor Bank

The no−load prediction flow diagram (code a) which is shown in Fig. (2.4) commences by assuming initial trial values of terminal voltage V_t, generator

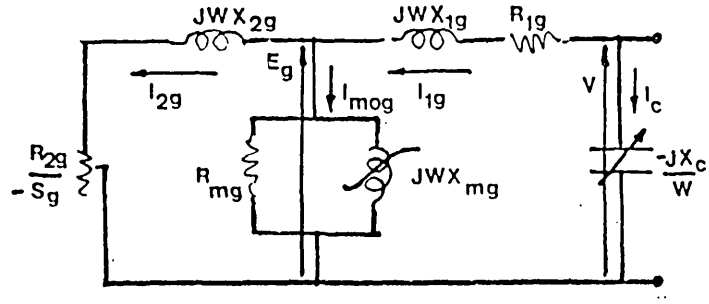

Fig. (2.3) No-load equivalent circuit of S.E.Ind. Gen.

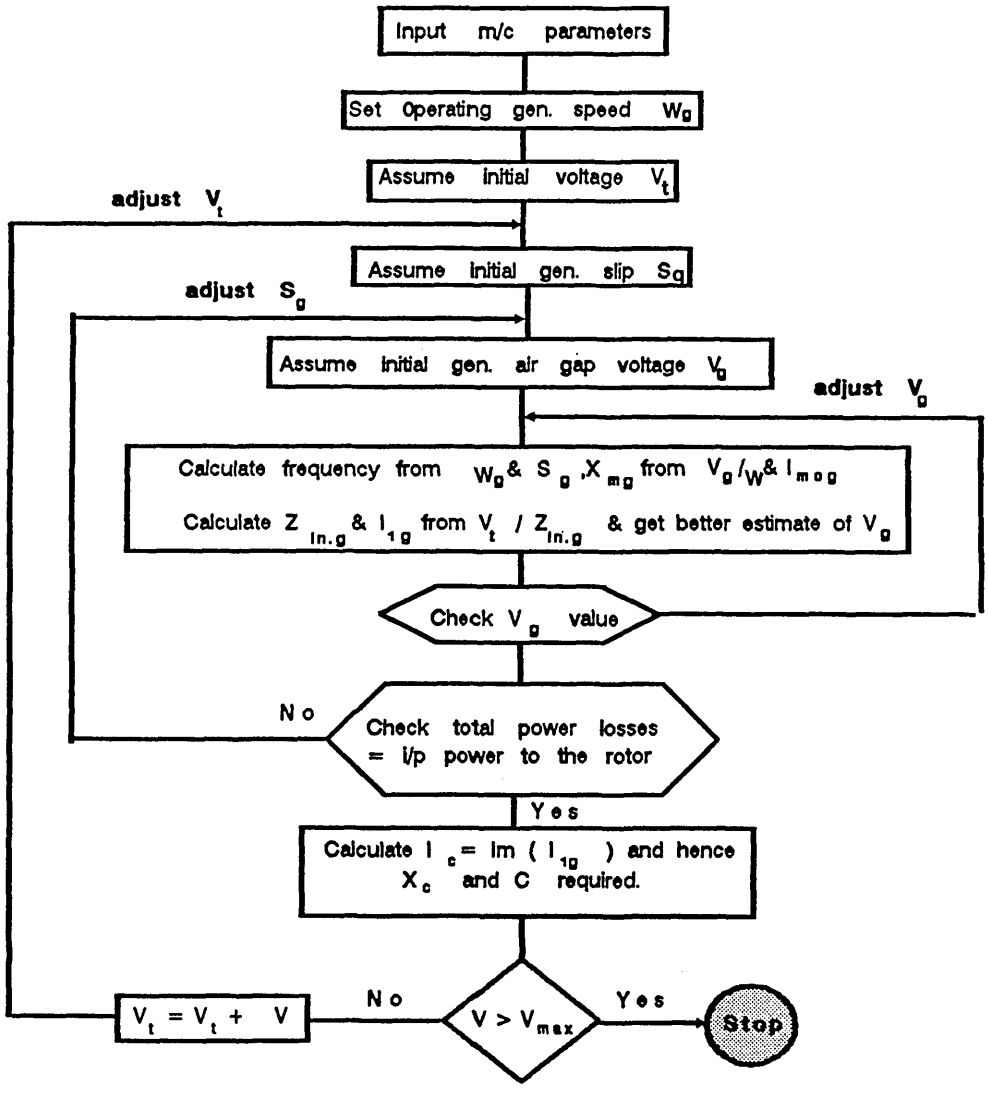

Fig, (2.4) No-load flow diagram (regulated capacitance).

slip S_g and generator air gap voltage V_g. The initial values used were generally 0.2 $\underline{/0^\circ}$, 0.001 p.u. and 0.18$\underline{/-20^\circ}$ respectively for these three quantities. The generator angular frequency is then calculated from:

$$w = w_g/(1-S_g) \tag{2-1}$$

and the magnetizing reactance X_{mg} is taken as

$$X_{mg} = V_g/w\ I_{mog} \tag{2-2}$$

where I_{mog} is obtained from the generator's magnetizing curve of I_{mog} versus V_g/w, the V_g/w being of course calculated from the initial assumed value of V_g and the value of w calculated from Eq [2-1]. The total generator terminal impedance can now be calculated from:

$$Z_{ing} = [(R_{2g}/-S_g+jwX_{2g})//(R_{mg})//(jwX_{mg})] + (R_{1g}+jwX_{1g}) \tag{2-3}$$

The generator stator current I_{1g} is then calculated from

$$I_{1g} = V_t/Z_{ing} \tag{2-4}$$

and a better value for V_g obtained from

$$\bar{V}_g = \bar{V}_t - \bar{I}_{1g}(R_{1g} + jwX_{1g}) \tag{2-5}$$

where R_{1g} and X_{1g} are the stator resistance and leaking reactance respectively. An updated value of X_{mg} corresponding to this new estimate of V_g is now

obtained – (Note the modulus of $\bar{V}_g$ is relevent here). Further iterations are conducted until convergence occurs (i.e. the V_g values on successive iterations change by less than 1%). Another iterative loop is needed to determine the correct value of slip. A comparison of the total power losses in the generator with the output power from the generator rotor forms the heart of this loop, the assumed generator slip being increased (typically by 0.05%) if the total power losses exceed the rotor output and decreased if less than the rotor output power. In this calculation, the rotor output power relation used was

$$P_{2g} = 3I_{2g}^2 R_{2g}/-S_g \qquad (2-6)$$

and the total generator electrical losses relation was

$$P_{gloss} = 3I_{2g}^2 R_{2g} + \quad 3I_{1g}^2 R_{1g} + \quad 3 V_g^2/R_{mg} + P_{wF} \qquad (2-7)$$

The generator windage and friction loss was taken as equal to the iron loss throughout the analysis.

Finally the value of capacitance required to give the assumed terminal voltage, V_t, was calculated from:

$$-j \frac{X_c}{w} = V_t/I_{1g} \qquad (2-8)$$

Note that at the end of the slip iteration, the net output power from the generator is zero and hence the input current must be purely inductive. The entire calculation can then be repeated as desired for other terminal voltage values, enabling a complete terminal voltage versus capacitance (or capacitor

current) characteristic to be built up.

2.3.2 Simulation of No–Load Operation with Specified Capacitor Values

A simulation code (code b) based on the no–load prediction technique described in section 2.3.1 for specified voltage conditions, was developed to determine the no–load characteristics when defined capacitor values are treated as input. The flow diagram is shown in Fig. (2.5). This program and the one described in section 2.3.1 make the same initial assumptions. The generator air–gap voltage V_g is similarly iteratively calculated until V_g values on successive iterations change by less than 1%. Again, an iterative loop is needed to determine the slip by comparing the total power losses in the generator with the output power from the generator rotor. However a second loop, through voltage adjustment, now matches the magnetizing and leakage inductance VAr needs of the generator with the leading VArs created by the capacitor bank. The value of terminal voltage corresponding to the input generator shaft speed and capacitor value is then determined. The entire calculation can then be repeated as desired for other generator shaft speed values, enabling a complete terminal voltage versus generator speed characteristic to be built up for the designated capacitor value.

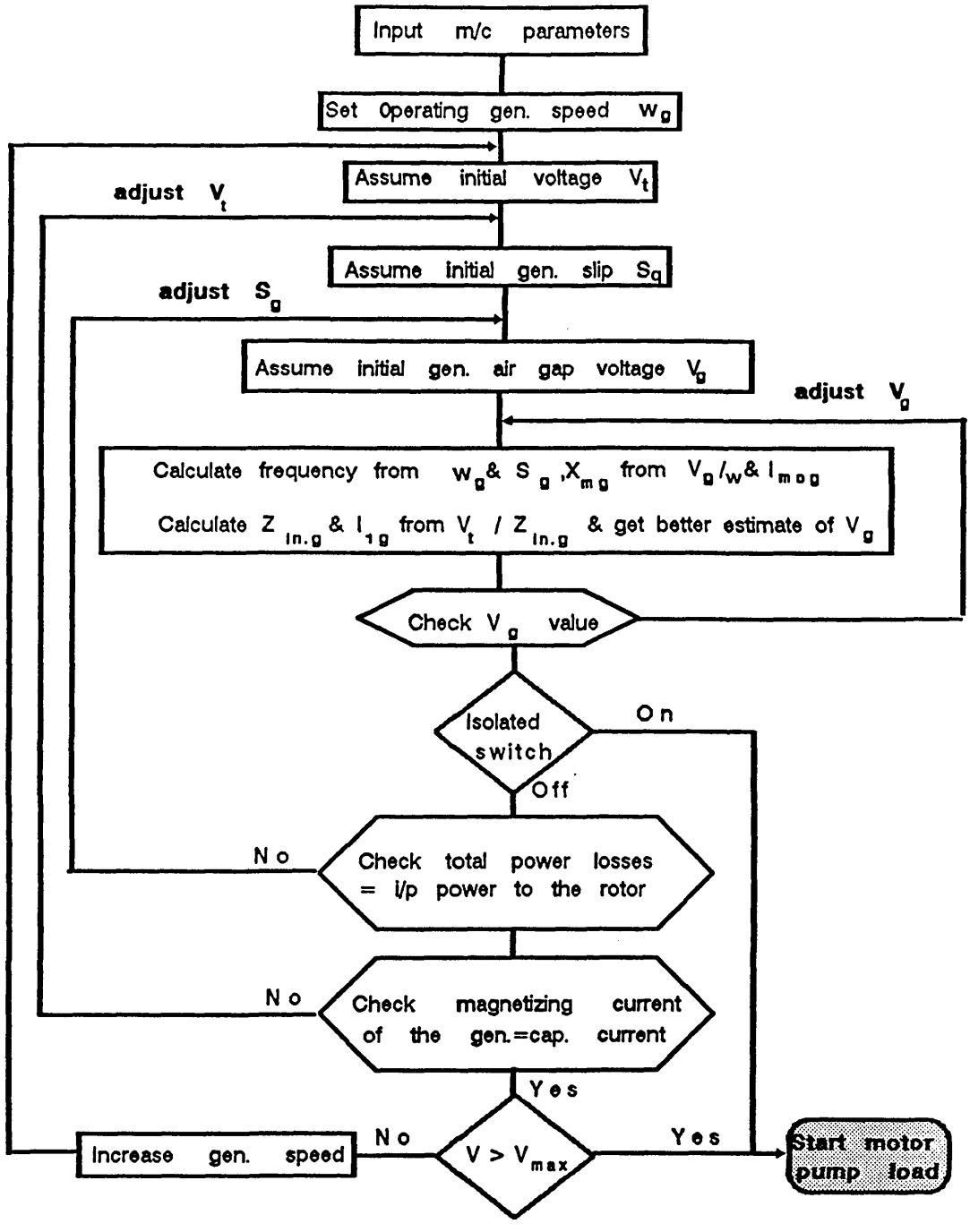

Fig. (2.5) No-load flow diagram (constant capacitance).

2.3.3 Simulation of Operation On–Load with Specified Output Voltage

The 'on–load' prediction technique Code (c) accounts for the mechanical load on the motor, a simple pump model being used. Fig (2.2) shows the equivalent circuit used and Fig. (2.6) shows the flow diagram.

For a particular operating point, the generator speed and terminal voltage are taken as known input quantities, and the system is then solved for all quantities including the capacitor value.

As before, initial assumptions are made for generator slip (now taken as 0.5% instead of 0.1% since the machine will now be generating into an external load) and air–gap voltage. Adjustments are made iteratively in the latter until the $\bar{V}_g$ from Eq(2–5) stabilises at a constant value, the I_{1g} again being calculated from V_t/Z_{ing} where Z_{ing} includes the X_{mg} value corresponding to the V_g/w value on the previous iteration. Trial values of motor air gap voltage V_m and slip are now assumed (typically initially set at $0.9V\angle{+20^\circ}$ and 100% respectively). In the same way as described before for the calculation of the generator magnetizing reactance, the motor magnetizing reactance is now obtained from the motor's magnetizing curve of I_{mom} versus V_m/w and the known generator output frequency w. The motor input impedance is then calculated from:

$$Z_{inm} = [(R_{2m}/S_m+jwX_{2m})||(R_{mm})||(jwX_{mm})] + (R_{1m}+jwX_{1m}) \quad (2-9)$$

and the motor stator current from:

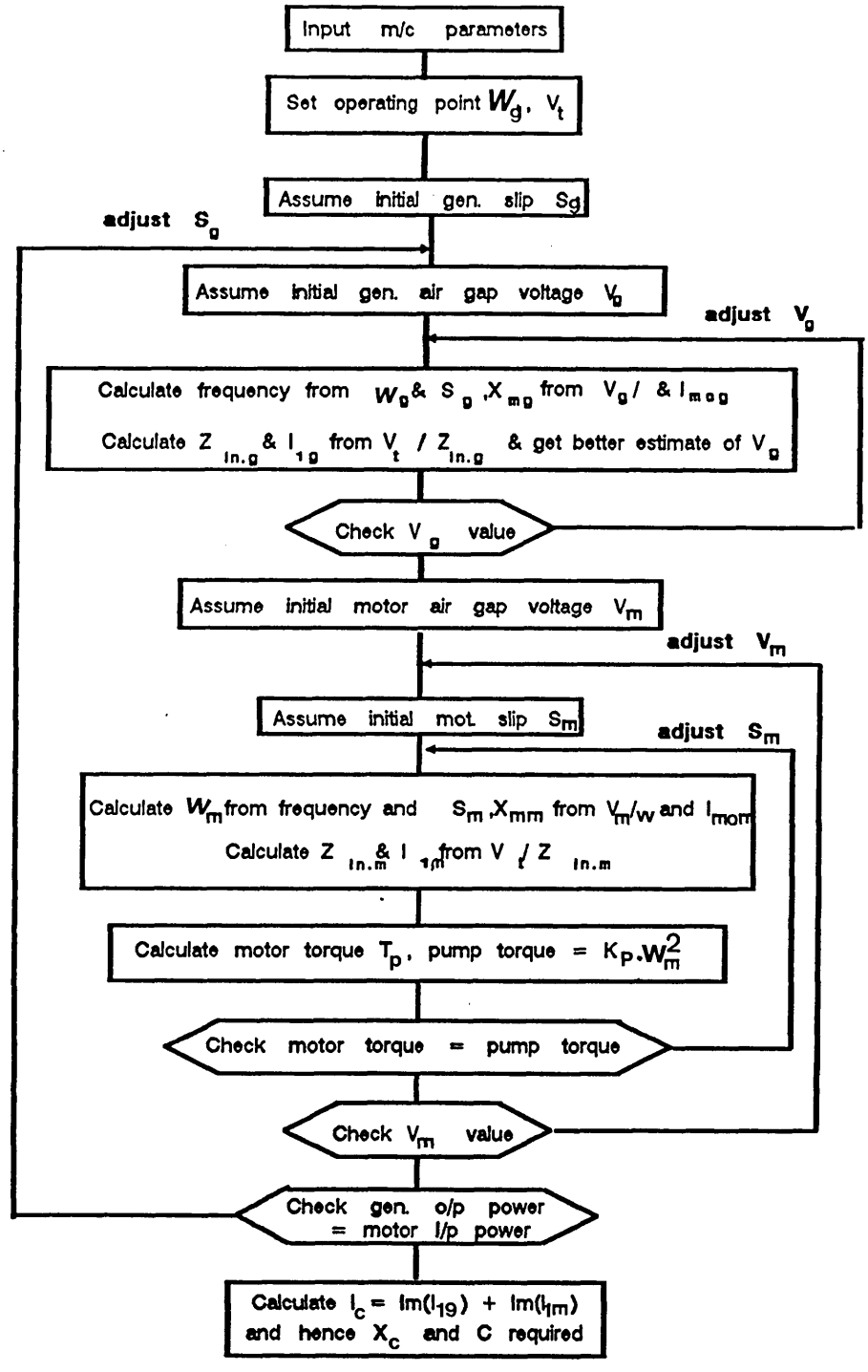

Fig. (2.6) Flow diagram for steady state performance (fully regulated capacitor bank).

$$\bar{I}_{1m} = \bar{V}_t/\bar{Z}_{inm} \qquad (2-10)$$

A comparison is then made between the calculated motor torque which is given by:

$$T_{elec.m} = \frac{1}{w}(I_{2m}^2)(R_{2m}/S_m) \qquad (2-11)$$

where

I_{2m} is the motor rotor current and equal to

$$\bar{I}_{2m} = \bar{V}_m/(R_{2m}/S_m + jwX_{2m}) \qquad (2-12)$$

and the pump torque which is given by:

$$T_p = k_p \cdot w_m^2 \qquad (2-13)$$

where the constant k_p in effect sets of pump rating.

The motor speed w_m is of course given by:

$$w_m = w(1-S_m) \qquad (2-14)$$

The motor slip estimate is now updated, being decreased (typically by 1%). The motor input current and torque are now recalculated and the process repeated until the motor and pump torques balance. A new estimate for the motor air gap voltage is now calculated using

$$\bar{V}_m = \bar{V}_t - \bar{I}_{1m}(R_{1m} + jwX_{mm}) \qquad (2-15)$$

and the Z_{inm} and I_{1m} recalculated together with a new value for the slip at which motor and pump torque equate. The entire process is then repeated

until the motor air gap voltage stabilises. A check is finally made on the power balance. If the generator output power is found to be less than/greater than the motor input power, the generator slip is adjusted upwards/downwards (typically by 0.5%). As can be seen from the Fig (2.5) flow chart, the new generator slip estimate is then used as the basis for a new set of claculations. The procedure is repeated until the powers balance. Finally, the capacitor current I_C is calculated by summing the reactive components of both generator and motor currents, and the corresponding capacitance per phase found from V_t/I_C. A complete set of system characteristics can be evolved if required by repeating the entire procedure for a set of generator speed figures, the voltage V_t being held fixed or made equal to $(V_t/w)\cdot.w$ as required.

2.3.4 Simulation of 'On–Load' Operation with Specified Capacitor Valued

Finally, the last of the steady–state simulation codes (code d) was developed to determine the on–load steady state performance when defined capacitor values are treated as input quantities. The 'on–load' prediction flow–diagram is shown in Fig (2–7). As in the previous section (2.3.3), the flow diagram commences by assuming initial values of terminal voltage, generator slip and generator air gap voltage, and for a particular operating point, the generator speed and the corresponding capacitor value are taken as known input quantities. The I_{1g} is again calculated from V_t/Z_{ing} where Z_{ing} includes the X_{mg} value corresponding to a particular V_g/w value. The generator equivalent circuit is then solved iteratively until the V_g from Eq(2–5) stabilises at a constant value. Also, trial values of motor air gap voltage V_m and motor slip are assumed. As described in Section (2.3.3), the motor magnetizing

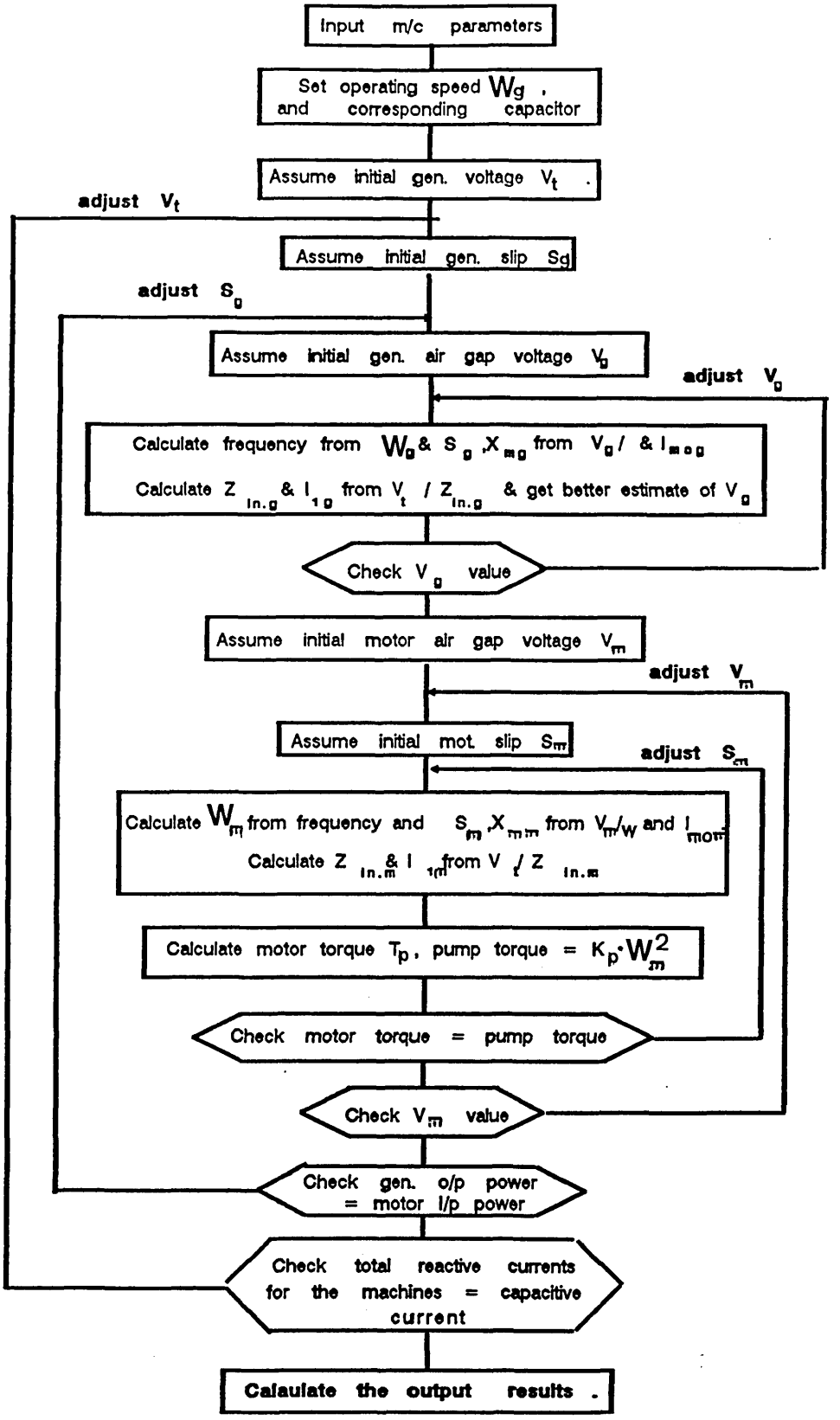

Fig. (2.7) Flow diagram for steady state performance (constant capacitance).

reactance can be obtained in the same manner described for the calculation of the generator magnetizing reactance.

The I_{1m} is then calculated from $V_t/Z_{in\cdot m}$. A comparison is made between the calculated motor torque and the pump torque. Adjustments are made iteratively for motor slip until the motor and pump torques balance. A new estimate for the motor air gap voltage is calculated from Eq(2−15), and the $Z_{in\cdot m}$ and I_{im} recalculated together with a new value for the slip at which motor and pump torque equate. The entire process is then repeated until the motor air gap voltage stabilises. A check is made on the balance of the power between the generator output power and the motor input power. Adjustments are made iteratively for generator slip until the powers balance. The last loop – a new one with this code – now matches via voltage adjustment, the magnetizing and leakage inductance VAr needs for the generator and motor with the leading VArs created by the capacitor bank. The value of terminal voltage corresponding to the input generator shaft speed and capacitor value is then determined. The entire calculation can then be repeated as desired for other, increasing generator shaft speeds until the generator current becomes too high. To avoid excessive voltages, saturation levels and magnetizing currents with the consequent risk of capacitor failure, it is necessary to switch out a portion of the capacitor bank. The program automatically assesses the critical speed/s involved, resets the capacitor bank to a new, preset, lower value/s and proceeds with further calculations.

CHAPTER 3

STEADY STATE OPERATING CHARACTERISTICS

3.1 Introduction

Results from the four prediction programs described in chapter 2 are presented in this chapter, together with some experimental test results. The magnetization characteristics of the induction generator and induction motor are also presented. Complete no–load terminal voltage versus capacitance (or capacitor current) characteristics at different generator speeds are obtained.

In a second group of no load results, the electrical characteristics under varying rotor speed, with fixed capacitor values are shown. The generator speed at which voltage build–up occurs and the value of the final voltage at the end of build–up period are shown. The effects of using large capacitor values are examined.

The on–load prediction technique has been used to demonstrate the way in which the scheme operates:

a) when the capacitance is varied to maintain constant voltage;

b) when the capacitance is varied to maintain constant voltage/frequency.

In each of these cases, a capacitance regulator in the form of a stepped switching scheme or regulator using a parallel inductor would be needed. The influence of the pump size in relation to the power rating of the two induction machines has been investigated and the results are included.

Estimates of power, efficiency, slip, current, frequency and voltage against speed for the typical system incorporating a regulated capacitor bank are presented, together with comparisons between predicted behaviour and steady–state experimental results from a laboratory rig. The test rig power circuit is shown in outline in Fig (3.1). The induction machine was a three phase delta connected, 11 Kw, 4 pole, 415V, 25A, 50Hz squirrel cage machine, manufactured as a standard, totally–enclosed 'Alpak' motor by GEC. (size D160M).

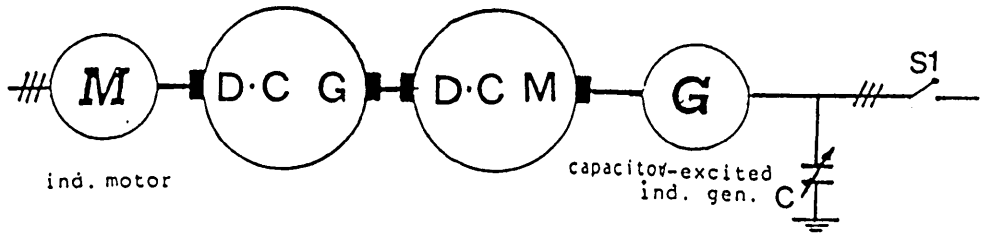

Fig .(3.1) NO -load capacitor - excited ind.-gen.

The d.c. drive motor was Ward Leonard supplied, was dynomometer – mounted and was equipped with a spring–balance torque measuring system and tachometer. Electrical quantities measured were line voltage and current, a plug box being used to check for balance. The capacitor bank was rated at 415V line and contained a multiplicity of paper capacitors switchable by means of manually operated switches.

3.2 Magetization Curve Test Results

The vital non–linear relationships between the air–gap e.m.f's V_g and V_m and the magnetization currents I_{mog}, I_{mom} were obtained from magnetization tests on the machines (in practice the mag. curve could perhaps be obtained from design data). The magnetization characteristics of the induction generator and induction motor used in the project are shown in Fig. (3.2a) and Fig (3.2b). They were obtained by exciting the induction machines from a 50 Hz variable–voltage supply while the machines were driven at synchronous speed. Allowance for the drop across the stator resistance R_{1g} and stator leakage reactance X_{1g} enables the air voltage V_g to be obtained from Eq [2-5]. The magnetizing reactance X_{mg}, corresponding to any V_g/w, is taken as the slope of the line from the origin to the operating point on the magnetising curve, i.e.

$$X_{mg} = V_g/w/I_{mog}.$$

The corresponding quantities can be similarly calculated for the motoring machine. The results are of course valid when the machine is capacitor (self)–excited. As is well known, for generation to occur, the capacitive reactance must have a value equal to or lower than the initial (air gap) slope of the mag.curve. It is, therefore, obvious that under these conditions an induction generator will always operate with the magnetic circuit saturated.

3.3 The Capacitor–Excitation Process

As stated in references [1-50] and [1-59), when the machine is being driven by a prime–mover, the residual rotor magnetism induces a small e.m.f. in the stator

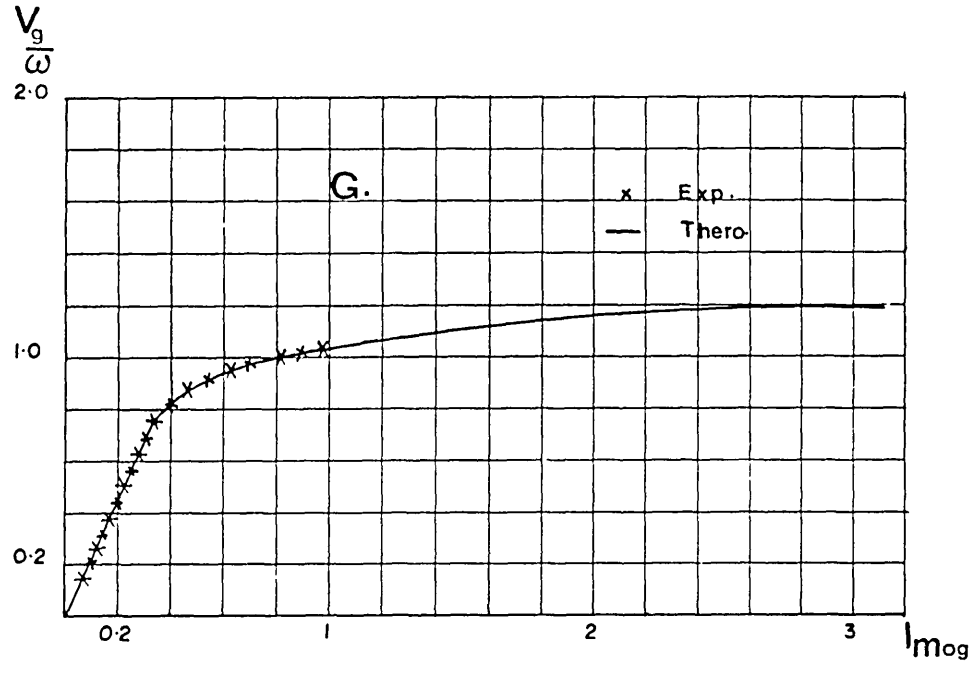

Fig. (3.2a) V_g/ω as a function of I_{mog} .

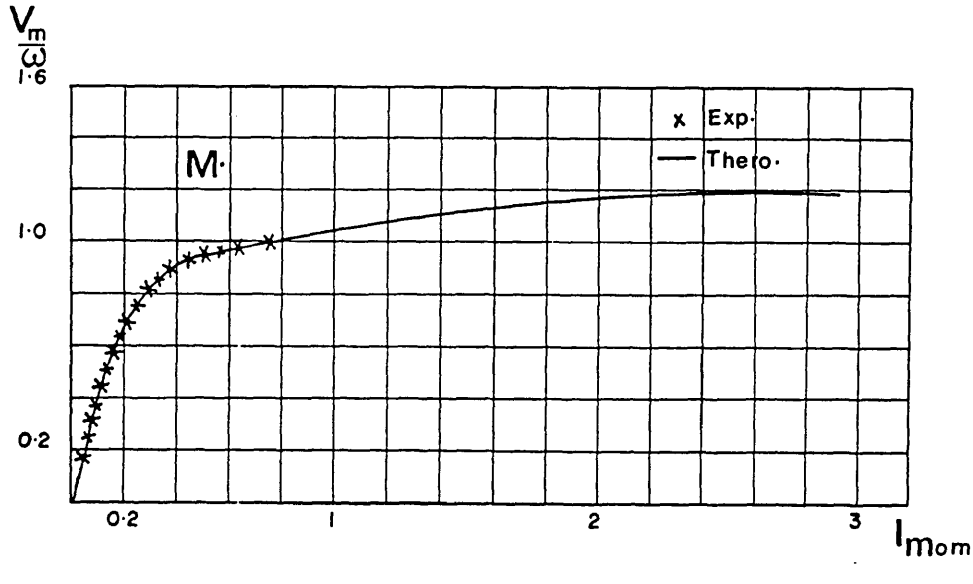

Fig. (3.2b) V_m/ω as a function of I_{mom} .

windings at a frequency proportional to the rotor speed. If under such conditions a leading current is provided by means of static capacitors across the stator terminals, the same current passing through the stator winding, an armature reaction flux is produced which assists the original residual flux. If the capacitors are of sufficient value, the voltage builds up. The e.m.f. and current build–up in the winding will increase up to a level governed by magnetic saturation in the machine and set by intersection of the capacitor and magnetization lines.

The machine is then self excited and can operate as an induction generator in isolation from an active power system.

3.4 Self–Excitation Characteristics

Curves of terminal voltage versus capacitor current can be obtained by varying the capacitor value, keeping the rotor speed fixed. Since the rotor current is negligible at no–load, the no–load stator current is essentially the magnetizing current, and the terminal voltage differs from the V_g e.m.f. by $I_{mog}(R_{1g}+jwX_{1g})$. Fig (3.3) shows the measured curves for the generator tested, at rotor speed of 0.6, 0.8 p.u respectively, together with predictions for these and other speeds obtained from the measured V_g/w versus I_{mog} curve (Fig .3.2a) using the computer code of Fig 2.4.

Obviously at the higher speeds the no load voltage can be dangerously high. However, when the load is applied there is a considerable fall in voltage level and the current rating of the apparatus may then be the limiting factor. The useful speed range is thus limited by the minimum excitation speed at the lower

end, and by the voltage and current ratings of the individual components at higher speeds [1-54]. As stated in reference [1-58], a useful physical picture of the system's operation under no−load conditions can be obtained by approximating the machine/capacitor single−phase equivalent circuit to a parallel R−L−C circuit comprising the magnetizing branches (X_{mog} and R_{mg}) and the excitation capacitors. The minimum input excitation point for such a circuit occurs when the currents in the inductor and the capacitor are equal. It can be observed that for each capacitance value there is a single operating point where the inductor and capacitor current are equal. This point is at the intersection of the inductor (magnetizing) curve and the linear capacitor voltage −current characteristic at the selected constant frequency. The voltage in such a circuit is defined by the saturable inductor which tends to steal current from the balanced circuit if the voltage increases beyond the value defined by the intersection. On the other hand, the excessive capacitive current before current equilibrium tends to increase the voltage towards the equilibrium point. This circuit is therefore inherently stable and self−regulating, the stability of the circuit voltage being based on the nonlinearity of the generator magnetizing curve. At low magnetizing current, where the magnetizing curve is practically linear, intersection with another linear (capacitor) line is not well−defined. The consequent poor voltage regulation results in flux instability in this region, in which a small decrease of capacitance can result in collapse of the voltage [1.58]. If capacitance is decreased after excitation has occurred, there is a minimum value of capacitance (smaller than the value needed for build−up) below which the machine loses excitation. This hysteresis type of effect is shown in Fig (3.4), the experimental points being obtained by gradually increasing and decreasing the terminal capacitance while the generator was driven at a constant 900 rev/min. Fig (3.4) also shows the computed values of

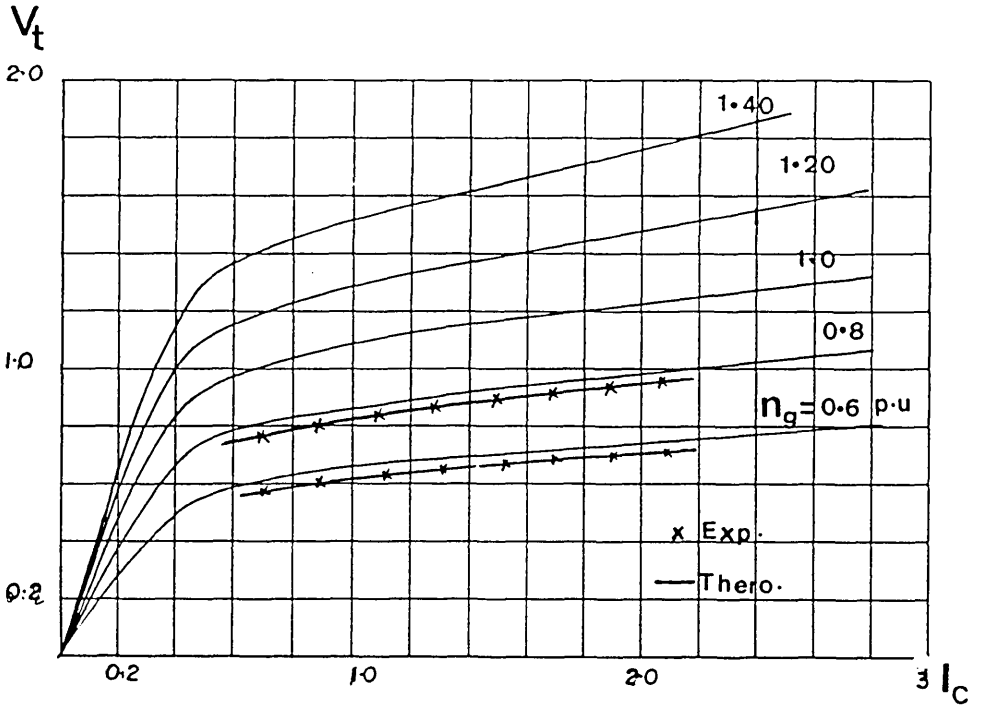

Fig. (3.3) Variation of the gen. voltage V_t against capacitance current I_c at 5 different gen. rotor speeds (n_g) .

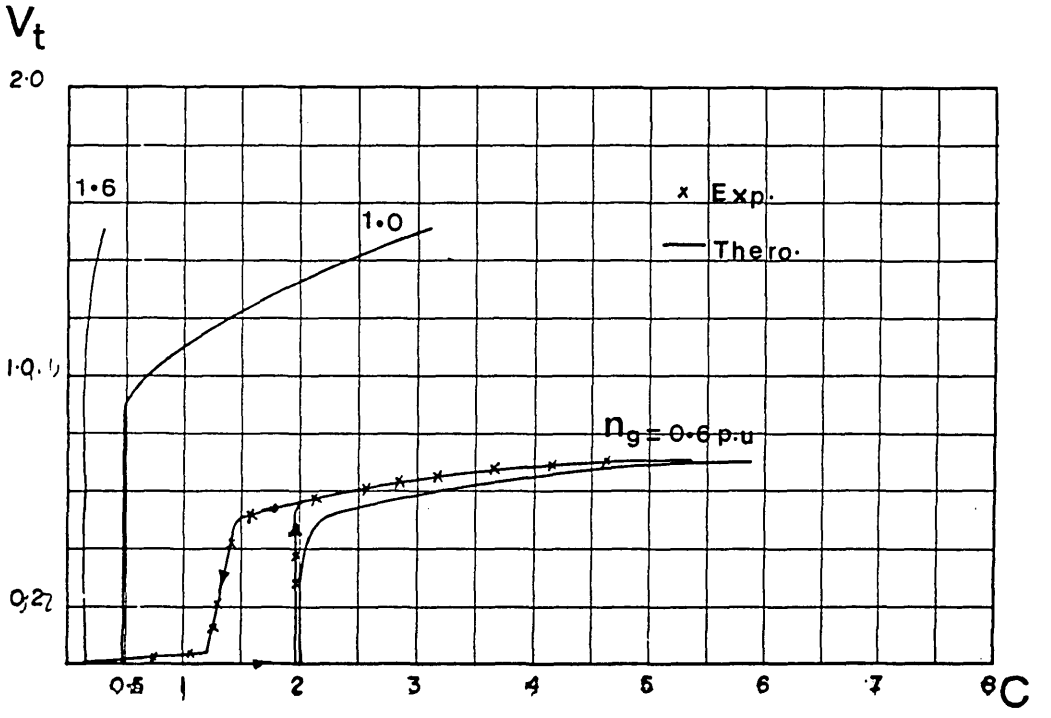

Fig. (3.4) Variation of the gen. voltage V_t against capacitance C at 3 different gen. rotor speeds (n_g) .

minimum per-unit terminal capacitance required for self excitation under no–load conditions at speeds of 0.6, 1 and 1.6 p.u. . Agreement between the computed and measured values of capacitance is very good in the saturated region. The curves reinforce the point that for stable operation, the capacitor should have a value such that the machine always operates more or less saturated. It is also clear from this figure that the capacitance requirement increases appreciably with decreasing speed.

3.5 No–Load Operation Under Constant Capacitance Variable Speed Conditions

As is well known, the minimum capacitor value needed for generating any significant voltage at no–load corresponds to a V_t/I_c reactance value at least equal to the slope V_t/I_{mog} of the air gap of the generator's magnetizing curve shown in Fig (3.2a). Fig (3.5) shows the build–up of voltage as generator speed increases at constant capacitor value (c= 6.372 p.u). Also, it shows the variation of frequency against generator speed. The generator slip under these 'no–load' conditions needs to be only high enough for the 3 I_{2g}^2 R_{2g}/S_g electrical output power from the rotor to supply the sum of the I.W.F. and 3 I_{mog}^2 R_{1g} copper losses. Since this will be a small slip, the generator frequency on no load is closely tied to the generator speed, so long as the system is in a self–excited state. Any increase in speed and hence frequency reduces the slope of the capacitor load line and increases the magnitude of the air gap e.m.f. curve, thus increasing the generated voltage at the intersection point. Fig (3.6) shows the variation of air gap voltage/frequency against generator speed. Above a certain generator shaft speed ($n_g \geq 0.6$ p.u), the V_g/f is nearly constant due to the linearity of the generator magnetizing curve in the saturation region.

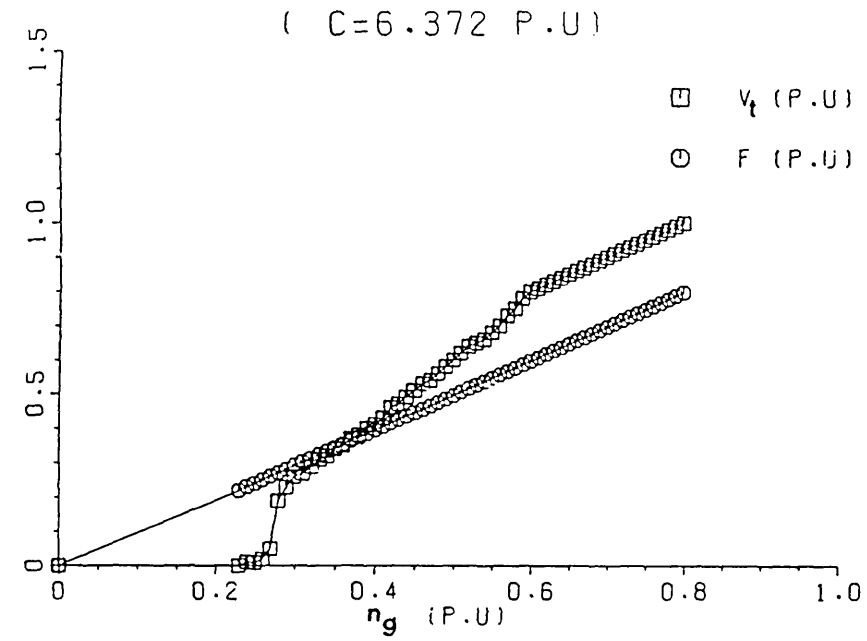

Fig. (3.5) Variation of gen. voltage and frequency against gen. speed .

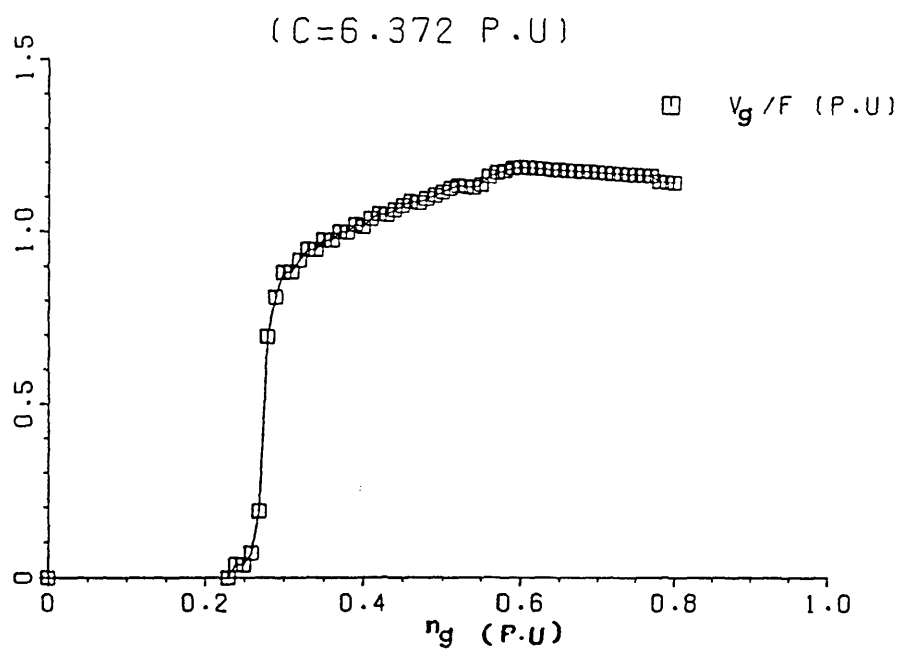

Fig. (3.6) Variation of gen. air gap voltage / frequency against gen. speed .

Fig (3.7) shows the variation of the no–load generator current against generator speed. The peak at 0.6 p.u. speed occurs due to the maximum in the V_g/f curve at about this speed, the peakier nature of the current curve probably being due to simultaneous variation in X_{mog} due to saturation changes.

The Fig (3.8) curve of X_{mog} versus speed shows, as expected, a minimum at a speed corresponding to the max generator current. Figs (3.9) to (3.12) show the predicted effects of increasing capacitance values. Fig (3.9) shows that, as expected, the speed for voltage build–up decreases as the capacitance is raised. It is also evident that, below 0.6 p.u. speed, the generated voltage increases with capacitance, but that – above this speed, due to saturation, the generated voltage is not affected by variation in capacitance over the range investigated. Corresponding curves of generator stator current I_{1g} and magnetizing reactance are also shown (Figs (3.11) and (3.12)). The generator magnetizing reactance is lower with the higher capacitor value due to the higher level of V_g/f.

3.6 On–Load Operation with Regulated Capacitor Bank

3.6.1 Experimental Rig and Test Procedure

The rig described in section 3.1 was added to by connecting a 5.5 Kw, 415V, 3 phase, 4 pole, TEFC squirrel–cage induction motor to the generator output (see Fig (3.13)). The motor was mounted on a base–plate with a resistively–loaded, dynomometer–mounted d.c machine. A.c. electrical power was monitored using two high quality electrodynamic wattmeters in the two wattmeter connection, and torques and speeds measured using spring balances and tachometers respectively. Since the use of a fixed resistive load on the d.c load machine would provide a load torque varying approximate linearly with

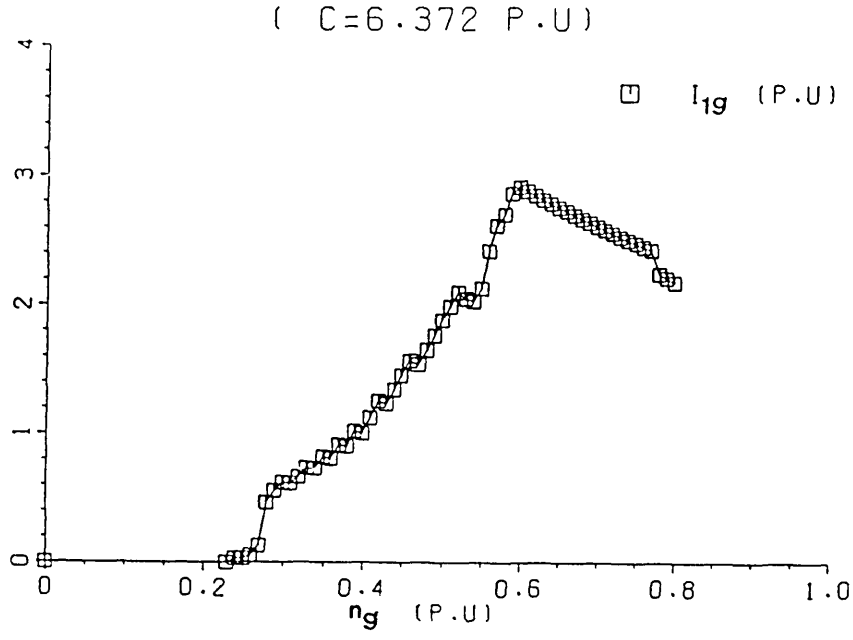

Fig. (3.7) Variation of gen. no-load current against gen. speed .

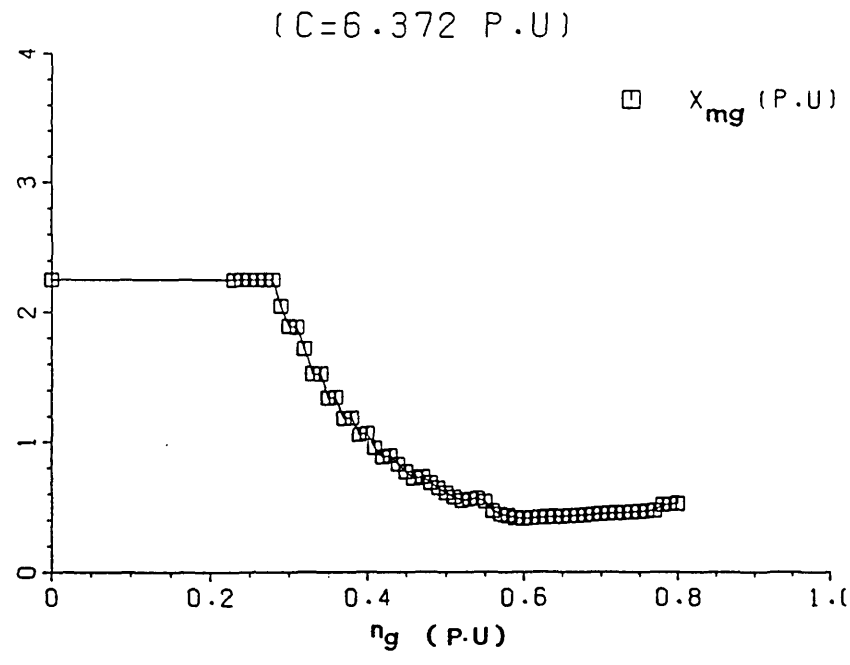

Fig. (3.8) Variation of gen. magnetizing reactance against gen. speed .

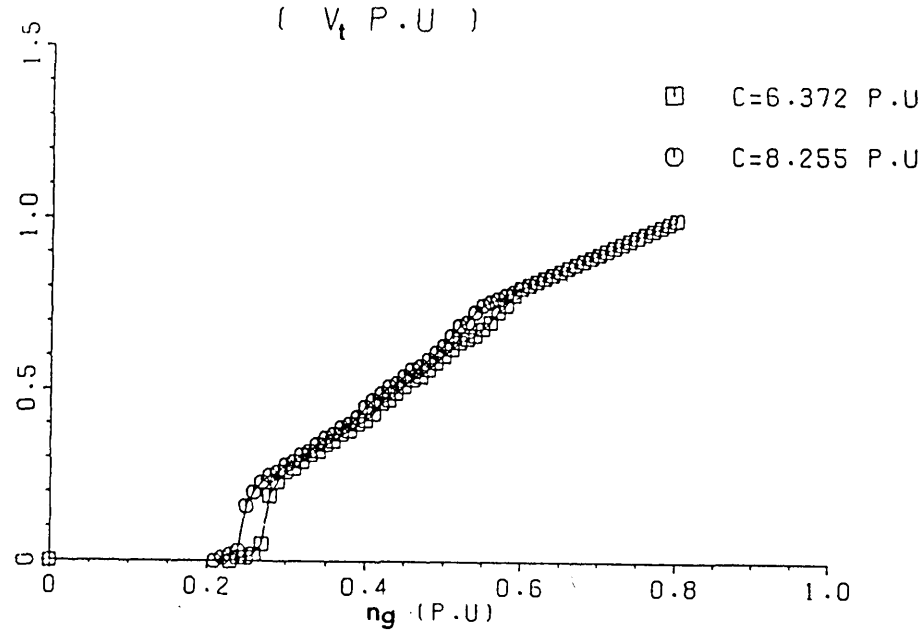

Fig. (3.9) Variation of gen. voltage against gen. speed at 2 different capacitor values

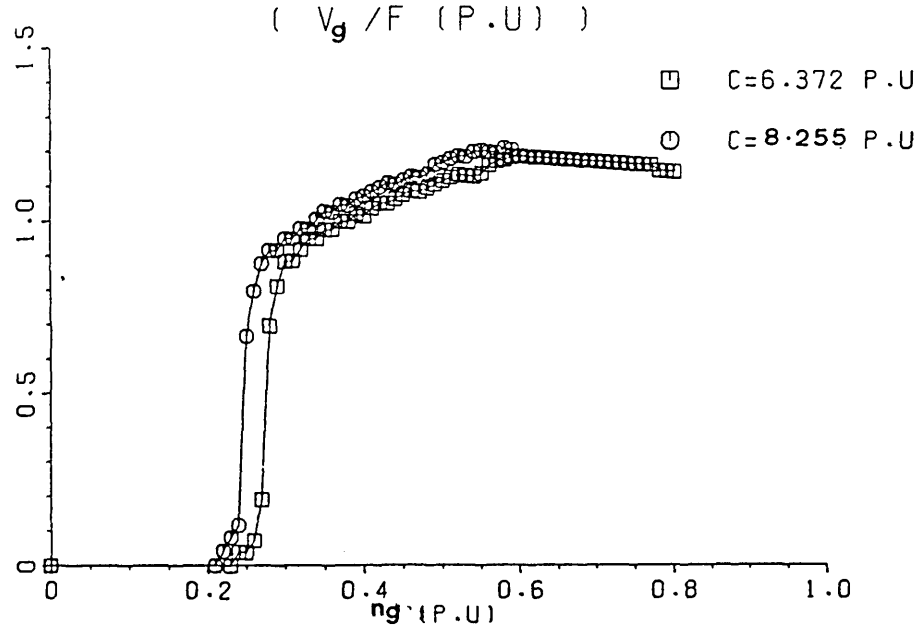

Fig. (3.10) Variation of gen. air gap voltage over frequency against gen. speed at 2 different capacitor values

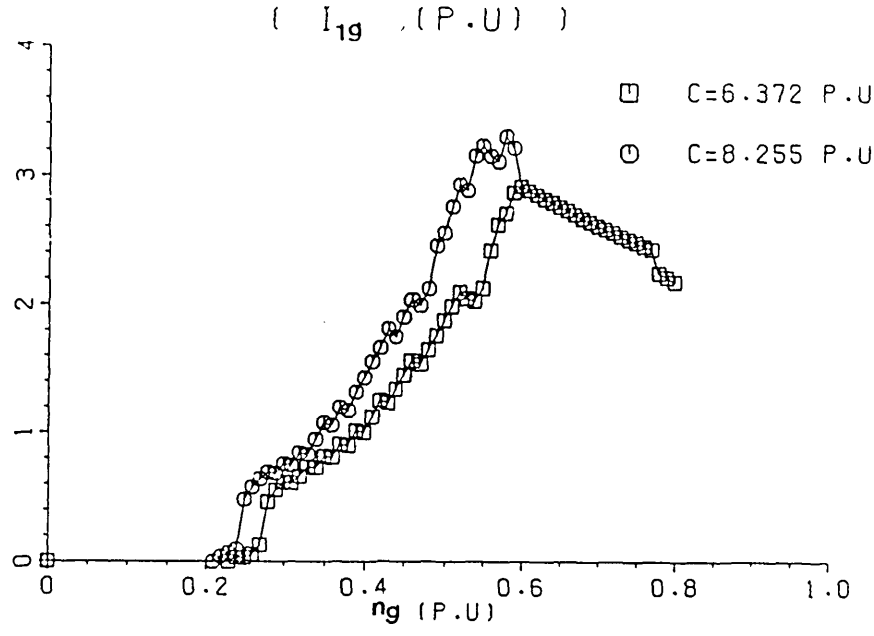

Fig. (3.11) Variation of gen. no-load current against gen. speed at 2 different capacitor values

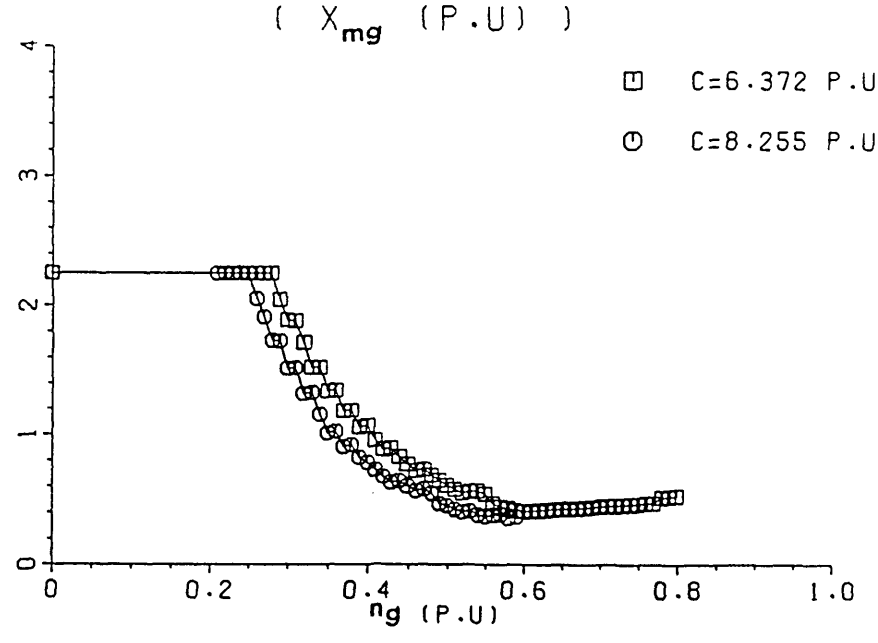

Fig. (3.12) Variation of gen. magnetizing reactance against gen. speed at 2 different capacitor values

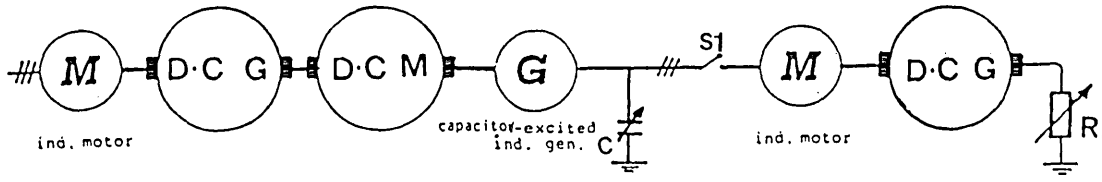

Fig. (3.13) Laboratory rig.

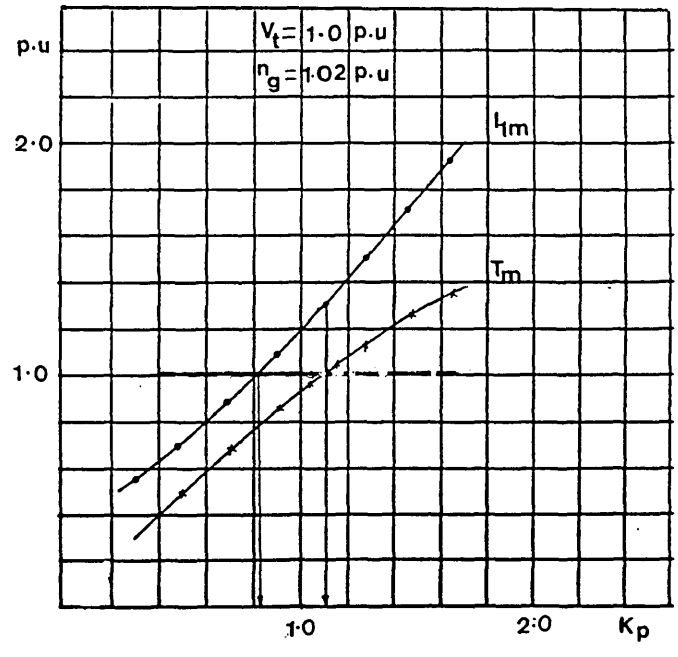

Fig. (3.14) Variation of motor torque & motor current against pump constant at constant gen.speed .

speed instead of a square law relationship, adjustment of R_L was needed during tests.

A common procedure was used for all the steady state load tests mentioned in the remainder of this chapter. With motor isolating switch S1 open, the induction generator speed was first set to a value corresponding to a value for which predictions had been made. With the capacitance and d.c. load resistance R_L both set to high values, S1 was then closed. After the induction motor had accelerated to a stable speed, the capacitance was reduced so that it was equal to the predicted value involved. R_L was then similarly reduced until the a.c. voltage between motor and generator was equal to the predicted value. The generator speed was held constant during these adjustments by suitable changes in the d.c. drive motor's supply voltage. Measurements of all currents together with motor and generator torques, motor speed and electrical power were then made. This procedure differs from the equivalent one used for the predictions, where after setting the generator speed and voltage, the capacitance and all electrical quantities are then calculated, but is obviously more convenient in practice.

3.6.2 Operating Modes Investigated and Pump Characteristic

Investigations were made of the scheme's operation under conditions of:

a) constant voltage

b) constant voltage/frequency

c) constant capacitance.

Regimes (a) and (b) are reported in this chapter. Scheme (c) is reported in chapter 4. The results presented in this chapter comprise predictions made using the codes described in section 2.3.4 together with measurements made on the rig.

Throughout the project, the mechanical load on the motor was assumed to consist of a centrifugal pump having an ideal square law characteristic (i.e. Torque = $kp.w_m^2$; power = $kp.w_m^3$), and the Kp factor was chosen to load the motor suitably at its rated speed.

3.6.3 Influence of Pump Size on System Operation

Before commencing the test program, a brief investigation was made of how pump size affects system operation. In the system examined, the generator rating (11Kw mechanical output as a motor) was double that of the motor (5.5Kw). This was a deliberate choice made partly in view of the expected VA loading on the generator under motor starting conditions. The pump constant K_p in effect sets the pump rating. A number of different K_p values were tried (see Fig (3.14)) and calculations performed for operation at a single specified voltage (1 p.u.) and generator speed (1.02 p.u), the capacitor values being chosen appropriately. Fig (3.15) shows the input VArs of each induction machine against pump constant. It is clear that the required total VArs increase with K_p. The pump constant giving rated motor torque with rated voltage (with an appropriate value of capacitance per phase $C_{p.u}$ = 1.6) was found to be 1.12 p.u. The corresponding generator slip and current were however 0.019 and 1.414 p.u. respectively, with a corresponding motor slip and motor current of 0.056 and 1.315 whereas the generator rated current was

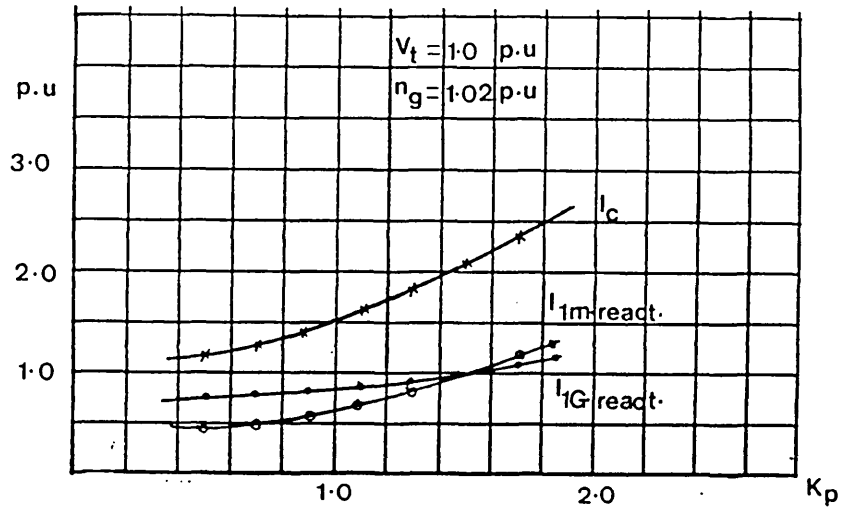

Fig. (3.15) Gen. , motor and total leakage VArs against pump constant at constant gen.speed .

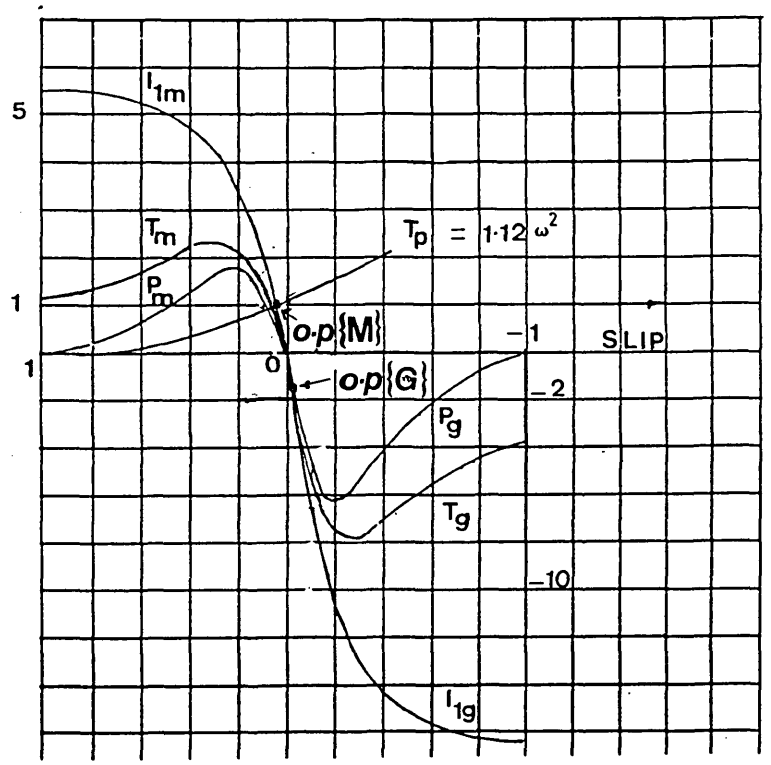

Fig. (3.16) Complete gen., motor and pump torque / speed curve obtaining at full load operating point for motor .

2 p.u. (on the base KVA chosen). The motor operating point would thus unfortunately result in over heating (the motor rated current being 1 p.u.)[1]. Fig. (3.16) shows the generator, motor and pump conditions versus slip (at the operating point's particular voltage and frequency) and the positions of this operating point on these curves. Smaller pump constants were then tried and a value found (K_p = 0.835) that resulted in rated voltage, current and frequency in the motor. The motor is then run at a power, torque and slip a little below its rated values.

The voltage and current phasor diagram of the induction scheme corresponding to rated voltage, current and frequency in the motor is shown in Fig (3.17). The generator stator current I_{1g} consists of two terms. One is the magnetizing current I_{mog} and the second is the rotor current I_{2g}. The imaginary component of I_{2g} is added to the imaginary component of I_{mog} to get the reactive component of I_{1g}. A similar phasor diagram representing the induction motor is drawn alongside. It is noticed that the capacitive current I_c is equal and opposite to the sum of the reactive components of generator and motor currents.

The active components of the generator and motor currents are also seen to be equal.

The 0.835 value of K_p was used for almost all the work reported in chapters (3 to 5).

---

[1]Two possible reasons for the unexpected motor current overload for rated torque, rated voltage and near rated frequency conditions are:

a) the frequency was in fact enough below nominal thus causing a significant V/f reduction and a corresponding mag.current increase

b) the motor design was perhaps optimistic.

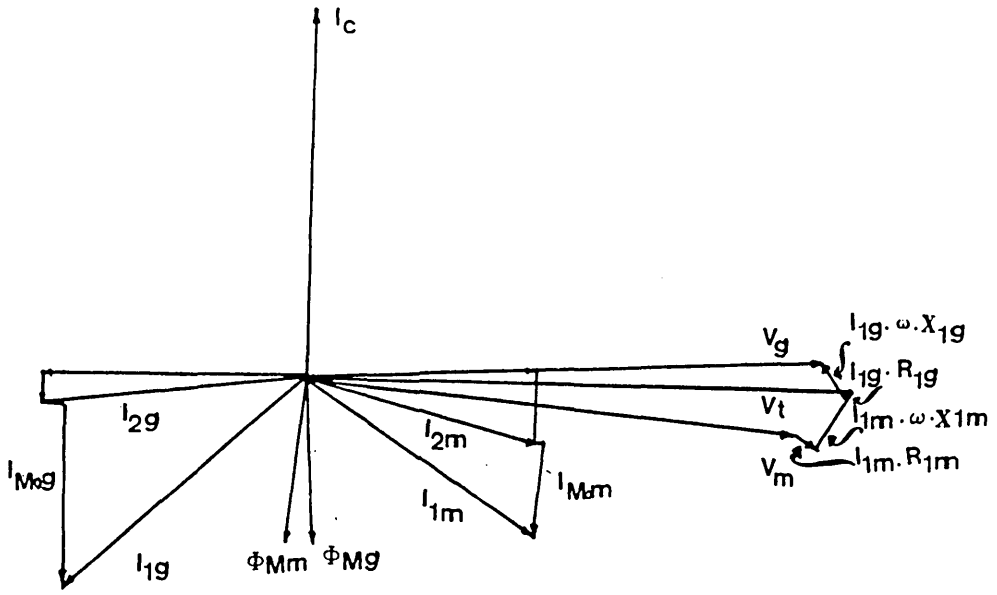

Fig. (3.17) Phasor diagram.

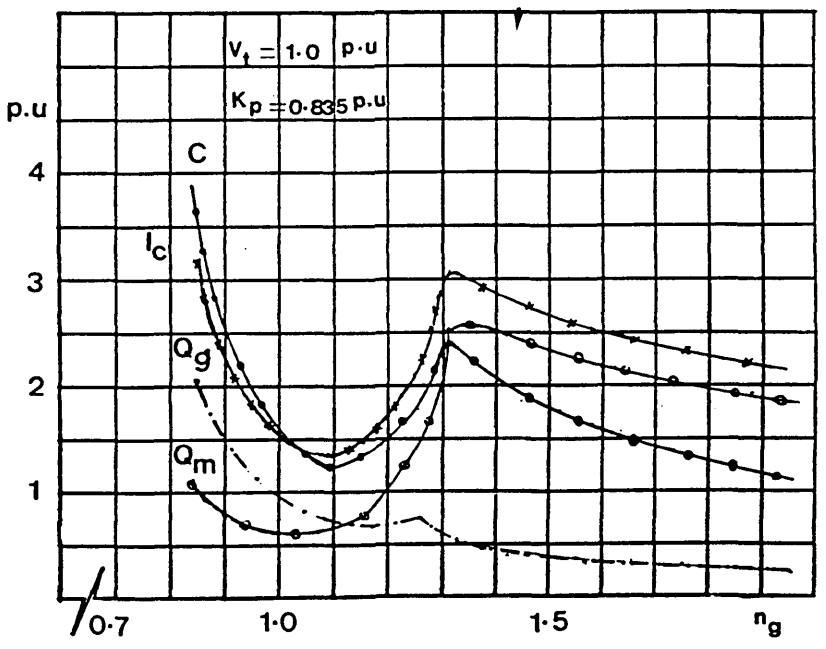

Fig. (3.18) Variation of the capacitor, capacitor current , gen. leakage VArs and motor leakage VArs against gen. speed (n_g).

3.6.4 Constant Voltage Condition with Pump Sized to Avoid Motor Overloading within Normal Speed Range

This regime was not investigated experimentally. Calculations were however performed for the system with its two induction machines (11Kw generator plus 5Kw motor), and a pump load having 0.835 as K_p. The prediction technique was found to converge satisfactorily. Conditions were examined for a number of different generator speeds n_g, the capacitor value being adjusted to maintain rated voltage. Fig (3.18) shows how the capacitor current and the input VArs of the generator and motor vary with generator speed n_g. The minimum in the capacitance value curve is interesting. At low generator speed, machine saturation levels with constant voltage operation are high, and result in high magnetization VAr needs. At higher generator speeds (1.1 to 1.25 p.u.) magnetization VArs are low but the VArs absorbed ($3\ I_{lg}^2\ wL_{\ell t}$) in the machine's leakage reactances become high .

Fig (3.19) shows the variation in generator slip, generator current and frequency with generator speed, and Fig (3.20) the variation in motor slip and motor current with generator speed. The decrease in generator slip that occurs for generator speeds beyond 1.25 p.u. and the tremendous increase in motor slip is caused by the pump's cubic power characteristic with speed, which in effect produces near stalling conditions (sometimes beyond 'pull–out') in the motor. Fig (3.21) shows a family of torque/speed curves for the motor, generator and pumps, each curve corrresponding to the frequency obtainted at the different generator speed values examined. Fig (3.22) shows the variation in motor speed and motor torque with generator speed n_g. It is clear that, for generator speeds beyond 1.25 p.u., the motor speed and torque decrease rapidly as the

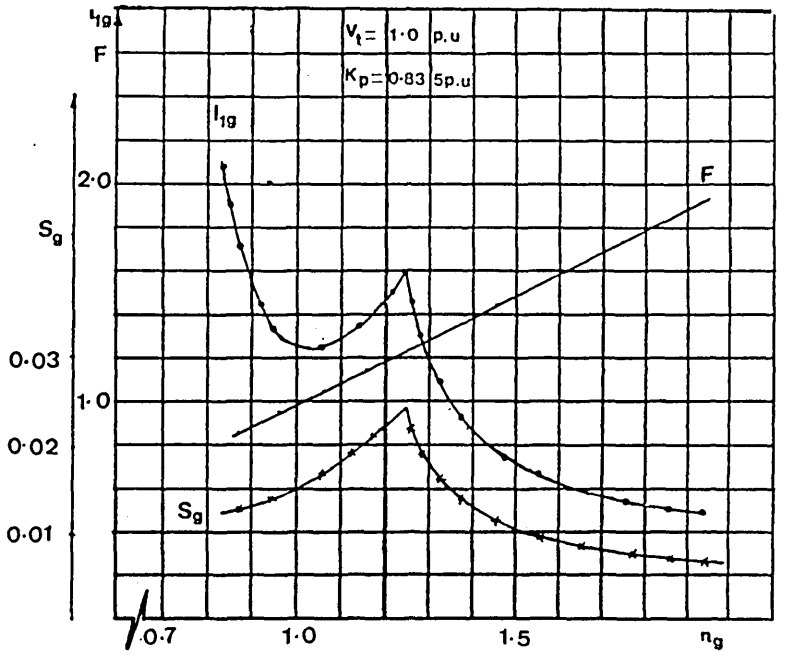

Fig. (3.19) variation of gen. current , gen. slip and frequency against gen. speed (n_g).

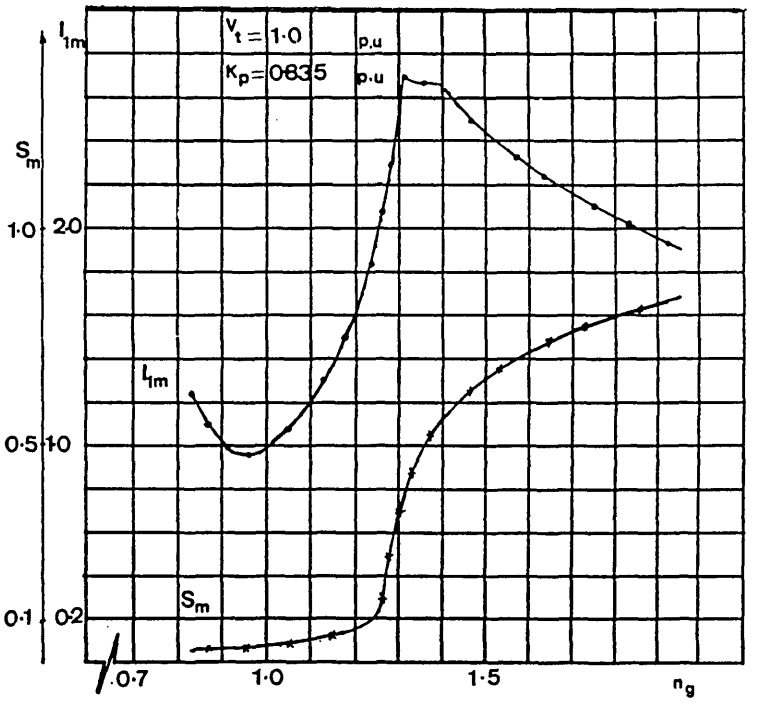

Fig. (3.20) variation of motor current and motor slip against gen. speed (n_g).

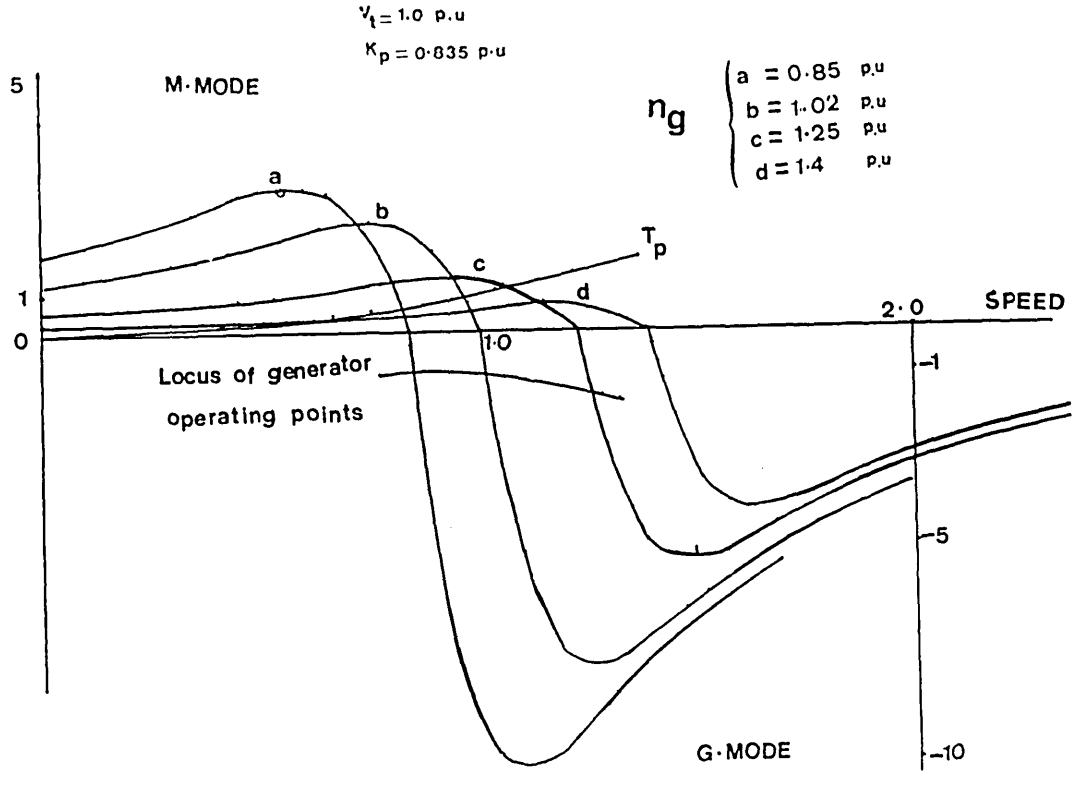

Fig. (3.21) Family of torque / speed curve for the motor , gen. and pump at 4 different generator speeds(n_g)

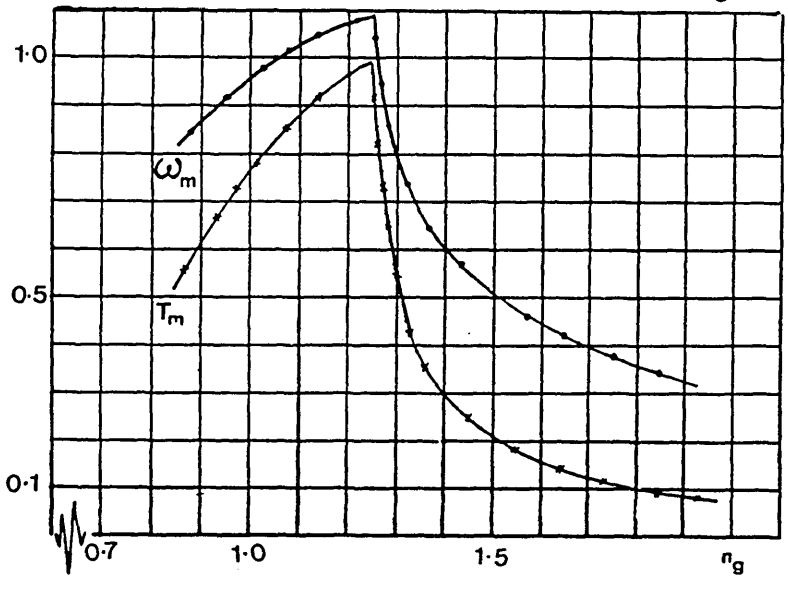

Fig. (3.22) Variation of motor speed and motor torque against gen. speed (n_g).

motor slip increases beyond the pull–out value.

Fig (3.23) shows the variation with generator speed in the generator's mechanical input power, electrical output power and electrical efficiency. Finally Fig (3.24) shows the variation with generator speed in the motor's electrical input power, mechanical output power and electrical efficiency. Fig (3.20) shows that, under constant voltage conditons, the system is limited by excessive saturation at low speeds and excessive motor slip due to mechanical overloading at high speeds. Each causes excessive currents (and hence heating) in the motor and at low speeds in the generator. Assuming a limit current of 1.2 p.u. the feasible estimated generator speed range is 0.83 to 1.09 p.u. This gives a pump power range of 0.36 to 0.82 p.u (i.e. 2.8:1) as shown in Fig (3.24).

The capacitance must be varied over a 2.9:1 range from 3.9 to 1.35 p.u as shown in Fig (3.18). The maximum capacitor KVAr required in the specific scheme examined was estimated as 10.86 for a maximum power transfer to the pump (at 1.02 p.u speed or 1530 rev/min) of 6.6 Kw with a generator speed of 1.09 p.u or 1635 rev/min and generator input power of 9.5 Kw. Higher speeds and/or large pump powers would involve motor over loads that would be unacceptable on a continuous basis. As can be seen in Figs (3.23) and (3.24), the generator and motor electrical efficiencies each lie between 72% and 82% over the feasible speed range. The overall system electrical efficiencies hence lie in the 52% to 67% range.

Although the maintenance of constant voltage may be useful if the system is to feed other (non–frequency–sensitive) electrical equipment, it is evident that the $\phi \alpha 1/f$ variation in motor and generator flux levels severely restricts the

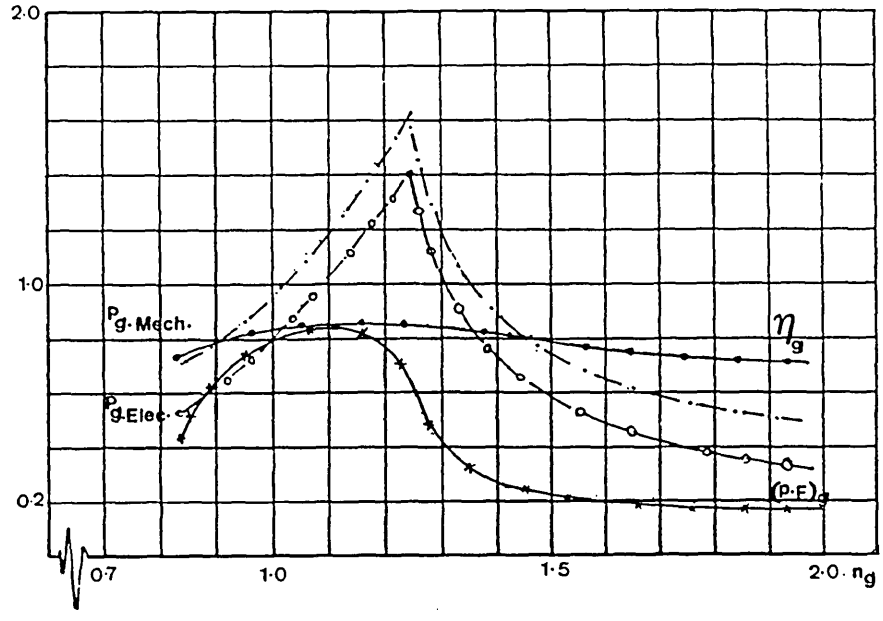

Fig. (3.23) Variation of mech. i/p power, elec. o/p power, power factor and efficiency for the gen. against gen. speed (n).

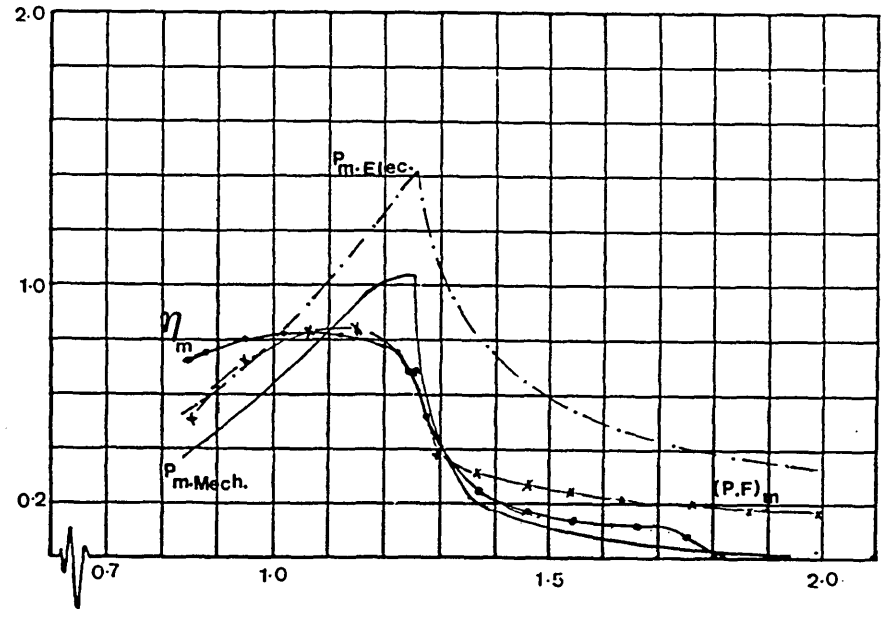

Fig. (3.24) Variation of elec. i/p power, mech. o/p power, power factor and efficiency for the motor against gen. speed (n).

system's feasible speed range, and worsens the motor's propensity to operate beyond pull–out at high speeds.

3.6.5 Operation at Constant Voltage/Frequency

In this part of the work, attention was again focussed on the specific generator–motor–pump system described in section 3.6. (11 and 5.5 Kw ratings with a pump having a K_p of 0.835). The choice of a relatively large generator was made partly on the basis of the expected starting KVA demand as stated earlier, partly because the generator had to carry both the motor and the capacitor currents ($\overline{I}_{1g} = \overline{I}_{1m} + \overline{I}_c > \overline{I}_{1m}$ at typical operating points), and partly in order to allow the generator to operate somewhat derated uner running conditons, hence hopefully raising its efficiency.

This last factor was felt to be important in obtaining respectable system efficiency values from a system whose efficiency might be adversely affected by the double mechanical to electrical to mechanical conversion stages inherent in the scheme. The voltage/frequency ratio chosen was one giving rated voltage (415v line) at rated frequency (50Hz). Constant voltage/frequency operation of course gives more favourable conditions in the machines in that their levels of magnetization remain approximately constant. The following results, which are all plotted on a base of generator speed, show both theoretical and measured results. Fig (3.25) shows how the capacitance per phase must ideally be varied in order to maintain constant voltage/frequency. Fig (3.26) shows the variation in capacitor current. Fig (3.27) shows the variation of motor current, generator current, system frequency and terminal voltage. Fig (3.28) shows the variation in generator and motor slips, and Fig (3.29) the variation in motor

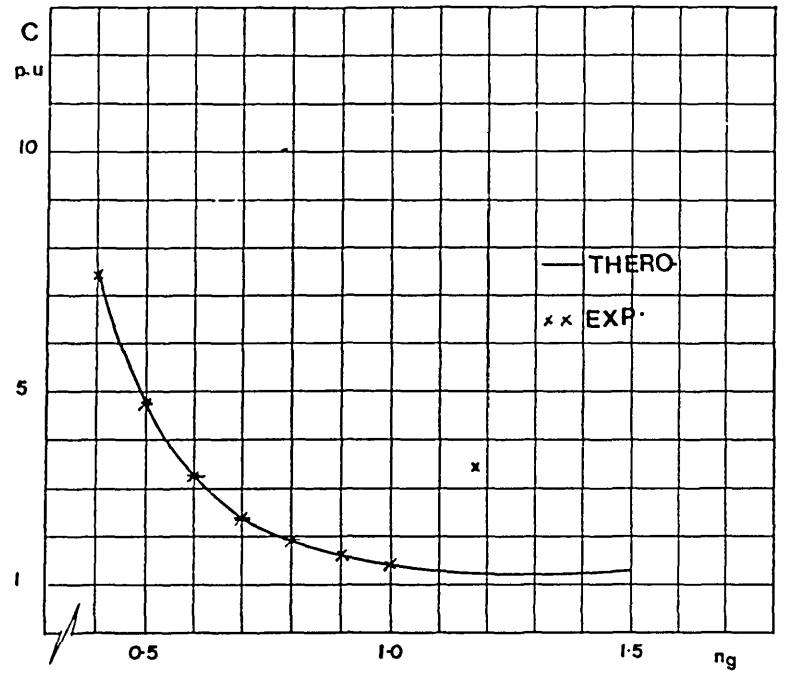

Fig. (3.25) Variation of required capacitance against gen. speed (n_g).

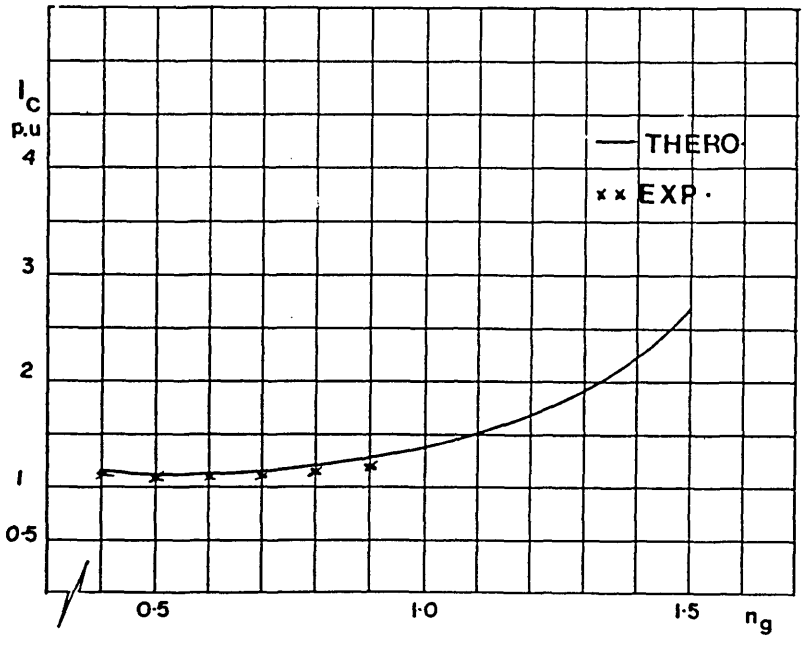

Fig. (3.26) Variation of capacitor current

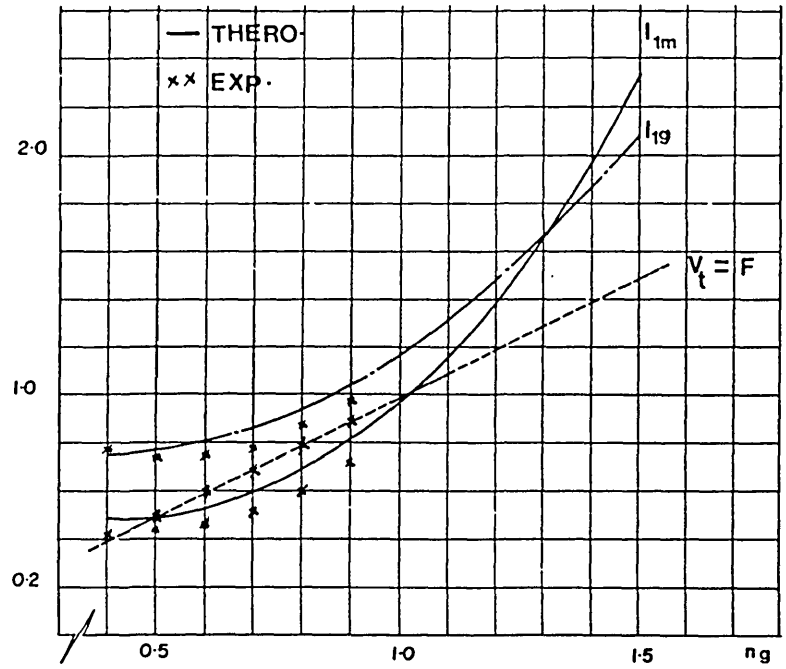

Fig. (3.27) Variation of gen. current, motor current ,gen. voltage and system frequency

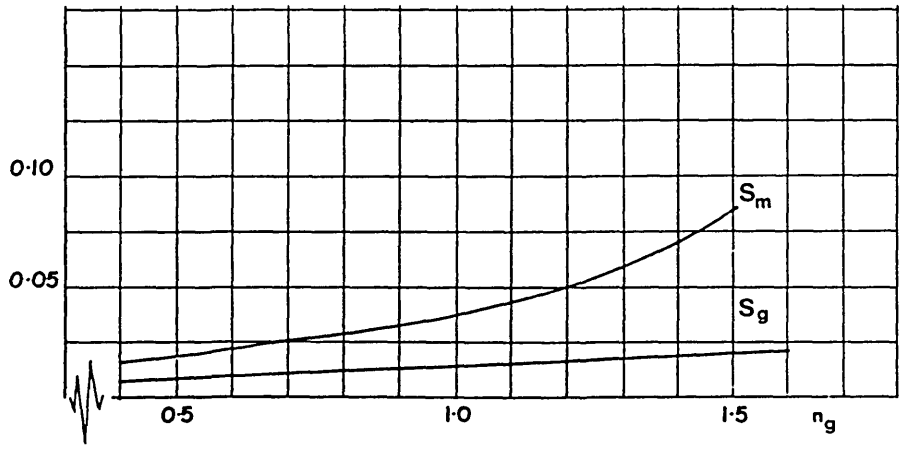

Fig. (3.28) Variation of gen. slip and motor slip

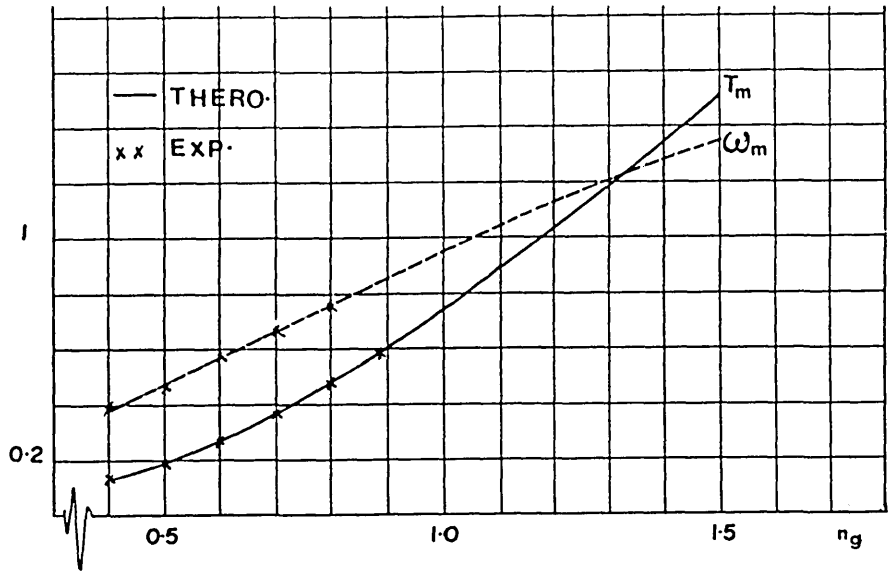

Fig. (3.29) Variation of motor o/p torque and motor speed

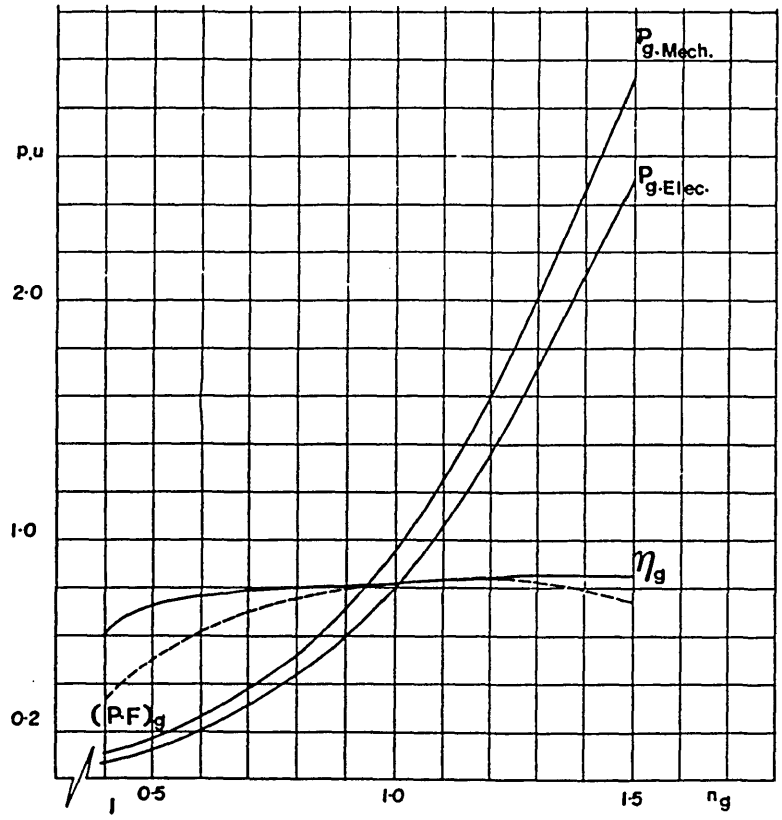

Fig. (3.30) Variation of gen. mech. i/p power, elec. o/p power, power factor and efficiency

output torque and speed.

Fig. (3.30) shows the variation of the generator's mechanical input power, electrical output power, power factor and efficiency. Fig (3.31) also shows the variation of the motor's mechanical output power, electrical input power, power factor and efficiency. Overall electrical efficiency ($\eta_g \cdot \eta_m$) is indicated in Fig (3.32). Since the capacitor bank has to supply the magnetizing and leakage VArs of both machines, the bank's installed KVAr is hence considerable as shown in Fig (3.25). 11.2KVAr is required for the test rig for rated current operation of the motor at 1522 rev/min and 415 line voltage. This compares with corresponding Kw figures of 6.713 and 5.52 for the generator output power and pump input power respectively. However, the bank can utilise standard, low cost, 50Hz capacitors (as developed for power factor correction installations) whose weight is low, and the bank's volume is typically comparable with the combined volume of the two machines.

It can be seen that the constant V/F mode of operation considerably extends the speed range, particularly in the lower speed region. Fig (3.27) shows that the system can now operate safety over a range of generator speeds from zero to 1.135 p.u, corresponding to a pump power range from zero to 0.95 p.u. Beyond this, the pump is apt to overload the motor. The need for a capacitor bank of large value able to work at high voltage is now avoided. Large capacitor values are still required for successful low speed operation but these need not be rated for high voltage. The cubic nature of the pump power characteristic means that it is probably sensible not to seek to make the system operate much below 0.6 p.u. This gives a pump power range of 0.15 p.u to 0.95 p.u[1](i.e. 5:1), and in this case the capacitor must be varied over a 2.4:1 range only, from 3.3 to 1.4

[1]Assuming a 20% overload in motor current

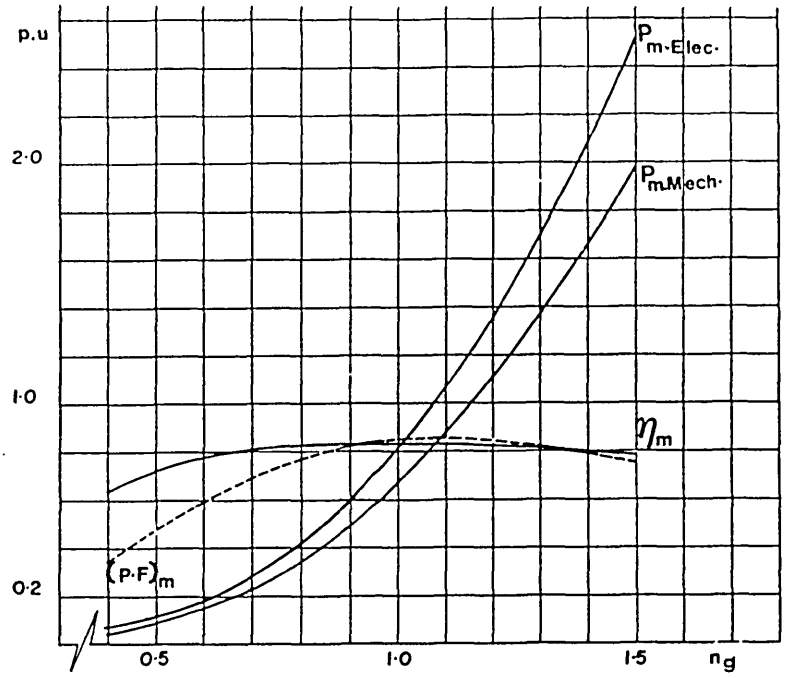

Fig. (3.31) Variation of motor elec. i/p power, mech. o/p power, power factor and efficiency

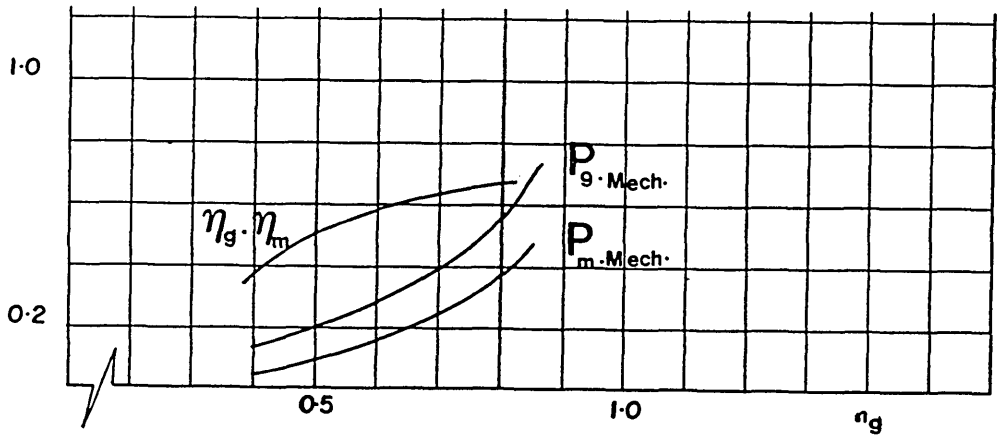

Fig. (3.32) Variation of gen. mech. i/p power, motor mech. o/p power, and overall electrical efficiency against gen. speed.

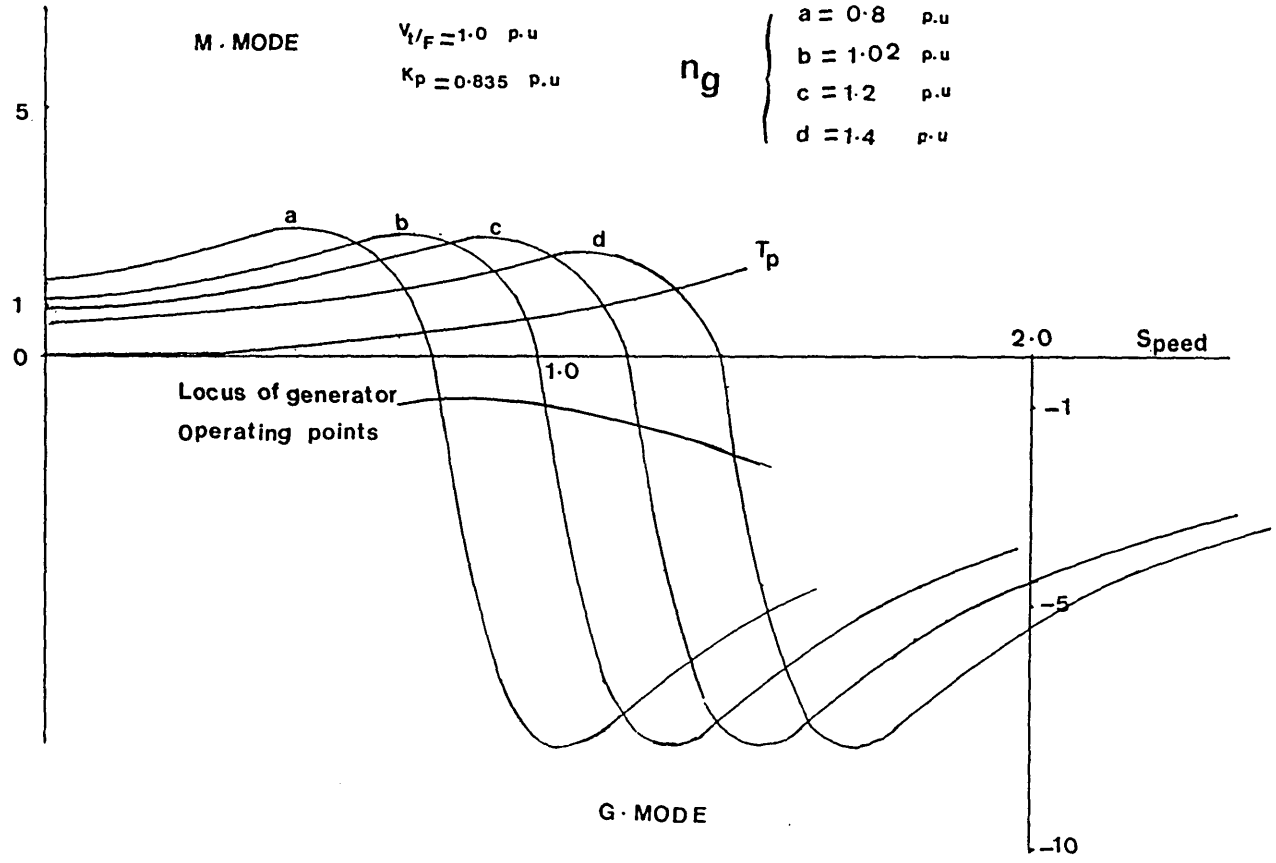

Fig. (3.33) Family of torque / speed curves for the gen., motor and pump at 4 different speeds (n_g).

p.u. The average overall electrical efficiency ($\eta_m \cdot \eta_g$) is approximately 65% over the 0.6 to 1.1 p.u speed range.

Finally the build–up of voltage with speed and torque means that slips are kept low and machine pull–out risks virtually are reduced, although turbine over–speeding could still pose generator heating risks, as shown in Fig (3.33).

3.6.6 Influence of Generator Sizes

A brief theoretical investigation was made of this topic in order to assess whether the postulated benefits of using a larger generator were borne out so far as operation at normal speeds was concerned. Starting conditions were considered later. The performance characteristics of a specific system (system 2) employing two identical squirrel–cage, three phase, 5.5Kw, 4 pole, 415V, 11.2A induction machines were estimated using the prediction code c, and compared with these obtained for the 11Kw/5.5Kw system (system 1) in section 3.6.5. The machines' parameters and the base values for the per unit quantities are given in Appendix 3. A number of different constant K_p values were tried and calculation again performed for operation at constant voltage per frequency (V/F = 1.0). The pump constant resulting in rated voltage, current and output frequency in the generator was found to be 0.685. The motor then runs at a current and slip a little below its rated values.

Figs (3.34) to (3.40) show the theoretical results for system 2. These Figures correspond to Figs (3.25) to (3.31) for system 1. It can be seen that the feasible speed range (limited by motor and generator currrents $\leq$ 1.2 p.u) is very similar (zero to 1.17 p.u compared with zero to 1.13 p.u). However,

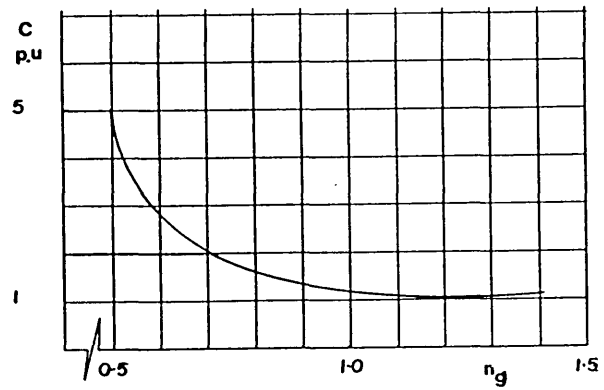

Fig. (3.34) Variation of capacitance against gen. speed (n_g).

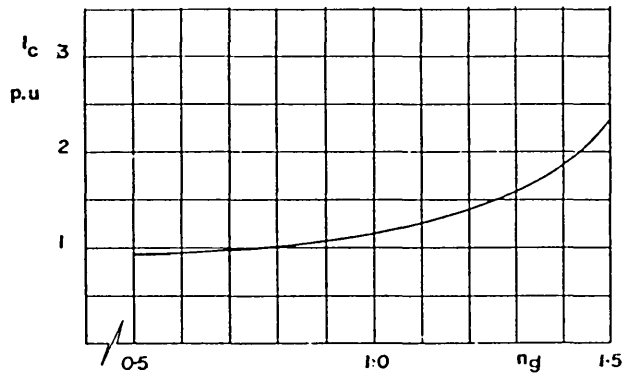

Fig. (3.35) Variation of capacitor current

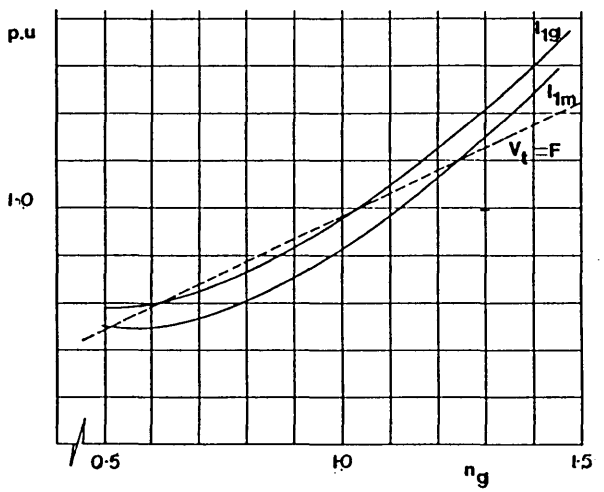

Fig. (3.36) Variation of gen. current, motor current, gen. voltage and system frequency.

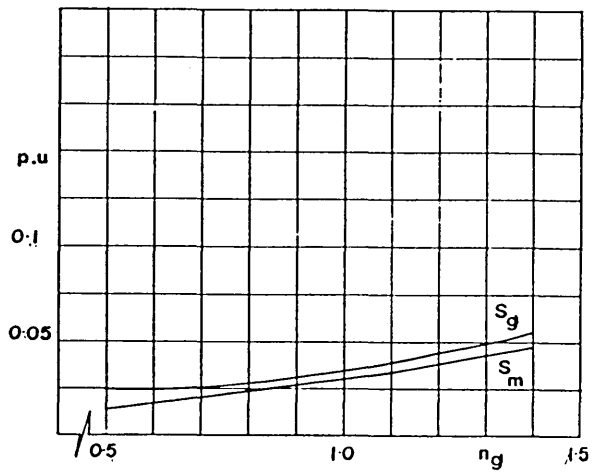

Fig. (3.37) Variation of gen. slip and motor slip

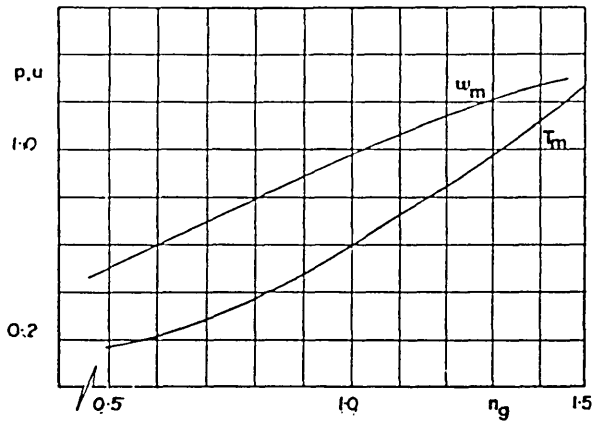

Fig. (3.38) Variation of motor o/p torque and motor speed

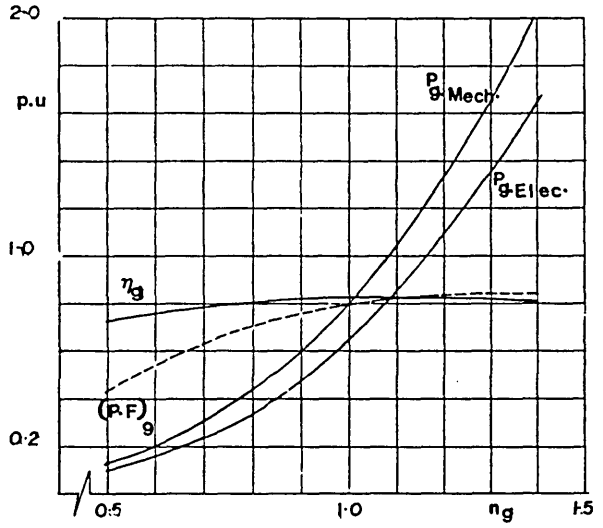

Fig. (3.39) Variation of gen. mech. i/p power, elec. o/p power, power factor and efficiency

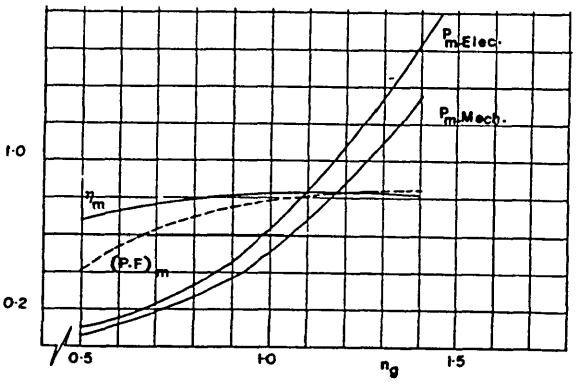

Fig. (3.40) Variation of motor elec. i/p power, mech. o/p power, power factor and efficiency

whereas with system 1 the motor current reached 1.2 p.u first, as generator speed was raised, with system 2, the generator current reaches this limit first as shown in Fig (3.36).

The corresponding range in pump power now ranges from zero to 0.82 p.u as shown in Fig (3.40). The max pump power for system 2 is of course less than that for system 1. The capacitance and reactive KVAr requirements for system 2 are a little less than for system 1 (see Figs (3.34) and (3.35)). As before, a sensible minimum operating generator speed is say 0.7 p.u. This gives a pump power range of 0.18 to 0.82 (i.e. 4.5:1), and in this case the capacitance must be varied over 2:1 range only from 2.1 to 1.05. The average overall electrical efficiency (η_m η_g) is approximately 66% over the 0.7 to 1.17 p.u speed range, as shown in Figs (3.39) and (3.40). It can be seen that the overall electrical efficiencies for system 1 and system 2 are virtually the same.

Generalising from the comparison, it is thus probably true to state: (a) that oversizing the generator enables the motor to work nearer its rated power (0.72 instead of 0.6 p.u) and to drive a larger pump (b) that the efficiency of the two schemes, designed so that one or other of the electrical machines is at maximum current at the nominal maximum frequency, is very similar.

Figs (3.41) and (3.42) show variations in the generator stator power loss and rotor power loss in the two systems against generator speed. From these two figures, it is clear that the power loss in the stator and rotor of the generator for system 2 is higher than for system 1, due to the high p.u stator and rotor resistances (0.0452 p.u and 0.0405 p.u respectively, instead of 0.0133 p.u and 0.015 p.u.)

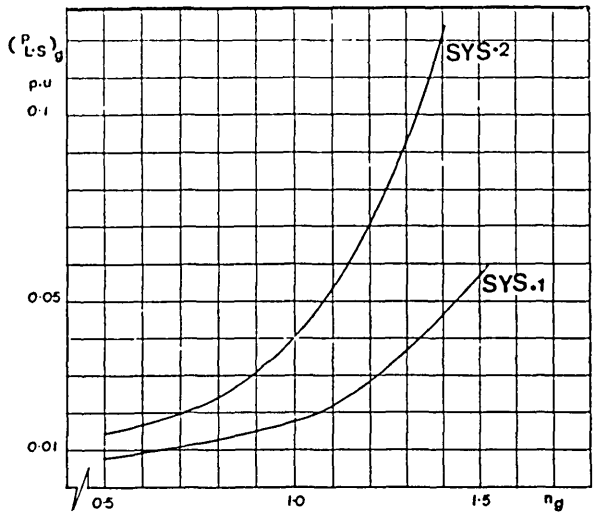

Fig. (3.41) Variation of the stator power losses for the gen. against gen. speed (n_g).

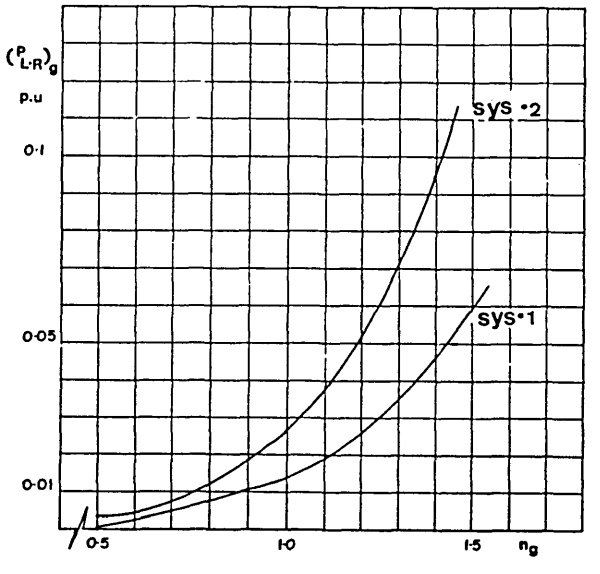

Fig. (3.42) Variation of the rotor power losses for the gen. against gen. speed (n_g).

Fig (3.43) shows the variation in the generator no load power loss (estimated using equation 2.7) against generator speed. The no load power loss in system 1 is higher because the iron loss resistance (22.32 p.u) of 5.5 Kw generator of system 2 is higher than the iron loss resistance (13.52 p.u) for the 11 KW generator of system 1. If the iron loss is assumed equal to the windage and friction loss, it emerges that the total system 2 generator power loss is a little lower than that in system 1, as shown in Fig (3.44). It is fairly certain that, with an unchanged pump size, the situation would be reversed, the generator power loss with the larger generator option being lower.

3.7 Capacitor Bank Regulation

Pratical capacitor bank regulation schemes for systems in the field were not investigated within the project, partly because the technology involved is well established. In this section, two standard types of scheme and their principal features are outlined. The possibility of using simplified schemes with two or three, on/off switched, capacitor–bank sections only is discussed in chapter 4.

3.7.1 Fixed Capacitor with Thyristor Controlled Inductor

This scheme, shown in Fig (3.45)(***b***), incorporates a fixed capacitor selected to provide the maximum reactive power needed by the induction machines. The net VAr output can be varied by changing the firing angle α in order to reduce the mean current in the inductor. With increasing α, the inductor current decreases and consequently the VArs provided increase. At maximum VAr demand the thyristors would of course be left untriggered. The scheme has drawbacks due to the losses in the inductor and the creation of harmonics in

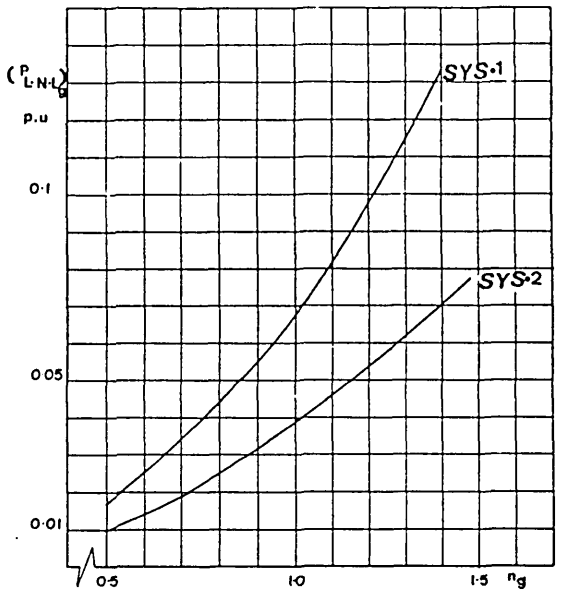

Fig. (3.43) Variation of the no-load power losses for the gen. against gen. speed (n_g).

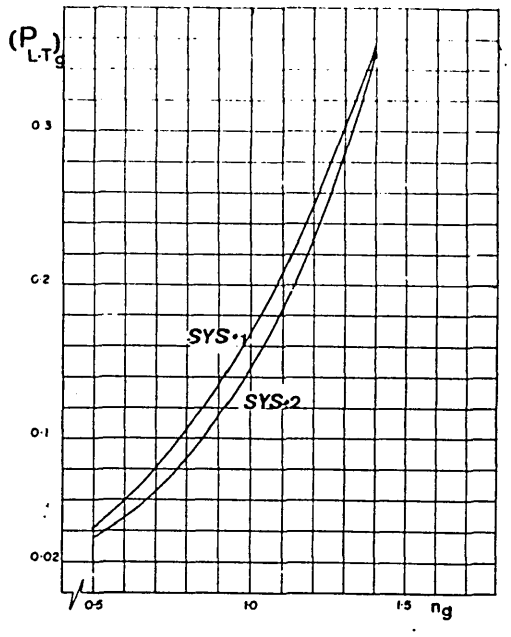

Fig. (3.44) Variation of the total power losses for the gen. against gen. speed (n_g).

the line currents due to the switching of the thyristors.

3.7.2 ON/OFF Switched Scheme with Sectionalised Bank

In this scheme, a number of discrete, 3 phase capacitor sections with thyristor or triac switches are used as shown in Fig (3.45)(*a*). With four or five sections having C values in a 16:8:4:2:1 ratio, the step sizes can be small enough to make the sudden changes in VAr output and hence voltage, frequency etc sufficiently small for practical purposs, even when close control of these quantities is essential.

In the literature, it is stated that this type of scheme with its 12 or 15 antiparallel thyristor pairs or triacs plus controller tends to be an expensive method for induction generator applications [1-49 and 1-58], but it is likely that the advent of low−cost programmable controllers and low cost thyristor assemblies have much improved this type of scheme's viability.

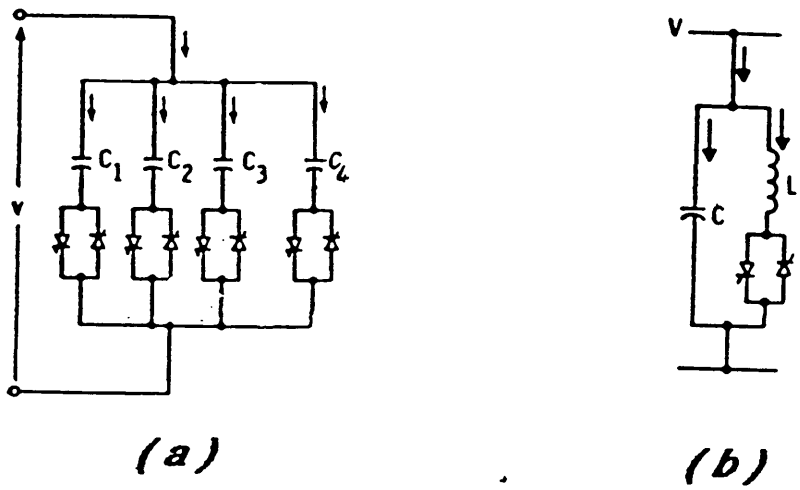

Fig. (3.45) Controllable capacitor bank using thyristor.

CHAPTER 4

STEADY-STATE PERFORMANCES WITH 2 OR 3 SECTIONS CAPACITOR BANK

4.1 Introduction

As will be evident from the results presented later in this chapter, the induction generator-plus induction motor scheme cannot operate successfully over any but an excessively narrow speed range if excitation is provided by a capacitor-bank of fixed value. Motor starting poses additional problems with a fixed value system due to the high VAr requirement at high motor slips.

In this chapter, the results of a study of a cost-effective capacitor bank configuration comprising two or three on/off-switched sections are presented. The measured results were obtained from the experimental rig described previously, with the capacitor values switched (manually) in a manner such as to simulate the presence of the two or three section banks envisaged in practice. The theoretical results were obtained using code D described in section 2.3.4. The two induction machines employed were the 11Kw generator and 5.5 Kw motor detailed in chapter 3 (scheme B). The pump K_p factor was again 0.835.

The results of two studies are presented:

(a) Investigation of operation with controlled capacitor at constant generator shaft speed.

(b) Investigation of operation with constant capacitance at different generator shaft speeds.

The objects of part (a) of the investigation were to establish the value of capacitance (C fixed) needed in the permanently–connected section of the bank. As will be seen, the presence of the induction motor plus pump load gives rise to a rather complex relationship between capacitance and voltage, and the choice of the fixed C is hence made rather more difficult. The objects of part (b) were to establish the width of the feasible speed range with C fixed, and hence to establish the speed (lower) boundaries at which the second and third (on/off switched) capacitor sections must be brought into circuit.

4.2 Operating Characteristics

It is assumed that the scheme has started successfully and the system has reached a steady state. Fig (4.1) (a) and (b) shows the computed variation of per unit terminal voltage V_t as capacitance is varied, plotted on a base of per unit capacitor current I_C. The results as stated above are for system 1 scheme B and the generator speed was assumed constant at six different values : 1.0, 0.85, 0.8, 0.7, 0.6 and 0.55 p.u respectively.

On Fig 4.1(b), a typical capacitor load line has been added. It is interesting to note that, with fixed capacitor conditions, there are generally two equilibrium operating points, (note that the use of a straight capacitor load line is based on a constancy of system frequency between the two operating points). The constant nature of the generator speed does in fact keep frequency approximately constant, but there is a small variation due to the change in

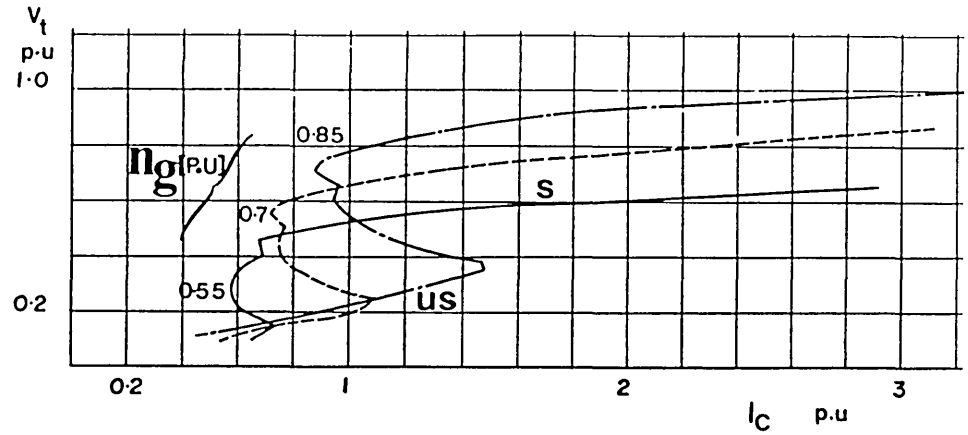

(a)

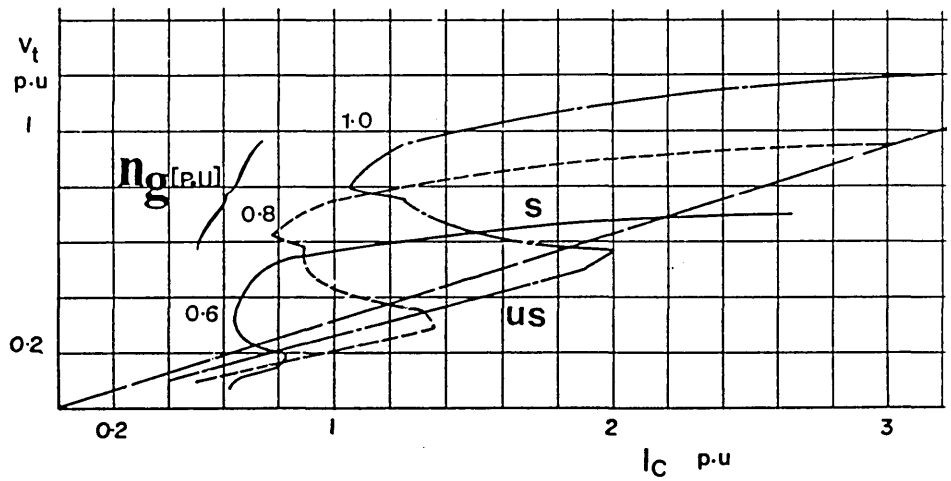

(b)

Fig. (4.1) Variation of gen. voltage against capacitor current at different gen. speeds.

system voltage and hence motor speed, power and generator slip.

Of the two equilibrium points, one lies at a lower voltage; the other lies in the saturation region. The first is unstable because slight reduction in the generator voltage leads to insufficient VAr output from the capacitor and hence to progressive loss of excitation. Any slight increase in voltage from the lower operating point leads to an excess of VArs and consequent movement of the machine operating point to the second position. The second operating point is stable in that a small change in voltage leads to a restoration of the operating point. Fig (4.2) corresponds to Fig (4.1) but a base of capacitance value instead of capacitor current is used. The curves show that so long as the voltage has exceeded a minimum value (e.g. 0.6 p.u with 0.7 p.u generator speed), increases of capacitance produce increases in steady state voltage. The minimum value corresponds to the turning point on the curves and this point divides the unstable operating region from the stable operating region.

Generator speed increases of course produce generally higher levels of voltage. Fig (4.2) also demonstrates that there is a minimum value of capacitance below which the system will not maintain or build up excitation. This minimum value of capacitance depends upon the generator speed. Fig (4.3) shows the variation of motor current against capacitance at different generator speeds. A high capacitance value is required as expected if rated current is to be maintained at lower generator speeds. Unfortunately, if the generator is then run at higher speeds, this value gives currents considerably above

allowable values. Hence capacitance must be reduced if over heating is to be avoided.

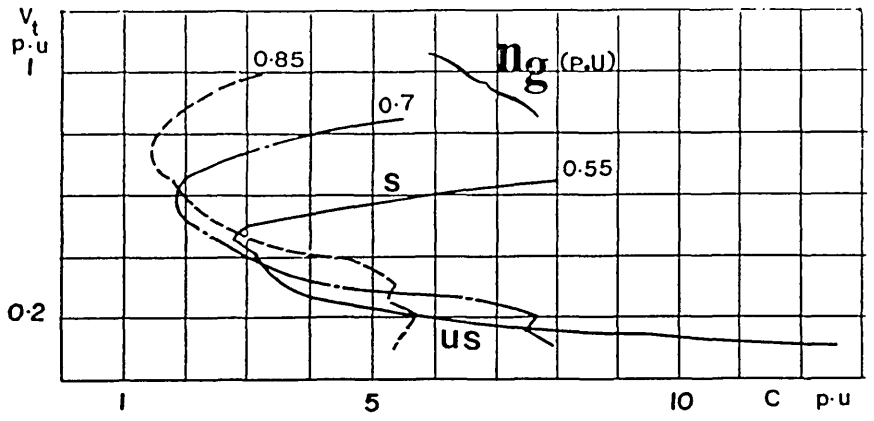

(a)

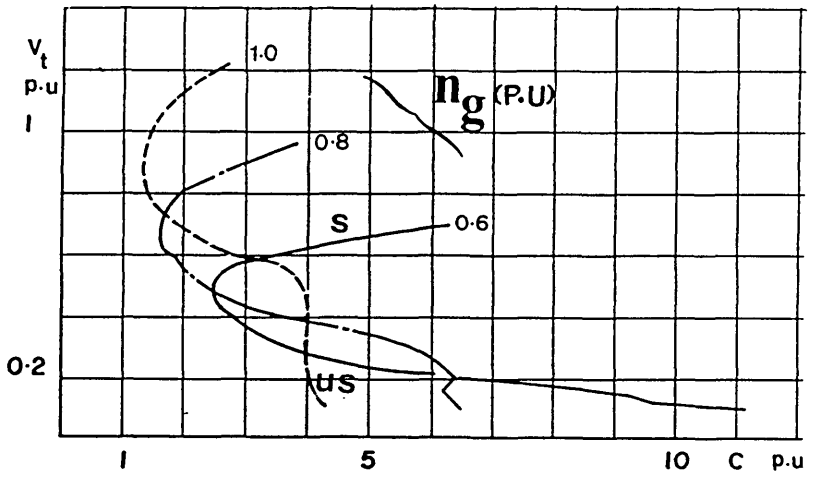

(b)

Fig. (4.2) Variation of gen. voltage against capacitor at different gen. speeds .

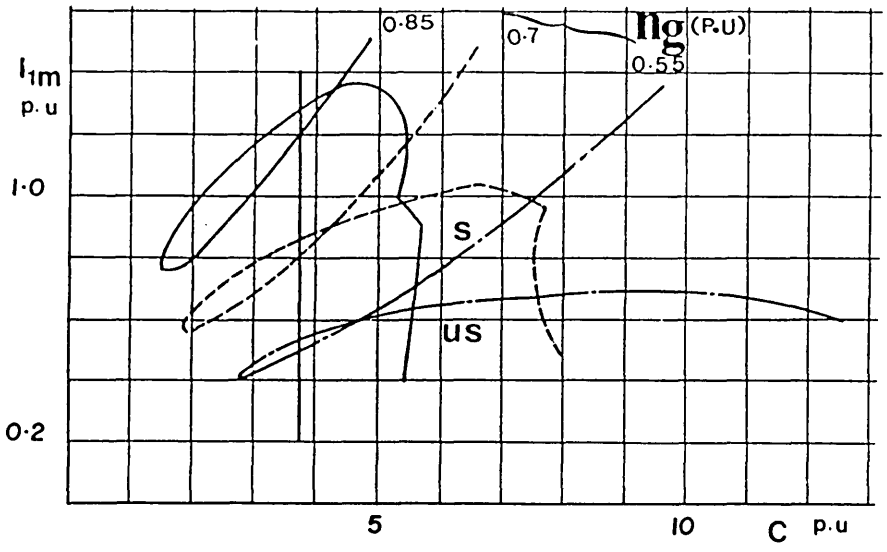

(a)

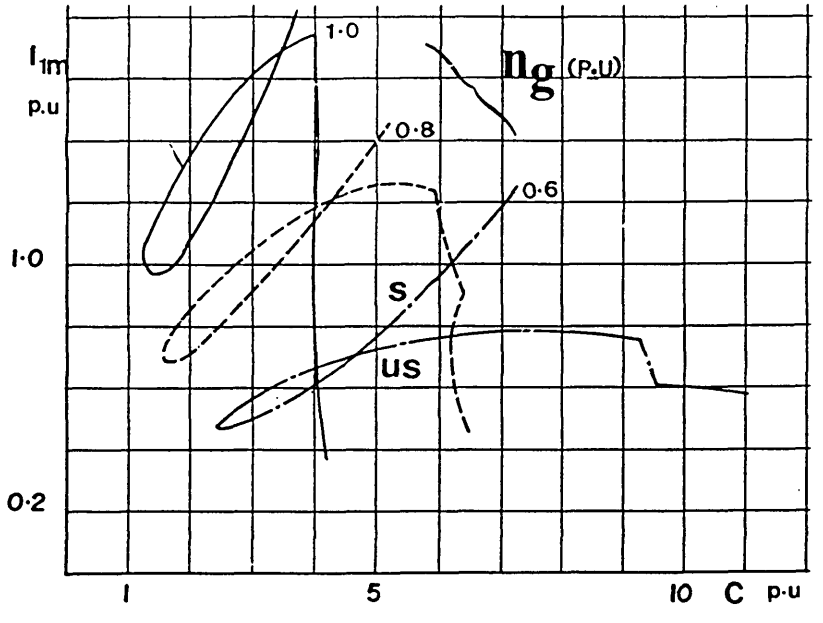

(b)

Fig. (4.3) Variation of gen. voltage against capacitor at different gen. speeds .

In general therefore, it appears that a single value of capacitance cannot provide satisfactory system operation with generator speed variation over a reasonably wide range. The basic reason for this is the strong dependence of the capacitor VArs on voltage and frequency (each of which is closely related to generator speed), even though the VAr demands of the machines also possess some frequency and voltage dependency.

4.3 Multi–stage Capacitor Bank

The multi–stage bank (where the number of stages is envisaged as relatively small, e.g. 2 or 3) is envisaged as consisting (see Fig (4.4)) of two discrete groups of permanently connected and switched capacitors respectively, relays or antiparallell, O° switched thyristor–pairs being used to connect and disconnect the stages within the second group.

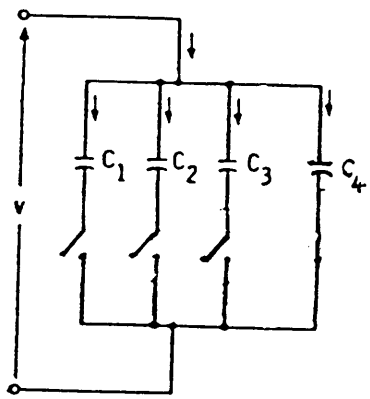

Fig. (4.4) Multi- stage, switched capacitor bank.

The number of switched capacitor stages would be kept to a minimum, in order to simplify the switching circuit, but not so few that the current could not be kept within upper and lower boundaries set by machine heating limits and motor stall limits respectively. The value of the final capacitance is carefully selected to provide the minimum amount of reactive power needed for satisfactory motor operation at some pre–set speed at which a first stage of extra capacitors would be switched in as generator speed fell. For operation at substantially lower speeds, it might be desirable to provide second and even third extra stages. Finally, under motor starting conditions, a special high value stage would be needed to furnish, in combination with the other stages of the bank, the motor's high starting VAr plus the generator's VAr requirements. The maximum value of the switched reactive power to be provided is of course the difference between the maximum VAr demanded by the scheme and the reactive power provided by the fixed capacitors.

This type of scheme, particularly when the number of switched stages can be held down to two, is considered to be relatively simple and inexpensive to build, and of course introduces no harmonic currents. The absence of such currents avoids extra machine losses and reduces resonance and noise risks.

4.4 Specific Scheme Investigated and Mode of Operation

The scheme examined is a 3 stage one, with one permanent and two switched stages, as is shown in Fig (4.5). The machines and pump details were as before and the scheme incorporates a motor isolating switch. The motor isolating switch S3 is normally closed only after the occurrence of self–excitation (i.e. after the voltage has built up to a reasonable value). This ensures (a) that

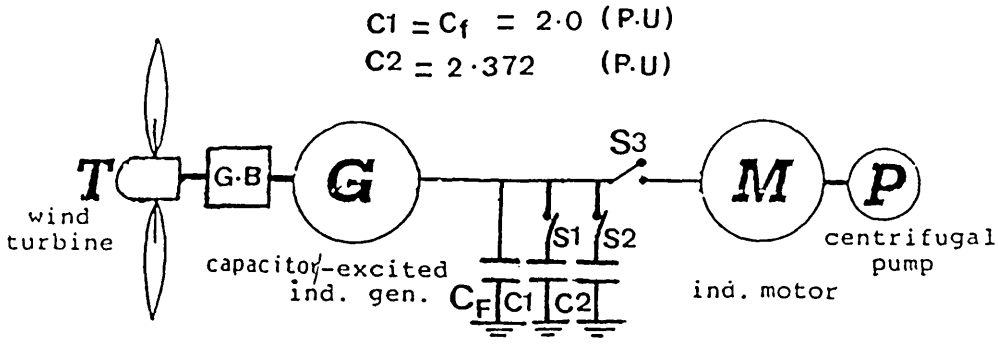

Fig. (4.5) Induction scheme with sectionalized capacitorbank.

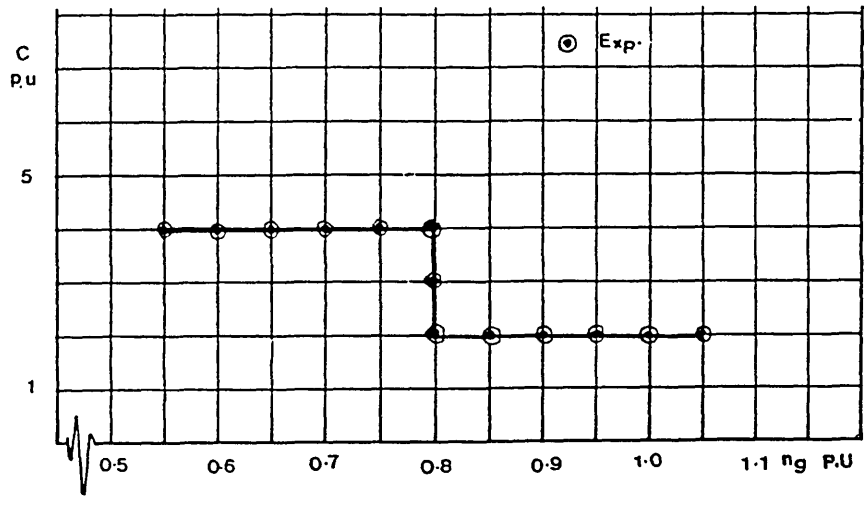

Fig. (4.6) Capacitance in circuit against gen. speed (n_g).

the build-up process can take place in the absence of the motor's very low standstill impedance (note that frequency will also be relatively low at typical desired self-excitation speeds) (b) that the load on the generator and hence the turbine is kept low until motor starting is required. The capacitance per phase must be reasonably high to avoid voltage collapse when the motor is connected (C_{st} = 6.372 p.u) and C2 is chosen to be fairly large in order to ensure this. In the scheme studied the total capacitance required (CF+C1+C2) for satisfactory motor starting (see chapter 5) at 0.8 p.u generator speed was 6.372 p.u. It is necesary to switch out C2 to avoid over excitation and excessive currents by opening S2. For the system studied, a C2 of 2.372 p.u was found to be satisfactory with a CF+C1 of 4 p.u.

The section switches S1 and S2 are envisaged as being operated by a simple logic controller which continually compares the max allowable motor current with a fixed reference, switching in an additional section or switching out C1 and possibly C2, depending on whether the motor current was respectively low or high.

4.5 System Characteristics

Theoretical steady-state results for this scheme, estimated using code D, are shown, together with test results, in the figures below. The 3 stage bank was simulated in the lab by means of the same, manually switched capacitor units as before. Figure (4.6) shows how the total C1+C2+CF capacitance is regulated as a function of generator speed (note that a generator speed-based rather than a current-based controller would be a possibility, subject to certainty about the load's torque/speed characteristic and non-steady-state

phenomena). Fig (4.7) shows terminal voltage and system frequency against generator speed (n_g).

Fig (4.8) shows the variation of the motor current and generator current and Fig (4.9) the variation in generator and motor slips. Fig (4.10) shows capacitor current and Fig (4.11) the machine magnetizing reactances.

Fig (4.12) shows the variation in motor output torque and speed and Fig (4.13) the variation of mechanical input power to the generator, electrical output power from the generator and mechanical output power from the motor.

Fig (4.14) shows the variation of generator efficiency, motor efficiency and overall efficiency against generator speed (n_g). Capacitor values of 2.0, 2.0 and 2.37 p.u were used for capacitor stages CF, C1 and C2 respectively, the changeover speed from CF to C1+CF being 0.8 p.u, the minimum feasible speed to avoid motor stall with CF+C1 being 0.55 p.u and the maximum speed to avoid motor overheating being 1.05 p.u. Fig (4.8) shows that, with the constant C1+CF capacitance in circuit, the motor current increases from 0.55 p.u to the limit value of 1.2 p.u as generator speed increases from 0.55 to 0.8 p.u. Beyond this generator speed the excessive motor current is caused by the pump's over loading the motor rather than by excessive voltage giving high magnetizing current. The same situation arises with CF only at 1.05 p.u generator speed. The generator current variation over the 0.55 to 0.8 speed range 0.82 to 2.01 p.u (the generator's rated current being 2 p.u) is shown in Fig (4.8). It can be seen that the feasible speed range with a totally unregulated capacitor bank is indeed rather small (e.g. 0.8 tp 1.05 p.u only with CF) and as is soon later, motor starting would be impossible.

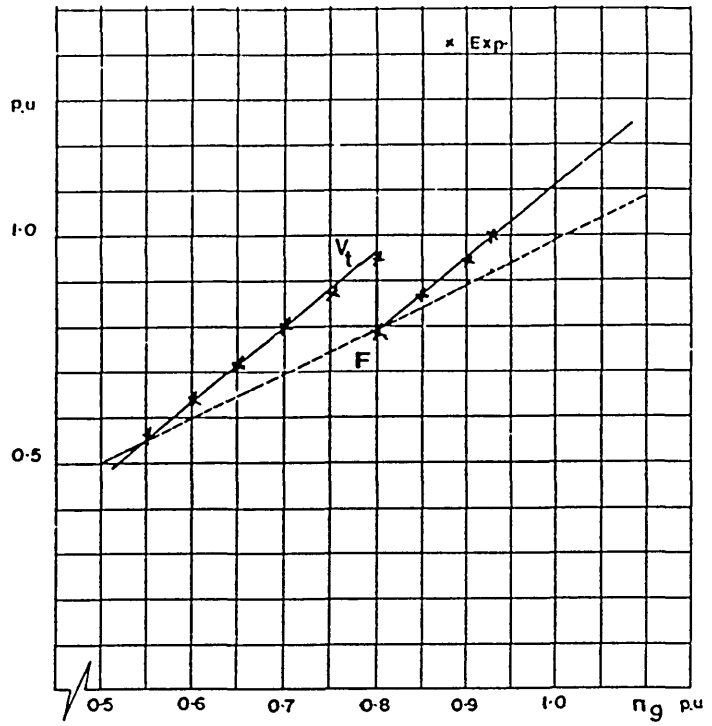

Fig. (4.7) Variation of system voltage and frequency.

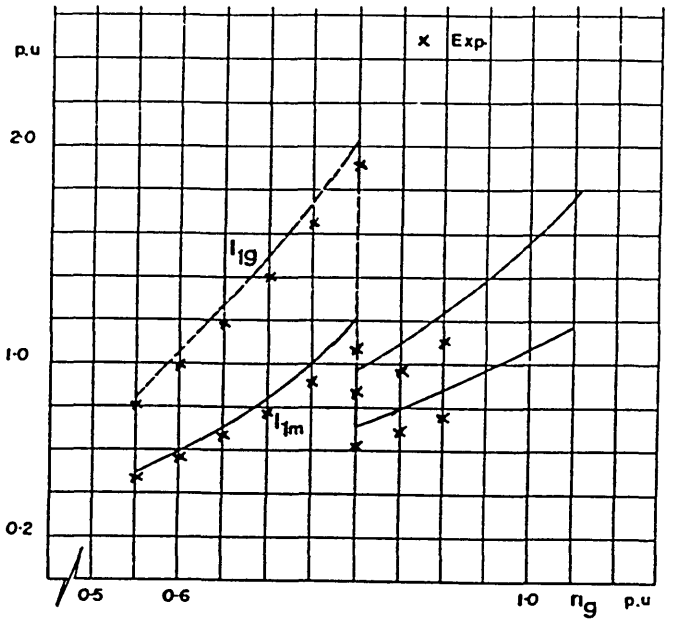

Fig. (4.8) Variation of gen. current and motor current against gen. speed (n_g).

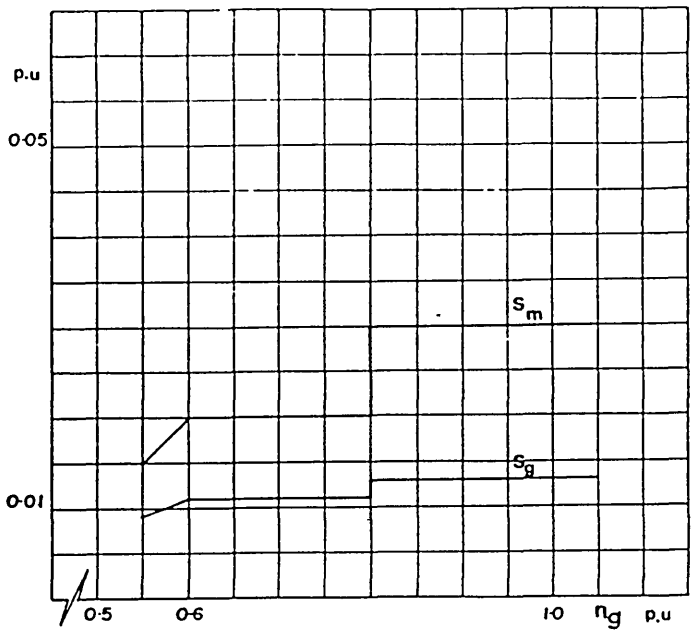

Fig. (4.9) Variation of gen. and motor slips.

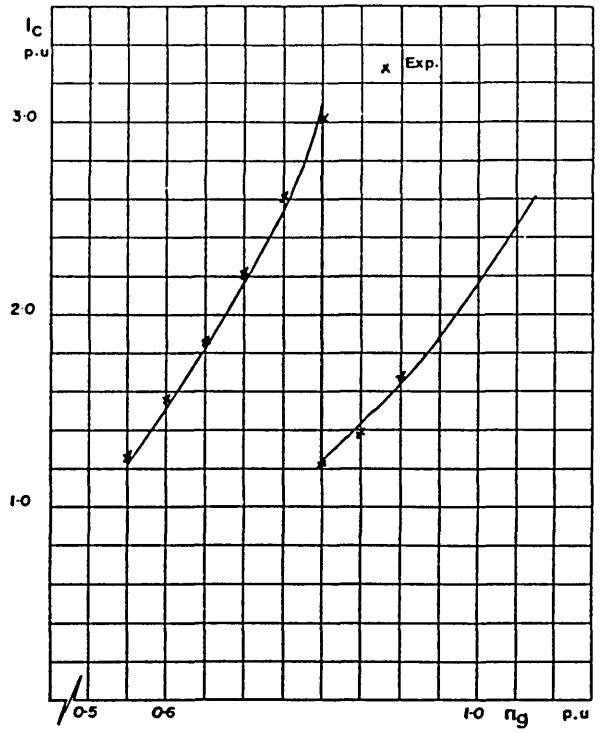

Fig. (4.10) Variation of capacitor current .

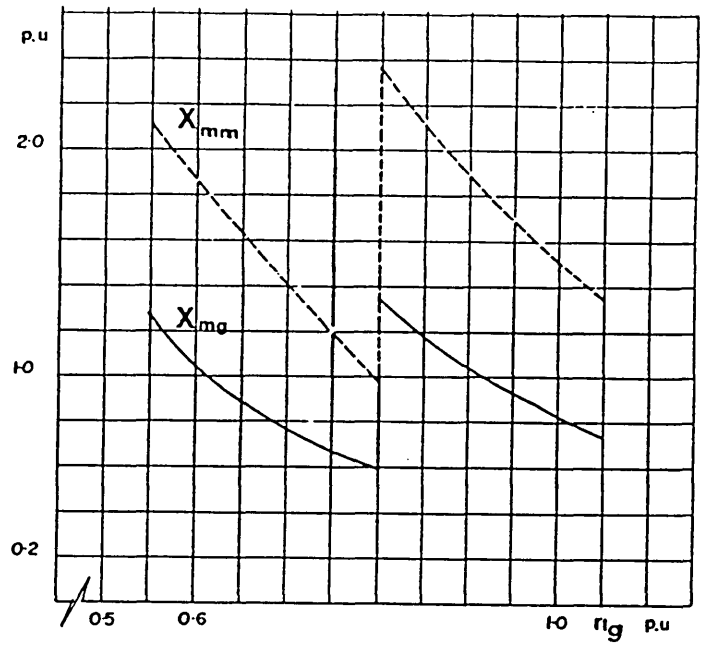

Fig. (4.11) Variation of gen. and motor magnetizing reactances against gen. speed (n_g).

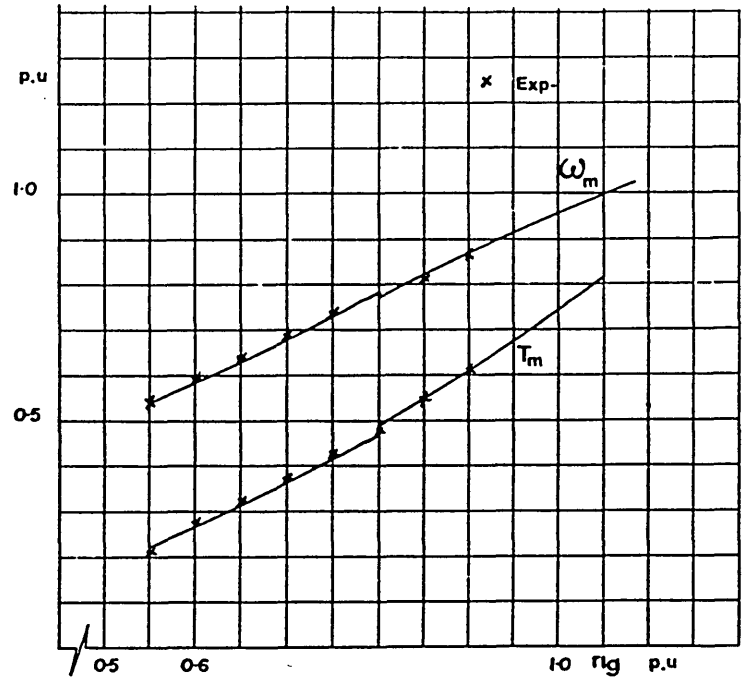

Fig. (4.12) Variation of motor o/p torque and speed against gen. speed (n_g).

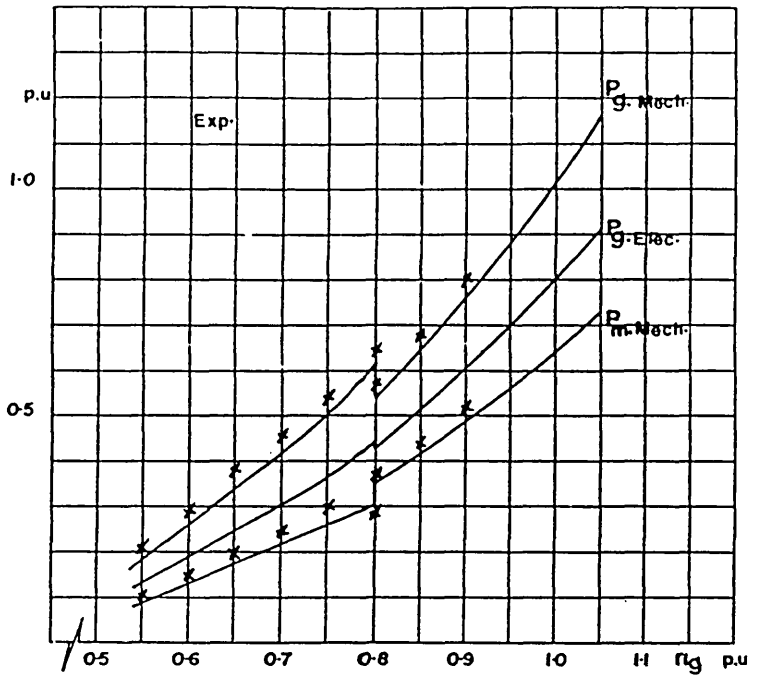

Fig. (4.13) Variation of gen. mech i/p power, elec. o/p power, and motor mech. o/p power

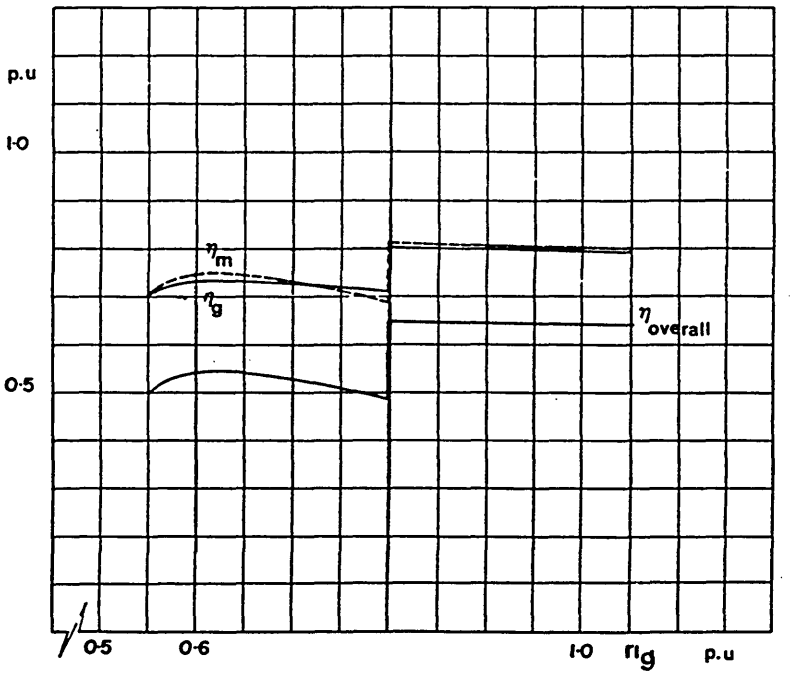

Fig. (4.14) Variation of gen. efficiency ,motor efficiency and overall elec. efficiency against gen. speed (n_g).

Fig (4.9) shows that, within a single portion of the operating speed range (i.e. while the capacitance is maintained constant), the variation in machine slips is remarkably small. This clearly is associated with a linear relation between frequency and speeds, and Fig (4.7) shows that the rate of change of terminal voltage is constant with speed. It can be seen that the V/F varies from 1 p.u at 0.55 speed to 1.1 p.u at the maximum 1.05 speed. Clearly the induction motor is able to operate satisfactorily with the pump load studied with V/F variation of this magnitude. Fig (4.10) shows the total reactive current required to supply the magnetizing and leakage VArs for both machines, clearly the VAr demand increases when magnetizing reactances are low due to high V/F (see Fig (4.11)). The overall speed range from 0.55 to 1.05 p.u corresponds to a pump power range of 0.08 p.u to 0.72 p.u (i.e. 1:9). This may well be a sufficiently wide range for practical purposes. The pump power at the capacitor–bank–switching–speed of 0.8 p.u was 0.3 p.u. Fig (4.14) shows that the overall electrical efficiency (η_m η_g) is approximately 52% over the 0.6 to 0.8 p.u generator speed range and approximately 64% over the 0.8 to 1.05 p.u generator speed range.

CHAPTER 5

SYSTEM BEHAVIOUR DURING MOTOR STARTING WITH CONSTANT GENERATOR SPEED

5.1 Introduction

This chapter describes an extension to the simulation code to enable it to predict the manner in which the motor accelerates from standstill to its final steady–state speed. In a later chapter, conditions under varying generator speed are considered, but here, generator speed is taken as constant. Switching operations carried out as appropriate with the motor isolating switch and on the capacitor bank are included in the treatment.

The extended code's validity is again restricted to the study of system operation where rates of change are relatively small within one cycle of a.c. operation, as, is generally expected to be the case due to the motor and load inertias. Clearly the effects of switching transients are taken as negligible.

Predictions have been made for the system operated in two ways

1] With a switched, three–section capacitor bank.

2] With a fully controlled capacitor bank operated so as to give a constant rate of voltage increase during the motor starting period.

As indicated in chapter 4, a motor isolating switch, closed only after self–excitation has occurred (see Fig 5.1), is necessary to facilitate voltage build up, free from the inhibiting influence of the motor's low standstill impedance.

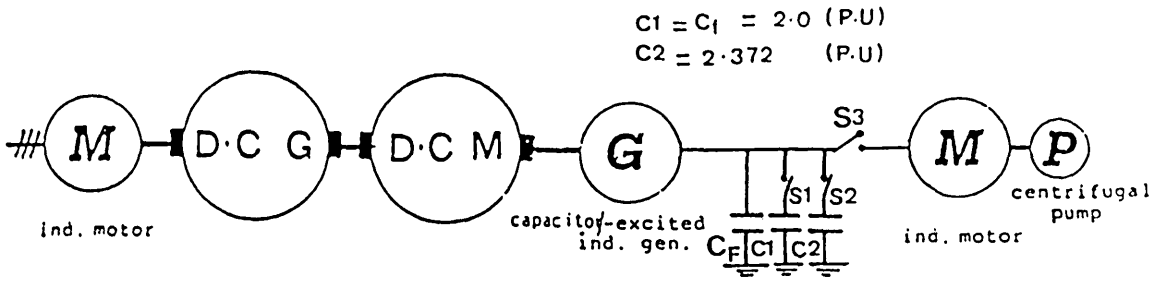

Fig. (5.1) No-load operation
(s1 , s2 are closed and s3 is open)

The need for some sectionalising of the capacitor bank in case 1] was confirmed during the investigation. The entire bank (giving the 'high' capacitance value) is used during generator self excitation with the motor isolating switch open and during motor start up. Two of these sections are used for low and medium speed operation, and just one section is used for higher speed operation. As mentioned earlier, by operating in this way, the capacitor bank is able to supply the large VArs needed at starting while avoiding excessive voltage and saturation when running over a reasonably wide speed range.

Estimates of voltage, current, frequency, generator torque, motor torque and pump torque versus time for the two cases are presented. Start up tests were performed on the laboratory rig and the results are commented on qualitatively. An experimentally–determined curve of minimum starting capacitance versus generator speed is included.

The analysis is based on the one described in chapter 2. Additional software was written (a) to deal with the changes in motor connection and capacitor

value caused by the switching operations, (b) to calculate, on a time–stepping basis, the motor's dynamic behaviour based on acceleration estimates.

5.2 Starting Sequence for Case (1)

The normal starting sequence would be:

1] check for sufficient generator speed (e.g. above 0.5 p.u);

2] initiate voltage build–up by switching in entire capacitor bank;

3] close motor isolating switch allowing current to flow through motor windings;

4] remove sections 1 and 2 depending on system conditions.

The use of starting resistors temporarily placed in series with the motor to reduce VAr demands was considered. These are likely to be required in cases where the generator maximum VA capability is relatively low, and where some reduction in motor starting torque is allowable. So far as the experimental rig was concerned, starting resistors were not found to be necessary (perhaps because the generator's rating was double that of the motor) and this aspect of the system's design was not considered further.

5.3 Simulation of Motor Start–up Operation with Specified Capacitor Values and Constant Generator Speed

The generator speed, generator voltage and total bank capacitor value are taken as known, input quantities for the simulation, whose flow–diagram is shown in Fig (5.2). As before (see section 2.3.4), trial asssumptions are made for generator slip and air gap voltage.

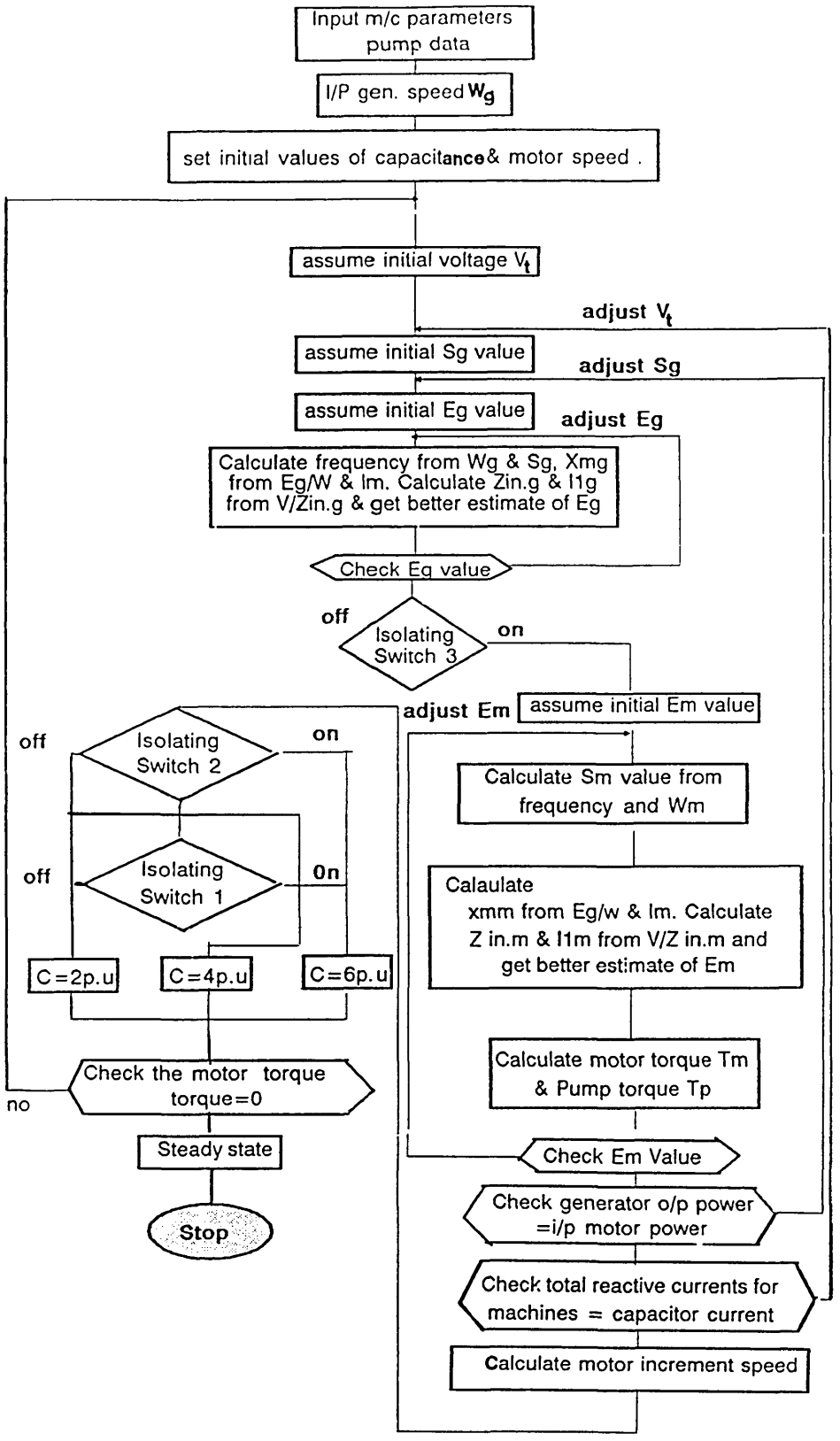

Fig. (5.2) Flow diagram for dynamic simulation with specified capacitor values and constant gen speed.

The generator angular frequency is then calculated from Eq (2−1), the air gap voltage per angular frequency being of course calculated for the inital assumed value of generator air gap voltage and the value of angular frequency calculated from Eq (2.1).

The rest of the calculation procedure for electrical quantities follows the sequence described before in section 2.3.4, except that the motor speed and hence slip are known quantities (viz 0 and 1 respectively initially, values calculated as described below during the start−up acceleration), rather than quantities whose determination requires a further iterative loop.

The new features of the program are:

a) the condition statements determing the operation of the isolating switch S3 and the section capacitor switches S1 and S2. S3 is turned on when the generator terminal voltage is estimated as reaching 1 p.u. S2 is turned off when the generator output current is estimated to have reached 2.2 p.u. This high current criterion was chosen in the light of the short period involved during motor acceleration, and the usefully high value to which the current falls after the extraction of the first, switched capacitor stage. Switch S1 is turned off when the motor speed is estimated to have reached 0.8 p.u and at least 1.0 seconds have elapsed since S2 was switched off.

b) The calculation of the motor's dynamic behaviour. A time−stepping loop surrounds the entire electrical calculation portion of the program. The motor acceleration at each time step is estimated on the basis of calculated motor and pump torques T_m and T_p given by equations (2−11) and (2−13).

The equation used to estimate the motor speed increase during each time step can be written in the form:

$$\delta w_m = \left(\frac{1}{(J_m + J_p + J_w)}\right)(T_m - T_p)\delta_t \qquad (5\text{-}1)$$

where J_m, J_p, J_w are the moment of inertia of the motor, pump and water respectively. The motor's initial speed is of course taken as zero and the motor speed is updated for the next set of electrical calculations. The calculations of moment of inertia of the motor, pump and water are included in the Appendix (4). A time step of 0.1 sec. was found to be satisfatory. The simulation was stopped when the net accelerating torque on the motor–pump shaft was estimated to have fallen to zero.

5.4 Simulation of Motor Start Up with Fully Regulated Capacitor Bank

The motor's starting time can be reduced and its starting conditions improved if, instead of large steps in capacitor occurring, the effective capacitance value is adjusted on a smooth, continuous basis. The particular adjustment strategy investigated here involved the setting of the capacitance value at each time step so as to give a constant, pre–set rate of rise of voltage up to a value corresponding to 1 p.u voltage/ frequency at the end of starting period.

Much of the code is identical to the one used for the case 1] starting process, but a few changes were made since capacitor value must now be calculated at each time step according to the voltage and frequency. Fig (5-3) shows the new flow diagram. It can be observed that the last loop of Fig (5-2) needed to

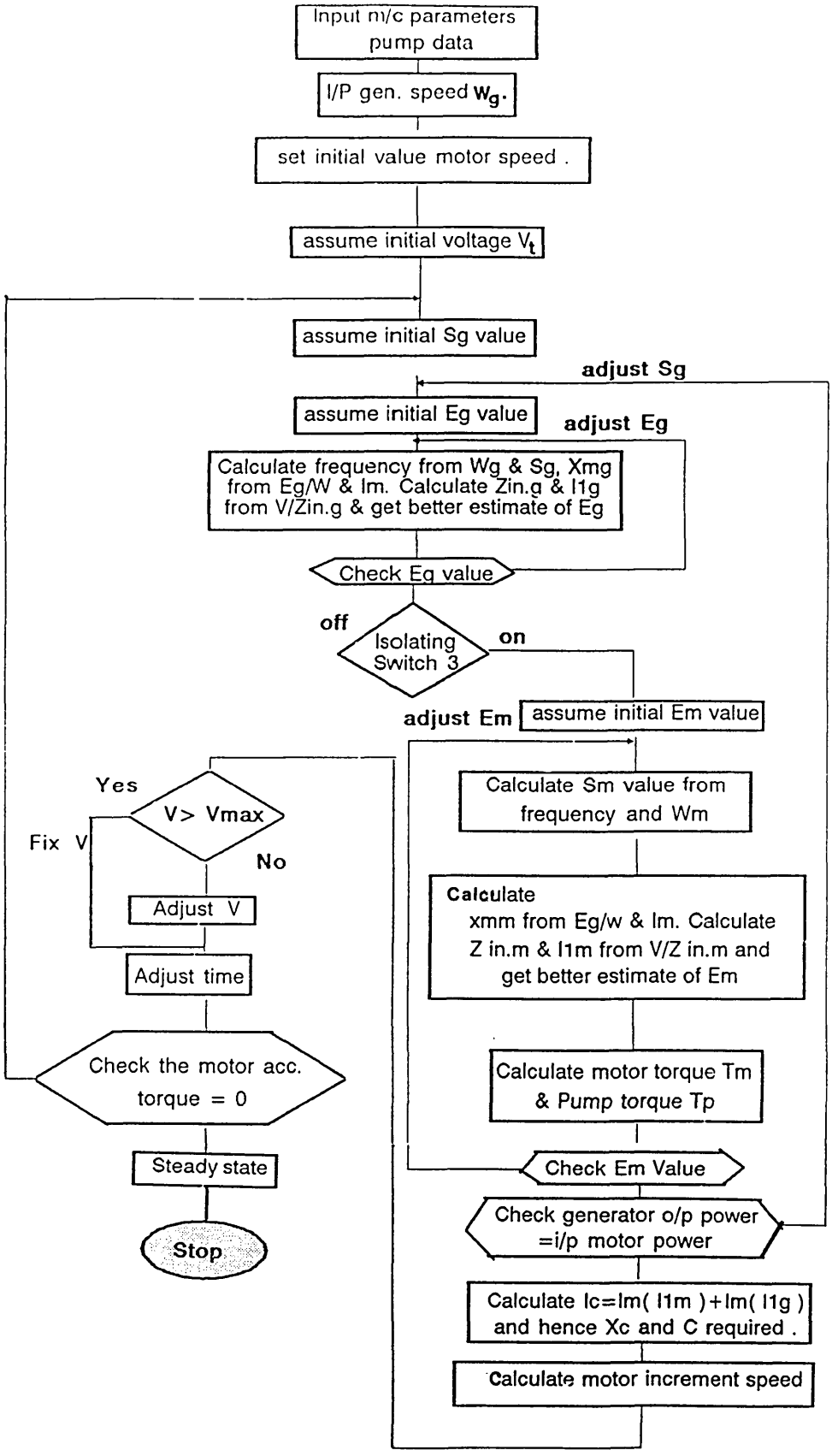

Fig. (5.3) Flow diagram for dynamic simulation with fully regulated capacitor bank and constant gen speed.

achieve VAr matching between the machines and the capacitor bank is now replaced by a simple calculation of the capacitor current I_C needed to supply the already–calculated reactive components of the generator and motor currents. The corresponding capacitance per phase is then found from I_C/V_tW.

5.5 Minimum Capacitance for the Voltage Collapse Avoidance

Fig (5.4) shows on a base of generator–speed the calculated value of capacitance needed to ensure that the voltage just after closing the motor isolating switch S3 exceeded 0.1 p.u. This was found to be the minimum voltage for avoidance of voltage collapse for the particular system examined. Fig (5.4) also shows an experimentally determined curve of minimum capacitance required to avoid complete voltage collapse on closing S3 versus generator speed. The difference between the two is probably mainly due to the difference between the criteria used (10% voltage as opposed to virtually 0% voltage).

5.6 Motor Start–Up Simulation Results with Switched Capacitor Bank (Case 1)

The following results all refer to a single scheme's (scheme 'B') start up behaviour. The generator shaft speed chosen was 0.8 p.u (constant). This choice of generator speed is believed to represent a typical value at which satisfactory motor start–up would occur. A lower figure would require an excessive total capacitance in order to avoid voltage collapse when the motor is first connected. A higher figure gives easier conditions electrically but would

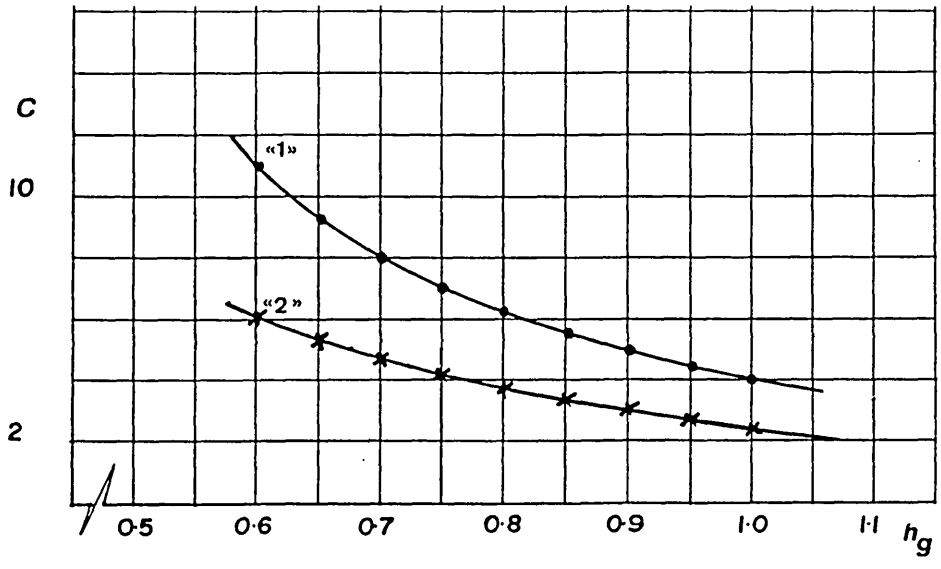

Fig. (5.4) (1) The calculated capacitances values needed to ensure that the voltage exceeded 0.1 p.u. just after closing s3

(2) The exp. min. capacitances values required to avoid complete voltage collapse on closing s3 .

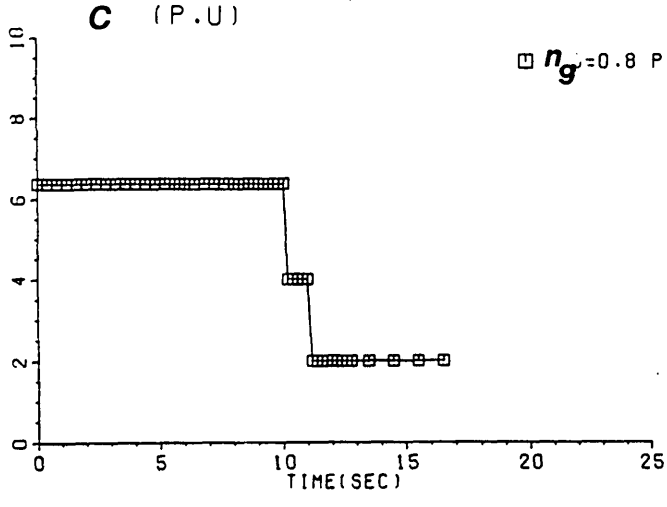

Fig. (5.5) Capacitance C (p.u)

imply an absence of pumping for an excessive part of the lower wind speed range. The three total capacitance values adopted in the simulations are shown in Fig (5.5). The values are 6.372 p.u (S1 and S2 closed), 4 p.u (S2 open, S1 closed) and 2 p.u (S2 and S1 open), corresponding to capacitor bank values of 2 p.u, 2 p.u and 2.372 p.u. The simulation starts with motor isolating switch S3 closed and the generator shaft speed set at the desired value (taken as 0.8 p.u in what follows). The steady state operating conditions for the system are then calculated assuming the motor to be at standstill. The motor acceleration process is then allowed to proceed, typical results being shown in Figs (5.6) to (5.9). The t=0 point on all graphs corresponds to the instant of S3 closure.

The figures correspond to a self–excitation, open circuit voltage of 1 p.u (i.e. with S3 open), and the total capacitance value of 6.372 p.u was chosen to give this particular voltage. Fig (5.6) shows how the terminal voltage builds after S3 closure from 0.12 p.u. The simulation predicts that 10.2 sec only elapses while speed and voltage build until the generator current reaches the threshold 2.2 p.u value. S2 then opens giving a voltage drop to 0.72 p.u. A further quick build–up of voltage then occurs until 2.2 p.u generator current is again obtained. S1 then opens and a final quick build–up of voltage to the final steady state value of 0.8 p.u then occurs. The rapidity of the later changes is caused by the relatively high motor torques and accelerations at the higher voltage and low slips. A satisfactory explanation is difficult to find for the behaviour of the slip at the 6 second point. A similar effect was observed experimentally. Figs (5.7), (5.8) and (5.9) show the capacitor VArs and the reactive requirements of both generator and motor. It can be seen that the motor needs a high reactive power at starting in comparison to the generator,

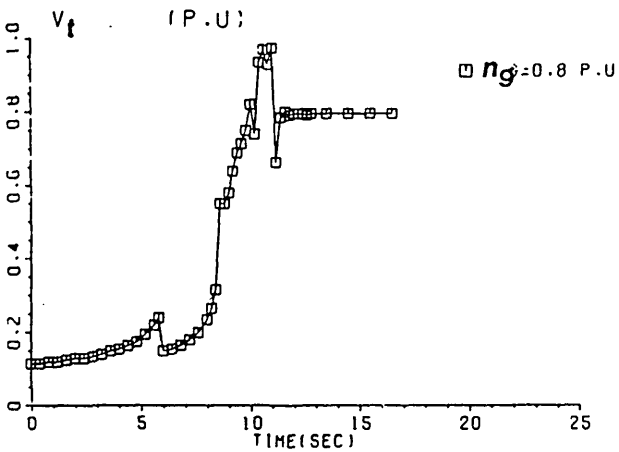

Fig. (5.6) Generator voltage

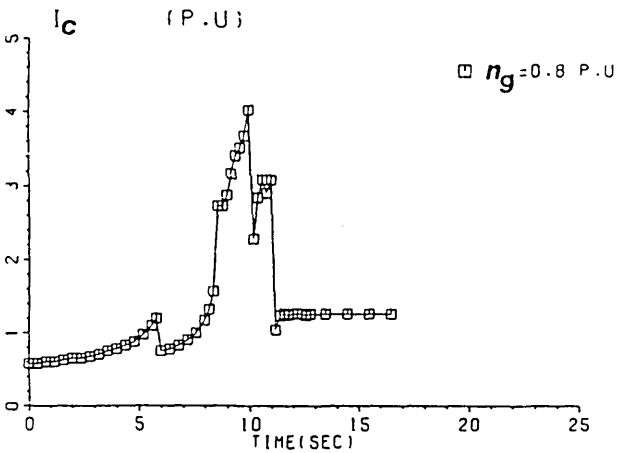

Fig. (5.7) capacitive current

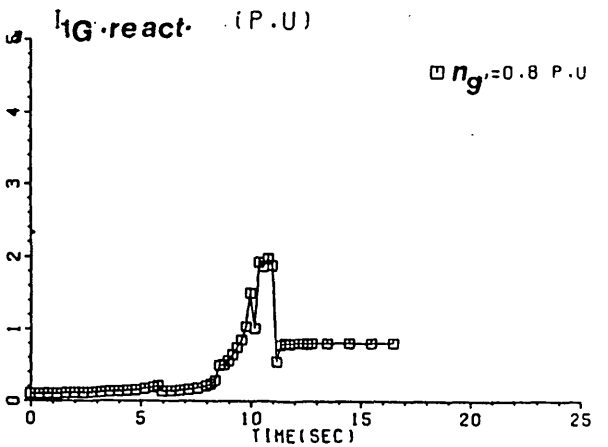

Fig. (5.8) Reactive component of gen. current

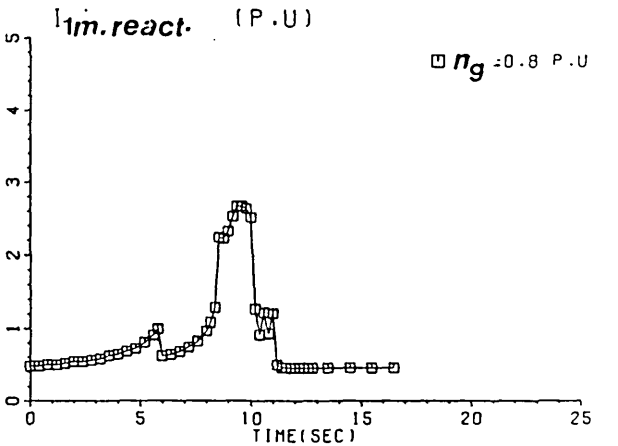

Fig. (5.9) Reactive component of motor current

and that the opening of S2 and S1 is vital to avoid over-excitation problems and the risk of capacitance failure.

The steady state motor VAr demand is less than the generator VAr demand due to the lower magnetizing reactance and higher magnetizing current of the generator, due in turn to its larger rating. Figs (5.10), (5.11), (5.12) and (5.13) show the air gap voltage per frequency, and the magnetizing reactance for both generator and motor. Although the frequency is nearly constant during the starting period, the motor air gap voltage per frequency is lower than generator air gap voltage per frequency within the first ten seconds, due to the higher stator impedance drop in the motor. As the motor accelerates and its impedance increases, the final steady state value of motor air gap voltage/frequency remains lower than that in the generator, even though the final generator current is higher because the motor stator resistance and reactance are higher. It can be seen that the final steady state values of magnetizing reactances differ (2.28 for the motor, 1.27 p.u for the generator), partly due to the generator is higher rating and partly to its somewhat lower magnetization curve. Figs (5.14), (5.15), (5.16) and (5.17) show generator current, motor current, gen. slip and motor slip. The high motor starting current can be observed, as can the effect on the currents of opening switches S1 and S2. Fig (5.16) shows that the generator slip remains little changed until the motor is nearly up to speed. The final steady state generator and motor slips are 0.012 and 0.024 respectively.

Figs (5.18) and (5.19) show the motor and pump torques. The difference between these torques, the net accelerating torque on the motor pump shaft, is shown in Fig (5.20). Fig (5.21) shows the motor shaft and pump speed. The

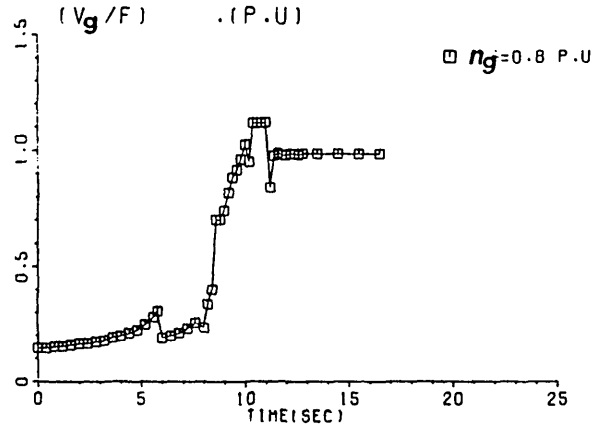

Fig. (5.10) Gen. air gap voltage per frequency

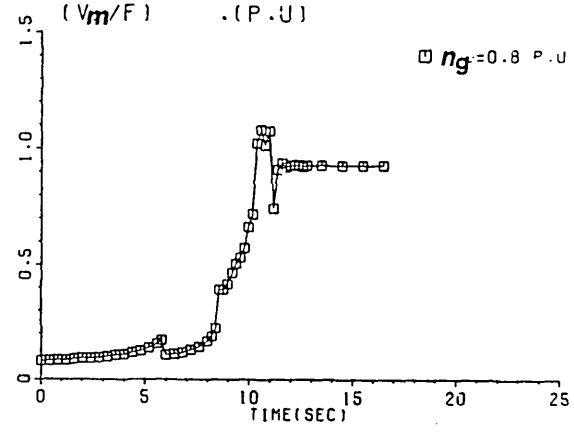

Fig. (5.11) Motor air gap voltage per frequency

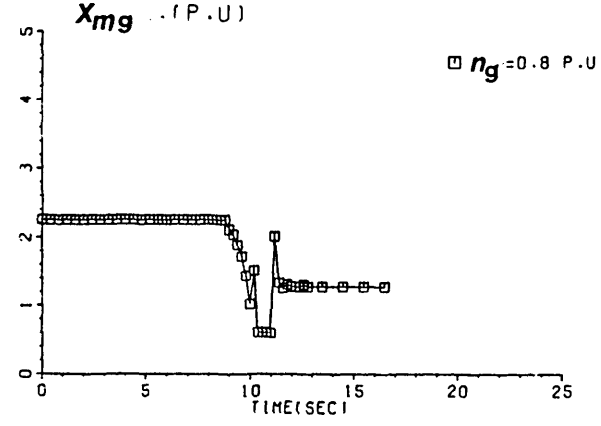

Fig. (5.12) Generator magnetizing reactance

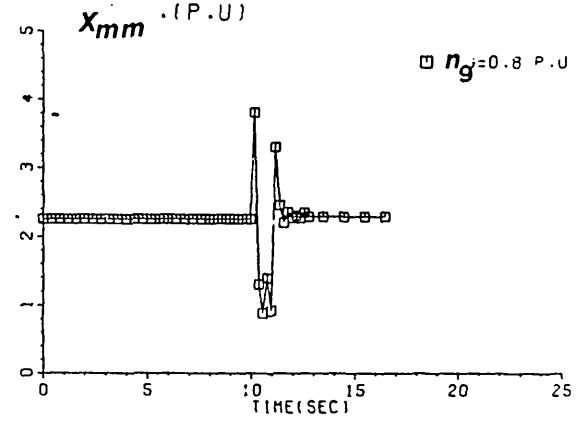

Fig. (5.13) Motor magnetizing reactance

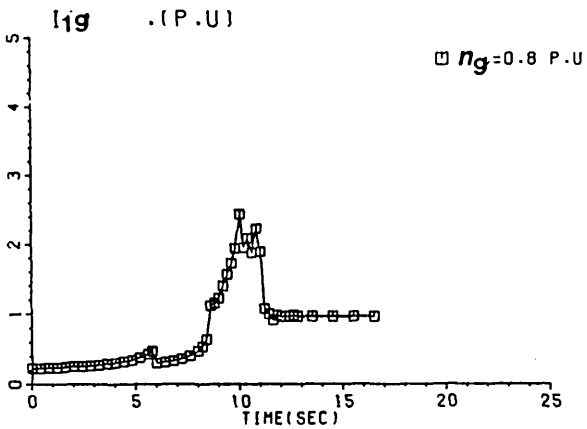

Fig. (5.14) Gen. current

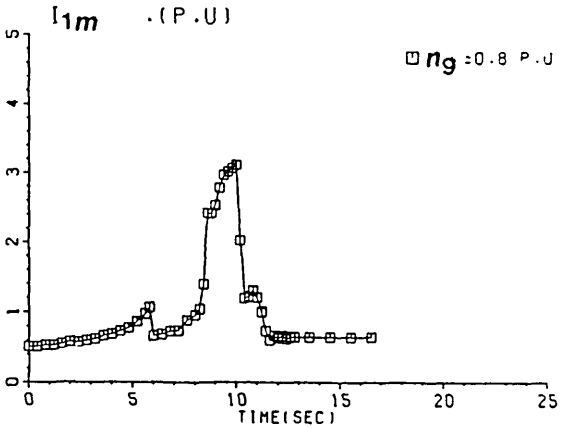

Fig. (5.15) Motor current

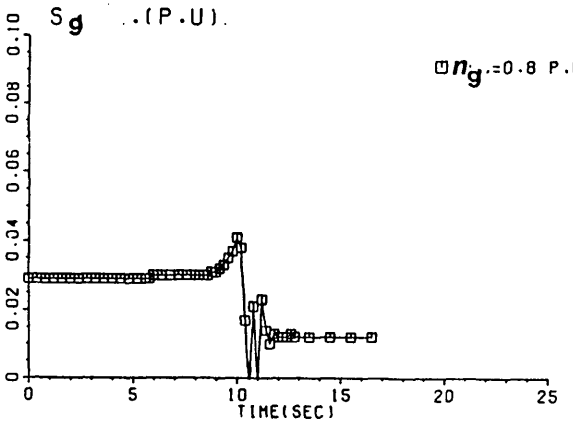

Fig. (5.16) Generator slip

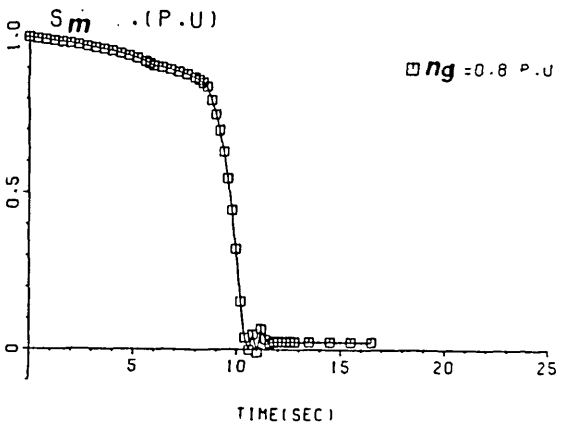

Fig. (5.17) Motor slip

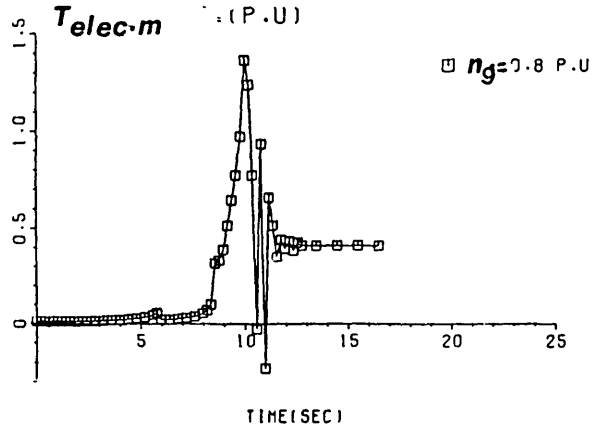

Fig. (5.18) Elec. i/p torque to the motor

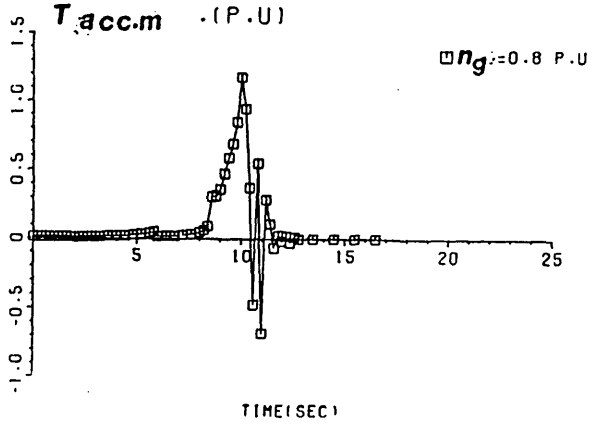

Fig. (5.20) Acceleration torque for the motor

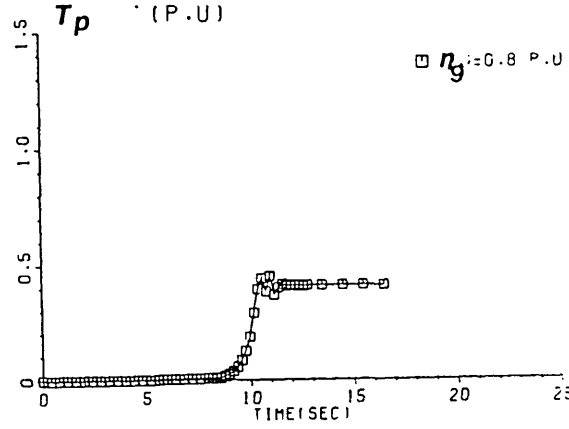

Fig. (5.19) Pump torque

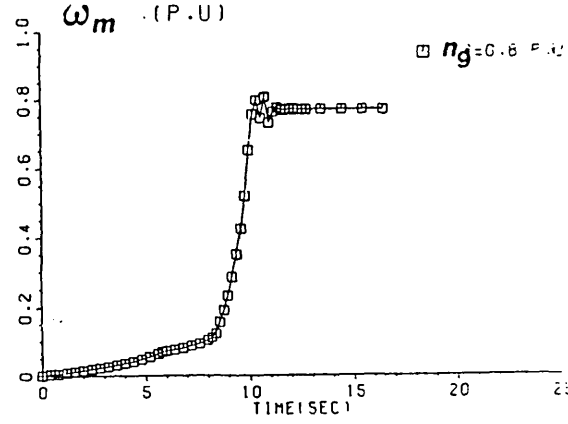

Fig. (5.21) Motor speed

electric torque produced by the motor is initially low (0<t<8.0 secs) due to the low voltage. This may cause problems in practice with pumps having appreciable friction. In the simulation, the torque absorbed by the pump is taken as zero at zero speed so motor acceleration nevertheless occurs. Most of the motor pump acceleration process occurs fairly quickly (8.0 < t < 10.0 secs).

Switching out C2 (2.372 p.u) reduces the motor electric torque to −0.03 p.u corresponding to motor and gen. slips equal to −0.001 and −0.004 respectively. The motor torque oscillates for 1.0 sec and then reduces to 0.35 p.u when C1 (2 p.u) is subsequently switched out; the torque oscillates again for another 1 sec before finally reaching steady state. The motor speed oscillations caused by the torque oscillations during the period 10 to12 sec can be observed on Fig (5.21). The final steady state speed is 0.77 p.u. Fig (5.21) also shows the high acceleration rate achieved in the previous period (8.0 < t < 10.0 secs) due to the high accelerating torque shown in Fig (5.20). The motor slip interestingly is predicted to become slightly negative value (−0.001) for a short period just after C2 is switched out. During this period, Fig (5.16) shows that a corresponding reduction in generator slip (hence output power etc) occurs. Figs (5.22) and (5.23) show mechanical input power to the generator and electrical output power from the generator. The max input power required, 1.75 p.u, occurs just before C2 capacitor is switched out. It then reduces to 0.24 p.u at t=10.6 secs, then oscillates and reaches a steady state of 0.475 p.u at t = 12.8 secs. The generator output power behaves similarly, reaching steady−state value of 0.366 p.u corresponding to a generator efficiency of 77%, as shown in Fig (5.24). Fig (5.25) shows that the generator power factor stays low, 0.37 p.u, during the first 8 secs. (due to the relatively low output current and voltage), but then increases with the voltage build to 0.78 p.u just before

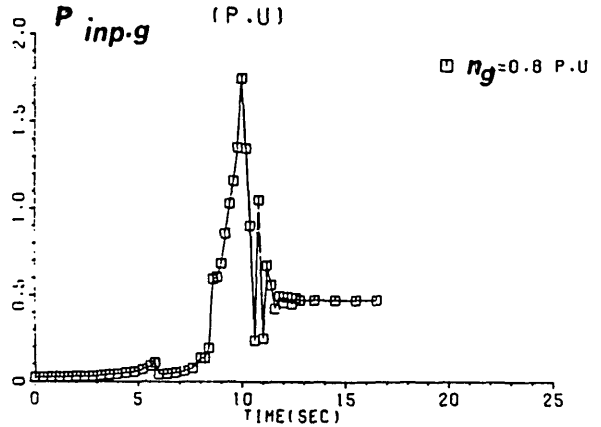

Fig. (5.22) Mech. i/p power to the gen.

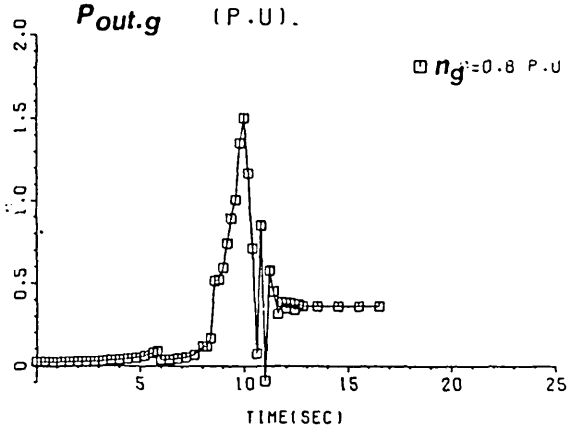

Fig. (5.23) Elec. o/p power to the gen.

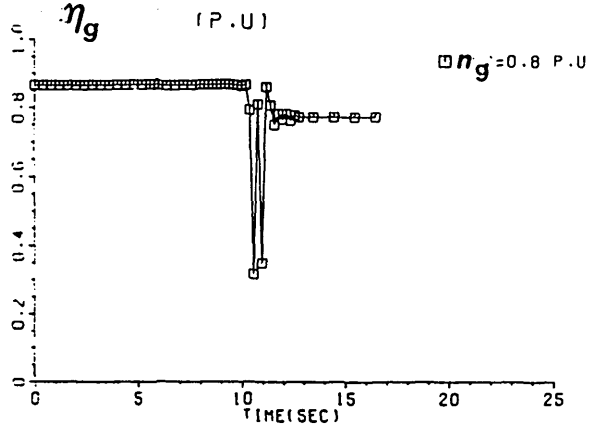

Fig. (5.24) Efficiency of the gen.

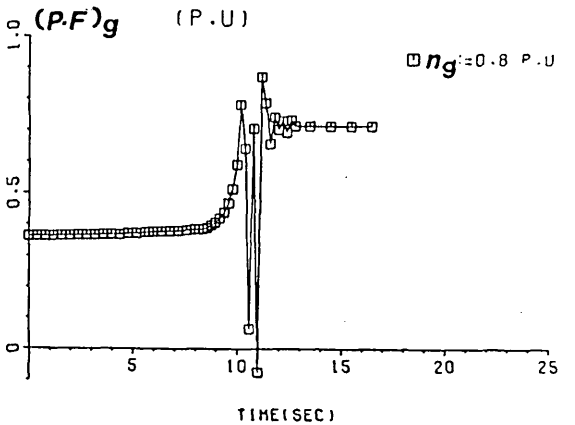

Fig. (5.25) Power factor of the gen.

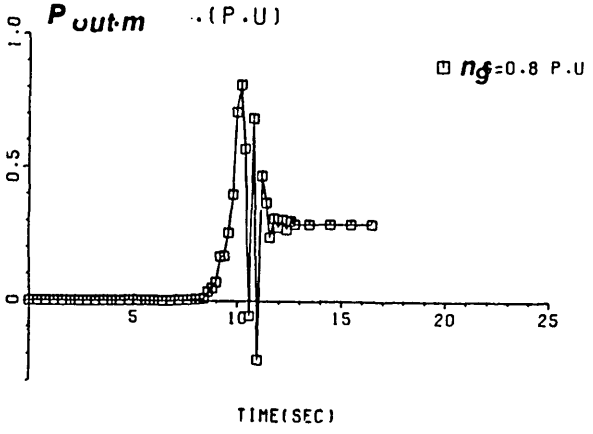

Fig. (5.26) Mech. o/p power of the motor

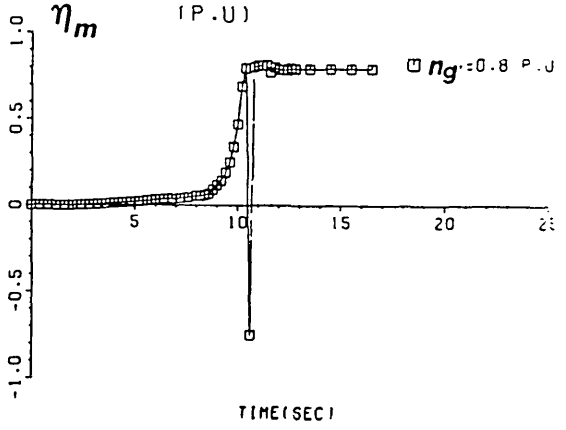

Fig. (5.27) Efficiency of the motor

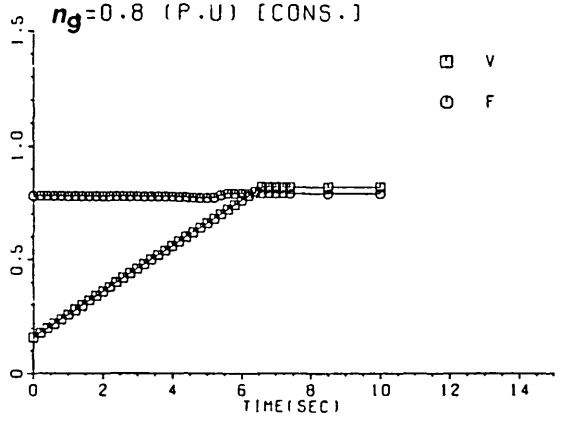

Fig. (5.28) Generator voltage and frequency

C2 switch−out. The final generator steady−state power factor is 0.71 p.u. Fig (5.26) shows the motor's output mechanical motor power. The short power reversal during the negative slip period can be observed. The final steady state output power is 0.29 p.u leading to a steady−state motor efficiency of 79% as shown in Fig (5.27). Note that the relatively low final motor power is caused by the original choice of generator speed 0.8 p.u and by the cubic power relation of the pump (the latter being sized to give approx 1 p.u power at 1 p.u speed). The overall electrical efficiency of the system is approximately 61%.

In general, the start−up behaviour of the laboratory rig has been observed to follow, in a qualitative sense, the theoretical results presented here.

5.7 Dynamic Response Results of On−Load Operation with Fully Regulated Capacitor Bank

Predictions were again made for the case of 0.8 generator shaft speed, and the motor was again initially isolated via the inclusion of the isolating switch S3 in the system. The initial value of capacitance was chosen to give a generator voltage, with S3 open , of 1 p.u. The isolating switch is closed when the voltage reaches 1 p.u and the capacitance value is then continuously adjusted so that the voltage follows a predetermined trajectory. The trajectory chosen is shown in Fig (5.28). The initial voltage (0.16 p.u) was in fact the value to which the voltage sank at initial S3 closure. The rate of voltage increase (0.2 p.u per sec) was chosen as giving satisfactory starting performance (a lower value leading to excessive starting time, a higher value giving motor stall and possibly voltage collapse risks). The simulation predicts a 6.6 sec period for the voltage to attain 0.82 p.u. After this point, the capacitance is adjusted so

as to maintain constant voltage, in line with a V/F ratio of approximately 1.0, given the steady state output frequency of 0.79. Fig (5.29) shows how the capacitance per phase would have to be varied in order to achieve this. The capacitance required would be approximately constant at 6.37 p.u for the first four seconds, would then decrease sharply to 1.52 p.u and finally increase again gradually to a final value of 2.14 p.u. The shape of Fig (5.29) suggests strongly that two fixed capacitance values (viz 6.37 and 2.14 p.u) will suffice, at least for operation at 0.8 p.u generator speed. The switchover from high C to low C would seen to be best done at the 5 sec point. (Section 4 describes the need for a further fixed C stage to cater for lower generator speeds). Figs (5.30), (5.31) and (5.32) show the capacitor current, and reactive current for motor and generator.

It is clear that the reactive requirement for the motor during the first 4 sec is higher than the reactive requirement for the generator, so the motors KVAr absorption accounts for most of the capacitor bank's KVAr output. Although the reactive component of the motor current starts to decrease after 4.4 secs as the motor slip decreases substantially, the reactive component of generator current steadily increases due to increase in terminal voltage .

Figs (5.33), (5.34), (5.35) and (5.36) show the ratio of air gap voltage to frequency for both generator and motor and the machines' magnetizing reactances. As mentioned before, the generator air gap voltage V_g is higher than the motor air gap voltage, particularly during the first 6 secs, due to the higher motor current and the higher motor stator impedances. Fig (5.35) shows that the generator magnetizing reactance is constant at its unsaturated values (i.e. for first 4 secs) when the generated voltage is below approximately

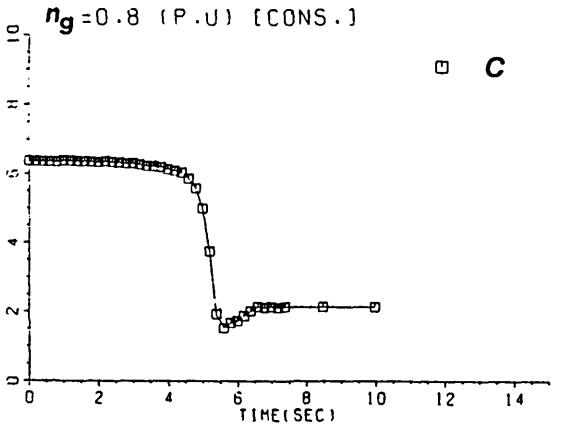

Fig. (5.29) Capacitance C (p.u)

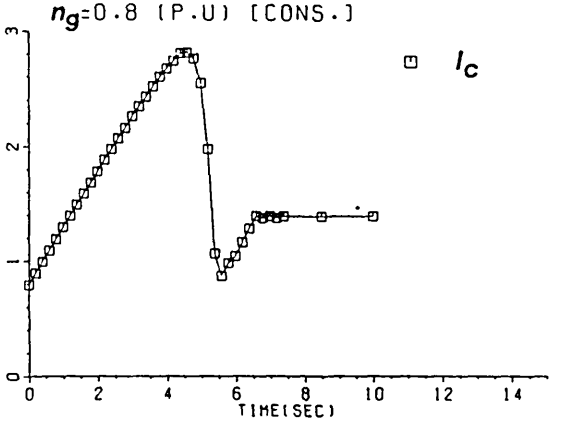

Fig. (5.30) capacitive current

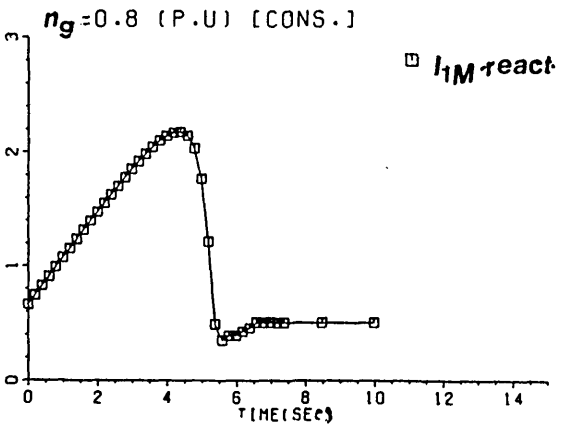

Fig. (5.31) Reactive component of motor current

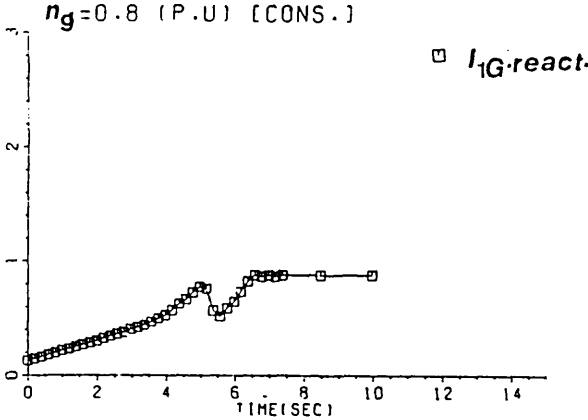

Fig. (5.32) Reactive component of gen. current

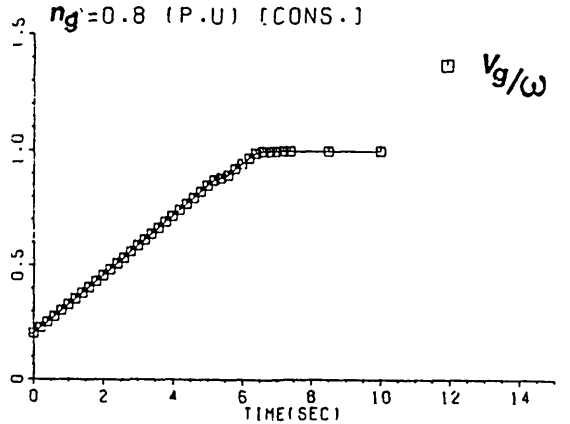

Fig. (5.33) Gen. air gap voltage per frequency

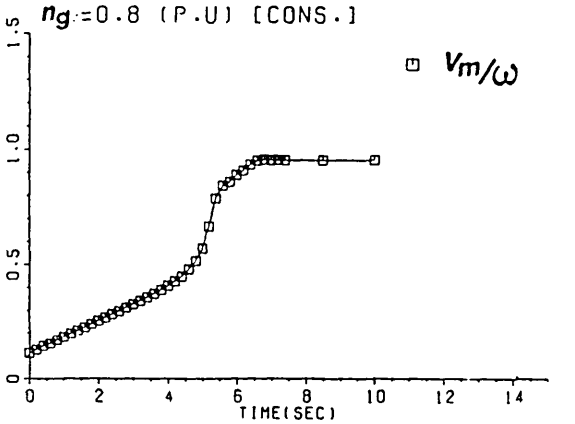

Fig. (5.34) Motor air gap voltage per frequency

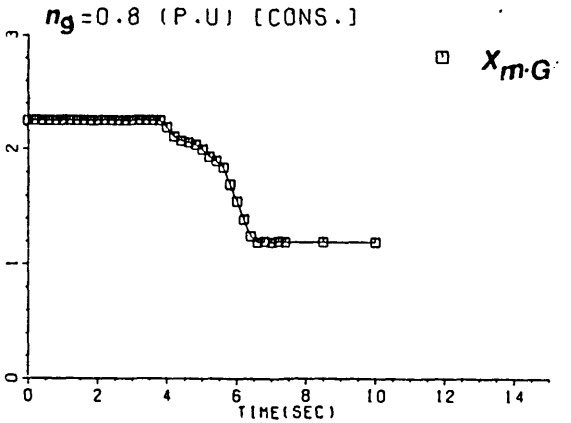

Fig. (5.35) Generator magnetizing reactance

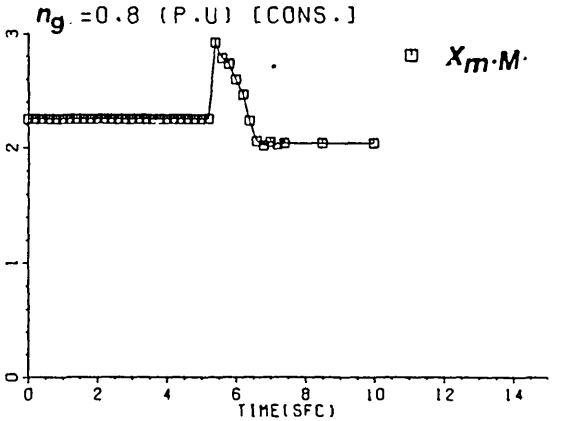

Fig. (5.36) Motor magnetizing reactance

0.56 p.u. After 4 seconds, the further increase in V/F (caused by the steady increase in V in the face of a virtually constant frequency) causes a saturation–induced fall–off in magnetising reactance. Fig (5.36) shows a similar initial pattern, but the motor's final state is virtually unsaturated due to its considerably higher saturated air gap voltage/frequency. The temporary rise in X_{mm} during $4.6 < t < 6.2$ is thought to be due to a shortcoming of the prediction technique.

Figs (5.37), (5.38), (5.39) and (5.40) show the variation of generator current, motor current, generator slip and motor slip against time. The 'soft start' nature of the voltage control strategy is seen to limit the starting current to 2.6 p.u (instead of the usual 5 or 6 p.u), but the motor acceleration in the final phase of the starting period is nevertheless quite satisfactory. The generator current is lower for the reason stated in respect of Fig (5.32). Fig (5.39) shows that the generator slip stays satisfactorily low during the entire starting period, only increasing above 3% when the motor is absorbing peak power near its pull–out speed. The final steady–state current values for motor and generator are 0.688 p.u and 1.0 p.u. The corresponding generator and motor slips are 0.011 p.u and 0.024 p.u respectively. Fig (5.41) shows the motor electric torque and pump torque against time. The difference between these torques, the net accelerating torque on the motor/pump shaft against time, is shown in Fig (5.42). The motor shaft and pump speeds are also shown. Due to the pump's square law characteristic, the torque absorbed by the pump remains less than 0.1 p.u as its speed increases during the first 4 secs from zero to 0.3 p.u. The net accelerating torque on the motor/pump shaft is hence virtually equal to the electric torque produced by the motor. A slight oscillation in the motor electric torque as it settles into its steady state value is observable on Fig

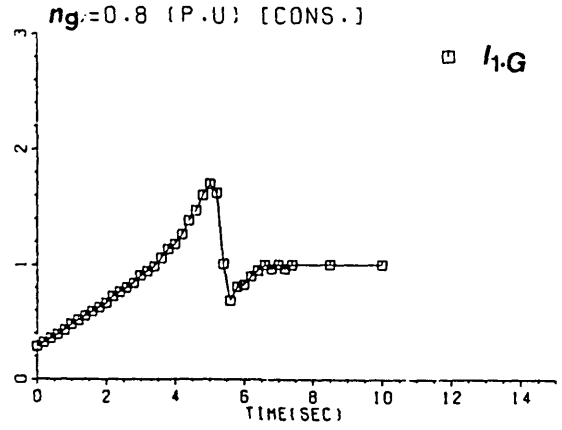

Fig. (5.37) Gen. current

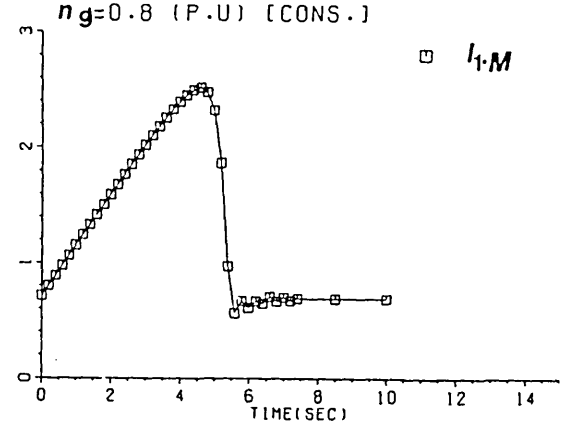

Fig. (5.38) Motor current

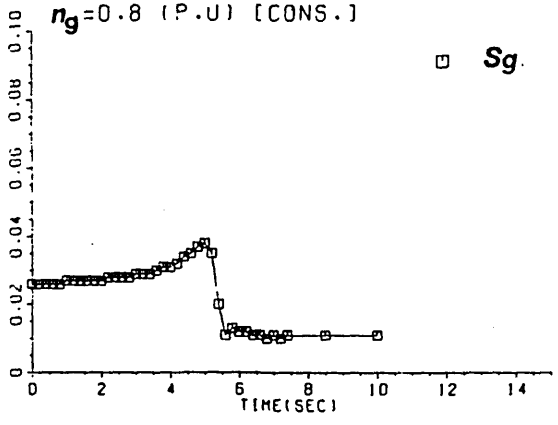

Fig. (5.39) Generator slip

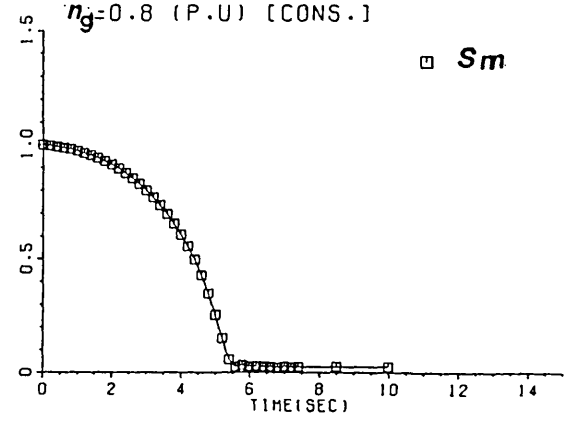

Fig. (5.40) Motor slip

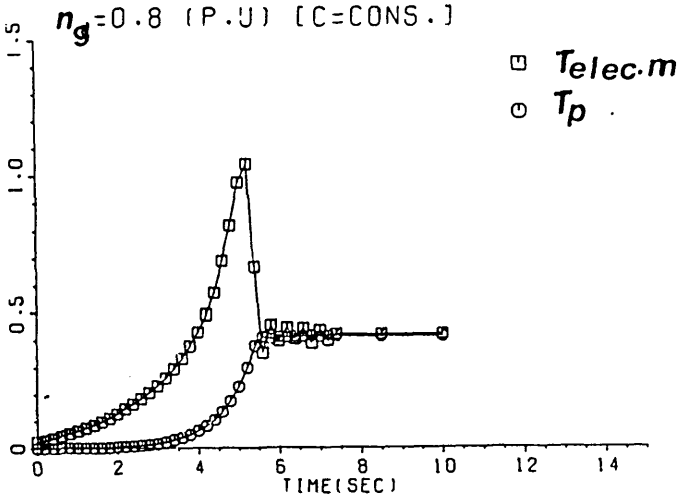

Fig. (5.41) Elec. i/p torque to the motor and pump torque

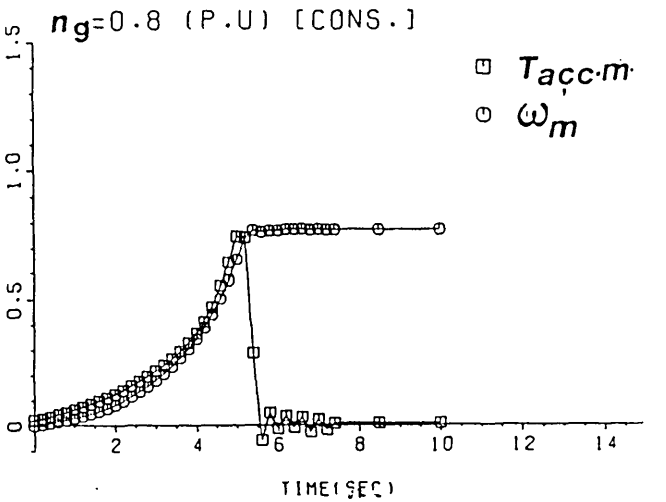

Fig. (5.42) Acceleration torque for the motor speed

(5.41). The steady−state motor speed of 0.77 is obtained after a total starting period of 7.5 secs.

Fig. (5.43) shows the variation of mechanical input power and electrical output power of the generator against time. A peak in each curve corresponding to the motor's peak accelerating period around pull−out slip is evident. Fig (5.45) shows the generator efficiency and generator power factor against time. The generator efficiency stays remarkably constant (η_g = 87.7%) during the first phase of the starting process, due probably to the generator's virtually constant slip and constant rotational losses (w_g = constant). The generator final steady state loss was 77.4%. Fig (5.45) shows the expected dependency of the generator power factor on output power and a final steady−state power factor value of 0.668. Fig (5.44) shows the variation of the electrical power and the mechanical output power of the motor against time. The motor's appreciable losses (mainly I^2R) during the starting period can be observed. Fig (5.46) shows the expected variation of motor efficiency. Its final steady−state value is 0.786.

A set of predictions for a lower, constant generator speed (0.7 p.u) was also made for comparison purposes. The starting capacitance value was chosen to give the same initial voltage (after closure of S3) as before (0.167 p.u). Figs (5.47) to (5.52) present the theoretical results of the starting process at both 0.8 and 0.7 p.u generator shaft speeds. A higher rate of rise of voltage than before was selected (see Fig 5.47) as the lower system frequency was expected to lead to higher motor torques per air gap power. The plateau value of voltage was set at 0.7 instead of 0.8 so as to give a final V/F of approximately 1 as before.

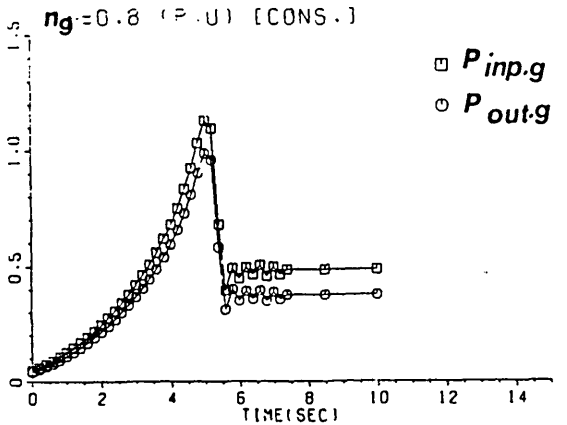

Fig. (5.43) Mech. i/p power and elec. o/p power to the gen.

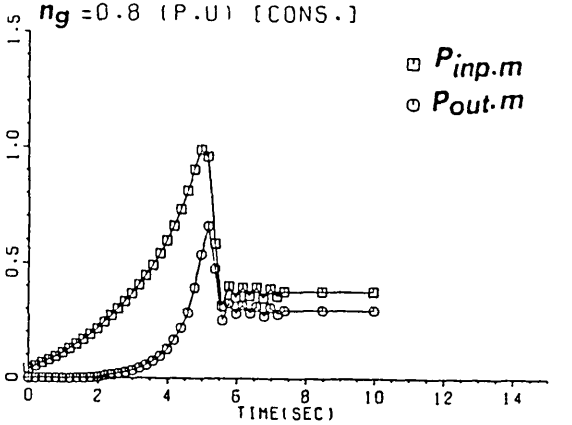

Fig. (5.44) Elec. 1/p power and mech. o/p power of the motor

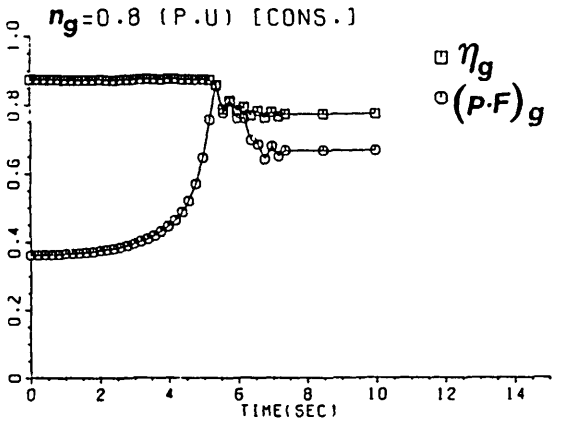

Fig. (5.45) Efficiency and power factor of the gen.

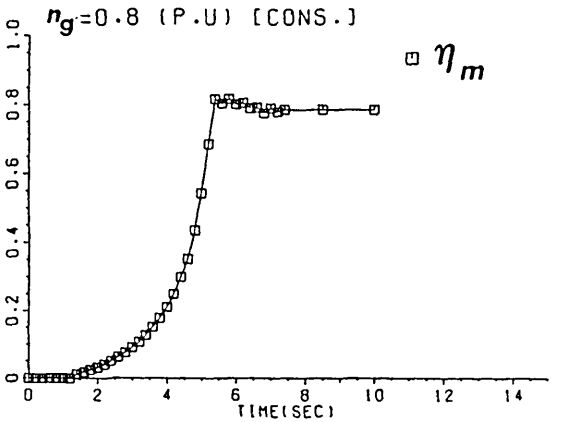

Fig. (5.46) Efficiency of the motor

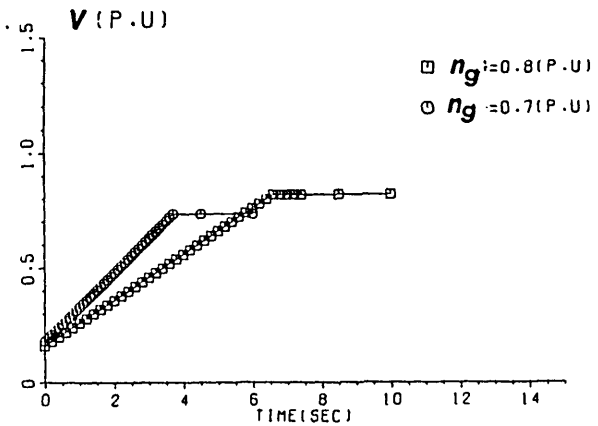

Fig. (5.47) Generator voltage

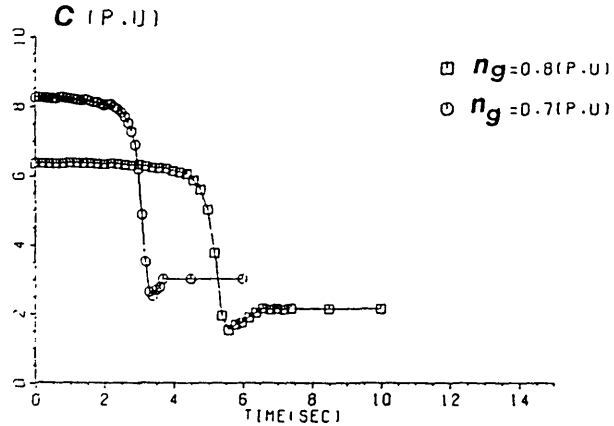

Fig. (5.48) Capacitance C (p.u)

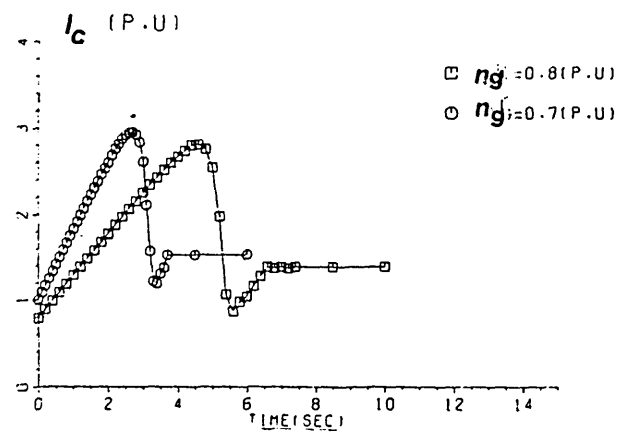

Fig. (5.49) Capacitive current

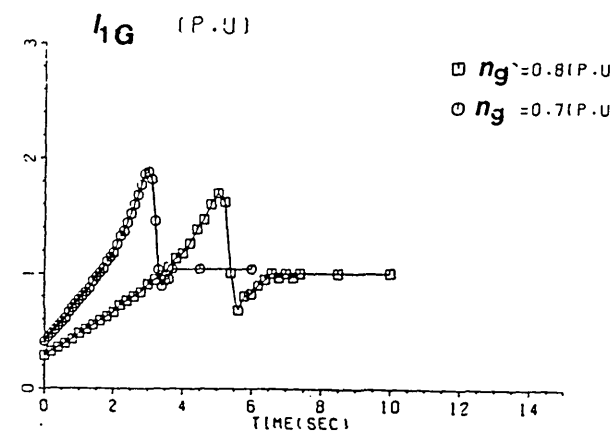

Fig. (5.50) Gen. current

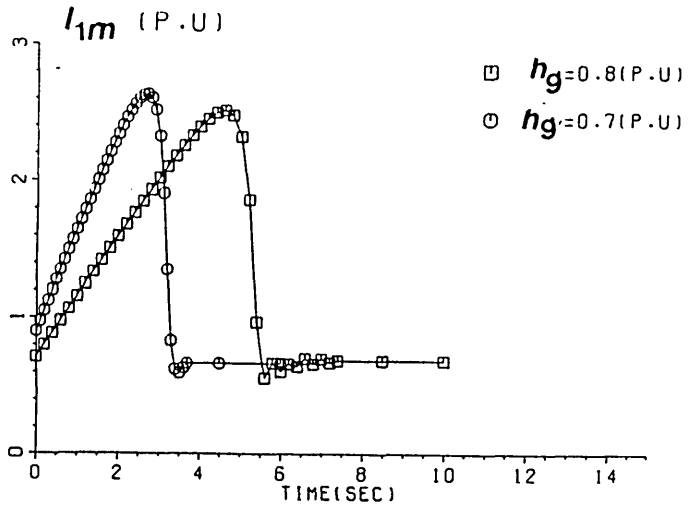

Fig. (5.51) Motor current

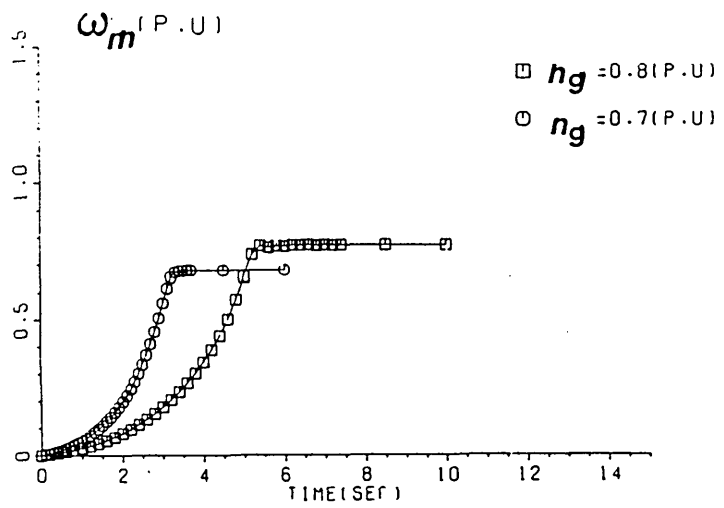

Fig. (5.52) Motor speed.

The motor was found to start satisfactorily with the higher dv/dt. Fig (5.48) shows, as expected, that a larger capacitor value is required both for starting and for running at the lower generator shaft speed, while Fig (5.49) shows that a somewhat higher maximum capacitor current (2.96 p.u) results as expected. Fig (5.49) shows the variation of capacitor current againt time. Figs (5.50) and (5.51) show the variation of the generator and motor currents against time at the same two generator shaft speeds. The steady state currents seem to be very little affected by the change in generator speed under the conditions chosen, in spite of the significant differences between the pump powers and torques. This probably stems from the dominance of the magnetizing currents under part-load conditions, (part load, saturated conditions in the case of the generator. Fig (5.52) shows the variation of motor shaft speed against time. The influence of the faster, preset dv/dt on reducing the motor starting time is clearly evident.

CHAPTER 6

SYSTEM BEHAVIOUR DURING MOTOR STARTING WITH CONSTANT WIND SPEED

6.1 Introduction

So far discussion of the scheme's operation has been restricted to specified generator shaft speed conditions. In this chapter, the simulation is extended to incorporate the wind turbine. The turbine is modelled using standard relations and the operation of the entire system studied for the particular case of start up behaviour under constant wind speed conditions.

Two capacitor conditions were examined:

a) Fully controlled capacitor bank, adjusted to provide a constant rate of rise of voltage, with rated voltage per frequency at the end of starting period.

b) Two section, unregulated capacitance bank.

A basis for the choice of gear box ratio is described in this chapter, together with a technique for determining the turbine torque referred to the generator shaft. Wind velocity is treated here as constant input quantity, though the code described could be used immediately if desired for system simulation under arbitrary, time–varying wind speed conditions. As will be seen, the results show how both start up behaviour and running performance are affected by wind speed. The simulation technique can hence help to determine the

optimum wind speed range for a given design installation, or conversely can help to arrive at a good installation design for a given wind regime.

6.2 Analysis

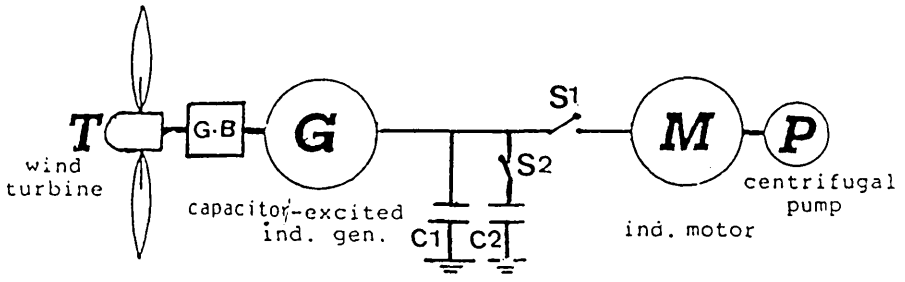

Fig. (6.1) Simplified system schematic
(note : switch states are for no load condition)

The simplified system schematic of the wind–electric pumping scheme is shown in Fig (6.1). As before, the dynamic prediction technique is based on the steady state, single phase equivalent circuit which is shown in Fig (2.2). If the use of quasi steady–state simulation basis is acceptable for most of the conditions experienced during system operation with a constant generator shaft speed, it is felt that it is also valid under varying generator shaft speed conditions, because for virtually all practical wind turbines, rates of change of turbine speeds are low.

The standard expression for turbine torque, derived in appendix A1, is:

$$T_{tur} = 0.5\ (K_g/w_g)\pi\cdot\rho\cdot R^2\cdot C_p(\lambda)\cdot V_w^3 \qquad [6\text{-}1]$$

where

k_g = gear box ratio

w_g = generator angular speed

ρ = air density

R = wind turbine radius

C_p = power coefficient

λ = tip−speed ratio

V_w = wind speed.

The theoretical results reported in this chapter were predicted for a system driven by a typical 3 bladed, 5 meter diameter wind turbine having a C_p versus λ characteristic shown in Fig A1−2 [1− 17].

For the system studied with fully regulated bank (designated as system 'A'), the two machines were identical, each being a 3 phase, 6 pole, 220v, 3.7 Kw, 16A induction machine. The base values and induction machine parameters are shown in Appendix (3). For the system studied with a 2 section unregulated capacitor bank (designated as system 'B'), the generator and motor were the 11 Kw and 5.5 Kw machines described in chapter 3. The estimated steady performance of scheme A is not included comprehensively in this thesis but is presented in reference [1−60]. The analysis techniques described in chapter 2 were used in each case. The steady state performance of scheme 'B' was presented in chapter 3.

6.3 Power and Torque Characteristics of the Wind Turbine

6.3.1 Selection of Gear Ratio "K_g"

Many factors in practice affect the selection of K_g. A very much simplified basis for K_g selection is to decide on the wind speed $V_{w(op)}$ at which rated current, rated voltage and frequency is required. The turbine speed w_{tur} for operation at this wind speed is then calculated

$$w_{tur} = \frac{\lambda\alpha \, V_{w(op.)}}{R} \qquad [6\text{-}2]$$

where the value of λ used (λ_α) corresponds to operation just to the right of the peak C_p point to reduce undesirable stalling risk. The corresponding generator speed chosen $w_{g(op.)}$ is that which results in rated voltage, current and frequency in the generator. The gear ratio is then found from

$$K_g = \frac{w_{g(op.)}}{w_{tur.}} = \frac{w_{g(op.)} \, R}{\lambda\alpha \, V_{w(op.)}} \qquad [6\text{-}3]$$

It is assumed that, if higher wind speeds are encountered, aerodynamic means will be employed to limit shaft speeds.

On this basis, a K_g of 22.1 was chosen, corresponding to a generator speed of 1080 r.p.m., a wind speed of 3 m/sec and a $\lambda\alpha$ of 4.3. Note that the low V_w corresponds to a wind regime for a typical Egyptian site.

6.3.2 Starting Turbine Torque

The turbine's starting torque can either be obtained from the turbine's characteristic C_Q versus λ curve where C_Q is the torque coefficient, or if this is not available from the initial slope of the C_p versus λ curve as follows:
The relation between tip speed ratio λ and turbine speed w_{tur} is

$$\lambda' = \frac{R}{V_w} \cdot w_{tur} \tag{6-4}$$

The slope of the C_p curve is

$$\frac{dC_p}{d\lambda} = \frac{C'_p}{\lambda'}$$

where C'_p and λ' are corresponding values at very small C_p and λ. Hence

$$C'_p = \frac{dC_p}{d\lambda} \cdot \lambda' \tag{6-5}$$

Sub. Eq. (6-4) into Eq. (6-5), gives:

$$C'_p = \frac{dC_p}{d\lambda} \cdot \frac{R}{V_w} \cdot w_{tur}. \tag{6-6}$$

This is now substituted, along with $w_g = K_g \cdot w_{tur}$ into Eq [6-1] and gives the following relation for the turbine starting torque:

$$T_{tur} = 0.5\ \rho\pi R^3 \frac{dC_p}{d\lambda} V_w^2 \tag{6-7}$$

where

$\frac{dC_p}{d\lambda}$: is the initial slope of the turbine's part of C_p versus λ curve.

Simple subroutines, whose flow charts are shown in Fig 6.2 and which calculate turbine torque and power, were written. In the flow diagram, initial values of wind speed and generator speed are treated as input. The tip–speed ratio λ is calculated from Eq [6-3]. The corresponding power coefficient is then calculated from either Eq [6-5] (for $\lambda <$ some λ'' below which the λ versus C_p curve is linear {1.25 in the present case}) or from the $C_p - \lambda$ curve itself if $\lambda > \lambda''$. The turbine torque $T_{tur.}$ is calculated using the standard torque relation (Eq 6-1) and turbine power calculated from

$$P_{tur.} = T_{tur.} \cdot w_g \qquad (6\text{-}8)$$

The calculations are repeated at fixed shaft speed increments (here chosen as 0.05 p.u) until the required max value ($w_g \leq 1.5$ p.u) is reached. The entire calculation can then be repeated as desired for other wind speeds. The wind rotor torque and power are outputted in per unit form. Fig (6.3) shows the calculated per–unit values of wind rotor torque referred to the generator shaft against generator speed at a series of wind speeds equal to 2, 2.6, 3.1, 3.9 and 4 m/sec. Superimposed is a predicted curve of the input mechanical torque to the generator needed for system 'A' (described in section 6.2) under constant voltage/frequency conditions. The electrical calculations showed that, for scheme A, a generator speed of 1080 r.p.m. gave rated voltage, frequency and rated generator current. Fig (6.3) shows that a wind speed of 3.1 m/sec gives an operating point corresponding to maximum turbine torque at this generator speed.

Fig [6-4] shows the per-unit values of wind rotor power against generator speed at the same set of wind speeds. Constant tip speed ratio operation is desirable

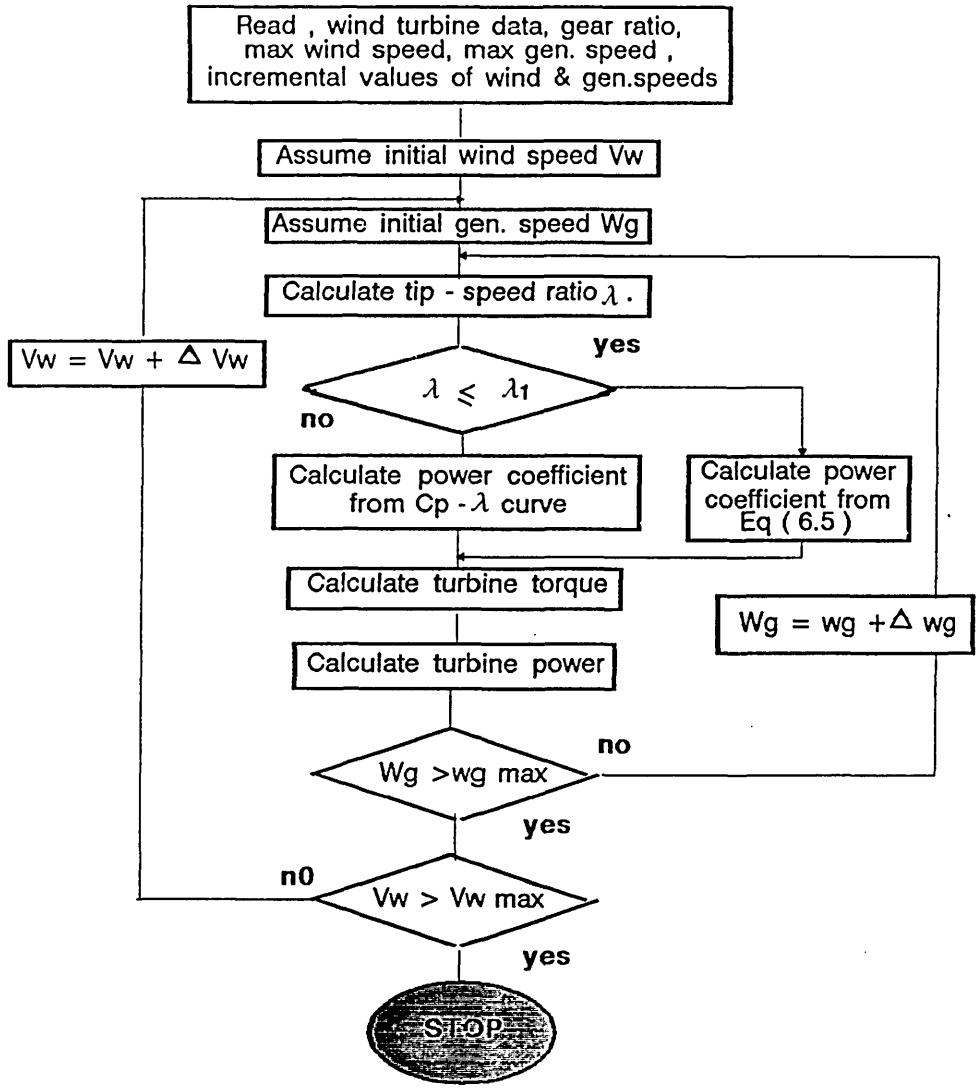

Fig. (6.2) Flow chart.

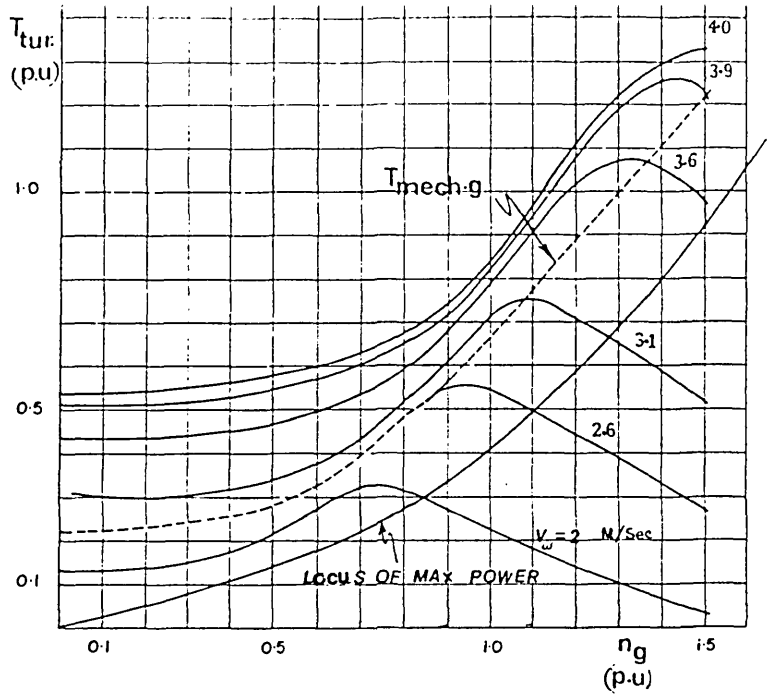

Fig. (6.3) Wind turbine torque and gen. i/p mech. torque versus gen. speed at different values of wind speeds..

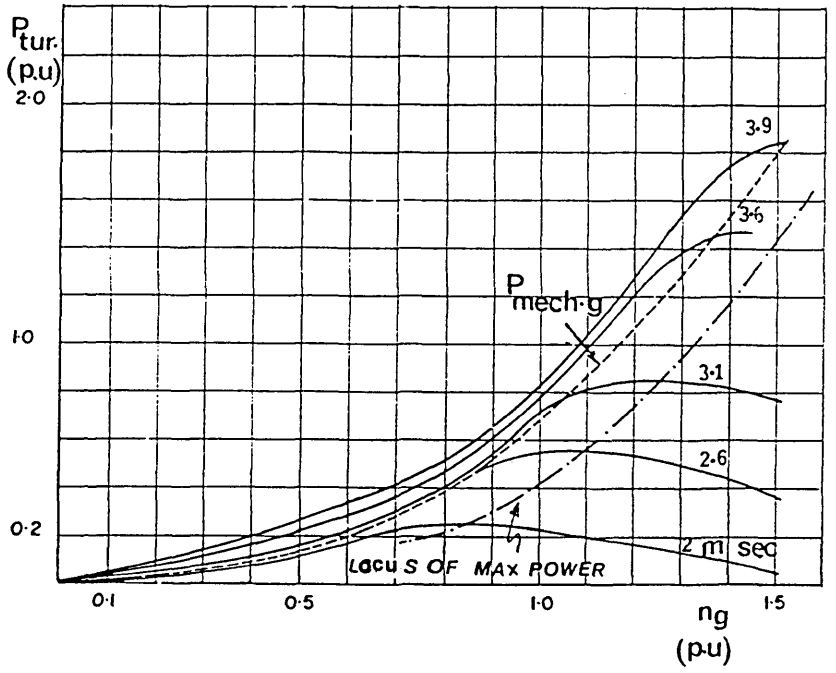

Fig. (6.4) Wind turbine power and gen. i/p mech. power versus gen. speed at different values of wind speeds..

for max energy extraction. The locus of the maximum power points is shown. Also shown is the required input mechanical power to the generator for constant voltage/frequency conditions calculated using the chapter 2 techniques.

It is clear that, whereas the max power locus is cubic with shaft speed ($T_W \alpha V_W^2$ and $w_g \alpha V_W$ at constant λ), the required mechanical power input to the generator unfortunately does not vary in this way. This is born out in table [6-1] which shows the generator speeds and corresponding required mechanical power inputs to the generator calculated using the chapter 2 prediction technique. From this table, it can be seen that K1, which is equal to P_m/w_g^3, is not constant, but varies from 0.798 to 0.582, while the generator speed varies frm 0.7 p.u to 1.3 p.u. The turbine will hence not operate at constant tip–speed ratio and hence its output power (proportional to C_p/λ^3) is generally somewhat below optimum, though the extent of the reduction seems to be fairly small, and the nature of the predicted operating points is stable (non–stalling) so far as the turbine is concerned.

6.4 Prediction of Steady State System Operation and Determination of Feasible Optimum Wind Speed Range

The flow chart for the program used to estimate the behaviour of the entire system is shown in Fig (6.5). In order to reduce computation time, it was decided to treat the generator speed rather than the wind speed as the independent variable. The generator speed is hence incremented by the outer–most loop of the program and calculations performed to establish the wind speed at which the turbine referred to the generator is equal to the generator gross electrical torque as calculated for the specific electrical and

Wg	P mech.g	Wg^3	K1	T mech.g
0.70	0.274	0.343	0.798	0.391
0.75	0.322	0.421	0.763	0.429
0.80	0.378	0.512	0.738	0.472
0.85	0.445	0.614	0.724	0.523
0.90	0.504	0.729	0.691	0.560
0.95	0.600	0.857	0.690	0.630
1.0	0.692	1.000	0.692	0.692
1.08	0.794	1.259	0.630	0.735
1.15	0.975	1.520	0.620	0.847
1.20	1.058	1.728	0.612	0.880
1.25	1.195	1.953	0.610	0.956
1.30	1.280	2.197	0.582	0.984

Table (6 . 1)

pump system by the method described in chapter (3). By envisaging a specific and constant value of V/F for the fully–regulated capacitor controller, each value of generator speed is of course associated with a unique value of generator gross electrical torque. The generator's gross torque versus speed charactedristic is pre–calculated and is input to the Fig (6.5) program at the start. An iterative loop is used to find the wind speed, the initial trial value being set at 1 m/sec. Equations [6-3] and [6-1] are used to calculate the tip speed ratio and turbine torque respectively as required. A comparison between the turbine torque and the gross generator torque forms the heart of the inner loop, the assumed wind speed being increased (typically in steps of $\frac{0.05}{\lambda}$ m/sec from an initially set value of 1 m/sec), until the torques become virtually equal.

6.5 Steady State System Operation Results

Fig (6.6) shows the turbine torque $T_{tur.(p.u)}$ and turbine power coefficient against generator speed. C_p is seen to cary from 0.3 to 0.465 over the generator speed range studied. The turbine's maximum C_p is 0.476, so the generator speed range over which C_p is better than 85% of its maximum value is 1000 r.p.m. to 1300 r.p.m. Speeds n_{g1} and n_{g2} marked on Fig (6.6) are the minimum and maximum satisfactory generator speed. Beyond n_{g2}, the generator current is predicted to become excessive (i.e. greater than 1.2 p.u). Below n_{g1} Fig (6.3) shows that the generator and turbine torque versus speed lines become virtually coincident and parallel, indicating that unstable operation leading to turbine stall is likely. Fig (6.7) shows the wind speed V_w and motor output power (i.e. pump input power). The limiting wind speeds corresponding to n_{g1} and n_{g2} are seen to be 2.7 m/sec and 3.5 m/sec. The corresponding range of pump output powers is 0.17 to 0.7, a range of 4:1, and of

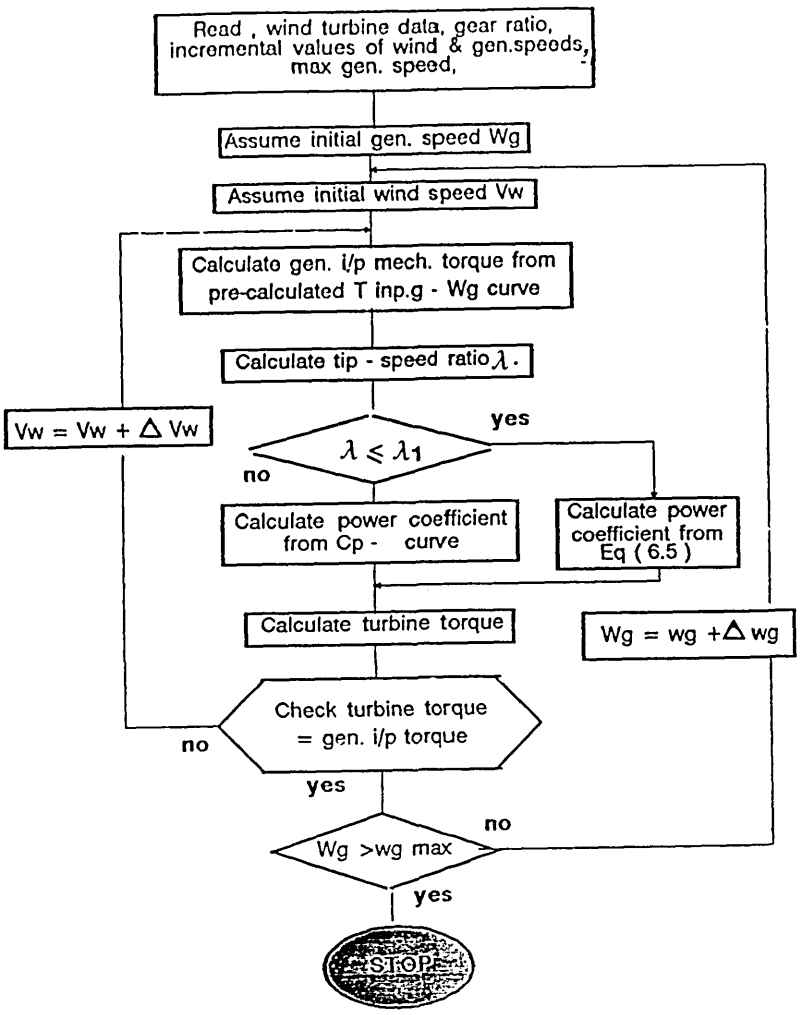

Fig. (6.5) Flow chart.

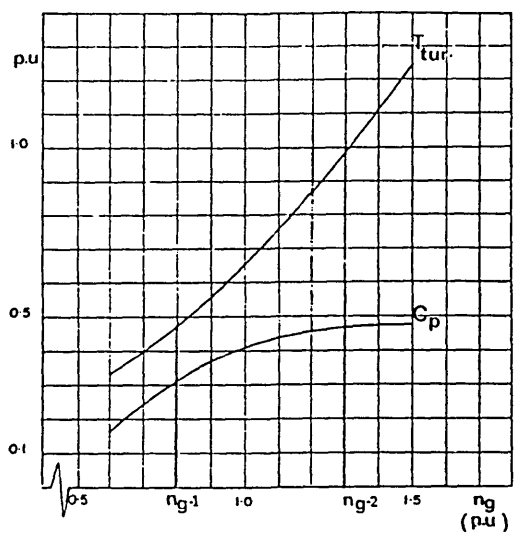

Fig. (6.6) Variation of wind turbine torque and power coefficient versus gen. speed.

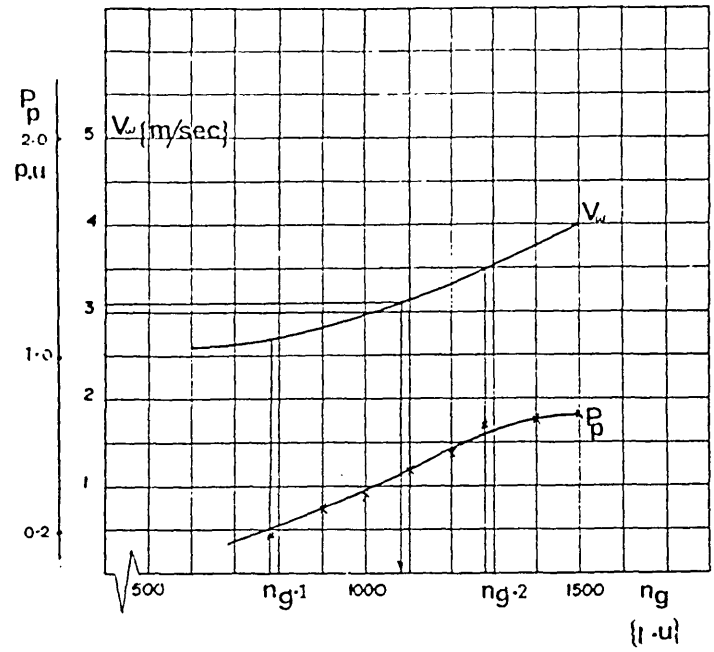

Fig. (6.7) Variation of wind speed and pump power versus gen. speed.

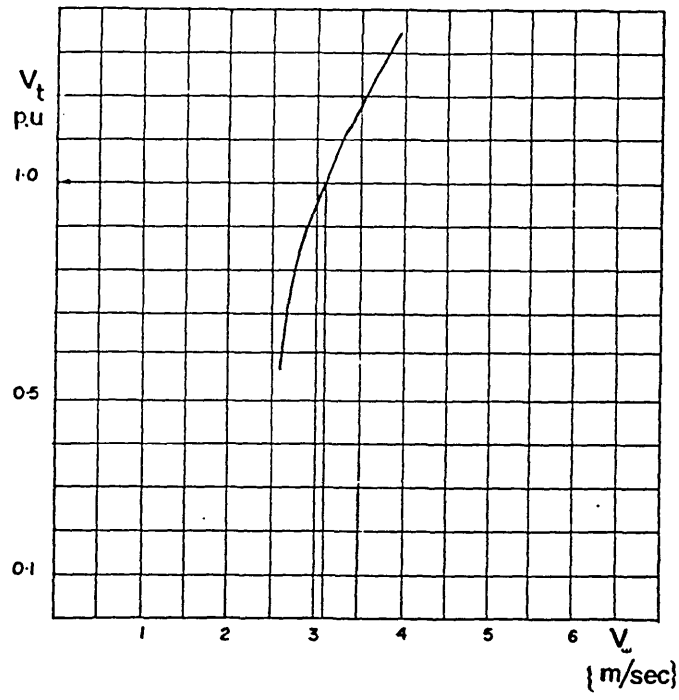

Fig. (6.8) Variation of gen. voltage against wind speed.

generator speed is 0.78 p.u to 1.28 p.u. The wind speed corresponding to rated current (1.0 p.u) in the generator and rated frequency and voltage is 3.1 m/sec. The graph shows that generator speed changes fast with wind speed within the operating range.

Fig (6.8) shows how the voltage V_t varies with wind speed. Note that, since the scheme is operated on a constant V/F basis, this curve also shows the shape of the frequency versus wind speed. It is clear that as would be expected from Fig (6.7), the rates of increase with respect to wind speed are high.

6.6 System Start Up Behaviour Under Constant Wind Speed Conditions

6.6.1 Motor Isolating Switch Open

Until the isolating switch is closed the generator operates on 'no–load'. Fig (6.9) shows the flow chart of the program written to simulate the system start–up behaviour from rest during this initial phase. Both generator and motor speeds are initially taken as zero and their speed increments are calculated from the equations of motion given later. The simulation code incorporates the 'no–load' code for electrical system prediction described in section 2.3.2. The turbine torque is calculated using the relations described in section 6.3.2. The wind velocity, though treated as a fixed quantity here, could be treated as a variable in a more comprehensive simulation. The generator speed increment is calculated at each time step from the estimated turbine torque $T_{tur.}$ Eq [6-1], from the generator electrical torque, given by:

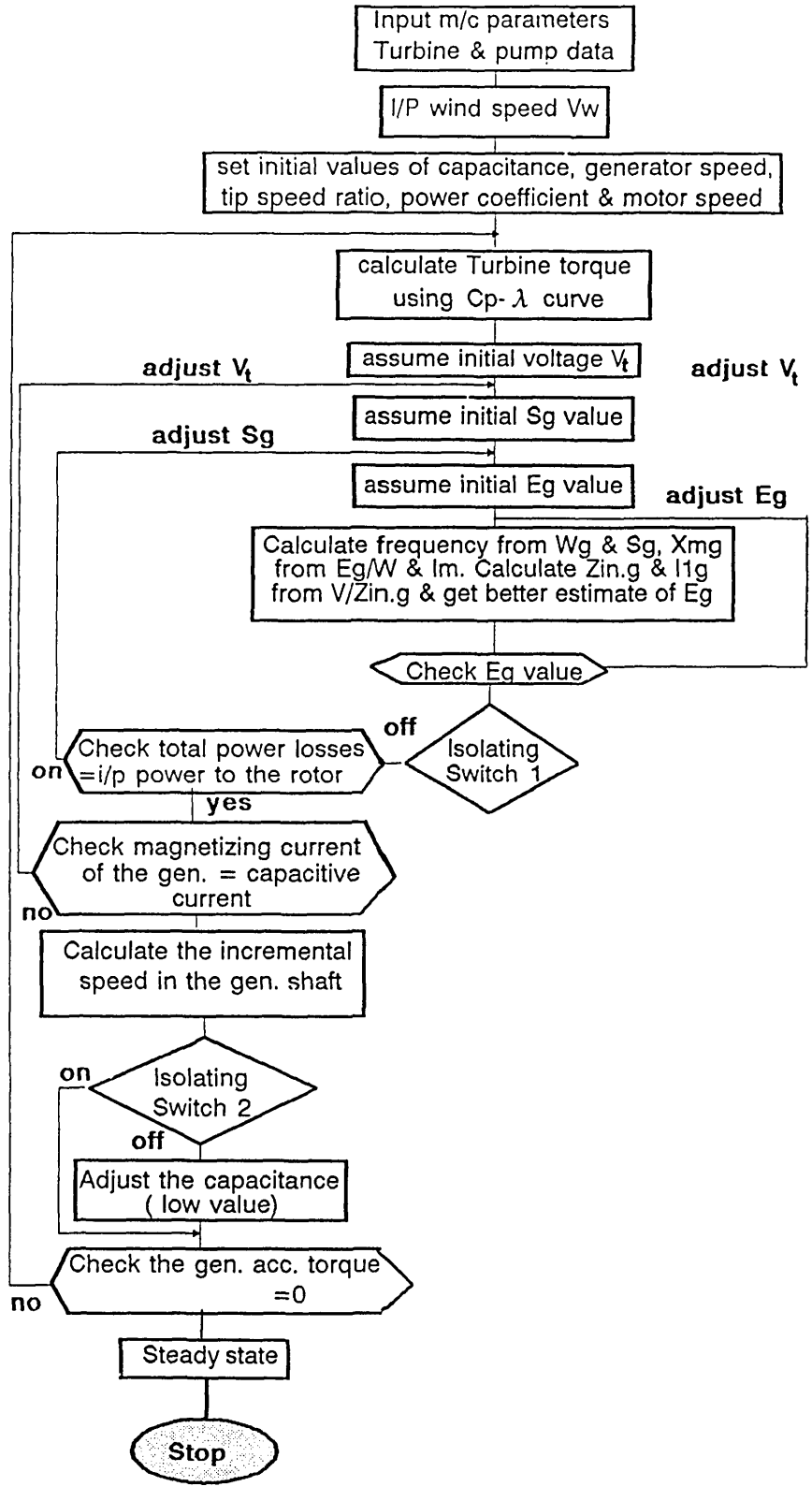

Fig. (6.9) Flow diagram of system start up behaviour from rest (isolating switch 3 is open)

$$T_{elec.g} = (\tfrac{1}{W})(I_{2g}^2)(R_{2g}/S_g) \qquad [6\text{-}9]$$

and from a relation derived directly from the system's equation of motion:

$$\delta_{wg} = \frac{1}{J_g + 1/K_g \cdot J_{tur}}\left(T_{tur.} - T_{elec.g}\right)\delta_t \qquad [6\text{-}10]$$

where J_g and $J_{tur.}$ are the moments of inertia of the generator and turbine respectively. The calculation of moment of inertia of the generator and turbine is included in Appendix 4.

6.6.2 'No-load' Results with Specified Capacitor Values

The theoretical results shown in Figs (6-10) to (6-17) for system start-up with motor isolator switch open with constant capacitor values were predicted for system A (described in 6.2). Fig (6.10) shows the build up of voltage versus time with three different capacitor values (4.6 and 8 p.u). The absence of self excitation (and hence generator torque) at low speeds hoped for in order to facilitate starting with low turbine starting torques can be observed. Fig (6.10) also shows that, with larger capacitors, the initial voltage build-up (at about t=1.5 secs) is faster. Subsequent increases in voltage arising from further generator acceleration, however, are lower, due to the higher values of current (V_tWC) and resulting higher I^2R loss and generator electrical torque. High capacitance values are also seen slightly to reduce voltage. This is caused by the increase in generator current and electrical torque resulting from the raised capacitance values, causing in turn lower turbine accelerations, and hence delayed build ups in speed, frequency and voltage. This lowers the voltage at which the generator's magnetization curve crosses the capacitor line (the mag.

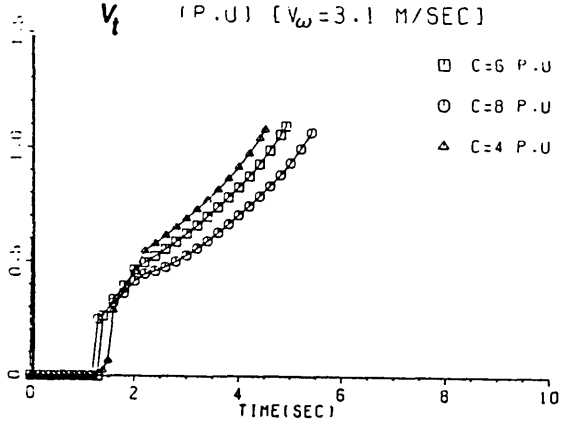

Fig. (6.10) Gen. voltage

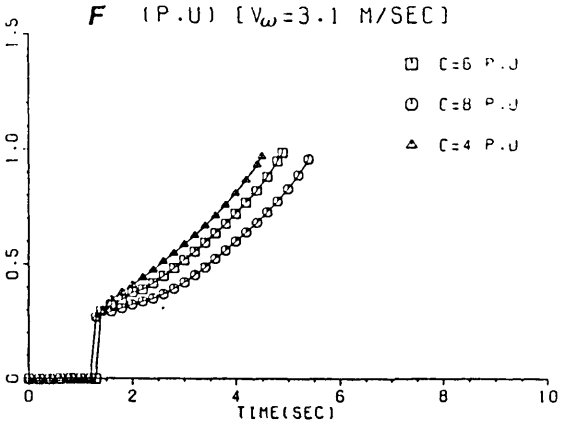

Fig. (6.11) Gen. frequency

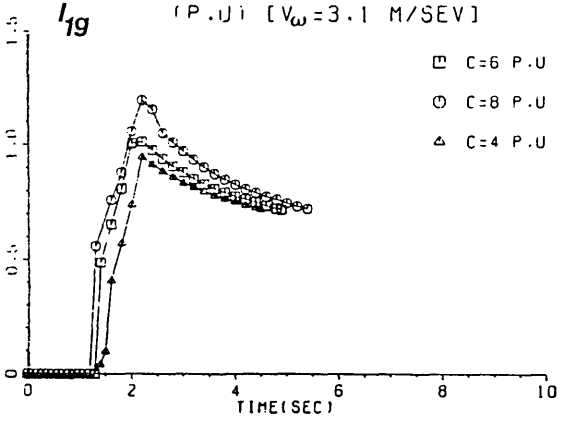

Fig. (6.12) Gen. current

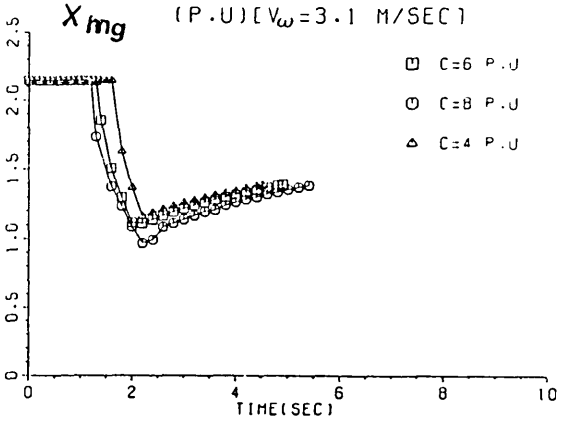

Fig. (6.13) Gen. magnetizing reactance

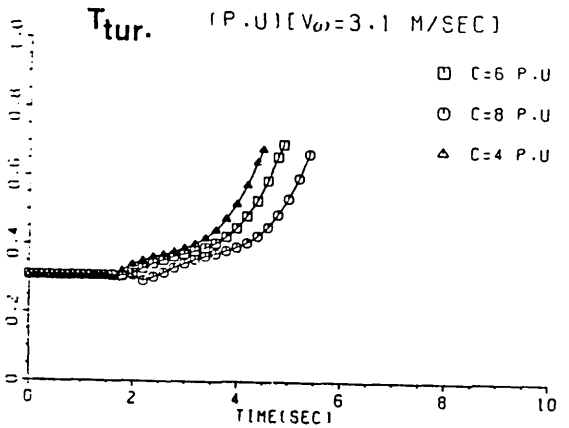

Fig. (6.14) Turbine torque

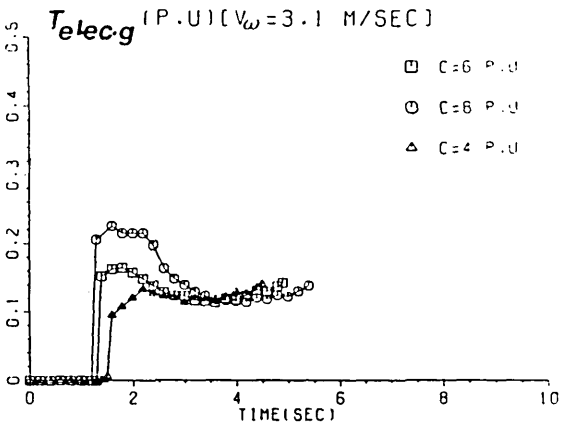

Fig. (6.15) Elec. O/p power to the gen.

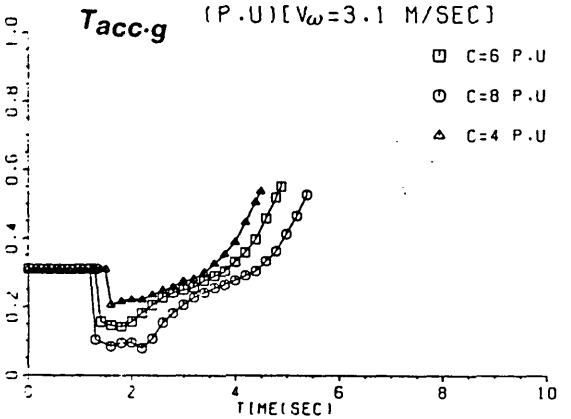

Fig. (6.16) Acceleration torque for the gen.

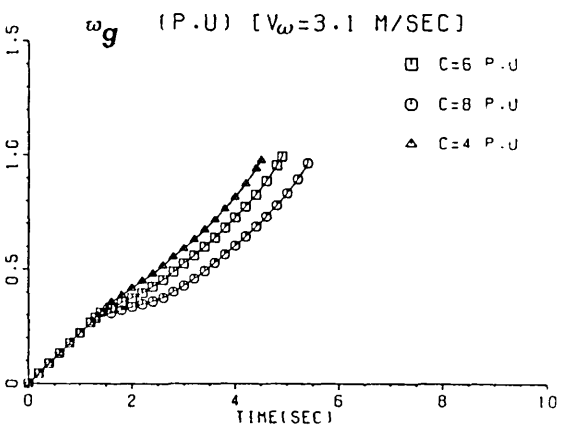

Fig. (6.17) Gen. speed.

curve scales with frequency). Changes are also caused by variations in the generator's magnetizing reactance. Fig (6.12) shows the variation of the generator current against time. The generator current is seen to peak when the frequency (set at no–load largely by the shaft speed) causes resonance between the capacitance and the machine's overall inductance. Since the generator's load current I'_{2g} is very small, the generator magnetizing reactance minimises when the generator output current peaks as shown in Fig (6.13). Fig (6.14) shows that the turbine torque is constant for the first 1.8 secs because, at lower generator shaft speeds ($w_g \leq 0.05\ w_{g\ rated}$), the turbine torque is virtually independent of generator shaft speed (Fig 6.7). Therefore, the turbine torque trajectory is affected by capacitor value due to the latter's effect on speed. A set of predictions for a higher, constant wind speed (V_w = 3.5 m/sec) was also made for comparison purposes. Figs (6.18) to (6.25) represent the theoretical results for start–up operation at this and the original wind speed. It is evident that, as expected, shaft acceleration is higher with the higher wind speed, leading to generally reduced time periods for voltage build up etc. but unchanged peak values etc.

6.7 Simulation of System Start–Up with Fully Regulated Capacitor Bank Under Constant Wind Speed Conditions

The code described in this section handles the entire start–up sequence for the above conditions. The capacitor bank is adjusted at each time step so as to give a constant, preset rate of rise of voltage, up to a value corresponding to 1 p.u voltage frequency at the end of the entire starting period. The voltage and frequency at which motor starting commences was made high by delaying closure of the motor isolating switch S1 until the voltage had built up to a value

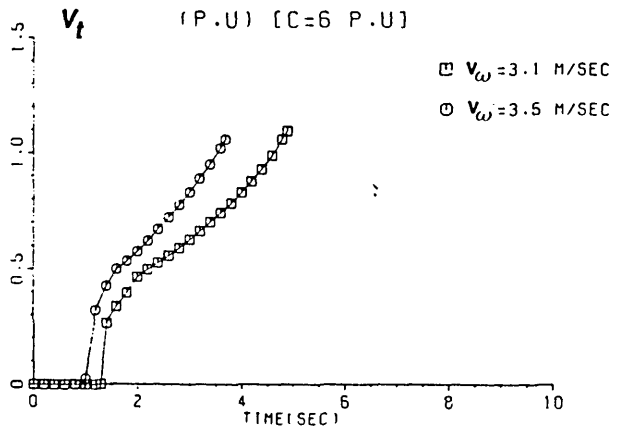

Fig. (6.18) Gen. voltage

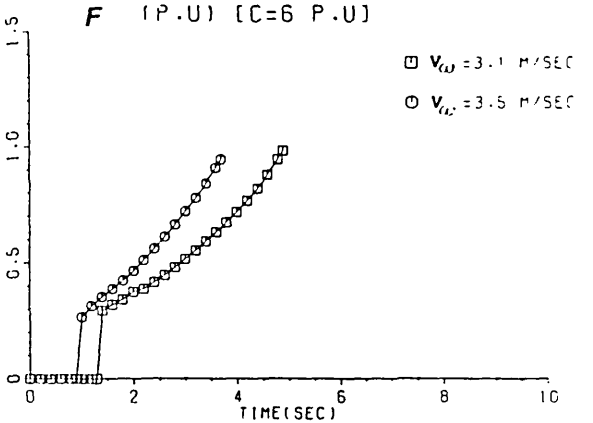

Fig. (6.19) Gen. frequency

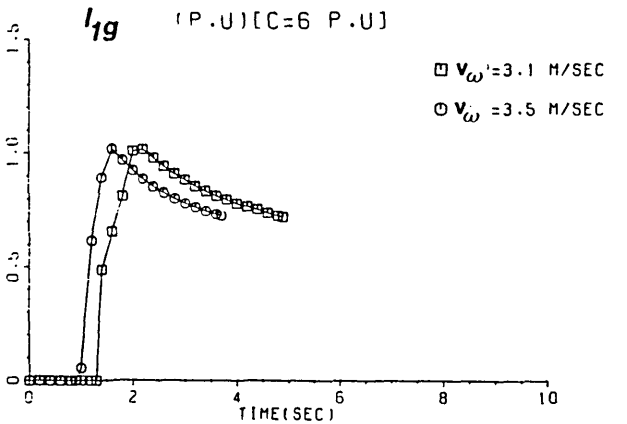

Fig. (6.20) Gen. current

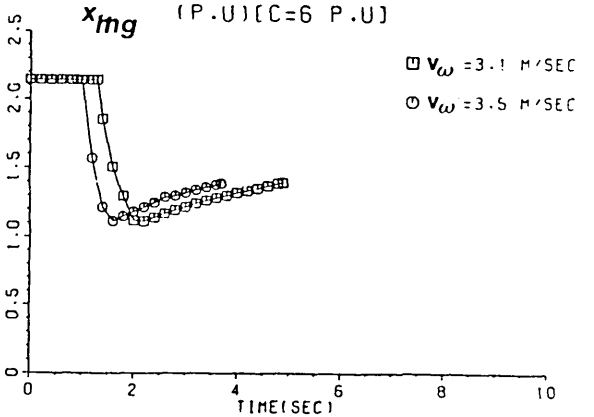

Fig. (6.21) Gen. magnetizing reactance

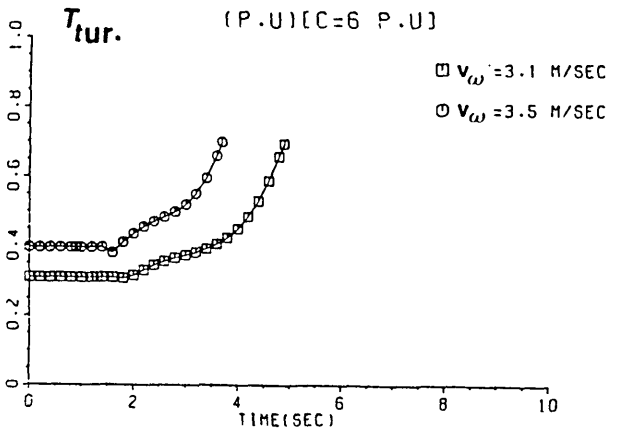

Fig. (6.22) Turbine torque

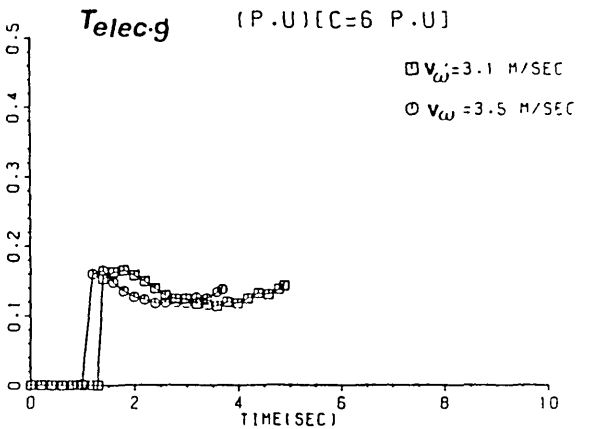

Fig. (6.23) Elec. O/p power to the gen.

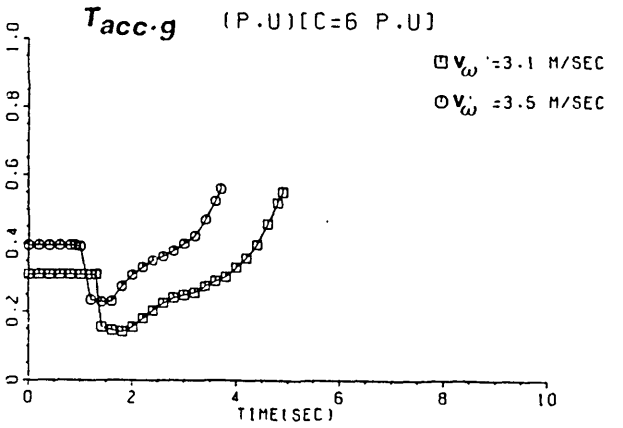

Fig. (6.24) Acceleration torque for the gen.

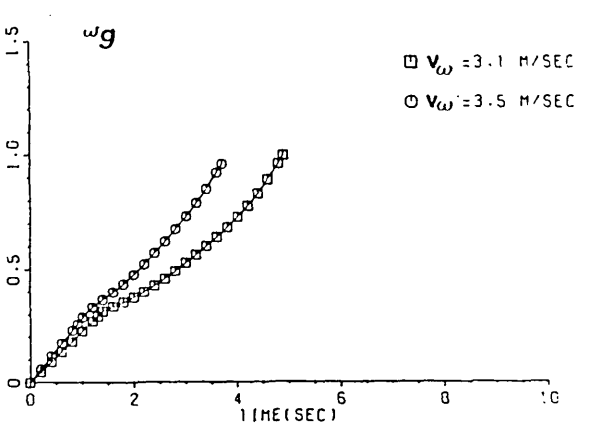

Fig. (6.25) Gen. speed.

such as 1 p.u. The capacitance per phase was, as before, made reasonably high to avoid voltage collapse when the motor is connected. Fig (6.26) shows the flow diagram. Wind velocity is treated as an input quantity. The turbine standstill torque is calculated using the relations given in section 6.2, and this enables the simulation to start. The no–load code relevant to system operation before S1 is closed is identical to the one used in section (6.5). Much of the motor start–up simulation code relevant to system operation when the isolating motor switch S1 is closed is similar to the code used in sections (2.3.4) and (5.4). The starting process reaches a conclusion when the net accelerating torques on the turbine–generator shaft and motor–pump shaft each fall to zero. The equations used are Eq (5-1) and Eq (6-10). The capacitor value is calculated at each time step as that needed to increment the voltage by the preset amount.

6.8 Results of System Start–up Simulation on Fully Regulated Capacitor Bank Scheme Under Constant Wind Speed Conditions

The results shown in this section were predicted for the particular wind turbine specified in section (6.2). The electrical system again incorporated two identical 3 phase, 3.7 Kw, 6–pole induction machines (system 'A'). The maximum value of capacitance was chosen to give a generator voltage, with S1 open, of 1 p.u. The isolating switch was closed when the voltage reached 1.1 p.u. When S1 is closed, it can be seen that the voltage falls to 0.5 p.u., this value being enough to ensure satisfactory motor starting. The rate of voltage increase $\left(\frac{\Delta V}{\Delta t} = \frac{0.02}{0.1}\right)$ p.u/sec after S1 closure was chosen at a value giving (as in the chapter 5 start–up simulations) satisfactory starting performance – a lower value leads to excessive starting time, a higher value gives motor stall. The

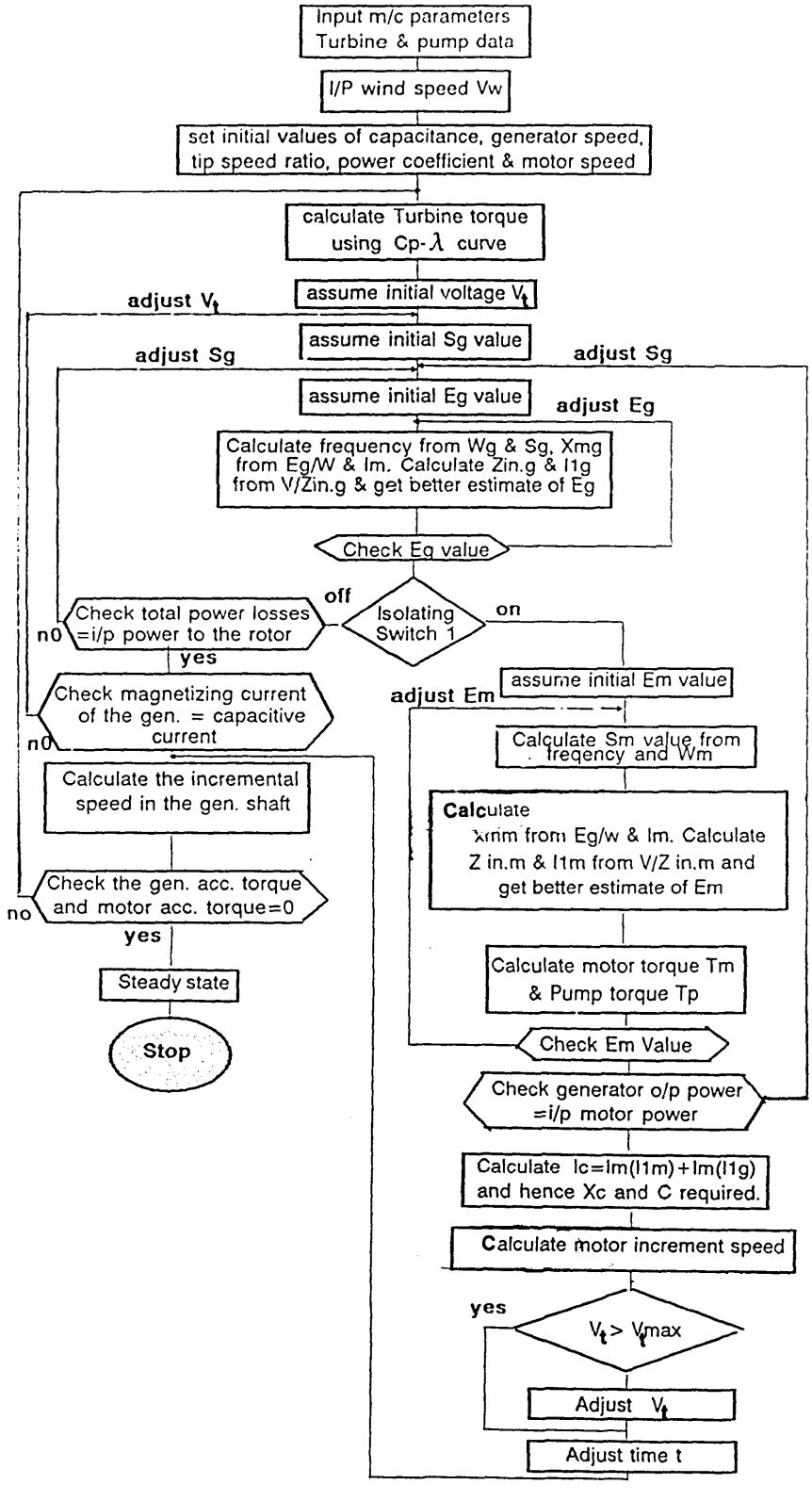

Fig. (6.26) Flow diagram for dynamic simulation of motor start up with fully regulated capacitor bank under constant wind speed condition.

simulation results are shown in Figs 6.27 and 6.28. The sequence of events is :

0 to 1.3 sec: turbine accelerates generator speed to 291 rev/sec: generator speed too low to cause voltage build up.

1.3 sec to 5 sec: voltage builds up to 0.26 p.u at t = 1.4 sec and continues to build as generator speed reaches 1036 rev/min.

5 sec: S1 closed; voltage falls to 0.5 p.u and motor–pump acceleration commences.

5 sec to 7.5 sec: voltage builds up at pre–set rate to 1 p.u due to further increase in generator speed and continuous adjustment of capacitor value.

5 sec to 13.3 sec: motor pump accelerates to peak motor torque point.

13.5 sec onwards: motor speed reaches final running value; steady electrical and mechanical conditions attained at about 14.5 sec. Fig (6.27) shows how the capacitance per phase has to be varied in order to achieve the desired voltage–time trajectory, which includes a constant voltage condition after the initial ramp rise during the 5 to 7.5 second period. The decrease in capacitance during the 5 to 7.5 period during a period of voltage increase is interesting and stems from the fast increasing system frequency. The temporary increase in capacitance requirement around t=13.3 sec is caused by the machines' high VAr requirements when the motor is operating near its pull-out (peak torque) point. The final capacitance value needed (1.36 p.u) is however quite modest. Fig (6.29) shows that the generator magnetizing reactance (a function of V_g/F

is constant at its unsaturated value for the first 1.3 sec before the build-up of generator voltage. After 2 seconds, the rate of increase of voltage is higher than the rate of increase of frequency, giving a V/F higher than 1 p.u.

The generater magnetizing reactance hence decreases gradually reaching a minimum value (X_{mg} = 1.1 p.u) after 2.1 secs. It then increases again to 1.4 p.u just before the isolating motor switch S1 is closed. When S1 is closed, the generator magnetizing reactance increases to its unsaturated value again ($X_{mg_{unsat.}}$ = 2.14 p.u) due to the big reduction in voltage (to 0.5 p.u) combined with a much smaller decrease (to 0.89 p.u) in frequency.

The final steady state value of 1.73 p.u (saturated), reflects the final V and f conditions. Fig (6.30) shows the motor magnetizing reactance. It is constant at its unsaturated value for the first 13.3 secs due to the high stator impedance drop in the motor at high slips resulting in a low motor air gap voltage. The sharp decrease in motor magnetizing reactance at 13.5 seconds is due to the temporary decrease in frequency, due in turn to the temporary decrease in generator speed as the motor passes through its peak-torque region. Figs (6.31), (6.32), (6.33) and (6.34) show generator slip, motor slip, generator current and motor current. As mentioned before in section (5.7), the 'soft start' nature of the voltage control strategy is seen to limit the starting current to 2.2 p.u. Fig (6.31) shows that the generator slip stays satisfactorily low and nearly constant during the entire starting period, only increasing to 0.84 p.u for a short period corresponding to the motor speed giving peak torque. The final steady state generator and motor slips are (0.087) and (0.072) respectively. The corresponding generator and motor currents are (1.053) and (0.942) respectively.

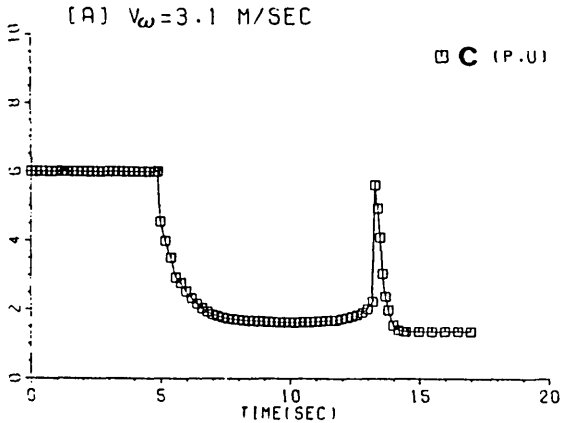

Fig. (6.27) Capacitance C (p.u)

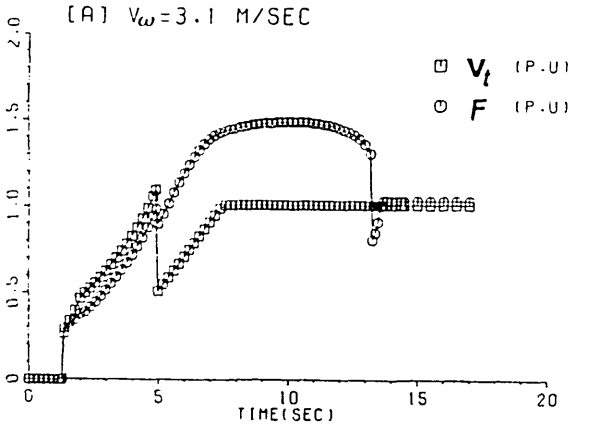

Fig. (6.28) Gen. voltage and frequency.

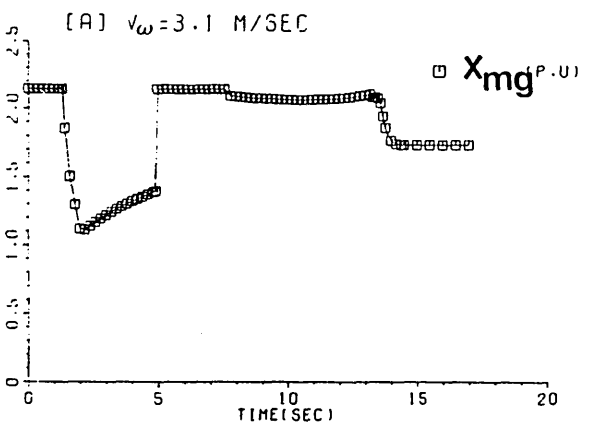

Fig. (6.29) Gen. magnetizing reactance

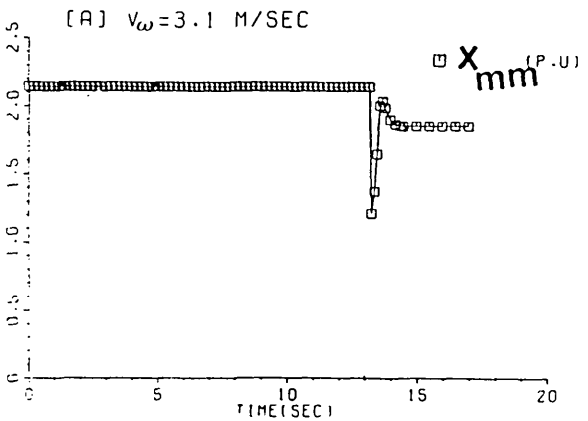

Fig. (6.30) Motor magnetizing reactance

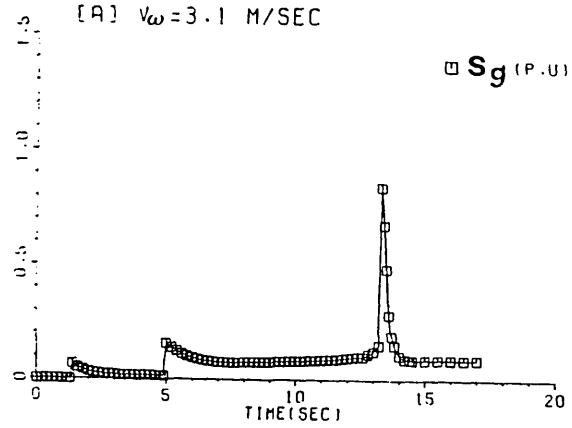

Fig. (6.31) Gen. slip

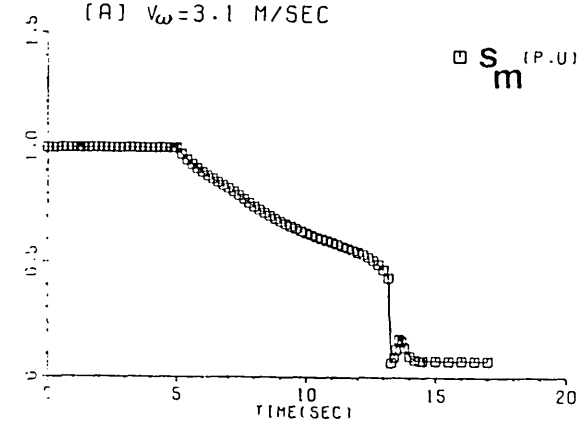

Fig. (6.32) Motor slip

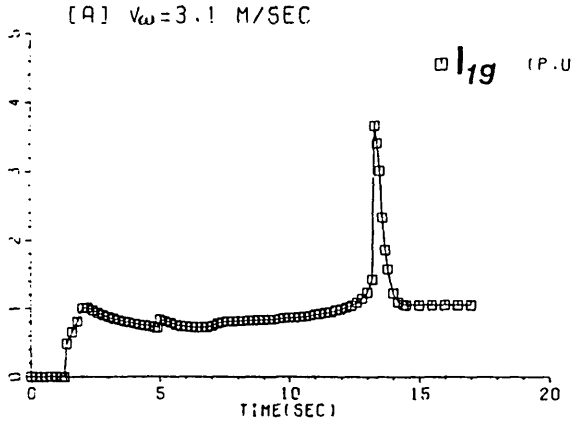

Fig. (6.33) Gen. current

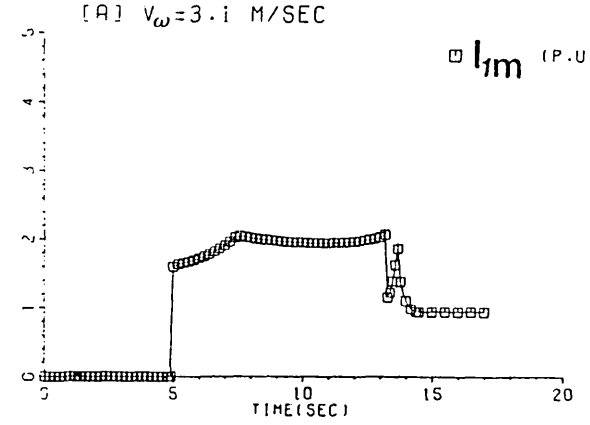

Fig. (6.34) Motor current

Fig (6.35) shows the turbine torque and the electric generator torque against time. It is seen that, with S1 open, electric generator torque is low due to the absence of self excitation resulting in a high turbine accelerating torque, facilitating the starting of the turbine. During the period $11 < t < 14.5$, the generator's electric torque is temporarily higher than the turbine torque, giving a temporary reduction in generator speed and frequency. This phenomenon is high–lighted in Fig (6.36), which shows the difference between the turbine torque and electric generator torque i.e. the net accelerating torque on the turbine/generator shaft. Fig (6.37) shows the electric input torque to the motor and pump torque against time. The pump torque is of course initially low, and hence a satisfactory pump acceleration occurs as seen as S2 is closed. As expected, the final stages in the pump acceleration occur at a fast rate due to the high motor torques around the pull–out slip. The variation of acceleration torque for the motor/pump and of motor speed are shown in Fig (6.38). Fig (6.39) shows the variation of mechanical input power, and electrical output power of the generator against time. A peak in each occurs corresponding to the motor's peak accelerating period. Fig (6.40) shows the generator efficiency against time. The generator efficiency changes little once S1 is closed ($\eta_G \simeq 0.77$) except during the events referred to above. This is due to the generator's constant slip. Fig (6.41) shows the variation of the input electrical power and the mechanical output power of the motor against time. During the starting period, the motor's losses are high, leading to low motor efficiency, as shown in Fig (6.42). The final steady state value is 0.75 p.u.

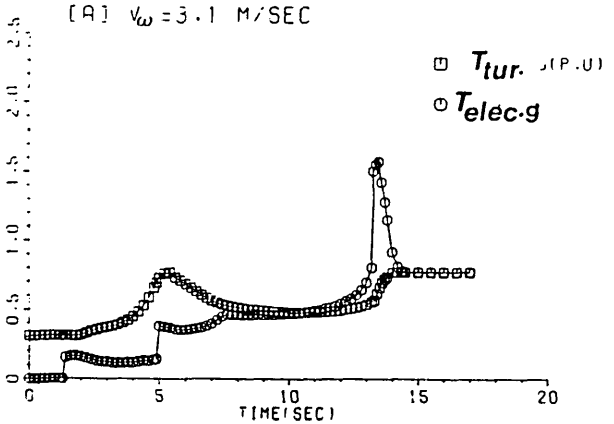

Fig. (6.35) Turbine and elec. gen. torques

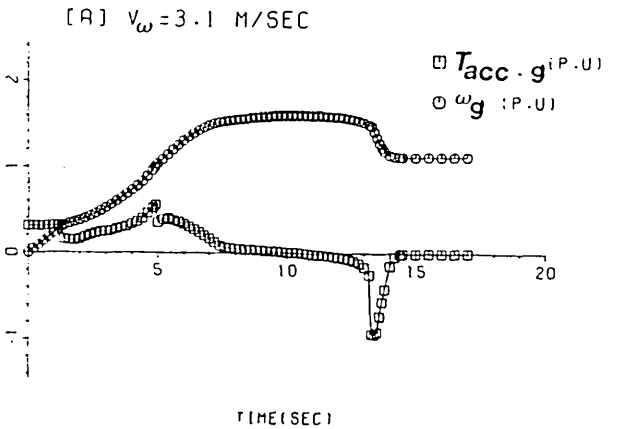

Fig. (6.36) Acceleration torque for the gen. and gen. speed.

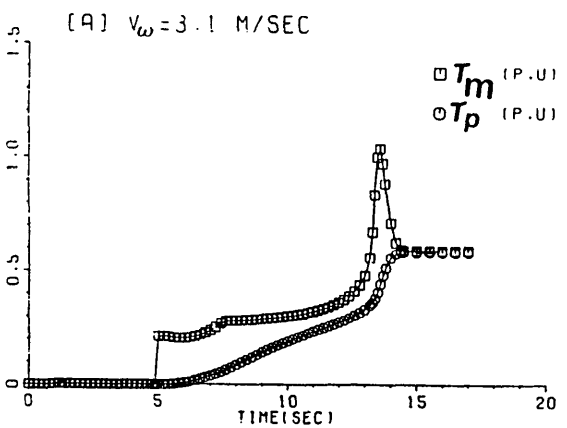

Fig. (6.37) Elec. i/p torque to the motor and pump torque

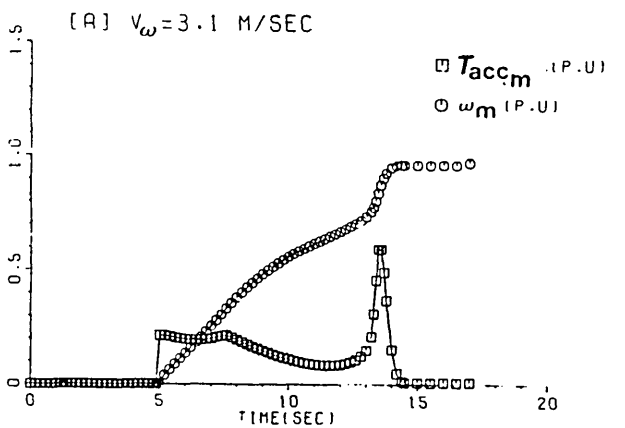

Fig. (6.38) Acceleration torque for the motor and motor speed.

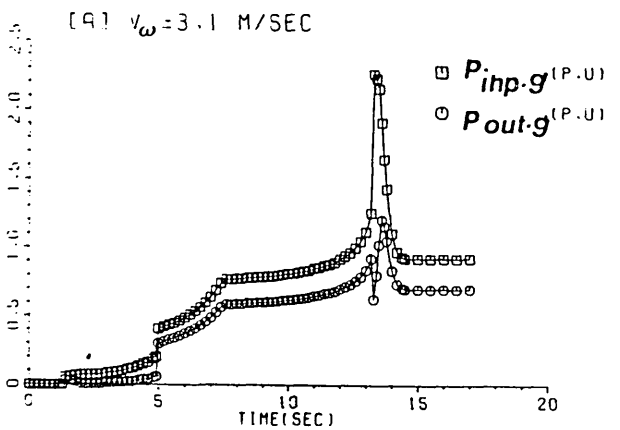

Fig. (6.39) Mech. i/p and elec. o/p power to the gen.

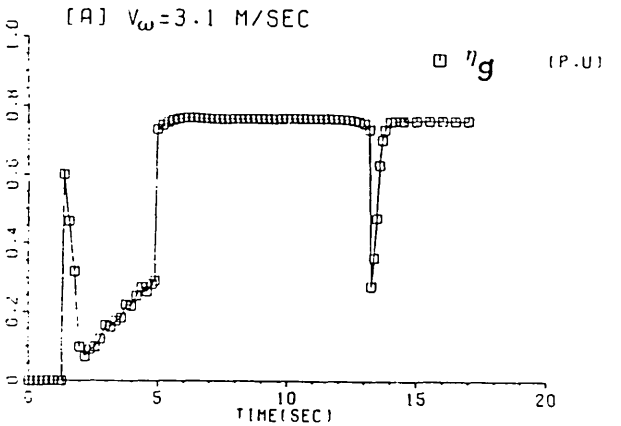

Fig. (6.40) Efficiency of the gen.

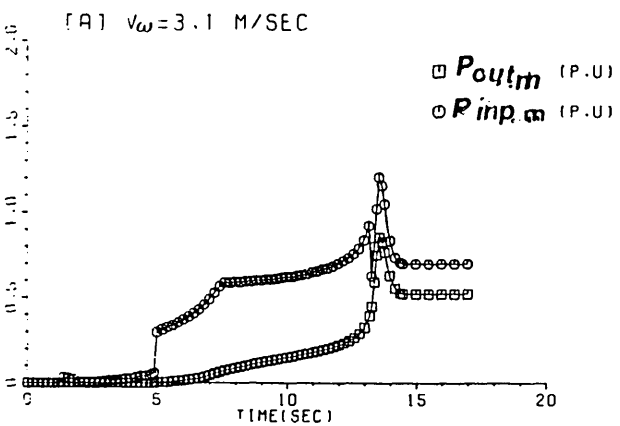

Fig. (6.41) Elec. i/p and mech. o/p power to the motor

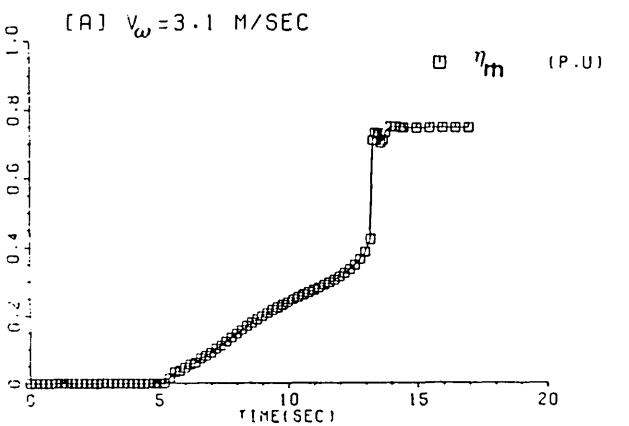

Fig. (6.42) Efficiency of the motor

6.9 Simulation of System Start-up with Switched Capacitor Bank Under Constant Wind Speed Condition

The analytical technique used for predicting the behaviour of the entire scheme when the capacitor bank consists of a capacitor bank simply switched in steps was described in a previous section (5.6). In this section, this analysis is extended to deal with varying speed behaviour. Operation is considered

a) for the pre-build-up and the build-up periods with the motor isolating switch S1 open and S2 (the starting capacitor switch) closed;

b) for the motor starting period with the motor isolating switch S1 closed and S2 closed;

c) in the post-motor-starting period with S1 closed and S2 open to avoid excessive voltage and saturation. The wind speed is again taken as a known, input quantity throughout.

The simulation was used to investigate the start-up behaviour of the system under constant wind speed conditions. This choice of wind speed (3 m/sec) was predicted to represent a typical value likely to give final steady-state conditions near rated for voltage, frequency and current. As described before in sections (5.3) and (6.6), the isolating switch S1 is closed when the generated voltage reaches 1 p.u.

The flow chart for the simulation is shown in Fig (6.43). Both generator and motor speeds are initially taken as zero and their speed increments are

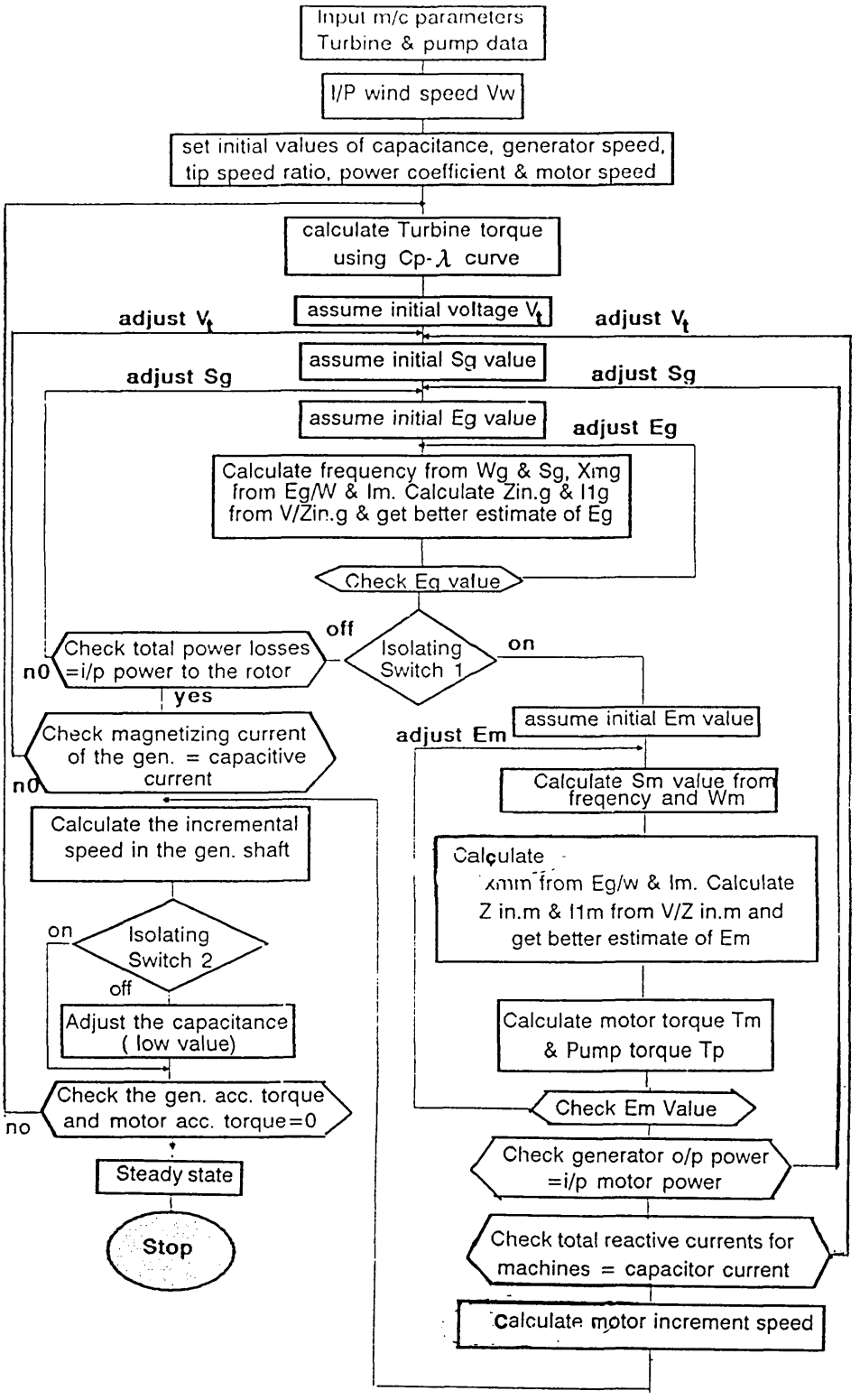

Flg. (6.43) Flow diagram for dynamic simulation of motor start-up with sectionalized capacitor bank under constant wind speed condition.

calculated from equations (5.1) and (6.10). The simulation code incorporates the 'on−load' code for electrical system prediction described in section (2.3.4).

6.10 System Start−up Results with Switched Capacitor Bank Under Constant Wind Speed Condition

Although results presented in this section are theoretical, good tie up of a set of final steady−state results has been obtained from the laboratory rig described in chapters 2 and 4. Table (6.2) defines the particular conditions at which the comparison was done, together with test and predicted results.

Results comparison

Pre - set operating point data

(1) Wind speed Vw = 3 m/sec

(2) Capacitance value = (4 x 148.8) μ F

(3) Switch condition S1 closed & S2 open

Vanables	*Test*	*Predicted*
Wg	*0.8*	*0.8*
V t	*0.951*	*0.96*
I g	*1.96*	*2.03*
I m	*1.02*	*1.20*
I c	*3.03*	*3.09*
Wm	*0.77*	*0.775*
Tm	*0.47*	*0.44*

Table (6.2)

No quantitative comparison of the system's dynamic behaviour was made, mainly because the d.c. motor representing the turbine in no way represented the turbine in a dynamic sense.

The theoretical results presented all refer to system 'B' described in sections (6.2), (3.1) and (3.2). In the simulations, it is assumed that S2 is opened when the generator current reaches 2 p.u and this sort of technique could be adopted in practice. The two capacitance values adopted in the simulations presented in Fig (6.44) are 6.4 p.u and 4 p.u with S2 closed and open respectively.
Fig (6.45) shows how the terminal voltage is predicted to vary with time. The motor isolating switch is initially open and the generator (and wind turbine) takes 6 secs. for the voltage−build−up speed to be attained. Switch S1 is scheduled to close when the voltage reaches 0.9 p.u. The simulation then predicts a 4.4 sec period of oscillatory behaviour. This is thought to be an L−C 'ringing' phenomenon excited by the sudden change in circuit configuration and compounded by sympathetic ripple effects on the motor and generator. However there is a possibility that the oscillatory behaviour stems from the discrete time stepping prediction technique used, i.e. that the phenomenon is a vagary of the computing method with no physical reality. Obviously, further investigations with a smaller time step are required to check this.

The motor pump acceleration during the $6 < t < 10$ sec period leads finally to an increase in voltage and generator current (the latter caused by raised VWC current and machine magnetizing currents) and switch S2 is scheduled to open when the generator current reaches 2 p.u.

The reduction in capacitance value brought about by opening S2 results in an immediate and beneficial reduction in voltage, and the value of C is chosen to give a final steady−state voltage of approximately 1 p.u. It is seen that, for the conditions studied, approximately 20 seconds elapses before the system reaches a steady−state. Obviously this period would be considerably reduced

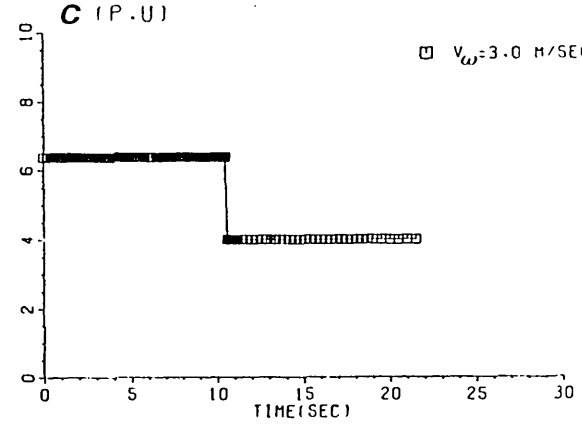

Fig. (6.44) Capacitance C (p.u)

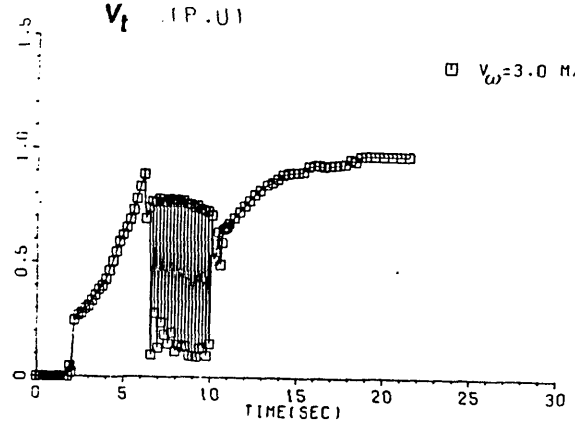

Fig. (6.45) Gen. voltage

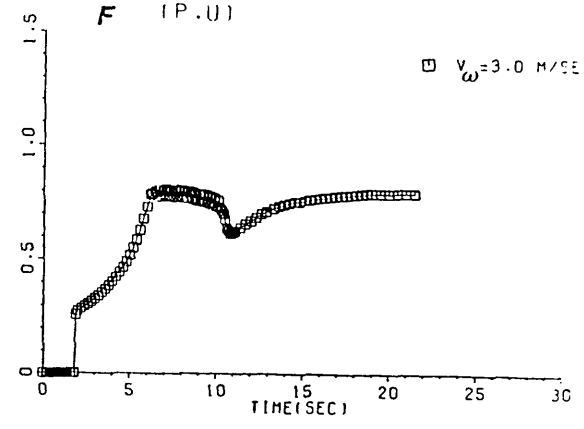

Fig. (6.46) Gen. frequency

with higher wind speeds.

Fig (6.46) shows the variation in system frequency during starting. Figs (6.47), (6.48) and (6.49) show the capacitor VArs and reactive requirement of both

generator and motor. It can be seen that the motor needs a high reactive input VA at starting (S1 is closed after 6 secs) in comparison to the generator, and that the opening of S2 is vital to avoid over excitation problems and the risk of capacitance failure. The steady−state motor VAr demand is less than the generator VAr demand due to lower magnetizing reactance of the generator. Figs (6.50), (6.51), (6.52) and (5.53) show the air gap voltage per frequency and magnetizing reactance for both generator and motor. The motor air gap voltage per frequency is lower than that of the generator within the $6.0 < t < 10$ sec period due to the higher stator impedance voltage drop in the motor. The final steady state value of motor air gap voltage/frequency remains a little lower than that in the generator because the air gap voltage V_g is higher than V_m. It can be seen that the final steady state value of generator and motor magnetizing reactances are 0.55 and 1.0 p.u respectively, the difference being due to the difference between the air gap voltages.

Figs (6.54), (6.55), (6.56) and (6.57) show generator slip, motor slip, generator current and motor current. The high motor starting current can be observed, as can the effect on the current of opening S2. The motor starting current is predicted to oscillate between approximately 3.3 and 0.6 times full load current. Fig (6.54) shows that the generator slip is approximately constant after opening S2 until it reaches its steady state value. The motor accelerates from rest to approximately the steady state value in 4 secs ($6 < t < 10$ secs). The final

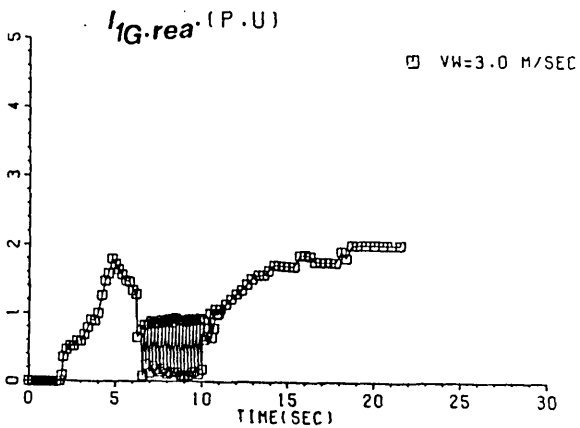

Fig. (6.47) Reactive component of gen. current

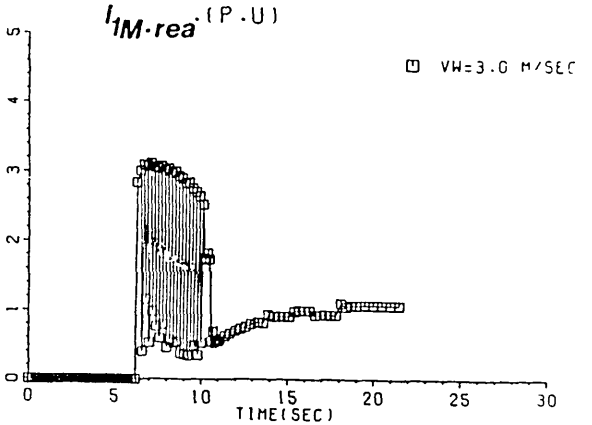

Fig. (6.48) Reactive component of motor current

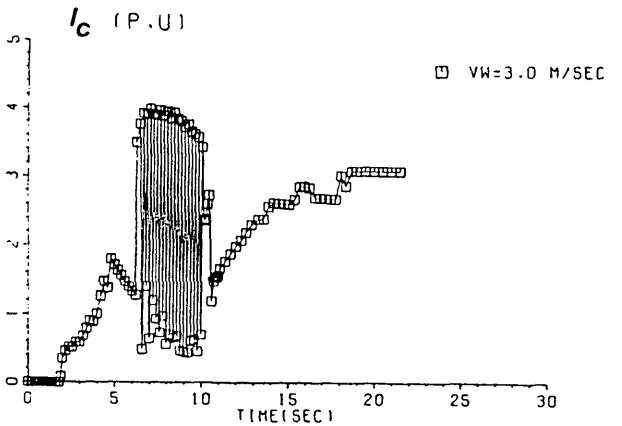

Fig. (6.49) capacitive current.

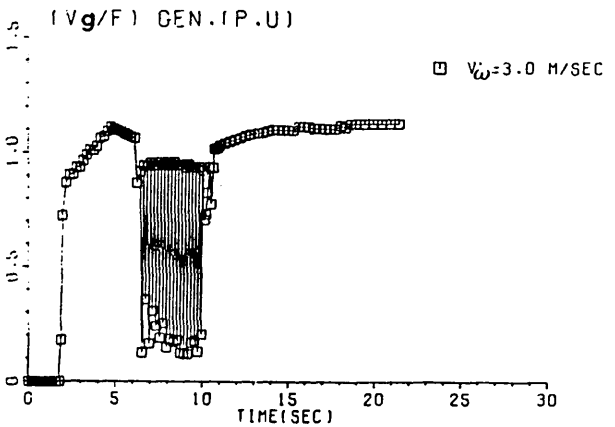

Fig. (6.50) Gen. air gap voltage per frequency

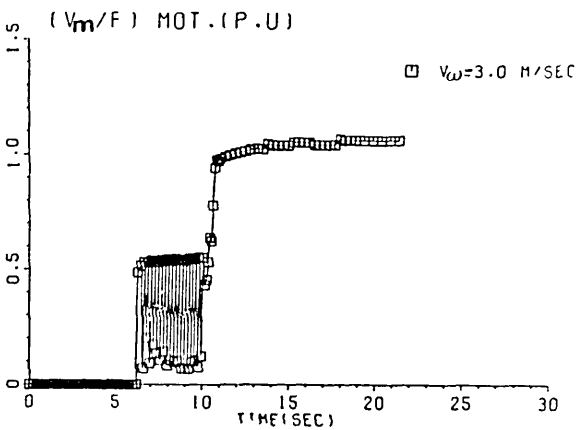

Fig. (6.51) Motor air gap voltage per frequency

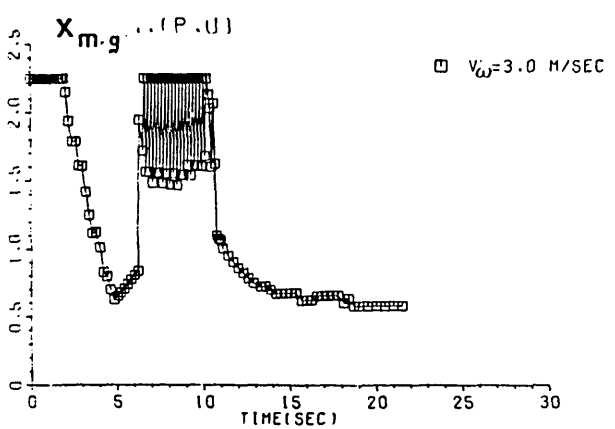

Fig. (6.52) Gen. magnetizing reactance

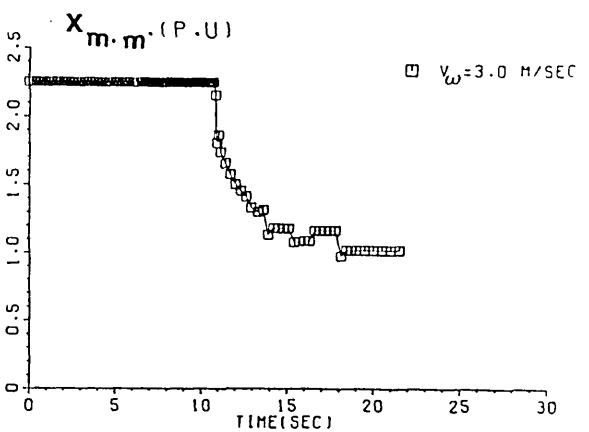

Fig. (6.53) Motor magnetizing reactance

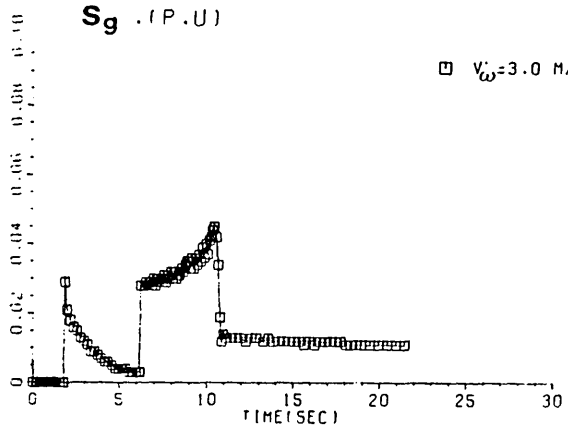

Fig. (6.54) Gen. slip

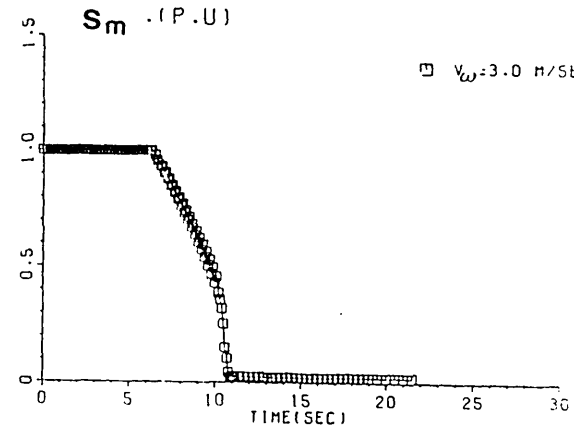

Fig. (6.55) Motor slip

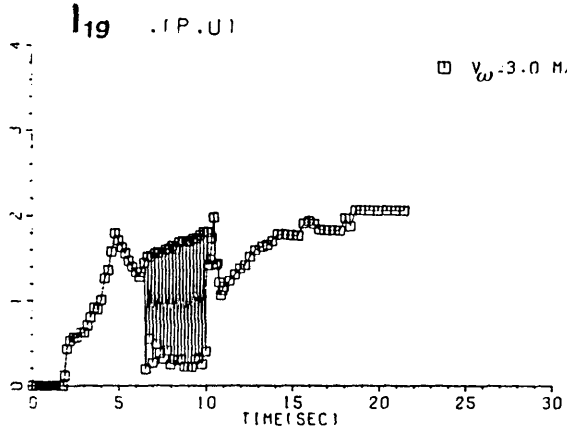

Fig. (6.56) Gen. current

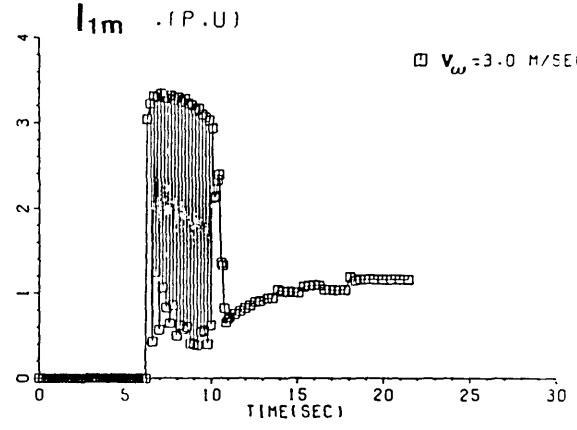

Fig. (6.57) Motor current

steady state generator and motor slips are 0.01 and 0.015 respectively.

Figs (6.58) and (6.59) show wind turbine torque and generator electrical torque. The difference between these torques, the net acceleration torque on the generator/turbine shaft, is shown in Fig (6.60). Fig (6.61) shows the generator shaft speed. During the $6 < t < 10$ period, the generator electrical torque is predicted to oscillate between values less than 0.2 p.u and values higher than 1.3 p.u, while the turbine torque is approximately constant at 0.8 p.u. This gives only a small mean accelerating torque resulting in little acceleration. After switching out C2 by opening S2, the turbine recovers and generator shaft speed starts to increase, reaching a steady state value of appoximately 0.8 p.u. The torques produced by the motor and absorbed by the pump are shown in Figs (6.62) and (6.63). The net accelerating torque on the motor/pump shaft is shown in Fig (6.64). Fig (6.65) shows motor and pump speed. Most of the pump acceleration between t=6.2 and 10.6 secs occurs fairly quickly under virtually constant generator speed conditions, but the considerable increase in motor power absorption ($10.6 < t < 11$ secs) that occurs as the motor's slip gets into the 20% to 0% range causes, as before, a significant drop in generator and turbine speed, and the final, rather lengthy portion of the pump acceleration process ($11 < t < 20$ secs) occurs as the turbine and generator speeds recover. Finally, Figs (6.66) to (6.71) show the power flow in the scheme.

Fig (6.68) and Fig (6.71) show generator and motor efficiencies. These are 72% for the generator and 70% for the motor at the final operating conditions giving an overall electrical efficiency (neglecting the power losses in the interconnecting cable) of 50%.

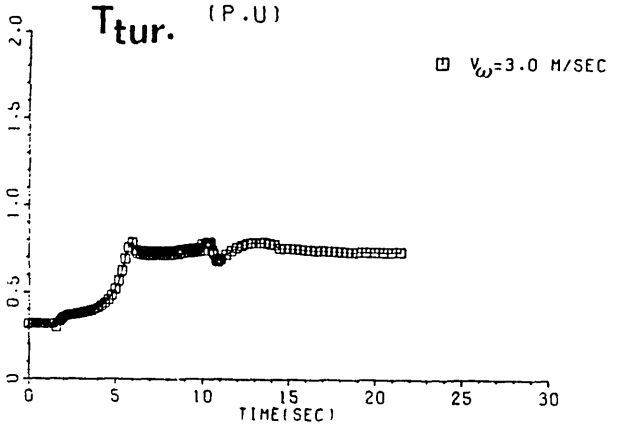

Fig. (6.58) Turbine torque.

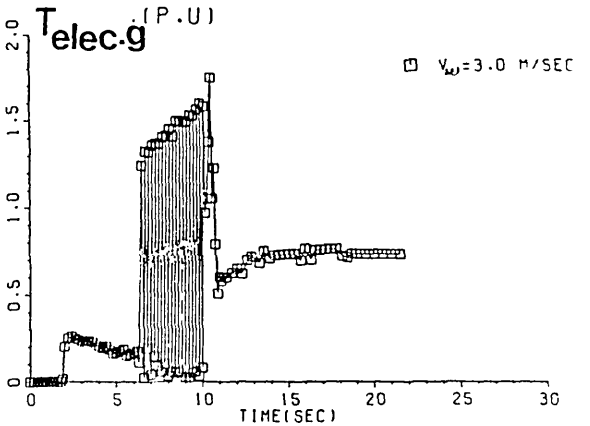

Fig. (6.59) Gen. elec. torque.

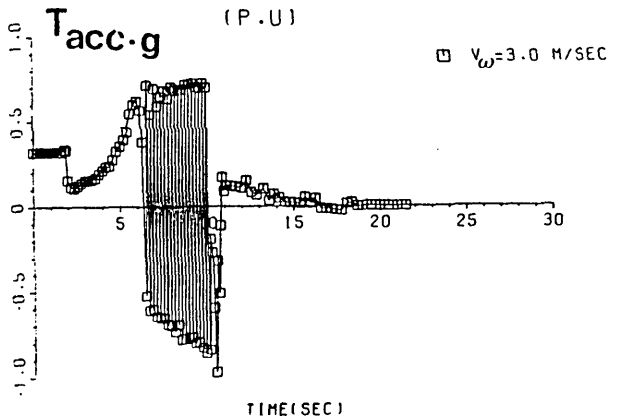

Fig. (6.60) Acceleration torque for the gen.

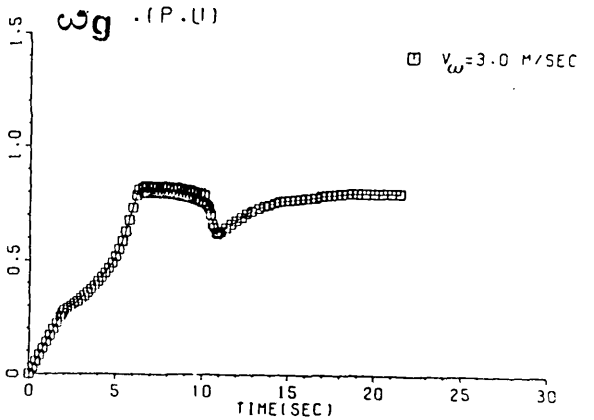

Fig. (6.61) Gen. speed.

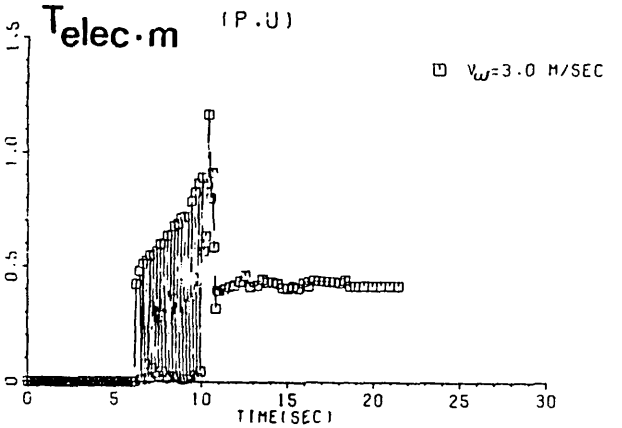

Fig. (6.62) Elec. i/p torque to the motor.

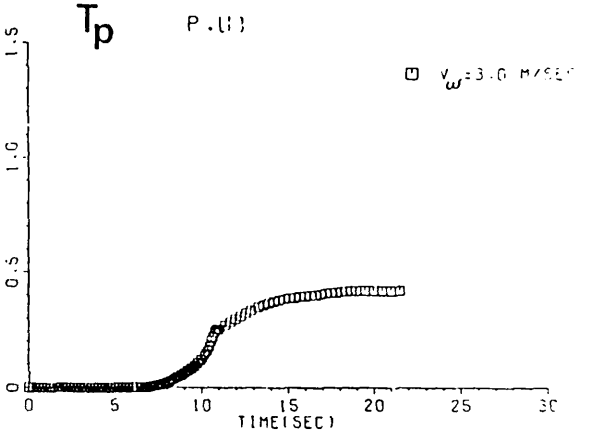

Fig. (6.63) Pump torque

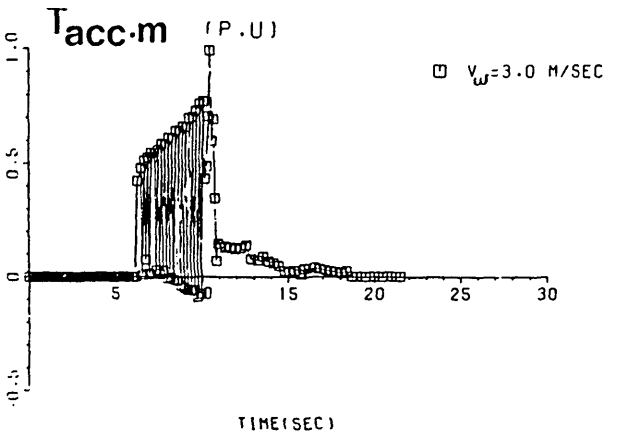

Fig. (6.64) Acceleration torque for the motor

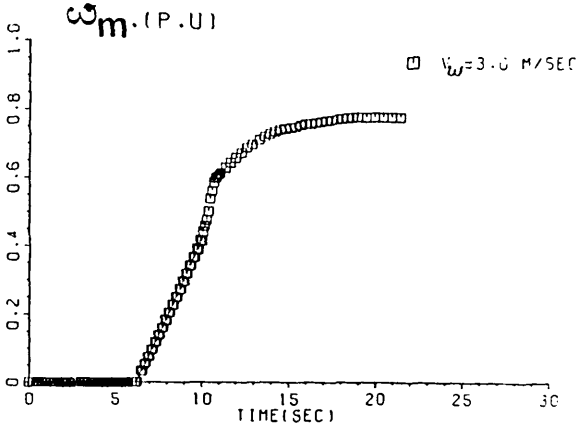

Fig. (6.65) Motor speed.

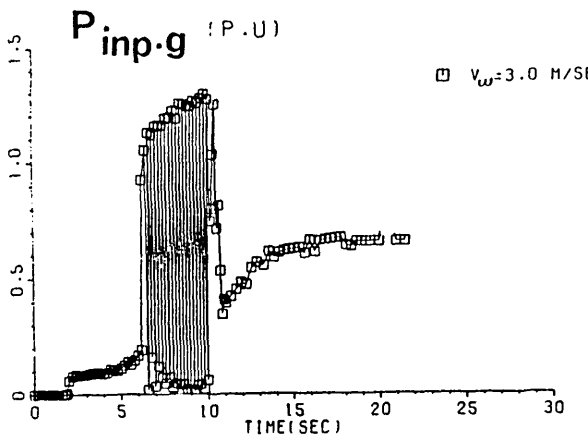

Fig. (6.66) Mech. i/p power to the gen.

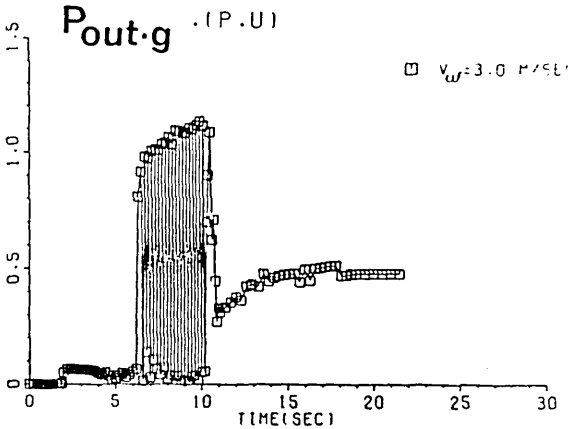

Fig. (6.67) Elec. o/p power of the gen.

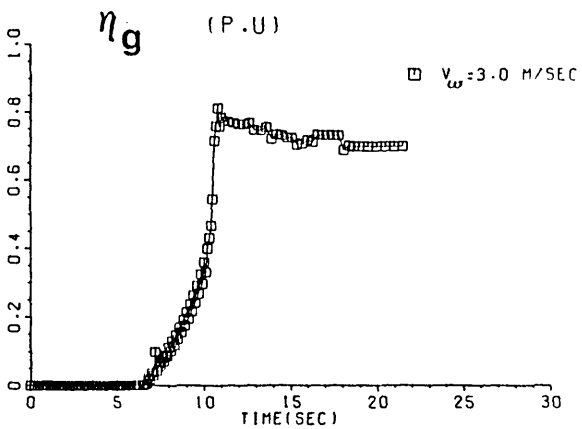

Fig. (6.68) Efficiency of the gen.

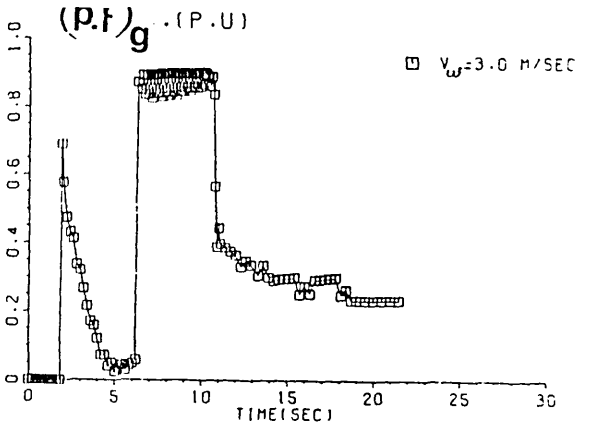

Fig. (6.69) Power factor Of the gen.

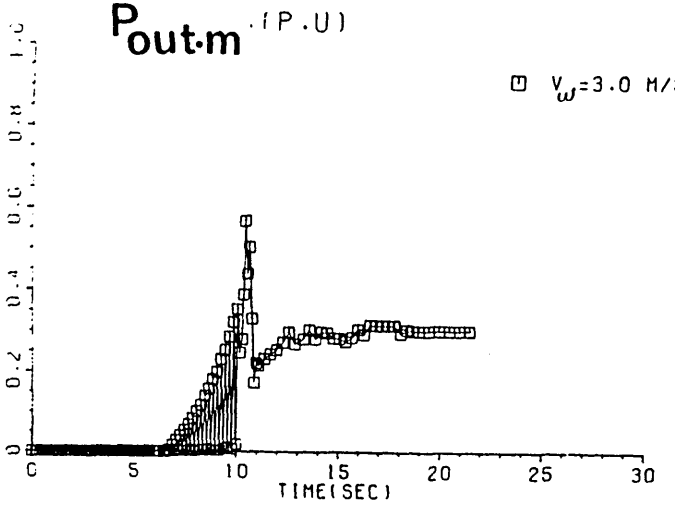

Fig. (6.70) Mech. o/p power of the motor

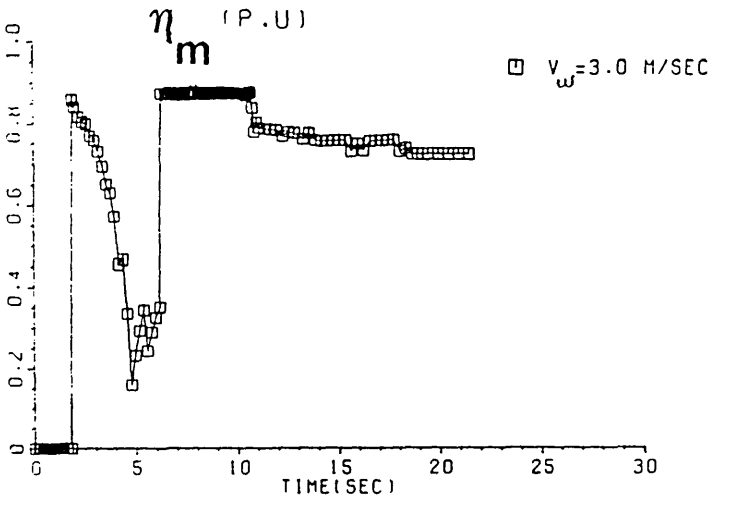

Fig. (6.71) Efficiency of the motor

CHAPTER 7

CONCLUSIONS

This thesis has analysed aspects of a wind pumping scheme based on the use of an electrical rather than a mechanical connection between turbine and pump. Aspects of the use of such a scheme have been investigated, and some eight codes for predicting various operating characteristics of a number of the scheme's variants have been drawn up. The use of such a scheme instaed of a direct mechanical connection can bring a number of advantage, as mentioned earlier, though the first–cost is likely to be higher, and the electrical nature of the scheme may introduce adverse development, maintenance and operational implications. Although the electrical parts of the scheme are simple constructionally, it has been seen that performance predictions are complicated by the strong coupling between the phenomena in the two machines and by the key role of saturation in fixing operating voltages. Although the analysis has been based on the steady state single phase equivalent circuit of the induction machine, with saturation taken into account by making each magnetizing inductancedependent on the calculated air gap flux level, the reasonably good correspondence between the test data obtained and predictions from some of the codes suggests that this simplification is allowable so far as many operating features of the scheme are concerned. It has to be admitted that, under certain conditions, (e.g. the fast generator voltage build up process and motor run–up in the vicinity of peak torque), the rate of change of r.m.s. electrical quantities will exceed occasionally the 10% per cycle figure suggested in thesis as the limit figure for 'steady state' operation. However, the analysis was found to be capable of predicting the generator speed at which voltage build–up occurs, and

the value of the final voltage at the end of the build–up period. Also, the final motor speed is likely to be predicted well in spite of probable errors in respect of the duration of the starting process.

A number of conclusions can be drawn from the work, many of which give guidance for the design of such systems:

1] Based on tests and predictions with two specific systems (viz system 1 with an 11Kw generator coupled to a 5.5 Kw motor, and system 2 with 5.5 Kw generator coupled to a 5.5 Kw motor), it appears that the maximum pump rating to avoid over–currents in the machines is approximately 85% of the motor rating when the generator rating is double that of the motor, falling to 70% approximately when the generator and motor rating are equal. In the former case, the limit is set by motor I^2R heating and in the latter case by generator heating. There is slight doubt about the influence of machine design on these guildline figures, since the tests showed that the 5.5 Kw machine at least could not deliver rated torque under rated voltage and frequency conditions without drawing an excessive supply current.

2] The most severe requirement so far as excitation requirements are concerned is the motor starting process, during which the capacitor bank must be large enough to supply the motor's heavy starting VAr requirement as well as the excitation needs of the generator. A trade–off was found between the selected generator speed at which the motor was started (by isolating–switch closure) and the size of the capacitor bank. Figures specific to the system studied but very probably typical of others, were 0.8 p.u speed and 6 p.u capacitor KVAr (where 1 p.u speed corresponds to 50 Hz synchronous speed

and 1 p.u KVA corresponds to the motor's input KVA at rated load). This means that the minimum operational speed of the system is approximately 0.8 p.u, a value which implies some 'wastage' of operating potential, though not an excessive wastage in view of the cubic law between generator speed and wind power capture.

3] As expected the excitation voltage prior to motor isolating switch closure was not found to be sensitive to capacitor values beyond those giving magnetic saturation in the generator. However, the size of capacitor was found to affect the speed at which self–excitation commenced.

4] The maximum system speed was found to be constrained almost entirely by excessive currents either in the motor (in system 1 with a generator of twice the motor rating) or in the generator (in system 2 with identical motor and generator).

Investigations were made of the scheme's operation with 3 specific operating modes:
a) constant voltage, b) constant voltage/frequency and c) constant capacitance.

5] With constant voltage operation, the system's speed range is severely limited by excessive saturation at low speeds (due to high V/F) and excessive motor slip due to mechanical overloading at high speeds (insufficient V/F). Each causes excessive currents (and hence heating) in the motor and at low speeds in the generator. Assuming limit currents of 1.2 p.u, the feasible estimated generator speed range is 0.83 to 1.09 p.u. This gives a pump power

range of 0.36 to 0.82 p.u (i.e 2.8:1). To maintain constant voltage it was found that the capacitance needed to be varied over a 2.9:1 range from 3.9 to 1.35 p.u. The maximum capacitor KVAr required during operation of system 1 was estimated as 10.86 (1.35 p.u) at 1.02 p.u pump speed with a pump input power of 6.6 Kw, a generator speed of 1.09 p.u or 1635 rev/min, and a generator input power of 9.5 Kw. The overall system electrical efficiency was found to vary between 52% and 67% range over the feasible speed range. Although the constant voltage operating mode may be useful if the generator is also to feed other (non−frequency−sensitive) electrical equipment, it is evident that the $\phi\alpha\frac{1}{f}$ variation in motor and generator flux levels severely restricts the system's feasible speed range, and warsens the motor's propensity to operate beyond pull−out at high speeds.

6] The constant voltage per frequency mode was, not surprisingly, found to give generally better results than the constant voltage scheme and would hence be generally preferred. With constant voltage per frequency operation, the system could theoretically operate over a wide range of generator speeds from zero to 1.135 p.u, corresponding to a pump power range from zero to 0.95 p.u. Beyond this, the pump is apt to over load the motor. However, large capacitor values are obviously required for successful low speed operation, but the capacitors switched in for low speeds need not be rated for high voltage. In view of these factors and the cubic nature of the pump power characteristic, it is probably sensible not to seek to make a constant V/F system operate much below 0.6 p.u. This gives a pump range of 0.15 p.u to 0.95 (i.e 5:1), and in this case the capacitance must be varied over a 2.4:1 range only, from 3.3 p.u to 1.4. The average overall electrical efficiency ($\eta_m \cdot \eta_g$) was found to be approximately 65% over the 0.6 to 1.1 p.u speed range.

Although controllable capacitor banks are now common, there is no doubt that the original concept of an electrical system comprising merely two induction machines and a sectionalized capacitor bank remains attractive in terms of reliability and simplicity, particularly for remote site applications.

7] The study of the 'fixed capacitance' operating mode showed that, in practice, a single value of capacitance was not in fact feasible. The prime reason for this was found to be the unavoidably high motor input KVAr requirement at starting. High input KVAr could not be avoided by starting the motor at a low frequency because the self–excitation process in the generator demands unrealistically high capacitance values at low speeds. Starting the motor even at 0.8 p.u speed required 6 p.u of capacitors on the system. Once the motor and pump are started and currents have fallen, capacitance must be reduced to a switchable lower value to avoid excessive V/F saturation. Over a restricted speed range (typically 0.55 to 0.8 p.u), maintenance of the capacitance constant at this lower value was found to give satisfactory operation. This can perhaps be explained by assuming a naturally–occurring constancy in V/F and machine VAr requirements varying as $I^2.wL$. Since motor torque α w^2 due to the pump load and $T \alpha I^2$ (neglecting magnetizing current), $I \alpha w$. Hence machine VAr α w^3 L. The capacitor VAr varies as V^2WC i.e. W^3C with constant V/F. This explanation is highly approximate and in practice, currents and voltages were found to increase excessively for speeds beyond 0.8 p.u. Hence for operation at speeds beyond the limiting value (0.8 here), a third, still lower value of capacitance was found to be necessary.

8] With the fixed capacitance mode, it was found theoretically that, over a considerable range of generator speeds, there existed not one system operating point at a given speed, but two.

One involves a relatively low system voltage, the other a higher voltage, leading to saturation in the machines. The first was predicted to be an unstable point either voltage collapse occurring with any slight disturbance in conditions, or voltage build–up, until the other, stable operating point is reached.

9] The choice of capacitance to be used in the fixed capacitance mode scheme is affected by several factors. The presence of the induction motor plus pump load was found to give rise in fact to a rather complex relationship between capacitance and voltage even when running conditions at a single speed are considered. There was of course found to be a generator speed–dependent minimum value of capacitance necessary for the maintenance of system voltage.

10] In spite of the break from the simplicity of the original, constant capacitance concept, the use of a two section (for restricted speed range) or a three section bank (for a wider speed range) is not felt to complicate matters unduly. Simple three–phase relay–contactors or anti–parallel thyristor solid state contactors can be used for section switching and for the motor isolating switch. Costs are relatively low and no harmonic currents need be introduced. The control for the contactors can be based on a simple voltage sensor for the motor isolating contactor and on a simple generator current sensor for the capacitor section contactors, the latter switching in or out an additional section depending on whether the motor current was respectively low or high. For one of the systems studied (system 1), desired per unit capacitor values were

estimated as 2.0 for the permanently connected section, and 2 and 2.37 for the switched sections.

As before, the system's maximum speed is limited (to 1.05 p.u. in the system studied) by excessive motor current caused by the pump's overloading the motor, due in turn to the pump's $T \alpha w^2$ characteristic. The overall electrical efficiency $\eta_m \ \eta_g$ of the scheme studied when operated in this 'constant capacitance' mode was found to be approximately 52% over the 0.6 to 0.8 p.u generator speed range and approximately 64% over the 0.8 to 1.05 p.u generator speed range.

11] System performance was investigated both with generator and motor identical and with a generator of twice the motor's rating. The use of a larger generator was found to enable the motor to be used (with a larger pump) up to its full rating, and to allow a somewhat wider system speed range. Alternatively the larger generator can be used to raise system efficiency somewhat. Recent laboratory tests have shown that motor starting may be difficult with too small a generator, particularly where seal friction or other adverse circumstances occur.

12] So far as voltage, frequency and harmonic conditions are concerned, the use in the capacitor banks of standard, low cost, 50 Hz capacitors (as developed for factory power factor correction installations) is thought to be feasible. Weight with modern units is low and the bank's volume is typically comparable with the combined volume of the two machines. Standard protection and safety discharge features would be incoporated in practical installations. The capacitor bank's physical environment may however be unsuitable for standard

factory P.F. correction capacitors, since ambient temperature and weather proofing needs are likely to be considerably more stringent.

13] The system's dynamic operation, both prior to and after motor start–up for both constant generator speed and constant wind speed, variable generator speed conditions, and for both fully regulated capacitor bank and sectionalised capacitor bank schemes was simulated. Although the simulation results were not correlated with test data, the general pattern of results line up very much with expectations and with qualitative observations on the lab rig, and the simulation technique is hence very likely to be valid so far as most aspects of system operation are concerned.

14] Simulation results showed that, if a fully regulated capacitor bank was used, 'soft start' conditions could be obtained for the motor and the starting current thus limited to only 2.6 p.u without unacceptable reductions in motor mean acceleration. A constant preset system dv/dt control startegy was assumed for the motor–starting period, and the influence of increases in the preset dv/dt was found to give rise to correspondingly reduced motor starting times.

15] Although fully regulated capacitor banks unquestionably improve the scheme's performance electrically (e.g. V/F maintained constant, motor soft–started, absence of oscillating behaviour predicted during starting), there is no doubt that the use of a sectionalized capacitor bank with a small number of sections is more practical, particularly for remote site applications. From previous work, we believe that the use of a single value of 'running' capacitor gives satisfactory system operation for generator speeds within a 1:1.5 band

corresponding to a roughly similar band of wind speeds. At lower speeds, voltage reduction tends to give rise to pump stall, while higher speeds lead to excessive magnetic saturation in the machines and excessive I^2R losses. The cost of a third capacitor section in order to widen the feasible speed range (typically into 2:1) can obviously be traded at the design stage against the extra annual pump output achieved, or the saving in the cost of turbine regulating features.

Although the investigation has tackled some of the major aspects of capacitor–excited induction generator schemes, a number of loose ends remain. Perhaps the principal items of further work are:

1] Investigation of short–time–scale transient phenomena particularly as regards voltage build–up and motor starting .

2] Investigation of the system behaviour (both 'starting' and 'running') during motor starting with real–time–varying wind speed conditions.

3] Investigation of the behaviour of systems incorporating two or more pump–motors fed from a single turbine–generator.

4] Evolution of protection schemes to avoid capacitance failure or overheating in case of:

   a) Inadvertent disconnection on open–circuit failure of motor–pump load.

   b) Short circuit faults on the cabling or in the machines.

5] Further work into the effect of turbine gear ratio on turbine behaviour under realistic wind conditions, including avoidance of stall.

6] Further work into the influence of generator size on system performance.

7] Evolution of simple controller designs for capacitor bank and motor isolating switches.

8] Investigation of and comparisons between schemes based on other types of electrical machine (e.g. incorporating brushless d.c pump motor or synchronous generator).

9] Field measurements using a real wind turbine and real pump.

10] Theoretical and practical investigations of the effects of hydraulic head variation and motor seal friction on system operation.

11] Incorporation of better iron−loss relations into the prediction codes.

APPENDIX 1

WIND TURBINE CHARACTERISTICS

The basic, simplified analysis of wind turbine behaviour was established before the war and is found in many texts. The following, from ref. [1−1], [1−16], [1−17] and [1−18] summarises the principal relations and their derivations.

The energy asociated with the wind is in the form of kinetic energy, so the energy of an air flow E_a^f, having a cross−sectional area of A, is given by

$$E_a^f = \tfrac{1}{2}\, m_W\, V_W^2 \qquad \text{Jole} \qquad (A1.1)$$

since the mass of air m_W flowing with a velocity of V_W through the area A in one second is:

$$m_W = \rho A\, V_W \qquad \text{Kg} \qquad (A1.2)$$

where ρ=air density Kg/m^3 (1.23 Kg/m^3 at normal conditions−t=15° and P=760 mmHg). The energy flux in one second is numerically equal to the power P_a

$$P_a = 1/2\ \rho A V_W^3 \qquad \text{w} \qquad (A1.3)$$

assuming the cross−sectional area of the wind to be circular in shape (as for horizontal axis propeller−type windmills)

$$P_a = \tfrac{1}{2}\rho\pi\ R^2 V_W^3 \qquad (A1.4)$$

where R is the radius of the windmill. The windmill can transform into useful work only part of the incident wind energy. The extraction efficiency is normally defined as the power coefficient C_p. The power coefficient is a complicated function of many quantities including rotor and air foil geometry, tip−to−wind speed ratio, hub and tip losses, etc. (In practice C_p may also vary periodically with rotation but this is neglected in this thesis.) Betz showed in 1926 that the maximum theoretical power coefficient was 0.593. Generally C_p is defined as the ratio of the power delivered by the windmill (P_m) to the total power (P_a) available in the cross−sectional area of the wind stream subtended by the wind rotor.

Mathematically $$C_p = \frac{P_m}{\frac{1}{2}\rho\pi R^2 V_w^3} \qquad \text{(A1.5)}$$

Fig (A1.1) shows a diagram of the machinery arrangement of an aerogenerator. The mechanical power at the shaft of the wind rotor is:

$$P_m = \tfrac{1}{2}\,\rho\pi R^2\, C_p\, V_w^3 \qquad \text{w} \qquad \text{(A1.6)}$$

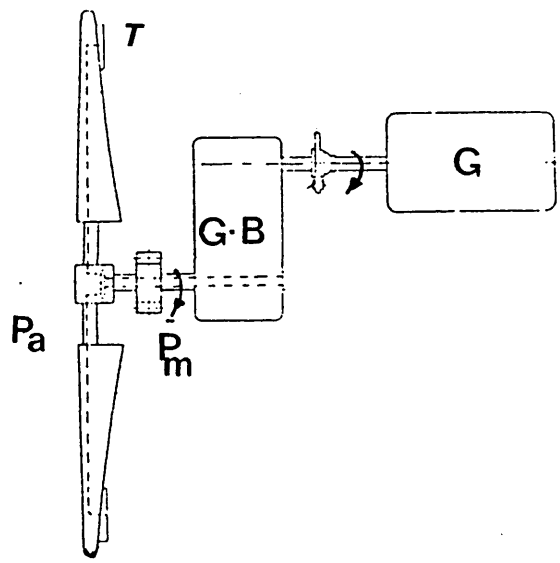

Fig. (A1-1) Diagramatic machinery arrangement of aerogenerator.

Thus, the mechanical power at the shaft is proportional to the square of the turbine rotor radius and the cube of the wind speed. The tip speed ratio λ is defined as the speed of the outermost extremity of the rotor blade divided by the free upstream wind speed i.e.

$$\lambda = \frac{w_g.R}{V_w} \cdot 1/k_g \qquad \text{(A1.7)}$$

where w_g = generator shaft speed and k_g = generator−turbine gear ratio and for a given fixed−geometry turbine, the C_p is usually taken to be a function of λ only. The $C_p(\lambda)$ curve in effect describes the efficiency of the wind turbine as a function of tip speed ratio. A typical efficiency curve for a typical fixed pitch horizontal axis windmill (a family of curves when blade pitch is adjustable) is shown in Fig (A1.2). This curve represents all the curves of different values of V_W. Using equations (A1.6) and (A1.7), the mechanical power at the shaft can be expressed in the form

$$P_m = \tfrac{1}{2}\rho\pi R^5(Cp/\lambda^3)\cdot 1/K_g^3 \cdot w_g^3 \qquad \text{(A1.8)}$$

For aerodynamic reasons wind powered turbines with a high value of tip speed ratio tend to be of "low solidity", i.e. there is only a small proportion (around 15%) of the "swept area" actually occupied by rotor blade. Windmills with high solidity (usually with λ value of unity or less) have however the advantage of high starting torque, which is the reason for them being primarily chosen for water pumping with direct mechanical transmission. Lower solidity, higher λ rotor designs offer higher efficiency, lower turbine mass and higher shaft speeds,

lower gearing and/or generator costs and weights, but lower starting torques.

These are difficult to use with direct connected pumps due to many pump's high starting torque requirements but can be considered for indirect schemes. From Fig (A1.2), it is clear that maximum efficiency occurs at a particular tip speed ratio λ_α. If the wind turbine is to extract the maximum power from the wind, it must be run so as to maintain λ at λ_α. The output power from the wind turbine is then:

$$(P_m)_{max} = \{\tfrac{1}{2}\cdot\rho\cdot\pi\cdot R^5.\frac{C_{pmax}}{\lambda_\alpha^3}\cdot 1/K_g^3\}\cdot w_g^3 \qquad (A1.9)$$

or

$$(P_m)_{max} = K1\cdot w_g^3.$$

Hence, under this operating condition the maximum output power from the wind turbine is again proportional to the cube of the generator shaft speed. Fig (A1.3) shows the wind rotor power against rotational generator speed at various wind speeds. The locus of the maximum power points is shown.

The total torque developed by the wind turbine can be written as:

$$T_t = (K_g)\cdot P_m/w_g \qquad (A1.11)$$

From equations (A1.2) and (A1.11), the total torque can be expressed in the form

$$T_t = \{\tfrac{1}{2}\cdot\rho\cdot\pi\cdot R^5\cdot C_p/\lambda^3.\ 1/K_g^2\}\cdot w_g^2 \qquad (A1.12)$$

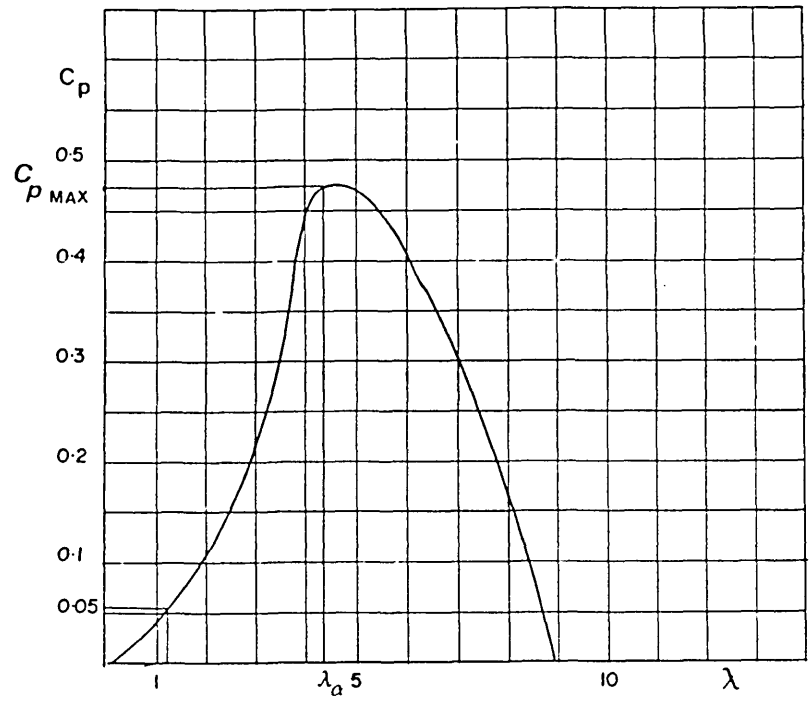

Fig. (A1-2) Power coefficient Cp versus tip speed ratio for a typical fixed pitch horizontal axis wind mill.

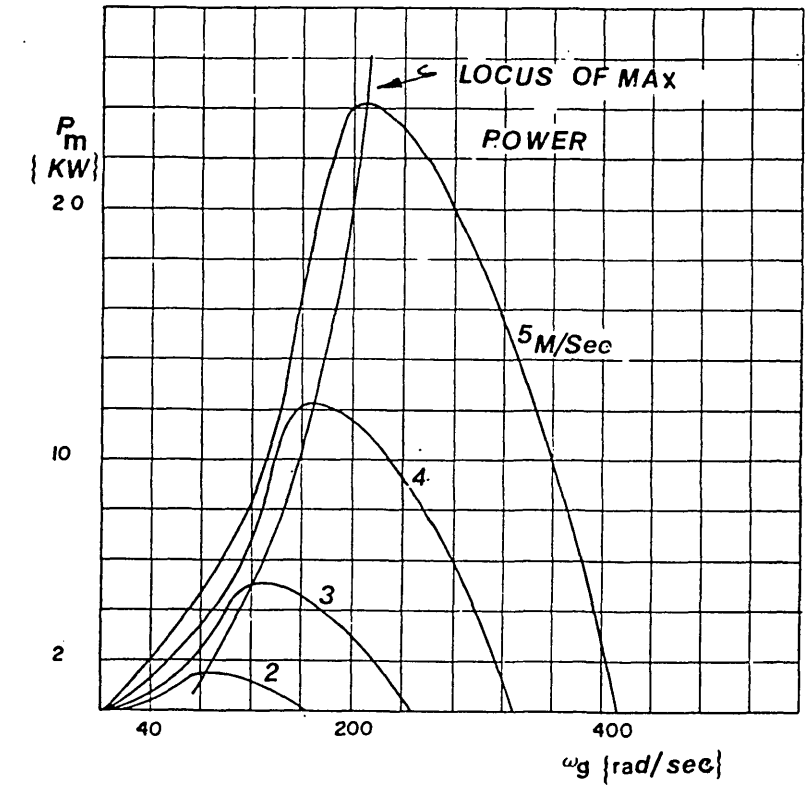

Fig. (A1-3) Wind rotor power Pm versus angular speed wg for different values of wind speed.

Using equations (A1.6), (A1.7) and (A1.11), the total torque developed by the wind turbine can be written as:

$$T_t = \tfrac{1}{2} \cdot \rho \cdot \pi \cdot R^3 \cdot V_w^2 \, C_p/\lambda \qquad \text{(A1.13)}$$

or

$$T_t = \tfrac{1}{2} \cdot \rho \cdot \pi \cdot R^3 \cdot V_w^2 \, C_Q \qquad \text{(A1.14)}$$

where $C_Q = C_p/\lambda$ is the torque coefficient of the wind turbine and can be taken as a function of the tip speed ratio λ only. Fig (A1.4) is a C_Q/λ curve for the same wind turbine. It can be noticed that a single maximum in C_Q occurs when the tip speed ratio takes a particular value of λ_β of λ. It can also be seen that this value of λ is different from the value λ_α of λ at which the wind turbine extracts the maximum power from the wind. The maximum torque and maximum power hence occur at different shaft speeds. Fig (A1.5) shows the wind rotor torque against rotational speed at various wind speeds. The loci of maximum torque and maximum power points obviously differ.

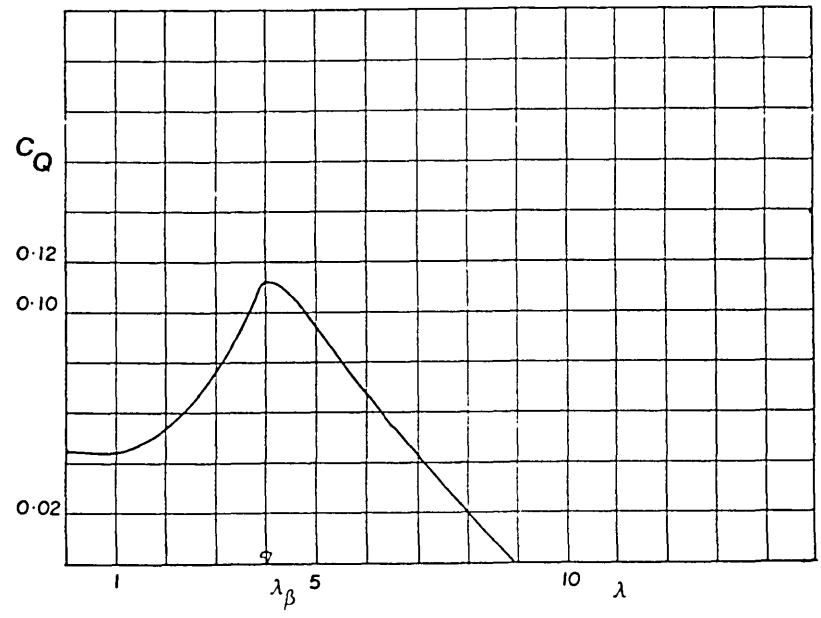

Fig. (A1-4) Torque coefficient C_Q versus tip speed ratio for a typical fixed pitch horizontal axis wind mill.

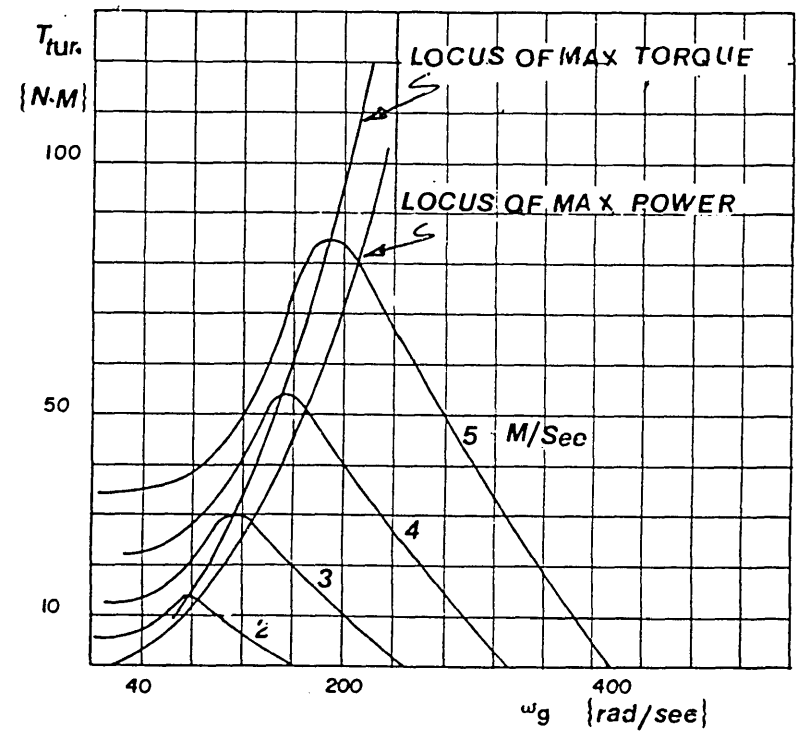

Fig. (A1-5) Wind rotor torque Tt versus angular speed wg for different values of wind speed.

APPENDIX 2

A2.1 Wind–Pumping System

The basic relations for pump behaviour are found in many texts. The following material, from ref [1-5], [1-6], [1-7], [1-19], [1-20], [1-21] and [1-22] summarises the principal factors concerning pump behaviour and selection.

Most motor pumps powered by windmills are of the reciprocating type or of some other positive displacement type [1-6].

A2.1.1 Rotary Displacement Pumps

Rotary pumps are characterized by steady (non pulsating) rates of discharge, high pressure delivery capabilities, high hydraulic efficiencies (90–95%), capacities proportional to shaft rotational speeds, and brake horse power proportional to shaft speed and dynamic head. If used down–hole in mechanical wind powered systems, rotary pumps require power shafting from gound to pump level [1-5].

A2.1.2 Reciprocating Pumps

Reciprocating pumps are characterized by a pulsating discharge, and the farm windmill is of this type. These pulsations occur at a frequency of $\sim$ 0.1 to 1 Hz. Therefore an analysis of the effect of this kind of load on the rotor cannot be made until wind data of comparable frequency of statistically reliable

representation are available, and one has a dynamic model for rotor and system performance. In general the rotational inertia of the system will smooth out the power demand to an average value, and the system becomes mathematically equivalent to the positive displacement rotary pump [1-5].

The variation of the stroke of a reciprocating water pump is one method of varying the pump load torque. Variable displacement designs exist for nearly every known positive–displacement type of pump. It may be said that the stroke–adjusting mechanism would permit the most efficient extraction of wind power for water–pumping over a wide range of wind speeds. It also permits a pump designed for a given wind and pumping head to be used at a different wind speed and over a different pumping head. The stroke adjusting facility also ensures relatively safe operation at higher wind speeds and permits the pump to operate at much lower wind speeds than possible with conventional–wind–driven pumps [1-6]

A2.1.3 Piston Pump

The classical wind pump system consists of a slow running wind turbine and piston [1-7]. Fig (A2.1) shows the schematic drawing of a piston pump connected to a wind rotor [1-9]. The piston pump is a load demanding a constant torque, which makes coupling to a wind machine rather difficult [1-7]. Although considerable effort has been expended by designers to improve wind turbine blade shapes, the higher values of C_p achieved in this way are frequency wasted through the inherent poor load matching with the pump [1-21]. Starting is even more difficult because of the cyclic variation of the pump's torque. The maximum torque is π times the average torque. When starting,

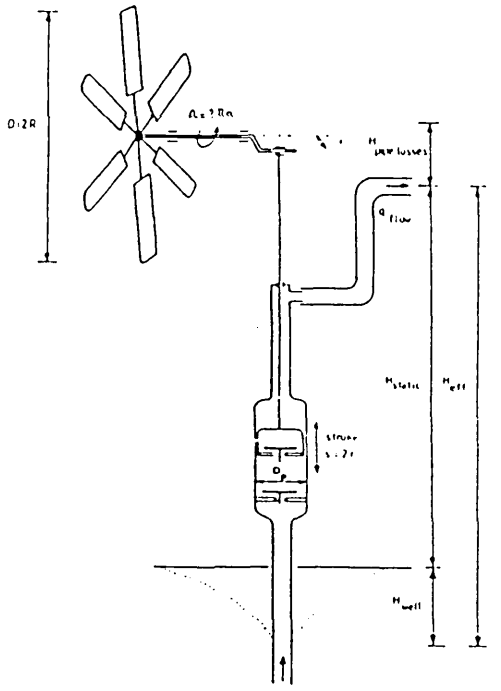

Fig. (A2-1) Schematic drawing of a piston pump connected to a wind rotor.

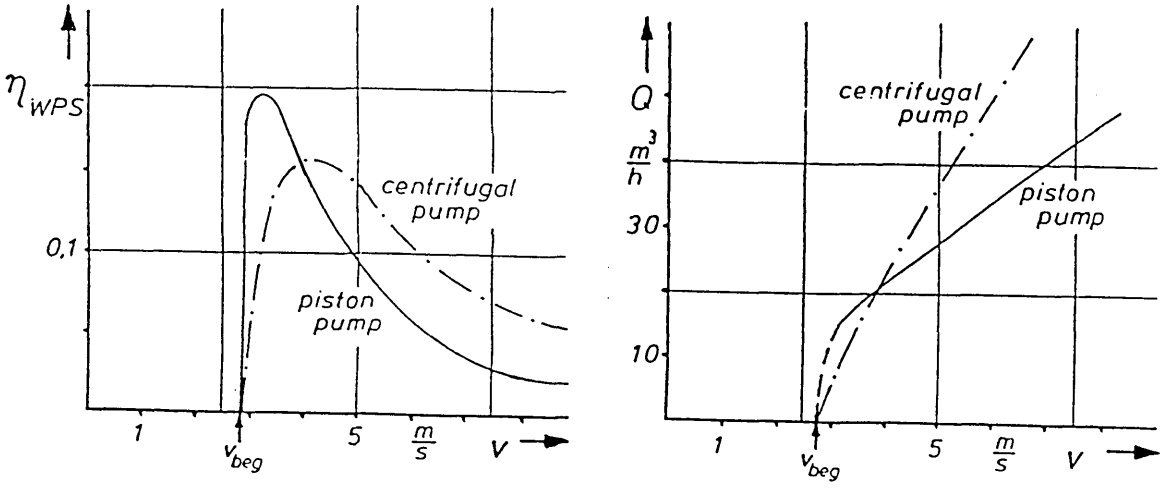

Fig. (A2-2) The total efficiency and the delivery versus wind speed.

the windmill has to overcome this maximum torque. Once it is running it "feels" only the average torque (due to the large inertia of the rotor). The power requirement of a piston is linearly dependent on the number of revolutions n, the working V and the total head H

$$P_{mech} = \rho_w \, g \, H \, V \, n/\eta_{mech} \qquad (A2.1)$$

where

ρ: The density of the water

g: acceleration due to gravity

η: mechanical efficiency.

If the graph of the power requirement of piston pump is superimposed on the characteristic of the wind turbine, the intersection point gives the rotational frequency dependent on wind speed, $n=n(V_w)$, and the ideal hydraulic pump output

$$P_{hydr} = \rho_w \, g \, H \, V \, n(V_w) \qquad (A2.2)$$

Thus, the hydraulic pump output power can be written in the form:

$$P_{hydr} = \rho_w \, g \, Q \, H \qquad (A2.3)$$

Since the pumping head is normally fixed and since the pumping rate is the most interesting quantity for users, the pumping rate Q instead of the net power is of interest [1-19]

$$Q_{(V_w)} = V\ n(V_w)/\eta_{vol} \tag{A2.4}$$

where η_{vol} : volumetric efficiency for piston pump $\simeq$ 80%

$$\eta_{vol} = \frac{Q_{(V_w)}}{n_{(V_w)} \cdot S\pi/4D_p^2} \tag{A2.5}$$

S: stork of the pump

D_p: Diameter of pump cylinder.

The total efficiency of the turbine and piston pump system [1-8] can be obtained from the product of the individual efficiencies $\eta_{wps} = C_p \cdot \eta$ (the turbine efficiency is equal to the power coefficient C_p and $\eta = \eta_{mech} \cdot \eta_{vol}$) or from the relation between pump output and theoretical wind power.

$$\eta_{wps} = P_{hydr(v)}/(\tfrac{1}{2}\rho V_w^3\ \pi\ R^2) \tag{A2.6}$$

η_{wps} is typically low, e.g. 20%. This is caused partly by the mismatch between the linear relationship between power demand and rotational speed for piston pumps, and the square law relationship between the peak power capacity of the windmill and rotational speed. However annual pump output is also adversly affected by starting problems, and the largest increases in annual pump output are likely to be achieved by minimising the starting windspeed, rather than by attempting to obtain full power matching over the entire range of operating wind speeds. The coupling between windmill and pump can be characterised conveniently by the design wind speed, which is the wind speed for which the overall power coefficient $C_p\eta$ reaches its maximum. The design wind speed can be found simply by equating the torque delivered by the

windmill, and that demanded by the pump due to the total static head [1-19].

$$\tfrac{1}{2}\rho \cdot V_w^2 \cdot C_Q \; \pi \; R^3 = i \; \tfrac{1}{\pi} \; \rho_w \; g \; H \; \tfrac{1}{2} S \tfrac{\pi}{4} \; D_p^2 \; \eta_{vol} / \eta_{mech} \qquad \text{(A2.7)}$$

where

i= transmission ratio (i<1 represents a speed–reducing transmission).

For the design point one may substitute $C_{Q_{max}} = C_{p_{max}} / \lambda_\alpha$ and find

$$V_d = \sqrt{\frac{\eta_{vol} \; S \; D_p^2 \; \lambda_\alpha \; \rho_w \; g \; H \; i}{4 C_{p_{max}} \; \eta_{mech} \rho \pi R^3}} \qquad \text{(A2.8)}$$

A high design wind speed corresponds to a relatively heavily loaded windmill (i.e. a large pump coupled to a relatively small windmill).

Another relationship [1-19] for calculating the wind power output in a given wind regime for a wind machine driving constant torque load "piston pump" is:

$$P_{(V_h)} = C_{p_{max}} \; \eta \cdot \tfrac{1}{2} \rho \; \tfrac{\pi}{4} \; D^2 \; V_d^2 \left\{ \frac{V_h}{V_d} \cdot \frac{\lambda_\alpha}{\lambda_d} - \frac{V_d}{V_h} \left(\frac{\lambda_\alpha}{\lambda_d} - 1 \right) \right\}$$

where

V_h: average hourly wind speed (m/s)

D: rotor diameter (m)

λ_α: design tip speed ratio

A2.1.4 Comparison between Piston and Centrifugal Pumps

In Fig (A2.2) (a) and (b), typical curves of water delivery rate for wind–powered pumps of the two types and their total efficiency are shown as functions of wind speed. It can be seen from the curves of delivery that, after delivery begins, the piston pump initially delivers more, but above a certain speed, the total efficiency of the wind pump system with centrifugal pump is higher. At high wind speeds, it is nearly twice as efficient. Another important aspect is that, if the graph of power requirement of the piston pump is superimposed on the characteristic of wind turbine, the intersection point gives the rotational frequency as a function of wind speed. The centrifugal pump, once delivery has commenced, operates close to the optimum even when wind speeds increase strongly. The power requirement of the centrifugal pump, a fluid–flow machine, fits the characteristic much better than in the case of the piston pump [1-7].

APPENDIX 3

System B parameters:

Electrical machines' name plate data:

Generator: GEC Kapac, totally enclosed, 3 phase, 4 pole, 50 Hz, cage induction motor 11Kw, 415v, 25A, delta connected

Motor: GEC Kapac, totally enclosed, 3 phase, 4 pole, 50 Hz, cage induction motor, 5.5 Kw, 415v, 11.2A, delta connected.

The machines' parameters and the base values for the pre−unit quantities quoted in the text and graphs are as follows:

A bar over a symbol refers to a base value.

$\overline{V}_{Line} = \overline{V}_{ph} = 415v$

$\overline{I}_{ph} = 11.2/\sqrt{3} = 6.47A$

$\overline{Z} = 64.18\ \Omega$

$\overline{f} = 50$ Hz

$\overline{n} = 1500$ rev/min

$\overline{C} = 148.8\ \mu F$

$\overline{KVA} = 3\overline{V}_{ph}\,\overline{I}_{ph} = 8.050$

$R_{1g} = 0.0133$ p.u

$X_{1g} = 0.0495$ p.u

$R_{2g} = 0.0152$ p.u

$X_{2g} = 0.060$ p.u

$R_{mg} = 13.52$ p.u

R_{1m} = 0.0452 p.u

X_{1m} = 0.117 p.u

R_{2m} = 0.0405 p.u

X_{2m} = 0.162 p.u

R_{mm} = 22.3 p.u

System A parameters

Electrical machines' name plate data:

Generator and motor

3 phase, 6 pole, 50 Hz, wound rotor, 5 Hp, 220v, 16A.

The machines' parameters and base values in this case were:

$\overline{V}$ = 220v (line)

$\overline{I}$ = 16 A (line)

$\overline{f}$ = 50H

$\overline{n}$ = 1000 r.p.m.

Base impedance = 7.95Ω

$R_{1g} = R_{1m}$ = .42 p.u

$R_{2g} = R_{2m}$ = 0.088 p.u

$X_{1g} = X_{2g} = X_{1m} = X_{2m}$ = 0.17 p.u

$R_{mg} = R_{mm}$ = 15.88 p.u

APPENDIX 4

Calculation of moments of inertia of the generator, motor, pump, water and wind turbine. The inertia figures used throughout the project, believed to be typical for the equipment involved, were estimated as follows:

1 Moment of inertia of the generator and motor

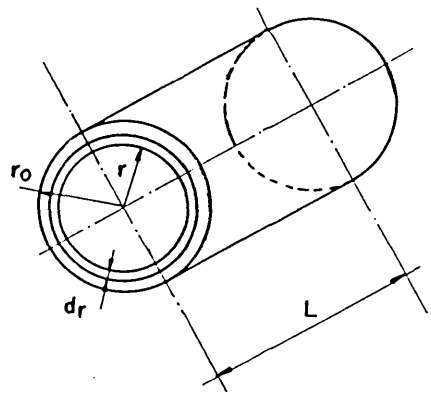

Fig. (A4-1) Motor dimension

For the 5.5 Kw induction machine shown in Fig (A4.1), the dimensions of the rotor are L=0.17m and r_0= 0.1m. The moment of inertia of the rotor is

$$J_m = \int_{r=0}^{r=r_0} dm \cdot r^2 dr$$

where

dm = mass of elementary annulus

$= 2\pi r \rho dr \cdot L.$

Hence

$$J_m = \int_{r=0}^{r=r_0} 2\pi\rho L r^3 dr = \frac{2\pi\rho L r_0^4}{4}$$

Putting $\rho_{\text{iron}} = 7.8 \times 10^3$ Kg/m^2 ,

$$J_m = 2\,\frac{\pi}{4}(7.8\times10^3) \times (0.17) \times (0.1)^4$$
$$= 0.208 \text{ Kg·m}^2$$

The moments of inertia of both the 11 Kw and the 5.5 Kw generators were taken, for simplicity as also equal to this figure. This is of course not so, but the effect on the simulation results is not drastic, and proper valves could be substituted easily. Simimarly the moment of inertia of the pump and water were assumed equal to $\frac{1}{4}$ J_m and 2 J_m respectively. Hence

$$\text{Motor–pump total inertia} = J_m + 0.25\ J_m + 2.0\ J_m$$
$$= 0.676 \quad \text{kg.m}^2$$

2. Moment Inertia of the Wind Turbine

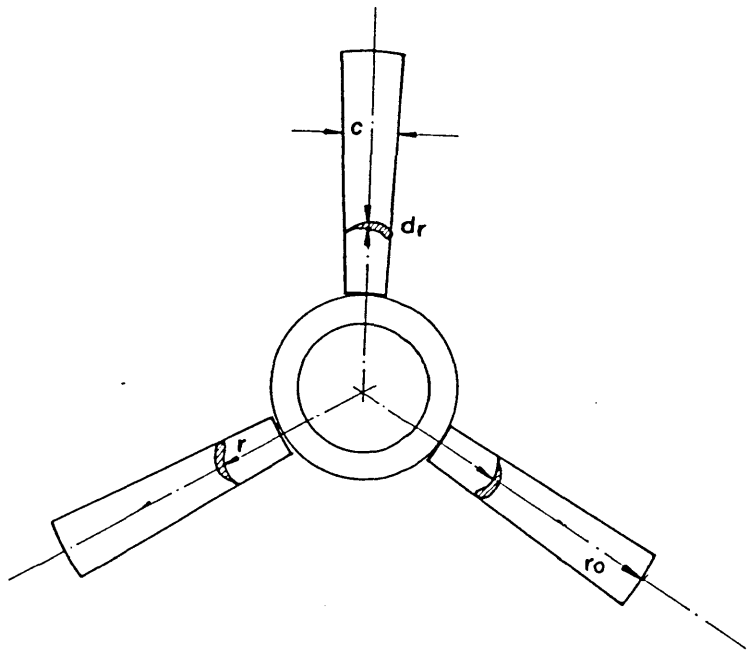

Fig. (A4-2) Rotor dimension

For the turbine used, shown in Fig (A4.2), the dimensions of the rotor blades are $r_0 = 2.5$ m and w = 0.004m. Assuming that the blade chord at mid span is equal to 15% of the blade pitch, then

$$c = 0.15 \frac{\pi D}{2} \cdot \frac{1}{3} = 0.3926\text{m}.$$

Moment of inertia of the turbine motor $= \int_{r=0}^{r=r_0} dm \cdot r^2 dr$ where $dm = 3c\rho dr \cdot w$.

Hence

$$J_t = \int_{r=0}^{r=r_0} 3c\rho w r^2 dr = c\rho w r_0^3$$

$$J_t = (0.3926)(7.8\times10^3)(0.004)(2.5)^3$$
$$= 191.39 \text{ Kg}\cdot\text{m}^2.$$

The turbine–generator total inertia referred to generator shaft is thus:

$$J_g + J_t/K_g^2 = 0.208 + 191.39/(23)^2 = 0.5697 \text{ Kg}\cdot\text{m}^2.$$

REFERENCES

[1.1] Doerner, H: 'Wind Energy Utilization – General View, Possibilities and Limitations'. Forschung Windenergie FWE 1985.

[1.2] Hurley, B.: 'Wind Energy for Load Drainage in Ireland'. Proc. of 8th BWEA conf. Cambridge 1986.

[1.3] Vandijk, H.J: 'Calculation of Required Storage Tank Capacity in Wind Pump Irrigation Systems'. Wind Engineering Vol. 10, No. 4, 1986.

[1.4] Nelson, V., Clark, R.N. and Barieau, R.E.: 'Wind Power Applications in the United States – Irrigation Pumping'. Wind Engineering Vol. 6, No. 2, 1982.

[1.5] Gilmore, E., Barieau, R.E. and Nelson, V.: 'Wind Power for Irrigation'. Wind Engineering, Vol. 1, No. 4, 1977.

[1.6] Vinayagalingam, T. and Sivasegaram, S. : 'A Variable–Stroke, Wind–Operated Water –Pumping System'. Wind Engineering, Vol. 3, No. 2, 1979.

[1.7] Gasch, R., Kortenkamp, R. and Twele, J. : 'A Simple Method for Near *Optimum* Design of Wind Turbine with *Centifugal* Pumps'. Wind Engineering, Vol. 11, No. 5, 1987.

[1.8] Fraenkel, P.L.: 'Review of Power Transmission Options for Wind–Powered Water Pumping'. Wind Engineering, Vol. 11, No. 3, 1987.

[1.9] Gray, P.A.: 'Science Research Council'. Wind Engineering, Vol 3, No. 4, 1979.

[1.10] *Tecnische* Hageschool, Eindhoven: 'Vakgroep Elecktromechanica en Vermogenselektronica, Afdelingden Elektrotechnick'. Rapport Nr EM 83–25, 1982.

[1.11] Geozinne, F. and Eilering, F.: 'Water Pumping Windmills with Electrical Transmission'. Wind Engineering, Vol. 8, No. 3, 1984.

[1.12] Batchelor, S.J. and Dunn, P.D.: 'Windpumps: A System Assessment. Wind Engineering, Vol. 11, No. 1, 1986.

[1.13] Todd, R.W.: 'Small Scale Wind Energy System'. Wind Engineering, Vol. 3, No. 4, 1979.

[1.14] Fraenkel, P.L. : 'Small Windmills for Pumping Water,.Wind Engineering, Vol. 3, No. 4, 1979.

[1.15] Halliday, J.A. and Lipman, N.H.: 'Wind Energy in Agriculture'. Wind Engineering, Vol. 6, No. 4, 1982.

[1.16] Watson, G.R. and Bainbridge, G.R.: 'The Design Construction & Proving of a Low Cost 5 Kw Wind Powered Turbine for Isolated Applications'. International Conference on Future Energy Concepts. 1979.

[1.17] Nicodemon, V.C.: 'Small Wind–Powered Electric Generators and Systems'. PhD Thesis, Imperial College, University of London, 1979.

[1.18] Wind Energy for the Eighties: A Review by Members of the British Wind Energy Association, England, 1982 (Book)

[1.19] Meel, J.V. and Oldenkamp, H.: 'Field Performance Monitoring System for Water Pumping Windmills'. Wind Engineering, Vol. 8, No. 4, 1984.

[1.20] Meel, J.V. and Smulders, P.: 'Some Results from CWP's Test Fields: Are the IEA Recommendations sufficient for windmills Driving Piston Pumps?' Wind Engineering, Vol. 11, No. 2, 1987.

[1.21] Swift, R.H.: 'On maximising the Long–term Efficiency of Water Pumping Windmills'. Wind Engineering, Vol. 11, No. 5, 1987.

[1.22] Burton, J.D. and Pinilla, A.E.: 'Water Pumps for Windmills: A comparison of Two Commercially Available Systems from South America.' Wind Engineering, Vol. 9, No.1, 1985.

[1.23] Falchetta, M. and Prischich, D.: 'Testing of Wind Pump with Electrical Transmission at the ENEA Test Facility'. Proc. 9th BWEA Conf., Edinburgh, April 1987.

[1.24] Rimmer, W.A.: 'Wind Pumping Electric Transmission'. Imperial College, 3rd year project report, 1985.

[1.25] Hegazy, M.: 'Wind Energy Utilization in Egypt'. EEA Report 1979.

[1.26] Elgmmal, A.H.: 'Prospect of Wind–Refrigeration System in Egypt'. Proc. of 10th BWEA Conf., London, 1988.

[1.27] Nour, S. : 'Ground Water Resources Hydrogeological Condition'. Vol. 3–A. Final Report (GPC) Sept. 1984.

[1.28] Umida, H., Sato, N. and Hayushi, Y 'Induction Generator Running in Parallel to Utility Power Network Requiring no Supply of Reactive Power'. Electr. Eng. J.P.N(U.S.A), Vol. 105, No. no2, 1985.

[1.29] Umida, H., Sato, N. and Hayashi, Y: 'Induction Generator Connected to Utility Network through DC Link Converters'. Elect. Eng. J.P.N(U.S.A), VOl. 105, No. no2, 1985.

[1.30] Velayndhan, C. and Bundell, J.H.: 'A Variable Speed, Constant Frequency Wind Power Generation Scheme Using a Slip–Ring Induction Generator'. 19th Inter Society Energy Conversion Engineering Conference, Vol. 4. (U.S.A) 1984.

[1.31] Velayudhan, C. and Bundell, J.H.: 'A New Automatic Generation Controller for a Wind–Driven Slip–Ring Induction Generator'. Proc. of IEEE (U.S.A), Vol. 72, No. 9, Sept. 1984.

[1.32] Hayashi, Y., Sato, N. and Funaki, S. : 'Self–Excited Induction Generator Parallel to AC Power Lines Through DC–Link Converters'. International Power Electronics Conference, Vol. 2, Tokyo, March 1983.

[1.33] Velayundhan, C., Bundell, J.H. and Leary, B.G. : 'An Adaptive Rotor Resistance Controller for Wind–Driven Slip–Ring Induction Generator'. Proc. of IEEE(U.S.A), Vol. 1, Sept. 1983.

[1.34] Reichert, K. : 'Stability of Asynchronous Generators'. Proc. International Conference on Evolution and Modern Aspects of Induction Machines, Torino, Italy, July 1986.

[1.35] Murthy, S.S.: 'Experience with the Analysis Design and Control of Induction Generator Operating in Autonomous or Grid Connected Mode'. Proc. International Conference on Evolution and Modern Aspects of Induction Machines, Torino, Italy, July 1986.

[1.36] Kliman, A.H.R.: 'The Asynchronous Generator, Mirage in Electrical Engineering'. IEEE Proc. Vol. 66, No. 8, August 1978.

[1.37] Eastham, J.F.: 'Principles and Characteristics of Induction Generator'. Electrical Review II November 1960.

[1.38] Adcock, N.C. : 'The Induction Generator'. The English Electric Journal, Vol. 12, December 1952.

[1.39] Velayudhan, C., Bundell, J.H. and Leary, B.G.: 'A Solid–state Controller for a Wind–driven Slip–ring Induction Generator'. Proc. of IEEE (U.S.A), VOl. 72, No. 8, Aug. 1984.

[1.40] Raina, G. and Malik, O.P. : 'Wind Energy Conversion Using a Self–Excited Induction Generator'. IEEE Trans. on Power Apparatus and Systems, VOl. PAS–102, No. 12, Dec. 1983.

[1.41] Malik, N. H. and Hague, S.F. : 'Steady State Analysis and Performance of an Isolated Self–excited Induction Generator.' IEEE Trans. on Energy Conversion, Vol. EC–1, No. 3, Sept. 1986.

[1.42] Ouazene, L. and McPherson, G.: 'Analysis of the Isolated Induction Generator'. IEEE Trans. on Power Apparatus and Systems, Vol. PAS–102, No. 8, Aug. 1983.

[1.43] Johnson, G.L. and Walker, H.S. : 'Three–phase Induction Motor Loads on a Variable Frequency Wind Electric Generator'. Wind Engineering, Vol. 1, No. 4, 1977.

[1.44] Irisa, T. Takata, S. and Ueda, R.: 'Dynamic Performance of Self–Excited Induction Generator with Voltage Controller'. IAS Annual Meeting. 1980 Cincinnati, U.S.A. Sept. Oct. 1980.

[1.45] Singh, B., Saxena, R.B., Marthy, S.S. and Singh, B.P.: 'Reactive Power Requirements of Single–Phase Self Excited Induction Generator to Obtain Constant Voltage Outputs'. ICEM'86. International Conference on Electrical Machines. Munchen, Sept. 1986.

[1.46] Daly, S.A., de Paor, A.M. and Simpson, R.J. : 'Modelling and Control of a Wind–Driven Induction Generator for Water Storage–Heating'. IEE Proc. Vol. 130, No. 9, Dec. 1983.

[1.47] Pinheira, R.E., Watanabe, E.H. and Careiro, S. Jr. : 'Reactive Power Compensator for Self–excited Induction Generator with Unbalanced Load' . Proc. ICEM Conf., Vol. 1, Munchen, Sept. 1986.

[1.48] Malik, N. H. and Mazi, A.A. : 'Capacitance Requirements for Isolated Self–Excited Induction Generators'. IEEE Trans. on Energy Conversion, Vol. EC–2, No. 1, March 1987.

[1.49] El–Sharkawi, M.A., Williams, T.S. and Butler, N. G.: 'An Adaptive Power Factor Controller for Three–Phase Induction Generator'. IEEE Trans. on Power Apparatus and Systems, Vol. PAS–104, No. 7, July 1985.

[1.50] Tandon, A.T., Murthy, S.S. and Berg, G.J. : 'Steady State Analysis of Capacitor Self–Excited Induction Generator'. IEEE Trans. on Power Apparatus and Systems, Vol. PAS–103, No. 3, March 1984.

[1.51] Elder, J.M., Boys, J.T. and Woodword, J.L. : 'Self–Excited Induction Machine as a Small Low–Cost Generator'. IEE Proc. VOl. 131, Pt. C, No. 2, March 1984.

[1.52] Elder, J.M., Boys, J.T. and Woodword, J.L. : 'The process of self–excitation in Induction Generators'. IEEE Proc. Vol. 130, Pt. B, No. 2, March 1983.

[1.53] Murthy, S. S., Malik, O. P. and Tandon, A. K.: 'Analysis of Self–Excited Generator'. IEE Proc. Vol. 129, Pt. C., No. 6, November 1982.

[1.54] Watson, D.B., Arrillaga, J. and Densem, T. : 'Controllable D.C Power Supply from Wind–Driven Self–Excited Induction Machines'. Proc. IEE, Vol. 120, No. 12, December 1979.

[1.55] Oai, B.T. and Davis, R.A.: 'Induction–General/ Synchronous Condenser System for Wind–Turbine Power'. Proc. IEEE, Vol. 126, No. 1, Jan. 1979.

[1.56] Arrillage, J. and Watson, D.B.: 'Static Power Conversion from Self–Excited Induction Generator'. Proc. IEE, Vol. 125, No. 8, Aug. 1978.

[1.57] Mohan, N. and Riaz, M.: 'Wind–driven, Capacitor–excited Electric Heating'. IEEE PES Winter Meeting, New York, Jan. 1978.

[1.58] Brenen, M.B. and Abbondanti, A. : 'Static Exciters for Induction Generators'. IEEE Trans. on Industry Applications, Vol. IA–13, No. 5, Sept/Oct. 1977.

[1.59] Doxey, B.C. : 'Theory and Application of the Capacitor–Excited Induction Generator'. The Engineer, Nov. 29, 1963.

[1.60] Bolton, H.R. and Abu–Adma, M.A. : 'Isolated Induction Motor Plus Capacitor–Excited Induction Generator Scheme for Borehole Pumping and Other Applications'. Proc. ICEM Conference, Munchen, 1986.

[1.61] Bolton, H.R. and ABu–Adma, M.A. : 'Electric Transmission Scheme for Wind–powered Borehole Pumping Applications'. Proc. 9th BWEA Conf. Edinburgh, 1987.

[1.62] Bolton, H.R. and ABu–Adma, M.A. : 'The Dynamic Response of Isolated Induction Generator, Induction Motor Schme for Wind–Powered Borehole Pumping Applications'. Proc. 10th BWEA Conf. London, 1988.

[1.63] Brook, D. and Mitchell, D. W. : 'Induction Generator Special Design Consideration for Turbines'. Proc. 9th BWEA Conf. Edinburgh, April 1987.

[1.64] Bolton, H.R. Lam, W.C. and Freris, L. L. : 'Double Output Induction Generator Scheme for Wind Energy Conversion'. Proc. 2nd BWEA Conf. April 1980.

[1.65] Bossanyi, E.A. and Jervis, B. : 'Compliance in Wind Turbines with Either Synchronous or Induction Generators'. Proc. 10th BWEA Conf. London, 1988.

[2.1] Grantham, C., Sutanto, D. and Mismail, B. : 'Steady State and Transient Analysis of Self–Excited Induction Generators'. Proc. IEE, Vol. 136, No. 2, March 1989.

BIBLIOGRAPHY

The following texts were used for general reference during the course of the project.

1] Twidell, S.: 'A Guide to small wind energy conversion systems'. England, 1987.

2] Simmons, D. M. : 'Wind power'. United States, 1975.

3] Selzer, H. : 'Potential of wind energy in the European community'. An assessment study, Brussels and Luxembourg, 1986.

4] Golding, E. W. : 'The generation of electricity by wind power'. England, First published 1955, Reprinted, with additonal material, 1976.

5] Cheremisinoff, N. P.: 'Fundamentals of wind energy'. United States, 1978.

6] Taylor, R. H. : 'Alternative energy sources for the centralised generation of electricity'. England, 1988.

7] McGuigan, D. : 'Small scale wind power'. England, 1978.